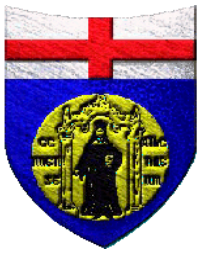

UNIVERSITA' DEGLI STUDI DI GENOVA

Corso di dottorato in Scienze e Tecnologie della Chimica e dei Materiali

Curriculum: Scienze e Tecnologie Chimiche
XXXIII Ciclo

Engineered poly(vinylidene fluoride) based composites containing inorganic inclusions as materials for energy-related applications: process-structure-properties correlations

ELISABETTA BRUNENGO

24/03/2021

Tutor: Prof. Maila Castellano
Co-tutor: Dr. Paola Stagnaro

to my husband
to my parents
to all my family

ABSTRACT

In recent years the continuous and rapid development of the electronic industry together with the need for more efficient electric energy harvesting have notably increased the demand for: *(i)* high dielectric constant and breakdown strength materials for high energy density capacitors and *(ii)* piezoelectric flexible materials, with the ability to bend into diverse shapes, for powering low-power portable devices and self-powered electronic systems.

Polymer-based composites and nanocomposites with inclusions of a ceramic active phase are very attractive for these applications because they combine materials with different characteristics, allowing the possibility to tune and optimize the dielectric and piezoelectric properties in the ensuing composite systems. In particular, many parameters can affect the material performance: *(i)* the nature of the polymer matrix and active component; (ii) the phases connectivity; *(iii)* the filler concentration, shape and dimensions; *(iv)* the filler/matrix interactions; *(v)* the preparation technique and processing. All this variability expands the possible applications of polymer-composites for energy-related purposes but also increases the difficulty in realistically predicting their ultimate properties. The design of polymer composites thus requires a rational selection of components, good interface engineering and proper processing optimization. To achieve this, a thorough comprehension of the process-structure-properties correlations is very important.

This is the principal aim of this thesis work, which focus on the preparation of poly(vinylidene fluoride) homopolymer (PVDF) or poly(vinylidene fluoride-*co*-hexafluoropropylene) copolymer (PVDF-HFP) based composites with 0-3 connectivity containing different perovskite fillers, namely, $BaTiO_3$ (BT), $Pb(Zr,Ti)O_3$ (PZT) and $Na_{0.5}Bi_{0.5}TiO_3$ - $BaTiO_3$ (BNBT). The filler particles were used as prepared or properly surface modified and several techniques were employed for the composites preparation (*i.e.*, solvent casting, melt blending, hot-pressing, compression moulding).

Initially, a study of the neat polymer matrices was performed, by using, for the first time in literature, the compression moulding technique to tune the polymorphism of PVDF. A principal component analysis was performed on the infrared spectra of the moulded films to validate the equation usually employed for determining the electroactive phase amount (F_{EA}) then multiple linear regression was applied to better understand how the processing parameters affect the F_{EA} value. A double-step procedure was proven fundamental in inducing the formation of PVDF β phase and improving the dielectric properties of the ensuing polymer films.

After this preparatory investigation, the study of the process-structure-properties correlations was extended to PVDF-based composites, addressing three main issues: *(i)* the influence of processing on the ultimate properties of the prepared samples; *(ii)* the influence of particles dimensions and surface modification on the dielectric behaviour of the composite materials; *(iii)* the response of flexible piezoelectric composites.

The preparation technique affects the microstructure at different levels, but it was found that not always a flawless particles dispersion necessary leads to the best final performance of the composite. Whereas, a proper moulding method, by affecting the polymorphism of the polymer matrix and the compactness of the film, can improve significantly the dielectric response.

The presence of an inorganic shell around BT particles allows a modulation of the effective permittivity of the composites; if intrinsic factors (*i.e.*, the permittivity of the components) prevail on extrinsic ones (*i.e.*, interfacial polarization), the composites response can be predicted by FEM calculations. However, in these conditions, the reduction in the dielectric constant compensates for the increase of the breakdown strength promoted by the shell and, as a whole, the stored energy decreases.

It is worth noting that the composites containing core-shell particles are characterized by low tunability, a condition which is important for application as dielectric capacitors.
The functionalization of the ceramic particles with the tested coupling agents, despite decreasing to a certain extent the dielectric permittivity of the ensuing composites (due to the intrinsic low permittivity of the silane moieties), increases the maximum electric field, thus leading to an energy recovering capability comparable or slightly higher than that of the composite containing pristine BT particles.
The dielectric response of the composites is affected by the particles dimensions even though the films containing pristine BT and those containing TiO_2-coated particles exhibit a different trend of dielectric permittivity with filler size; this suggests a not negligible contribution of the interfaces, which varies with the method of particles synthesis.
As concerns the piezoelectric composites, the piezoelectric coefficient (d_{33}), in general, increases if the filler dimensions increase significantly. The higher response of the samples containing sintered and crushed PZT or BNBT particles (with respect to simply calcined powders) probably derived from the higher particles connectivity inside the agglomerates, which in turn leads to higher local stresses inside the material. As far as we know, the piezoelectric properties of composites made of fluorinated polymer matrices and BNBT filler had not been studied yet. The obtained d_{33} are in line with those of many flexible lead-free composites made with particles different from BNBT, suggesting the potentiality of these composites in the field of energy harvesting.

As principal achievements, I obtained: *(i)* an alternative and smart method to tune the polymorphism of PVDF homopolymer and its copolymers, by exploiting a simple and easily-scalable processing technique; *(ii)* solvent-free fabrication of polymer-based composites with dielectric properties improved by the moulding process; *(iii)* a better comprehension about the role of the interfaces, useful to tune the final performance of the dielectric composites; *(iv)* flexible lead-free polymer-based composites with a good piezoelectric response for potential application as safe energy harvesting devices.

Summary

1 INTRODUCTION & SCOPE

1.1 Background

In a global strategy of reducing the use of fossil fuels motivated by worldwide warming and pollution, new technologies are emerging that allow more rational and sustainable use of energy. This trend has prompted the interest in the production of devices capable of storing a large amount of electric energy or converting it in different ways.

The choice of a particular dielectric or piezoelectric material for a specific energy-based application is not only limited to its electric or electro-active response but also depends on other parameters, such as the frequency to be applied, the mechanical characteristics required, the available volume, the processing leading to the final devices, etc.

Polymer-based composites and nanocomposites are very attractive for such kinds of applications because they combine materials with different, or even opposite, properties with the aim of exploiting the most suitable characteristics of single components. This allows to improve the performance of the ensuing composite materials or to extend their application to cases for which the common ceramic devices are not suitable.

This is the general background in which my PhD research activity fits.

In particular, I carried out my research activity without a university scholarship mainly at the Institute of Chemical Sciences and Technologies "Giulio Natta" (SCITEC) of the National Research Council (CNR), formerly Institute for Macromolecular Studies (ISMAC-CNR), and to a less extent at the Department of Chemistry and Industrial Chemistry (DCCI) of the University of Genoa.

The PhD research was largely developed in the framework of two CNR projects: the POLYCOM Project (2016-2018) and a Serbian-Italian Bilateral Cooperation Project (2019-2021).

The POLYCOM Project – "Engineered polymeric composites with high energy density" (IDROL 10359) was funded by the Bank Foundation Compagnia di San Paolo. The main scope of this project was to study and improve the dielectric properties of polymer-based composites and nanocomposites with ceramic inclusions through the engineering of polymer-inorganic filler interface and understand the factors that determine the performance of the material, with particular attention on the effect of the microstructure (size, distribution of the dispersed phase, interface morphology, connectivity).

POLYCOM was a very interdisciplinary project being based on the collaboration between three research groups:

- ICMATE-CNR (Institute of Condensed Matter Chemistry and Technologies for Energy) group (Genoa, Italy), that lead the project and carried out the *(i)* synthesis and characterization of barium titanate ($BaTiO_3$) particles (also labelled BT in the following) and their coating with different binary oxides (namely, TiO_2 and SiO_2) and *(ii)* evaluation of dielectric properties of simple capacitors *ad hoc* prepared with the polymer/ceramics composite materials;
- ISMAC-CNR (now SCITEC-CNR) group, (Genoa, Italy), that was involved in the *(i)* functionalization of BT particles, *(ii)* incorporation of various types of particles in suitable polymer matrices, such as poly(vinyldene fluoride) (PVDF) and its copolymers, exploiting different processing methods to obtain composite or nanocomposite materials, and *(iii)* characterization of the polymer matrices, inorganic fillers and ensuing composite materials;
- Physics Department of "Ioan A. Cuza" University of Iasi (Romania), that studied the role of composite material composition and structuring in determining dielectric properties, correlating FEM modeling and experimental data.

The Serbian-Italian Bilateral Cooperation Project, entitled "Lead-free piezoelectric and multiferroic flexible films for nanoelectronics, energy harvesting and energy storage" (Project code: RS19MO01), is funded by MAECI (Italian Minister of Foreign Affairs and International Cooperation).

The aim of this project is the preparation and characterization of PVDF-based composites containing Lead-free particles, principally consisting of doped $BaTiO_3$, to find the best formulations and proper design for producing flexible films for energy harvesting and storage.

Also this project is characterized by great interdisciplinarity, involving five research groups:

- ISM-CNR (Institute of Structure of Matter) group (Rome, Italy), responsible for the Italian side and in charge of the piezoelectric characterization and anelastic measurements;
- ISTEC-CNR (Institute of Science and Technology for Ceramics) group (Faenza, Italy), in charge of the ceramic particles synthesis and composites poling;
- ICMATE-CNR, in charge of the dielectric characterization of the composite materials;
- SCITEC-CNR, in charge of the the preparation of composites from solvent casting and their spectroscopic, morphological and thermal characterization;
- IMR-UB (Institute for Multidisciplinary Research, University of Belgrade) group (Belgrade, Serbia), responsible for the Serbian side and in charge of the preparation of composites from hot-pressing and ferroelectric measurements.

Within this framework, I spent a research period in Serbia, at the University of Belgrade.

1.2 Objectives

Taking into account the specific focuses of the projects in which my PhD research is framed, the principal aims of this thesis work are:

- The preparation of PVDF-based composites with 0-3 connectivity containing different inorganic inclusions (used as prepared or properly surface modified) by solvent casting, melt blending, or other techniques, followed by compression moulding in order to obtain final plates suitable for the subsequent characterization;

- The thorough characterization of the employed particles and achieved composites to study the influence of the preparation method and introduction of the inorganic particles on the polymorphism of the polymer matrix as well as on the ultimate properties of the ensuing materials.

1.3 Thesis outline

After this *Chapter 1*, in which the background of the study is presented, *Chapter 2* is focused on the state of the art. In particular, the principles of energy storage and conversion and the challenges in these fields are described in *Paragraph 2.1* where the theoretical background behind these topics, accompanied by the principal mathematical relationships, and the more diffuse methods of measurement used to determine the parameters of interest are reported. In *Paragraphs 2.2* and *2.3* the advantages of exploiting polymer/ceramics composites for energy-related applications are highlighted, with a summary of the factors affecting the final properties of these composite materials.

A general description of the principal materials employed is then reported. In particular, as concerns the matrix, after a brief *excursus* on the different polymers used in literature for dielectric or piezoelectric composites, the benefits of the fluorinated matrices are pointed out (*Paragraph 2.4*); a major exponent of this class of polar polymers, that is PVDF, is presented whit description of its molecular, thermal and structural characteristics, paying particular attention on its polymorphism.

Also some of the most common copolymers of PVDF, namely poly(vinylidene fluoride-*co*-trifluoroethylene) (PVDF-TrFE), poly(vinylidene fluoride-*co*-chlorotrifluoroethylene) (PVDF-CTFE) and poly(vinylidene fluoride-*co*-hexafluoropropylene) (PVDF-HFP), are briefly introduced.

As concerns the inorganic filler counterpart, *Paragraph 2.5* starts with a general presentation of the characteristics of the perovskite materials, with the advantages that distinguish them from other inorganic compounds and some examples and applications. Then, the focus shifts on the description of the three principal perovskites used in this research work: Barium Titanate (BT),

Lead Zirconate Titanate (PZT) and Bismuth Sodium Barium Titanate (BNBT), dwelling on their characteristics temperatures, crystalline structures and properties.

Chapter 3 is dedicated to the specific materials used in this work and the procedures adopted and customized: specifically, particles functionalization (*Paragraph 3.3*), composites preparation (*Paragraph 3.4*) and techniques employed for materials characterization (*Paragraph 3.5*).

Gathered results and their discussion are included in *Chapter 4*. This chapter is divided into 3 sub-chapters relative to the main issues addressed in this work:

(i) the influence of processing on the polymorphism of the polymer matrix and on the ultimate properties of the prepared composite samples, starting from the study of the neat polymer matrix (at first PVDF and then PVDF-HFP) and following with the composites (*Paragraphs 4.1.1, 4.1.2, 4.1.3, 4.1.4*);

(ii) the influence of particles dimensions and surface modification on the performance of the composite materials, considering both the particles functionalized with silane coupling agents and those coated with inorganic binary oxides (*Paragraphs 4.2.1, 4.2.2, 4.2.3*);

(iii) the response of piezoelectric composites, consisting of a preparatory study on PVDF/PZT films (*Paragraph 4.3.1*) followed by the investigation on lead-free composites containing BNBT particles (*Paragraph 4.3.2*).

Part of these Paragraphs are freely adapted from four papers derived from the work:

• E. Brunengo, L. Conzatti, I. Schizzi, C. Costa, M.T. Buscaglia, G. Canu, M. Castellano, V. Buscaglia, and P. Stagnaro, «PVDF/$BaTiO_3$ composites as dielectric materials: influence of processing on properties», AIP Conference Proceedings, 1981, 020132 (2018), Code 137840, ISBN: 978-073541697-0, ISSN: 0094-243X, Article n. 020132.

• E. Brunengo, M. Castellano, L. Conzatti, G. Canu, V. Buscaglia, P. Stagnaro, "PVDF-based composites containing PZT particles: How processing affects the final properties", Journal of Applied Polymer Science 137 (2020) 48871; DOI: 10.1002/APP.48871.

• E. Brunengo, G. Luciano, G. Canu, M. Canetti, L. Conzatti, M. Castellano, P. Stagnaro, "Double-step moulding: an effective method to induce the formation of β-phase in PVDF", Polymer 193 (2020) 122345; DOI: 10.1016/j.polymer.2020.122345.

• E. Brunengo, M. Castellano, L. Conzatti, I. Schizzi, C. Costa, M.T. Buscaglia, G. Canu, L. Curecheriu, L. Padurariu, L. Mitoseriu, P. Stagnaro, V. Buscaglia, "Improved dielectric properties of PVDF–$BaTiO_3$ composites by solvent-free processing", Journal of Applied Polymer Science 2021; 138:e50049; DOI: 10.1002/app.50049.

2 STATE OF THE ART

2.1 Energy storage and conversion

The term “energy harvesting” (also called energy scavenging) refers to the recovery of energy from one or more of the surrounding energy sources and its accumulation and storing for later use [1]. This requires two important capability: energy conversion and energy storage.
Nowadays, different types of plants that produce kW or MW power levels exploiting renewable sources such as water, wind, solar or geothermal energy are already widespread; this is called macro energy harvesting technology. However, some applications require much lower but portable power. This is usually provided by conventional batteries whose life is however limited compared to the working life of the devices they power. As an alternative, the interest in micro-energy harvesting technologies is growing up. Such technologies are based on the conversion and storing of waste energy from mechanical stress and strain, mechanical vibration, human body movement, chemical, or biological sources into viable electricity, obtaining mW or μW power levels.

As concerns energy storage applications, the four main types of devices employed are batteries, fuel cells, electrochemical capacitors and dielectric capacitors. Among these, dielectric capacitors are advantageous thanks to their high power density, high charge and discharge rate, long cycle time, and wide working temperature range. Not by chance, the total number of papers dealing with dielectric materials intended for energy storage has grown exponentially in the last dozen years (Figure 2.1). Furthermore, dielectric capacitors are passive components widely used in electronic systems also for other purposes such as filtering, current conversion, termination, decoupling, etc., each of these applications requiring different specific characteristics (Table 2.1).

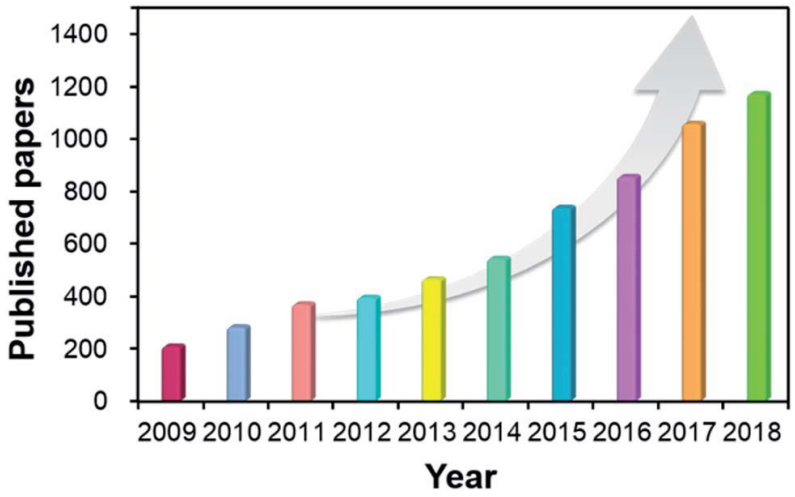

Figure 2.1: Number of publications per year concerning the dielectric materials for energy storage in the recent scientific literature [2].

Table 2.1: Major applications and properties of capacitors [3].

Application	**Value range**	**Stability required**	**Tolerance required**
Filtering	1 pF to 100 nF	Moderate	Moderate
A/D conversion	1 pF to 10 nF	Very high	Very high
Termination	50–200 pF	Low	Low
Decoupling	1–100 nF	Low	Low
Energy storage	> 1 µF	Low	Low

A capacitor consists of a dielectric material interposed in between two conductor plates, the electrodes, which typically are in a parallel-plate configuration. When an external electric field is applied to a capacitor, positive and negative charges, generated within the dielectric medium, accumulate in the two plates as a consequence of material polarization.
The higher the dielectric constant, the stronger the ability of the material to polarize. There are four main mechanisms of polarization that can occur in a dielectric medium as a consequence of an applied electric field. They are schematized in Figure 2.2 and briefly described in the following.

- Electronic polarization, due to the displacement of the electronic cloud with respect to the atomic nucleus. This polarization, also called optical polarization, typically occurs in the UV frequency range.
- Ionic or atomic polarization, associated with the displacement of the atomic nuclei in a molecule or of the ions in a crystal lattice, respectively, manifests at IR frequencies.
- Dipolar polarization, generated by the orientation of permanent dipoles present in polar materials. In this case, the range of frequencies is that of the microwaves
- Interfacial or Maxwell-Wagner polarization, consequence of the space charges which move inside the material and locate at discontinuity surfaces consisting of medium inhomogeneities, presence of defects and impurities or incomplete contact with the electrodes.

The first two mechanisms, both involving discrete energy levels, are characterized by a resonant behaviour and are independent by temperature while the second two, due to the limited mobility of the dipoles and/or charges, lead to relaxations phenomena and thus, to losses. In fact, in a real dielectric material, the permittivity can be expressed as a complex permittivity:

$$\varepsilon^* = \varepsilon' - i\varepsilon'' \tag{2.1}$$

where ε' is the real part, related to the stored energy, and ε'' the imaginary part of the permittivity, related to the lost energy, usually due to ohmic conduction losses and/or to losses associated with the absorption of energy to move charges within the material. These two dielectric parameters are related by the term called loss tangent, which is often used to indicate the dielectric losses:

$$tan\delta = \frac{\varepsilon''}{\varepsilon'} \tag{2.2}$$

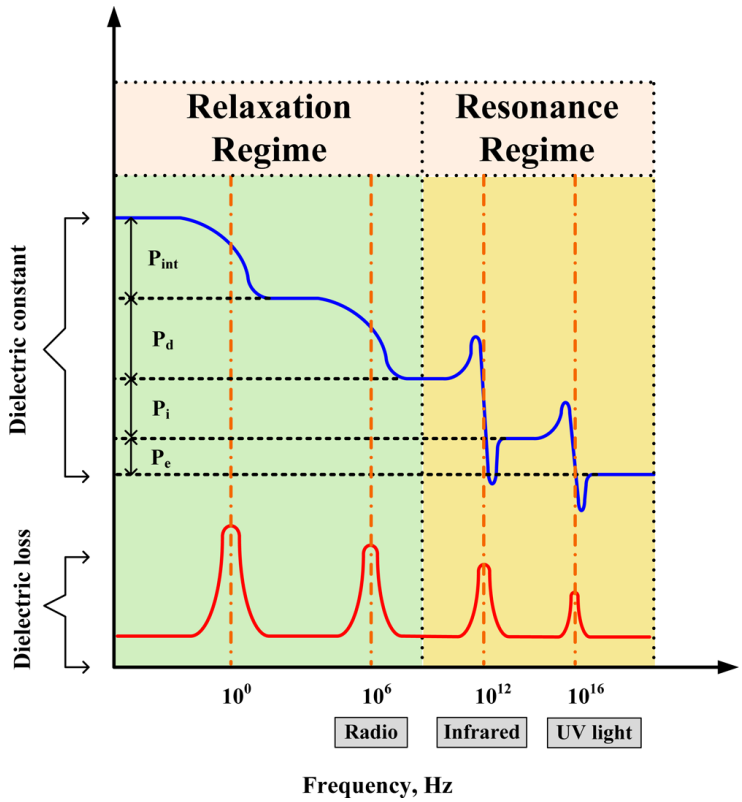

Figure 2.2: Different types of polarization and their frequency dependence [4].

The energy-stored ability of a capacitor is related to its capacitance (C) which depends on the geometry of the system and permittivity of the dielectric material:

$$C = \frac{Q}{V} = \varepsilon_0 \varepsilon_r \frac{A}{d} \tag{2.3}$$

where Q is the accumulated charge, V the applied electric voltage, ε_0 the vacuum permittivity (8.85 x 10^{-12} F/m), ε_r the relative permittivity, A the overlap area of the electrodes and d the distance between them (*i.e.*, the thickness of the dielectric material).

During the charging process, the external bias makes the charges move, indicating that a work must be done and at the same time that the electric energy is stored in the dielectric medium. The amount of the stored energy W could be obtained from:

$$W = \int_q^0 V dq = \frac{1}{2} C V^2 \tag{2.4}$$

Commonly, for the convenience of comparison, the energy stored per unit volume (U) of a given dielectrics is considered. This value could be measured by using two different methods: a static and a dynamic one.

In the static method, the capacitor is first charged and then connected to a load (R) to allow part of the stored energy discharging; this is accompanied by a transient current (I) formed in the closed circuit.

The energy density, which in this case is a recoverable energy density (U_{rec}), is obtained by:

$$U = U_{rec} = \frac{W}{Ad} = \frac{1}{Ad} \int I^2(t) R dt \tag{2.5}$$

In the dynamic method, the energy density can be calculated by measuring the electric field-polarization (E-P) loop and by integrating the area between the vertical axis and the obtained curve (Equation 2.6).

$$U = \frac{W}{Ad} = \int_0^{Emax} P dE = \int_0^{Emax} \varepsilon_0 \varepsilon_r E dE \tag{2.6}$$

In particular, for a linear dielectric material, whose permittivity is independent by the applied electric field, the Equation 2.6 is simplified in:

$$U = \frac{1}{2} \varepsilon_0 \varepsilon_r E^2 \tag{2.7}$$

In the case of an ideal linear dielectric material, the energy stored is equal to the energy recovered. However, for real materials, part of the energy accumulated during the polarization process is exhausted during depolarization because of the hysteresis loss; in this case, schematized in Figure 2.3, the energy loss (U_{loss}) corresponds to the area enclosed in the loop and just the remaining area corresponds to the energy effectively recovered during the discharge process.

Taking into account these considerations, the energy storage-efficiency can be defined as:

$$\eta = \frac{U_{rec}}{U_{rec} + U_{loss}} \tag{2.8}$$

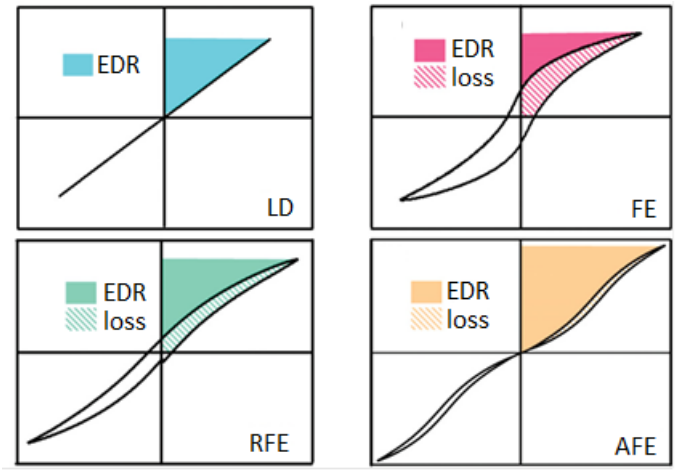

Figure 2.3: Scheme of the energy recovered (EDR) and loss for different types of materials: linear dielectric (LD); ferroelectric (FE); relaxor ferroelectric (RFE) and antiferroelectric (AFE). The image is taken and modified from [5].

In addition, because the energy accumulated in a capacitor depends on the applied electric field, one can easily guess that the higher the material resistance to the applied field, the higher its storage capability. Thus, another important factor in determining the properties of a given dielectric material is its breakdown strength. The dielectric breakdown of an insulating material is the abrupt failure under an external electric field leading to mechanical damage and electrical conduction [6]. In practice, when the electric field reaches a certain threshold, which depends on the nature of the material but also on extrinsic factors, such as defects or impurities, it causes irreversible modification of the dielectric medium, accompanied by the loss of insulation. The mechanism of this phenomenon is not yet completely unrevelled and different theories are present in literature, that ascribe the electrical breakdown to the electrons promotion from the valence to the conduction band (*i.e.*, intrinsic breakdown), to field localizations determined by conduction currents and losses from polarization (*i.e.*, thermal breakdown), to an avalanche process of the free electrons (*i.e.*, ionization breakdown), to the presence of pores that act as starting point of failure (*i.e.*, erosion breakdown) or to the formation of conducting channels as a consequence of the material degradation (*i.e.*, breakdown from tracking) [7–10]. One or, more plausibly, a combination of these different mechanisms can cause the breakdown of a solid insulator, depending on the duration of the applied field.

Anyhow, since the breakdown phenomenon limits the maximum energy that can be cumulated in a dielectric material as a consequence the breakdown threshold would be as high as possible to improve the performance of the device.

As concerns the energy conversion, piezoelectric systems seems to be very promising due to their simple configuration, high conversion capability, and the possibility of being integrated into more complex systems to be applied for the so called Internet of Things (IoT) [11].

The phenomenon of piezoelectric (from the Greek word "*piezo*" or "to press"), was discovered in 1880 by Pierre and Jaque Curie during a systematic study of the effect of pressure on the generation of electric charge by non-centrosymmetric crystals, such as quartz [12]. The first serious application of the piezoelectricity was carried out during the First World War by P. Langevin [13], who constructed the first underwater ultrasonic source (sonar).

With "piezoelectricity" is indicated the unusual characteristic of certain materials to convert the mechanical energy into electrical energy (*i.e.*, direct piezoelectric effect) and the electrical energy into mechanical energy (*i.e.*, converse piezoelectric effect). This ability is related to the peculiar crystalline structure of these materials. The necessary condition for the occurrence of piezoelectric effect is the absence of a centre of symmetry in the crystal, such a condition is responsible for the charge separation between positive and negative charges (ions, dipoles) as a consequence of an external mechanical stress. If the piezoelectric material is inserted in a circuit, the electric field so generated causes, in turn, a flow of current until the free charges neutralize the polarization effect; once the mechanical force applied to the material is removed, the flow of charge will reverse until the material reaches its original standstill state (Figure 2.4).

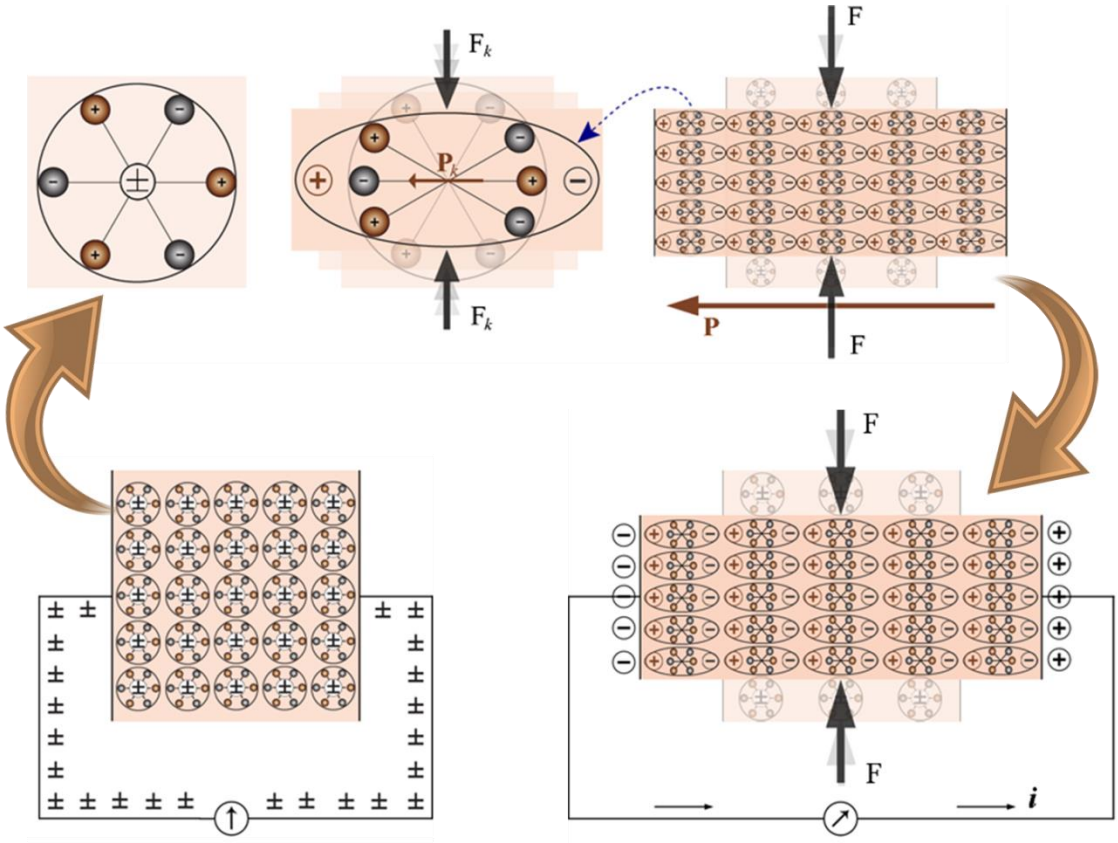

Figure 2.4: Direct piezoelectric effect explained with a molecular model and its consequences at a macroscale level when the material is connected to a galvanometer. The image is freely taken and modified from [14].

To describe the interconnection between the mechanical and electrical behaviour of the material the following constitutive Equations are used:

$$Direct\ effect: D = dT + \varepsilon E \tag{2.9}$$

$$Converse\ effect: S = sT + dE \tag{2.10}$$

where D is the electrical displacement, d the piezoelectric coefficient, T the applied stress, ε the permittivity of the material, E the electric field, S the strain and s the mechanical compliance (*i.e.,* the inverse of the elastic modulus). The above reported Equations are written in a generalized form, without the directional notation, but they are actually tensor relations. In fact, the piezoelectric coefficients, usually used to quantify the phenomenon in a given material, is expressed as follows:

$$d_{ij} = \left[\frac{\delta D_i}{\delta T_j}\right]_E \tag{2.11}$$

or

$$d_{ij} = \left[\frac{\delta S_j}{\delta E_i}\right]_T \tag{2.12}$$

where the subscript i is the direction of the electric field associated with the voltage applied or the charge produced while subscript j gives the direction of the mechanical stress or strain.

According to Equation 2.11, which is valid at constant electric field, d_{ij} express the charge collected on the electrodes as a consequence of the applied stress, while, according to Equation 2.12, valid for constant stress, d_{ij} represents the mechanical strain produced by an applied electric field.

Depending on the different modes with which the mechanical stress or the electric field can be applied, it is possible to have different d constants; among them, the most used are d_{33} (direct or longitudinal d), used when the force is applied along the polarization axis and d_{31} (transverse d) used when the force is applied perpendicularly to the polarization axis (as in the example of Figure 2.4).

The piezoelectric coefficients are the most important parameters defining the piezoelectric activity of a material, basically, the higher the d_{ij} values, the more active the material. Large d_{ij} constants relate to large mechanical displacements, which are usually sought in motional transducer devices. On the contrary, for applications as sensors, high sensitivity is required; this can be expressed by the voltage coefficient (g) which is the ratio between the open circuit electric field and the applied mechanical stress; g_{ij} is related to d_{ij} by the following Equation:

$$g_{ij} = \frac{d_{ij}}{\varepsilon_r \cdot \varepsilon_0} \tag{2.13}$$

The performances of a piezoelectric material are usually measured under dynamic or quasi-static conditions.

The first approach consists of measuring the response of a piezo-material when subjected to an alternating electric field or mechanical stress with a frequency close to the mechanical resonance of the sample. Due to the electromechanical coupling, it is possible to induce resonance in a piezoelectric material, without the need for external mechanical vibration, but simply applying an AC voltage across the device (Figure 2.5a); the material response is visible as peaks in the measured impedance curve, from which the piezoelectric coefficient can be calculated [15].

The second method, called of Berlincourt, is based on a more direct approach, consisting of applying a small oscillating force to the sample, usually via a loudspeaker type coil, and then measuring the charge output. A reference sample, often a PZT ceramics, is in line with the loading train and is used to measure the force applied (Figure 2.5b). In this way, the piezoelectric coefficient is got as the ratio of the charge signal from the reference material to that from the specimen under investigation (or their root mean square).

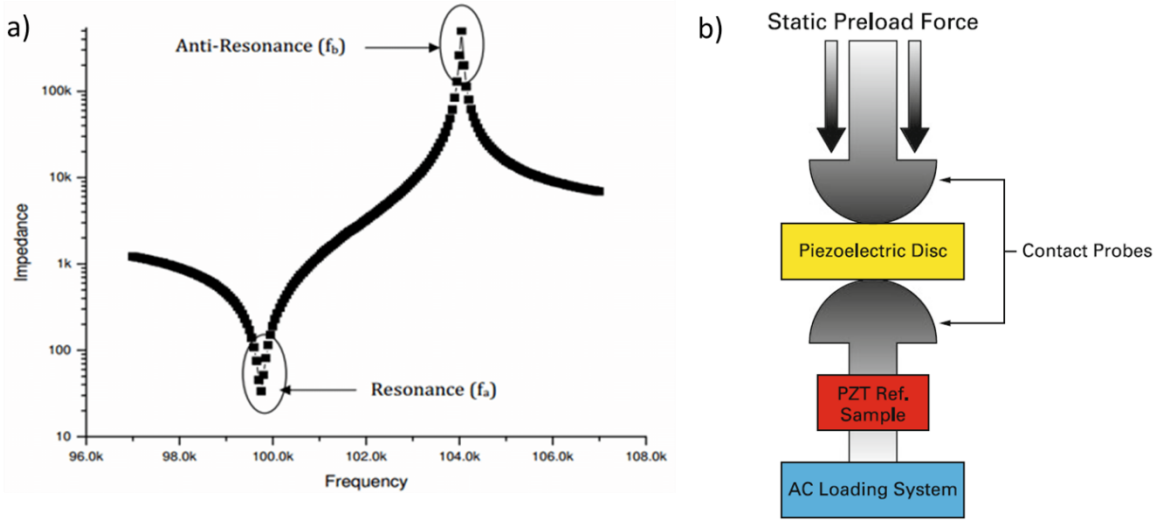

Figure 2.5: a) Resonance and anti-resonance frequency in the impedance curve of piezoelectric material [16]; b) Scheme of the force head used in the Berlincourt method [17].

Beyond the intrinsic piezoelectric characteristics of a composite, the possibility of exploiting its properties is also determined by *(i)* how the external stress is applied and *(ii)* the configuration of the device in which the piezoelectric material itself is integrated.

At the experimental level, as an example, C. K. Jeong *et al.* [18] measured a different output voltage by deforming a rubber-based piezoelectric hyper-stretchable composite in stretching, twisting, folding, and crumpling mode.

In view of a more industrial level, S. Mishra *et al.* [19] reviewed different possible configuration available for piezoelectric energy harvesting (PEH) systems (Figure 2.6): *(i)* the cantilever beam type (Figure 2.6a,b), obtained by bonding a thin layer of piezoelectric material to a non-piezoelectric layer and by fixing it at one end to achieve a structure operating in flexural mode. This geometry allows to generate the maximum amount of strain for a given amount of mechanical vibration; *(ii)* the circular diaphragm set-up (Figure 2.6c), much stiffer than the previous one, in

which a thin disk-shaped layer of piezoelectric material is attached to a metal shim and perpendicularly stressed; *(iii)* the cymbal type configuration, showed in Figure 2.6d, which allows producing an in-plane strain under a transverse external force, and is required for applications withstanding higher impact forces; *(iv)* the stack configuration (Figure 2.6e) which consists of multiple piezoelectric layers stacked over each other.

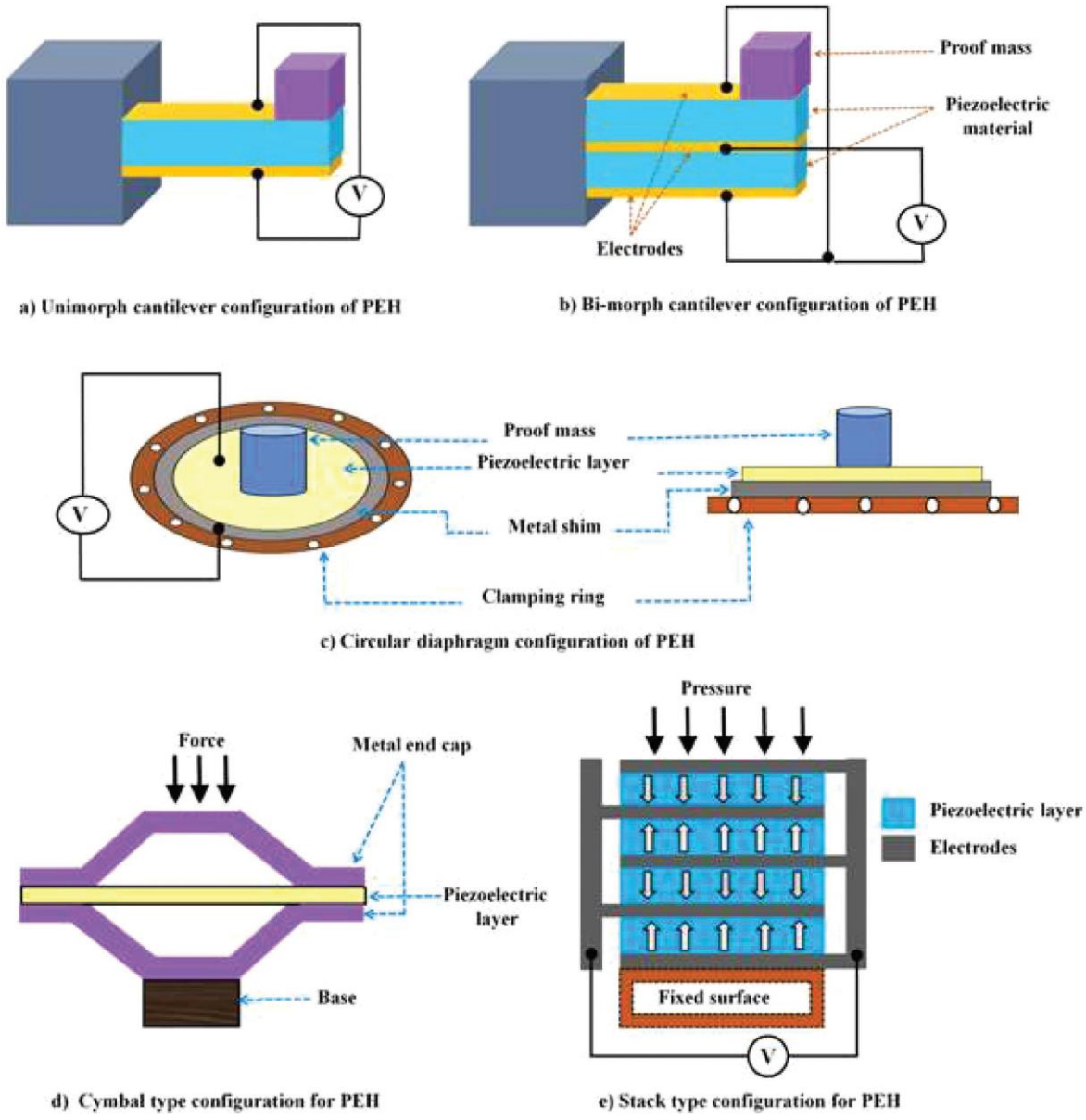

Figure 2.6: Different structural configurations of piezoelectric energy harvesting devices.

In general, the design of a piezoelectric energy harvesting device for a particular operation could always be specified depending upon the application perspective and operating mode.

2.2 Composites for energy storage

As one can infer from Equation 2.7, both high permittivity and high breakdown field are required for an efficient electric energy storage. However, single insulating materials do not satisfy these conditions at the same time. On one hand, ceramic materials are characterized by a high dielectric constant (10^2-10^3) but low breakdown strength (10 MV/m); on the other hand, polymers possess low dielectric constant (1-10) but high breakdown strength (100-1000 MV/m).

Polymer-based composites and nanocomposites are thus very attractive for these applications because the introduction of high permittivity inorganic particles into a polymer matrix, characterized by a high breakdown field, allows improving the amount of stored electric energy. Other advantages of such dielectric composite materials, with respect to all ceramics counterparts, are that *(i)* they can be produced using relatively low-temperature processes and *(ii)* their dielectric properties can be properly tailored by changing the nature of components and their concentration.

When two different materials are combined to exploit their dissimilar characteristics, the final properties of the ensuing composites depends on different factors, among which those playing an important role are listed below:

- nature of the polymer matrix and active component (*i.e.*, the ceramic filler);
- phase(s) connectivity;
- filler concentration;
- filler dimension;
- filler shape;
- filler/matrix interactions;
- preparation method and processing.

Some examples related to the influence of these variables are reported in the following.

Nature of components. First of all, the ultimate properties of a dielectric composite are strictly influenced by the type of filler and matrix that "compose" it. In particular, for energy-related applications, polymer-based composites containing insulating or conducting filler can be found in the literature. As conducting fillers, metals, such as Ni, Ag or Cu [20–22], and carbon, in the form of graphene or nanotubes [22], have been used. The preparation of percolated composites using conductive or semi-conductive fillers is a strategy used to obtain high-permittivity composites for dielectric applications; when the concentration of the conductive component is close to reaching the percolation threshold, the particles approximate to each other, remaining insulated by thin layers of dielectric material (*i.e.*, the polymer matrix), thus forming nanocapacitors and leading to very high permittivity values. However, the dielectric characteristics obtained are not a direct consequence of the intrinsically high-ε fillers, but are due to the huge increase in interfacial polarization. In addition, high dissipation factors arising from conductive network formation above the percolation threshold preclude the use of these composites for energy storage applications.

To avoid this, a more used approach, is based on the preparation of composites containing high-ε insulating ceramic fillers. In this case, the dielectric properties of the final material, despite could be affected by extrinsic factors, are mainly related to the intrinsic dielectric characteristics of the filler chosen. Perovskite compounds are good candidates as the active component for these kinds of composites (for more details on this class of materials, see *Paragraph 2.5*); among these, barium titanate, $BaTiO_3$, is undoubtedly one of the most widely used in this area [2], but also composites containing $SrTiO_3$, $(Ba_xSr_{1-x})TiO_3$, $(Na_xBi_{1-x})TiO_3$, $PbZr_{0.52}Ti_{0.48}O_3$ or $BiFeO_3$ are reported in the literature [23–27].

Besides the filler, also the type of polymer matrix is important to determine the final properties of the composites. As an example, Kim *et al.* prepared composites containing barium titanate particles and, in order to study the effect of the matrix, chose two types of polymeric host materials: namely, a low permittivity bisphenol A-type polycarbonate (PC) and a high permittivity poly(vinylidenefluoride-*co*-hexafluoropropylene) (PVDF-HFP), obtaining in the second case about a doubled effective permittivity while maintaining acceptable the dielectric losses. In general, PVDF and its copolymers are the most employed as polymer matrices in dielectric composites (for more details see *Paragraph 2.4*) and are also the subject of this study.

Connectivity. Properties of composite materials depend not only on the type of filler and matrix, but also on how they are coupled. Such a coupling concept was first introduced by Newnham [28] and it is known as connectivity. The connectivity describes the interspatial relationships in a multiphase material, depending on it the mechanical and the electrical properties as well as the thermal fluxes between the phases. In a binary composite, the connectivity is described by the combination of two numbers x-y which represent the number of directions through which the filler (x) and the matrix (y), respectively, are self-connected.

Theoretically, 10 different types of connectivity exist (Figure 2.7). However, only a few of these configurations are reproducible in practice, namely 0-3 (ceramic particle-filled polymer), 1-3 (unidirectional laminates of ceramic fibers), 2-2 (laminated sheets of ceramics and polymer).

In particular, in this work 0-3 composites are considered, which are the most widespread type of composite materials in the field of energy storage due to the good performance they can reach accompanied by the simplicity of fabrication.

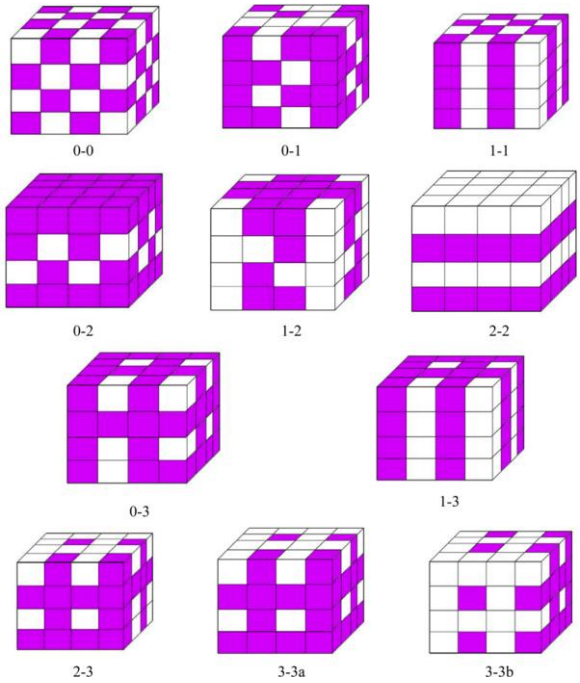

Figure 2.7: Possible connectivity patterns for a biphasic material [3].

Filler concentration. In general, the dielectric permittivity of a polymer composite containing a non-conducting inorganic filler increases by increasing the amount of filler because of the higher intrinsic permittivity of the latter, but also because of the increase of the interfacial area between the two components. However, in practice, this ideal trend does not hold for very high filler concentration. Kim *et al.* [29] prepared PVDF-HFP based composites containing from 10 to 80 Vol% of $BaTiO_3$ particles finding that the permittivity increases with the particle volume fraction reaching a maximum around 50-60 Vol%, after which the performance decreases (Figure 2.8). This is due to practical limits in composites preparation: at high loading, a filler dispersion such as to guarantee an ideal separation of filler particles and their covering with a polymer matrix layer become more and more difficult leading to an increase in porosity and a consequent decrease of dielectric properties (the permittivity of air is 1). For this reason, the filler concentration is usually maintained below 50-60 Vol%.

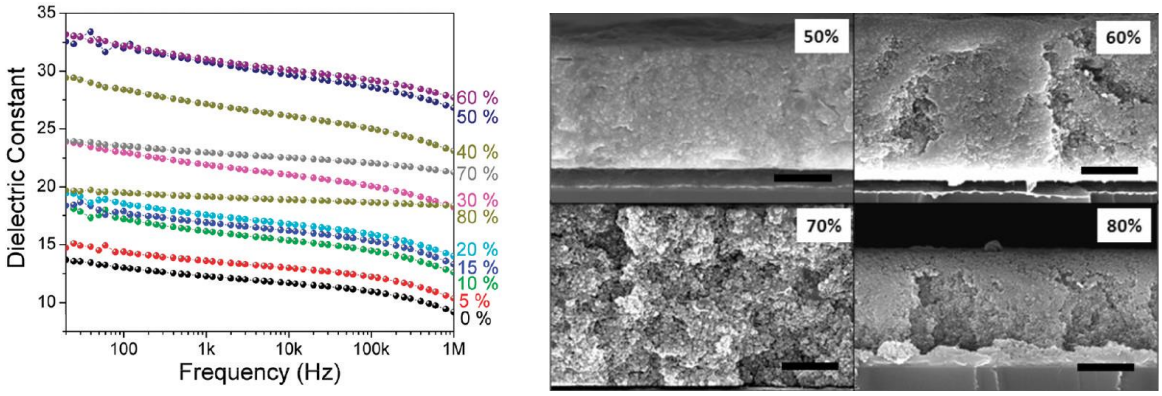

Figure 2.8: Dielectric permittivity of the PVDF-HFP/BT composites and relative morphology of the samples near the concentration threshold. Image modified from [29].

Filler dimension. In general, the dielectric permittivity of composites is clearly dependent upon the size of fillers, even though the dependence is not always the same. In some cases, the dielectric permittivity increases by increasing filler size and in others it decreases with the filler dimension; moreover, the trend can also change with the measurement conditions (Figure 2.9).

Two factors play an important role in determining these opposite trends: the intrinsic properties of the filler and the extrinsic contributions of the interfaces. As concerns the intrinsic properties of the filler, an emblematic case is that of $BaTiO_3$, whose permittivity is strictly related to the grain size following a non-monotonous trend (for more details see *Paragraph 4.2*), while more frequently, the dielectric response of ceramics tends to be higher for larger than for smaller particles. In addition, the change in dielectric properties with size in the micrometer scale is not necessarily the same as that in the nanoscale: the physical and chemical bulk properties of materials gradually disappear and approach molecular behaviour when the sizes approach the nanometric scale. Added to this is, in a composite, there is the fact that the filler is not isolated but surrounded by the polymer matrix; for small filler size, the surface markedly increases and the extrinsic contribution deriving from filler/matrix interfaces become more and more preeminent, surpassing in some cases the intrinsic properties of the single components involved.

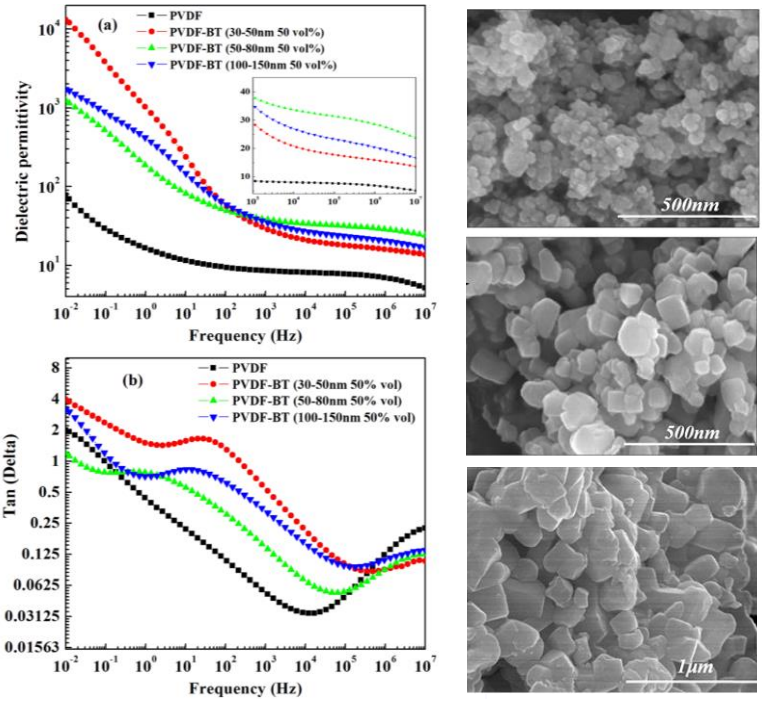

Figure 2.9: Dielectric response of PVDF/BT composites containing particles with different dimensions and corresponding SEM micrographs of the powders. Images modified from [30].

Filler shape. Along with the size, the shape of filler is as well important in determining the dielectric properties of the final composites. A general classification of fillers according to their shape is based on dimensionality: 0D (particles); 1D (fibers); 2D (sheets). Fillers with different shapes have different surface extension resulting in different interfacial areas in the composites

and, in some cases, in different connectivity. This leads to different interfacial polarization influencing the dielectric permittivity, but also to different electric field distribution affecting the electrical breakdown, especially if the anisotropic fillers are oriented. As an example, Z. H. Shen *et al.* [31] theoretically demonstrated that the breakdown strength of a composite film containing ceramic fibers or nanosheets is higher than that of a composite containing 0D particles only if the 1D or 2D filler is oriented parallel to the film surface and thus perpendicular to the applied electric field (Figure 2.10).

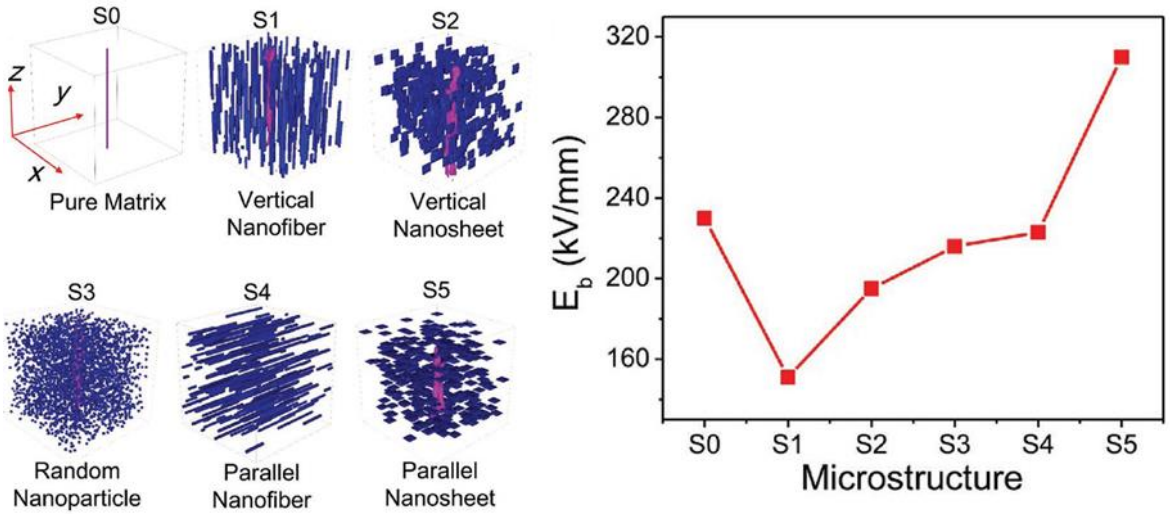

Figure 2.10: 3D simulations of microstructure effects on the breakdown. The volume fraction of the nanofiller is 10%. The aspect ratio of the nanofibers is r:h = 1:20 and the length scale of the nanosheets is 1:6:6. Image modified from [31].

In general, for both percolative and non-percolative composite systems, 0D fillers are amongst the most used, due to their easier syntheses.

Filler/matrix interactions. When two materials with different dielectric properties are put together to prepare a composite, the areas in which they are in contact show peculiar characteristics. Due to the high difference in dielectric permittivity, polymer/particle interfaces can be sites of significant local field fluctuation and thus can negatively affect the final performance of the composite material, especially from the point of view of dielectric losses and breakdown strength (for more details see *Paragraph 4.2*).

In order to mitigate the electric field concentration, the most common method is to modify the filler surface by following two principal "engineering" approaches: *(i)* the compatibilization with the polymer matrix, which can potentially increase the mechanical resistance of the composites and limit the dielectric losses at interfaces (Figure 2.11); *(ii)* the formation of a gradient in dielectric permittivity with a shell of a third material having intermediate properties between those of the filler and matrix.

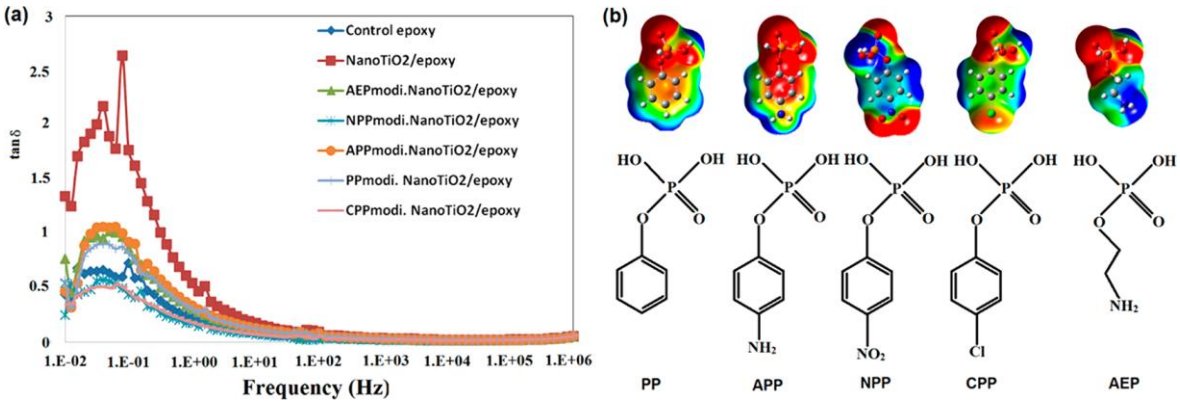

Figure 2.11: a) Dielectric losses of polymer and epoxy-based composites with 5 Vol % filler and b) molecular structures of organophosphate ligands and their electrostatic potential maps obtained from density functional theory (DFT) modeling (red and blue colour represent negative and positive charges, respectively). Image taken from [32].

Fabrication method. Besides all the previously cited factors, also the methods used to prepare a composite lead to a not negligible effect on their final properties. At equal type of components, filler shape, dimensions and amount, different processing can lead to different performances of the composites.

The two principal approaches employed for composites preparation are techniques that involve the use of solvents (*e.g.*, solvent casting, spin coating, etc.) or those which pass through the polymer melting (*e.g.*, melt mixing, extrusion, hot-pressing, etc.). In both cases, the procedure chosen to add the filler to the polymer matrix, instrumentation, temperature and time used to mix the components as well as the conditions set for obtaining the final films can modify: *(i)* the polymorphism of the polymer matrix [33]; *(ii)* its crystallinity degree [34]; *(iii)* polymer chains orientation [35]; *(iv)* filler dispersion [36]; *(v)* microstructure or the density of the composite [24].

Obviously, besides the improvement of the dielectric response also the difficulties in the preparation of the composite both in terms of costs, time and process scalability have to be considered. Indeed, for applicative purposes, one must take into account both the technologies involved in the preparation of the composites and the performance of the ensuing films.

Taking into account all possible variants, one can easily guess that a realistic prediction of the final properties of a composite intended for energy storage is very difficult. The design of polymer composites requires a rational selection of components (in terms of nature, dimensions, shape, concentration, etc.), a good interface engineering and proper processing optimization.

2.3 Composites for energy conversion

Similarly to what is reported in the field of energy storage, also for energy conversion applications, the design and fabrication of polymer-ceramic composites can be a smart strategy to modulate and enhance the properties of different piezoelectric materials. Indeed, composite materials have been

found to exhibit several improved piezoelectric properties as compared to ceramics and polymer single components.

In fact, piezoceramics have a large piezoelectric coefficients and provide high energy conversion rates, but they are too brittle to be used in general-shape energy transducers. On the contrary, piezopolymers have smaller electromechanical coupling constants but they are characterized by lightweight, low density, low cost and capability to withstand much higher strain due to their inherent flexibility, all this making them more suitable for applications demanding a large amount of bending or twisting. In addition, their low permittivity leads to higher voltage coefficient values which signify them as good sensor materials.

The same variables considered for the polymer/ceramics composites for energy storage (*e.g*, nature of the polymer matrix and active component, connectivity, filler concentration, filler dimension and shape, filler/matrix interactions, fabrication method) play an important role in determining the piezoelectric properties in the analogous counterparts intended for energy conversion [37].

Nature of components. Similarly to what described in *Paragraph 2.2* for the dielectric properties, also the piezoelectric properties, obviously depends on the nature of the components. M. Alexandre *et al.* [38], studied the effect of the polymer matrix in PVDF or polyamide 11 (PA11) based composites containing sodium niobate ($NaNbO_3$) particles; they ascribed the differences in the d_{33} values to the different state of the amorphous phase of the polymer matrices (vitreous for the PA11 and rubbery for the PVDF). Riquelme *et al.* [39] prepared instead PVDF-based composites containing different types of filler, BZT-BCTZ, $0.50[Ba(Zr_{0.2}Ti_{0.8})O_3]$-$0.50(Ba_{0.7}Ca_{0.3})TiO_3$, and KNNS-BNKZ, $0.96(K_{0.48}Na_{0.52})(Nb_{0.95}Sb_{0.05})O_3$-$0.04Bi_{0.5}(Na_{0.82}K_{0.18})0.5ZrO_3$; even if the differences in the dielectric permittivity are low and non-monotonous with the filler amount, the piezoelectric coefficient of the composites containing BZT-BCTZ is double of that of the samples with KNNS-BNKZ, at equal composition (Figure 2.12a).

Filler concentration. Also for piezoelectric composites, in general, the piezoelectric response increases by increasing the ceramic filler content. As an example, K. Yu *et al.* [40], by preparing PVDF-based composites containing particles of KNNL-Z ($(K_{0.475}Na_{0.495}Li_{0.03})NbO_3$-$0.003ZrO_2$) found that d_{33} coefficient increased from about 5 to about 40 by increasing the filler content from 40 to 80 wt% and the same trend was observed for the g_{33} coefficient. However, the increase of the filler amount also leads to an increase of the stiffness of the composite, as evidenced by A. Kumar *et al.* [41]; they prepared PVDF/BCZT (*i.e.*, 0.05 $(Ba_{0.7}Ca_{0.3})TiO_3$-$0.05Ba(Zr_{0.2}Ti_{0.8})O_3$) and tested the power generation by means of drop weight impact technique finding a decrease of the actual applied mechanical force as a consequence of the increasing hardness due to the increasing filler quantity. A too high filler content can compromise the flexibility of the piezo-composites, limiting their applicability in the range of low deformations.

Filler shape. As concerns the filler shape, G. Malucelli *et al.* [42] studied the effect of the particles morphology on the piezoelectric response of composites based on a UV-curable acrylic matrix, by using filler with spherical, bipyramidal, flower-like and long needles structures (Figure 2.12b). The piezoelectric effect of the different ZnO nanostructures was interpreted on the basis of the possible orientation of the 002 crystallographic planes with respect to the direction of the applied mechanical stress; this is perpendicular in the case of flower-like particles, which lead to the highest voltage output and parallel for the needles structures, leading to the lowest voltage output.

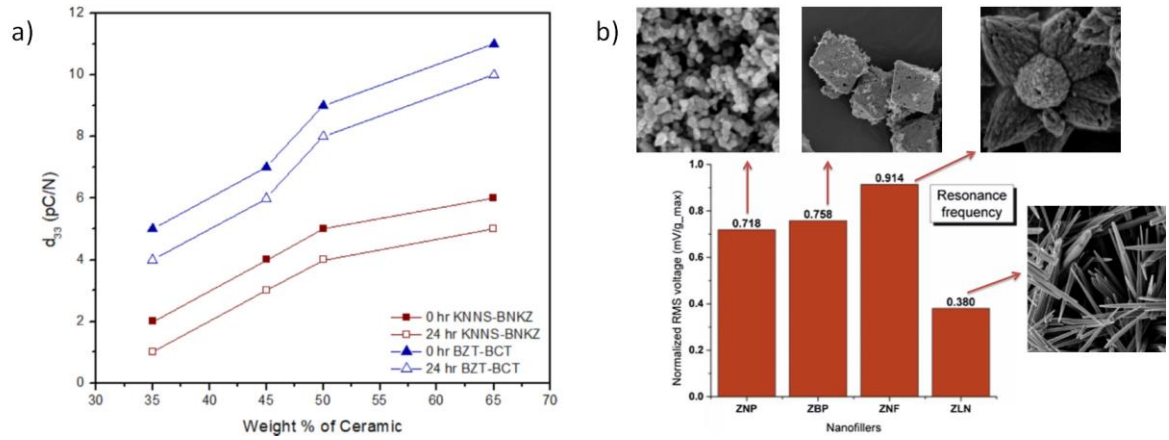

Figure 2.12: a) Piezoelectric coefficient (d_{33}) of xBZT-BCT-(1-x)PVDF and xKNNSBNKZ-(1-x)PVDF composites at RT [39]; b) Normalized voltage RMS values (for the four different nanofillers) at resonance frequency [42].

Filler dimensions. Also the particles size can have an effect on the final piezoelectric response of the composites; in literature, some examples describing an improvement of the piezoelectric performances with the particles dimensions are reported but the reasons have been not disambiguated; G. Rujijanagul *et al.* [43] ascribed the higher d_{33} coefficients of PE-PZT (polyethylene/lead zirconate titanate) composites containing larger particles to a more effective poling whereas T. Greeshma *et al.* [44] working on PVDF/PZT composites, reported that the differences observed related to the particles dimensions are instead due to their effect on the crystallinity degree and the β phase formation induced in the polymer matrix.

Filler/matrix interactions. The surface modification of the filler can be beneficial or detrimental for the piezoelectric properties of the composites depending on how it influences the particles dispersion and the interactions with the polymer matrix; as an example, Min *et al.* [45] found that the hydroxylation of PLZT (*i.e.*, lead lanthanum zirconate titanate) particles improve their dispersion and their compatibility with PVDF matrix, leading to a higher piezoelectric coefficient with respect to that obtained for analogous composites containing untreated particles. R. Li *et al.*, [46] clearly showed how the introduction of a coupling agent can have a contrasting effect; they prepared PVDF/PZT composites by modifying the particles with a silane (KH-570) or titanate (NDZ-101) coupling agent finding that the former decreases d_{33} and g_{33} due to an insulating effect

induced at the filler surface, while the latter leads to a maximum in the piezoelectric coefficients at a specific content (Figure 2.13).

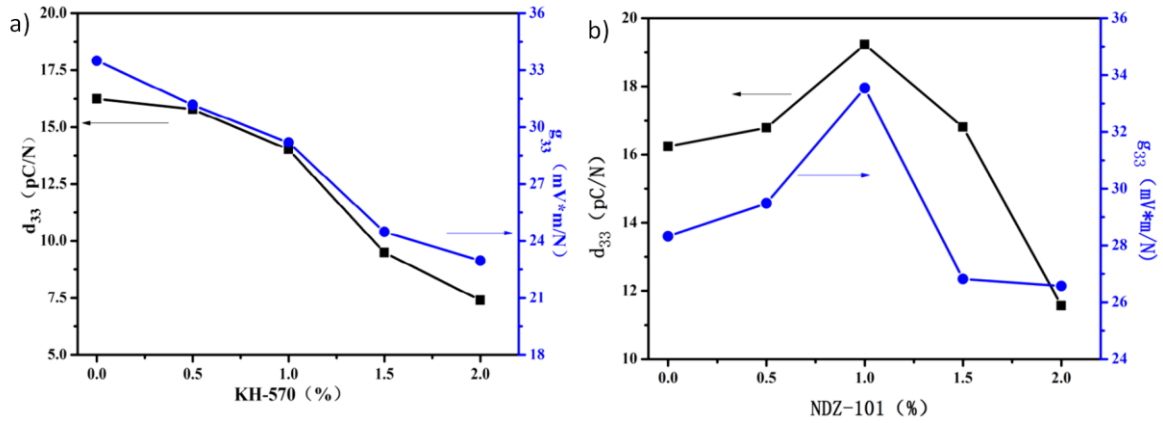

Figure 2.13: Piezoelectric coefficients of the PVDF/PZT composites containing particles modified with two different coupling agents [46].

Dealing with piezoelectric composites, it is important to underline another factor. Indeed, in their virgin state, piezoelectric polymers as well as polycrystalline ceramics do not show any polarization and exhibit no piezoelectric effect, because they are characterized by an irregular alignment of dipoles. In order to acquire piezoelectricity, an important operation known as "poling" has to be done to these materials; poling procedure comprises the application of a strong electric field, commonly at a temperature close to the Curie temperature, with the aim of aligning the electric dipoles along one single orientation. This polarization is, at least partially, maintained once the temperature is brought down to room temperature and the electric field is removed, the whole procedure resulting in a material with piezoelectric properties, as schematized in Figure 2.14.

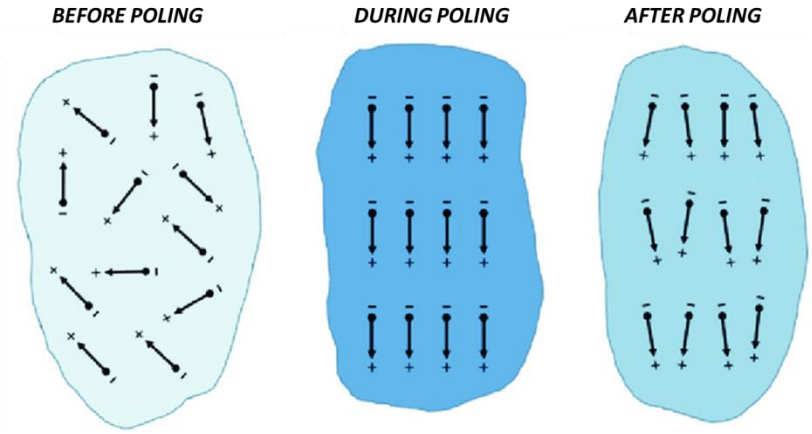

Figure 2.14: Scheme of the evolution of piezoelectric domains in piezoelectric materials with poling [47].

In general, the degree of polarization can be tailored easily by varying the poling method and conditions.

J. Pei *et al.* [48] studied the effect of poling time, temperature and electric field intensity on the d_{33} values of PVDF/PZT composites finding that the piezoelectric response increases by increasing the above mentioned parameters, being the effect more pronounced for high filler amount. K. Arlt and M. Wegener [49] compared the piezoelectric properties achieved in PVDF-TrFE/ PZT and PVDF-HFP/PZT composites by poling for different times, at different temperature regimes and by using two poling methods: corona discharge or poling in direct contact. They demonstrated that the d_{33} value and sign can change due to the fact that, under the applied conditions, also a not negligible polarization of the polymer matrix, whose response is opposite than that of the ceramics, is induced.

Thus, contrary to what happens for composites employed as capacitors, in the case of piezo-composites, the final performances are not only determined by the components used and the processing employed for the composites preparation but they are also affected by external factors related to the method and conditions used, at first, to make the material piezo-active, and then to stimulate its response (see *Paragraph 2.1*).

2.4 Fluorinated polymer matrices

A large number of polymer matrices have been used, on the basis of on their different properties, to prepare composites and nanocomposites useful in the wider field of electronics encompassing energy harvesting and storage devices. In general, polyethylene (PE), poly(methyl methacrylate) (PMMA), epoxy resins, and polyimides have been largely employed for these purposes [50–56]. For example, Z. M. Dang *et al.* prepared $BaTiO_3$/polyimide composites by *in-situ* polymerization obtaining high dielectric breakdown [57], M. J. K. Kumar *et al.* obtained Lanthanum Zirconium Oxide (LZO)/PMMA composites with low dielectric losses [58], B. Fan *et al.* realized sandwich-structured polydimethylsiloxane/carbon nanotube composites endowed with good dielectric properties [59]. Also, bi-axially oriented polypropylene (BOPP) is considered a promising solution for film capacitors due to its high dielectric strength and self-healing dielectric breakdown capability, even if its dielectric constant of only 2.2 severely prevents further development in the field of energy storage [60].

The restraint common to all the above cited polymers is their low dielectric permittivity, which, ranging from 2 to 5, is significantly inferior than that of their inorganic counterparts thus limiting the energy density obtained within the polymer matrix and consequently, in the resulting composites.

In general, polymers can be classified into polar and non-polar ones based on their mean dipole moments. In a non-polar polymer, the individual dipole moments are not present at all or cancel out each other (due to symmetry) being hence responsible for lower dielectric constant values. On the contrary, in polar polymers, the dipoles, generated by the high electronegativity difference between

the atomic elements of individual bonds, do not cancel out each other giving rise to a reinforcement of individual dipole moments and leading to comparatively higher dielectric constant than nonpolar polymers.

Fluorinated polymers exhibit large spontaneous polarization and high dielectric constants (10-12 at 1 kHz) because of the presence of fluorine atoms along the polymer chains. Fluorine has very high electronegativity (4.193) and very small size (its van der Waals radius, 1.35 Å, is only slightly larger than that of hydrogen,1.2 Å); this leads not only to a high dipole moment (μ = 1.92 D) of C-F bonds but also to high packing density of structures containing such bonds [61]. Beside the best known fluoropolymer that is polytetrafluoroethylene (PTFE, commonly called Teflon from its major tradename), a main representative polymer of this category is poly(vinylidene fluoride) (PVDF). PVDF is even one of the most intriguing and challenging semi-crystalline polymers studied nowadays, due to its peculiar dielectric, piezoelectric and ferroelectric properties, which are accompanied by other interesting characteristics, such as good mechanical properties, chemical inertia and biocompatibility [62]. PVDF is a polymer with chemical formula $(CH_2\text{-}CF_2)_n$, containing 59.4 wt % fluorine and 3 wt % hydrogen atoms. It is characterized by a crystallinity degree ranging from 50 to 70%, glass and melting temperatures in the range of −40 to −30°C and 155−190°C, respectively, and a Curie temperature between 195−197°C. PVDF was first polymerized in the 1940s but its ferroelectric nature was discovered in the late 1970s when D. Naegele and D. Y. Yoon observed the orientation of molecular dipoles as well as ferroelectric behaviour using infrared spectroscopy [63]. Two IR absorptions at 512 and 446 cm^{-1} were associated with transition moments along and perpendicular to the $C\text{-}F_2$ dipole. R.G. Kepler and R. A. Anderson found that the axes of crystalline regions of PVDF oriented themselves on the application of an external electric field, based on the X-ray diffraction (XRD) of the sample before and after field application [64].

Nowadays, it is known that the electroactive properties of PVDF and its copolymers are strictly related to crystal polymorphism. In fact, as a consequence of different processing conditions, this polymer can be obtained in the form of five distinct crystalline phases, which differ from each other in terms of molecular conformation and packing: α, β, γ, δ and ε [33]. Among the phases, α and ε are non-polar, because of the antiparallel packing of the C-F dipoles (TGTG' and T_3GT_3G', respectively). On the contrary, the other three polymorphs are characterized by a neat dipole moment, whose value is particularly high for the β phase (TTT conformation and dipolar moment per unit cell 8×10^{-30} C m), and show useful electroactive properties, exploitable for capacitors, sensors, actuators, etc. [65]. A representation of the three principal PVDF crystalline forms is reported in Figure 2.15.

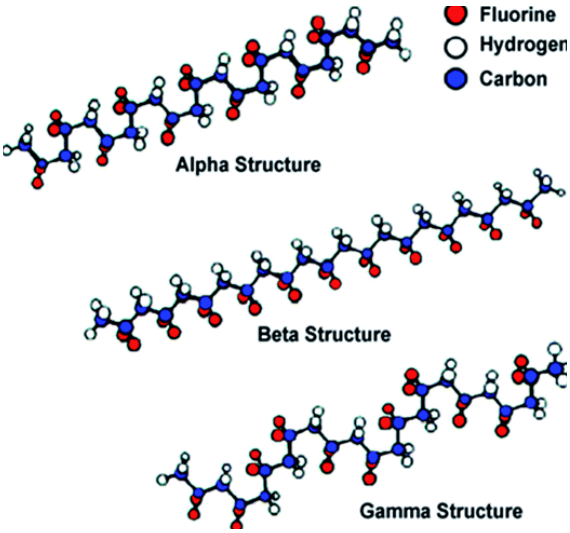

Figure 2.15: Scheme of the chain conformation for α, β and γ crystalline phases of PVDF [66].

Not only the polymorphism, but also the direction of *c*-axes (that is of PVDF macromolecule backbones) with respect to the applied electric field affect the dielectric properties. Relatively higher dielectric constant can be obtained for the dipoles that are arranged in the parallel direction to the field, as the orientation of the dipoles will be easier in the presence of an applied voltage. In contrast, if the dipoles are arranged in the perpendicular direction to the field, the orientation of the dipoles would be restricted, resulting in relatively lower dielectric constant [4].

In addition, the size of the crystalline domains in PVDF has an effect on its polarization. Smaller domains are more flexible and can respond more quickly to the change in electric field than larger domains, leading to lower dielectric losses and higher energy density of the material. Therefore, the degree of crystallinity, the relative content of various crystal phases, polymer chain orientation and size of domains all affect the dielectric response of PVDF [2].

Beside PVDF homopolymer, also its copolymers are widely used for energy-related applications. PVDF copolymers have been indeed developed with the aim of improving the properties of the homopolymer and adapting to the increasing technological demands (Figure 2.16).

Poly(vinylidene fluoride-*co*-trifluoroethylene), PVDF-TrFE, is one of the most studied copolymers. Contrary to its homopolimeric parent, if the VDF unit content is between 50 and 80%, this copolymer crystallizes as β phase independently of the adopted processing method. This is due to the large presence (20÷50%) of TrFE comonomer units which induce a large steric hindrance, favoring the all-*trans* conformation. This copolymer possesses a dielectric constant (≈ 18) higher than that of PVDF homopolymer (9-12) and its Curie temperature is below the melting temperature, allowing the study of ferroelectric (FE) to paraelectric (PE) phase transition. However, PVDF-TrFE is characterized by relatively higher remnant polarization (7.5 μC/cm^2) than that of PVDF, this resulting in lower energy density.

The introduction of chloride trifluoride ethylene (CTFE) units along the PVDF polymer chain, results in the formation of poly(vinylidene fluoride-*co*-chlorotrifluoroethylene) PVDF-CTFE copolymer. The content of CTFE determines different properties: if the amount of such comonomer

is small (lower than 16 mol%) the ensuing copolymer is semi-crystalline, while it becomes completely amorphous for higher CTFE concentrations; as a consequence, also the glass transition changes, varying between -40 and 45°C. The dielectric constant of this copolymer (≈ 13) is slightly higher than that of PVDF homopolymer while its piezoelectric properties are markedly superior (d_{33} can reach 140 pC/N). However, the presence of chlorine atoms makes P(VDF-CTFE) less suitable in a general contest of environmental sustainability.

PVDF-HFP is obtained by introducing hexafluoropropylene (HFP) co-units along the PVDF macromolecular chains. Also in this case, different contents of HFP in PVDF-HFP lead to a variety of attractive properties. Low HFP contents (about 5-15 mol %) corresponds to a flexible but still semi-crystalline copolymer, having a crystallinity degree comparatively lower than that of PVDF due to the presence of the bulky CF_3 groups, while comonomer amounts higher than 20 mol% make PVDF-HFP copolymer amorphous. The electroactive properties of this copolymer are adjustable by changing the processing conditions: solvent-cast and quenched samples present the typical ferroelectric behaviour which is absent in the case of slowly cooled films. PVDF-HFP has comparatively higher energy density (11−13.5 J/cm^3 at ~6000 kV/cm) than PVDF and PVDF-TrFE and its piezoelectric coefficient d_{31} (30 pC/N) makes it a promising material in some piezo and ferroelectric application areas, such as the development of magnetoelectric sensors and actuators.

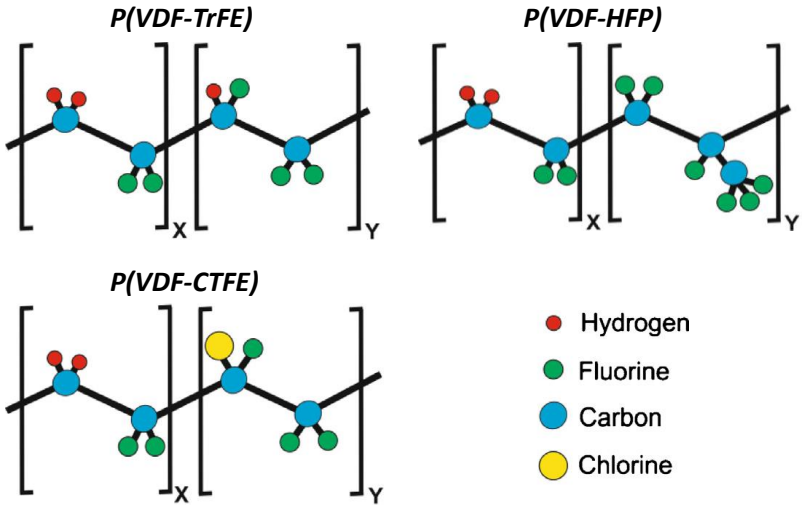

Figure 2.16: Schematic representation of the three principal copolymers of PVDF. Modified from [33].

2.5 Perovskite ceramic fillers

Perovskites are a family of inorganic materials of considerable technological importance due to their physical and electrical characteristics, such as dielectric and superconducting properties, pyro and piezoelectricity, and linear and non-linear electro-optical effects.

The perovskite structure, characterized by the cubic space group *Pm3m*, is one of the most extensively studied structures in materials science and can be schematized by the general formula ABX_3 (X = O, F) where A is a large radius metal cation, coordinated with 12 X anions, and B is a smaller radius metal cation, coordinated with 6 X anions Figure 2.17.

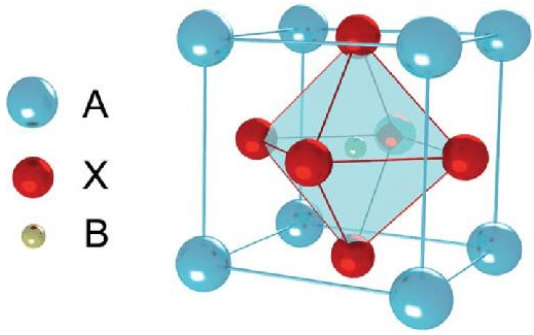

Figure 2.17: Schematic representation of the ABX_3 perovskite structure [67].

Since ABF_3 materials, in general, exhibit relatively high dielectric loss factors, we only consider ABO_3 type materials, which are also the most widely used. The atomic arrangement for ABO_3 perovskite structure was first found for the mineral $CaTiO_3$, which was discovered in 1839 by G. Rose. However, one of the principal researchers involved in this topic was V. M. Goldschmidt, who studied and synthesized a large number of perovskites and introduced the concept of the "tolerance factor", which dictated the limits of the radius of the A and B atoms leading to a stable perovskite structure [68].

Despite sharing the same ideal structure, many properties of the perovskites vary markedly from one compound to another, making them more suitable for one or another application (Table 2.2).

Table 2.2: List of properties and applications of the principal perovskite compounds.

Reference compound	**Properties**	**Existing and potential applications**	**Ref.**
$BaTiO_3$	Ferroelectricity, piezoelectricity, high dielectric constant	Multilayer ceramic capacitors (MLCCs), PTCR resistors, embedded capacitance	[2] [69]
$(Ba,Sr)TiO_3$	Non-linear dielectric properties	Tunable microwave devices	[70]
$Pb(Zr,Ti)O_3$	Ferroelectricity, piezoelectricity	Piezoelectric transducers and actuators, ferroelectric memories (FERAMs)	[71][72]
$Bi_4Ti_3O_{12}$	Ferroelectric with high Curie temperature	High-temperature actuators, FeRAMs	[73][74]

$(K_{0.5}Na_{0.5})NbO_3$, $Na_{0.5}Bi_{0.5}TiO_3$	Ferroelectricity, piezoelectricity	Lead-free piezoceramics	[75]
$(Pb,La)(Ti,Zr)O_3$	Transparent ferroelectric	Optoelectronic devices	[76]
$BiFeO_3$	Multiferoic, magnetoelectric coupling, high Curie temperature	Magnetic field detectors, 4-state memories	[77]
$PbMg_{1/3}Nb_{2/3}O_3$	Relaxor ferroelectric	Capacitors, actuators, transducers (medical imaging)	[78][79]
$SrRuO_3$	Ferromagnetism	Electrode material for epitaxial ferroelectric thin films	[80]
$(La, A)MnO_3$ A = Ca, Sr, Ba	Ferromagnetism, giant magnetoresistance, spin-polarized electrons	Magnetic field sensors, spin electronic devices	[81]
$SrTiO_3$	Incipient ferroelectricity, thermoelectric power, metallic electronic conduction when n-doped, mixed conduction when p-doped, photocatalyst	Alternative gate dielectric material, barrier layer capacitors, substrate for epitaxial growth, photoassisted water splitting	[82][83]
$LaGaO_3$ $BaIn_2O_5$	Oxyde-ion conduction	Electrolyte in solid oxide fuel cells (SOFCs)	[84]
$BaCeO_3$ $BaZrO_3$	Proton conduction	Electrolyte in protonic solid oxide fuel cells (P-SOFCs)	[85]
$(La,Sr)BO_3$ (B = Mn, Fe, Co)	Mixed conduction, catalyst	Cathode material in SOFCs, oxygen separation membranes, membrane reactors, controlled oxidation of hydrocarbons	[62][86][87]
$CH_3NH_3PbX_3$ (X = Cl, Br, I)	Appropriate band gab, high light absorption efficiency	Photovoltaic cells	[88][89]

For more convenience, the following description is restricted to three compounds only: $BaTiO_3$, $Pb(Zr,Ti)O_3$ and $Na_{0.5}Bi_{0.5}TiO_3$ - $BaTiO_3$ which are the principal perovskites used in this work.

Barium Titanate. Barium titanate (BT in the following), which was first studied in the 1950s, is perhaps the most widely investigated oxide in the field of dielectrics, having a dielectric permittivity in the order of 1000. Its impressive dielectric properties arise from a structural change for which the center Ba^{2+} and Ti^{4+} cations are displaced relatively to the O^{2-} ions, leading to the formation of electric dipoles.

BT is indeed characterized by five crystal forms which are stable at different temperatures: namely, a trigonal phase (below -90°C), an orthogonal structure (between -90°C and 5°C), a tetragonal structure (in the range 5÷120°C) and a cubic (above 120°C) phase (Figure 2.18).

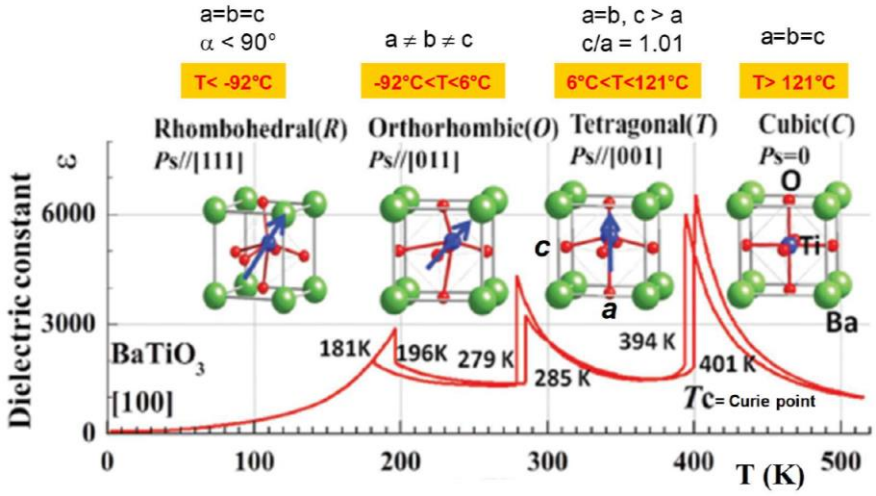

Figure 2.18: Scheme of the structural evolution of barium titanate as a function of temperature [90].

The Curie temperature, at which BT undergoes a paraelectric to ferroelectric phase transition, is around 120°C; however, this as well as the other transition temperatures can be affected by the exact chemical composition and grain size. For example, increasing Sr^{2+} substitutions on the A-site has been found to reduce the Curie point linearly to room temperature, while the introduction of Pb^{2+} in place of Ba^{2+} raises the Curie point [6]. In addition, the Curie temperature slightly increases by increasing the grain size while an opposite trend was found for the other transition temperatures [91,92].

Other BT properties can be tuned by doping it or modifying its microstructure. As an example, cobalt-doped $BaTiO_3$ shows a greater resistance than other piezoceramics to depoling by compressive stresses [93], while it is known that BT dielectric permittivity changes with a non-monotonous way by increasing the grain size [94] and a similar trend was also found for the piezoelectric coefficient [91].

Lead zirconate titanate. Another interesting ceramics characterized by a perovskite structure and used for energy-related applications is lead zirconate titanate $PbZrO_3$*$PbTiO_3$, commercially called PZT, which is a solid solution of orthorhombic $PbZrO_3$ and tetragonal $PbTiO_3$ [95]. Different percentages of the two compounds determine different crystalline structures and, in particular, compositions near the morphotropic phase boundary (*i.e*, between tetragonal and rhombohedral phase, $PbZrO_3$:$PbTiO_3$ = 43:47) lead to high values of electromechanical coupling coefficients and electrical permittivity (Figure 2.19).

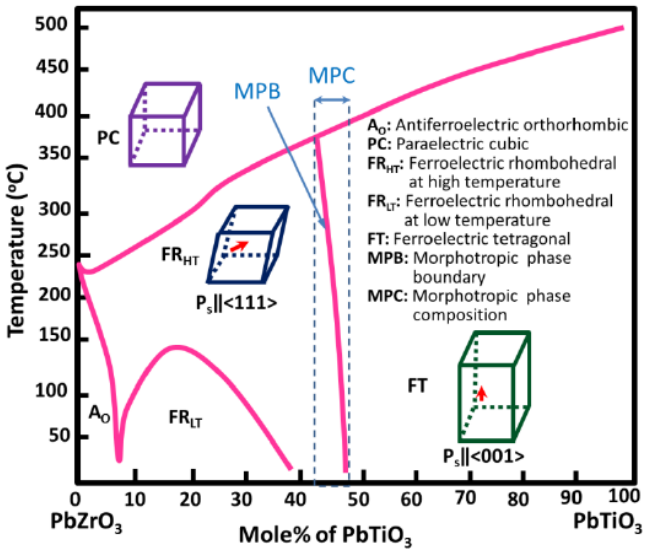

Figure 2.19: Phase diagram for PZT ceramics, with relevant regions labeled [95].

Also in this case, by controlling chemistry and processing, PZT properties can be optimized for specific applications. Two classes of PZTs are available on the market, called soft and hard PZTs, where the terms "soft" and "hard" refer to the mobility of the dipoles or domains, as well as to the polarization and depolarization behaviour. Soft PZT is obtained by adding donor dopants, which cause cation vacancies in the crystal structure, enhancing the domain reorientation. Soft PZTs have large piezoelectric coefficients, large permittivity, high electrical losses, large electromechanical coupling factors, very high electrical resistance, low mechanical factors. These characteristics make them interesting for actuators (micro- and nano-positioning), sensors such as conventional vibration pickups, electro-acoustic applications as sound transducers and microphones [96].

Hard PZTs derive from doping with acceptor atoms, that cause oxygen vacancies and pin the domain walls; this leads to low piezoelectric coefficients, low permittivity, low losses, low electrical resistivity and high mechanical factors. These piezo elements are used for example for ultrasonic cleaning, in biomedical fields and sonar technologies.

An interesting study based on different mixing of these two PZT types was carried out by N. Horchidan [96].

Bismuth Sodium Barium Titanate. Despite the interesting properties of PZT ceramics, it is important to remind that lead oxide is highly toxic and its toxicity is further enhanced due to its volatilization at high temperature, particularly during calcination and sintering. Thus, keeping in mind environmental sustainability, serious attempts are being made to develop lead-free ferroelectric, piezoelectric and related materials having potential characteristics for piezo-devices.

Lead-free piezo materials can be grouped into three categories [75]: *(i)* perovskites, *(ii)* non-perovskite bismuth layer structured ferroelectrics (BLSF), and *(iii)* non-perovskite tungsten bronze type ferroelectrics. The perovskite compounds include $BaTiO_3$ (BT), $BiNaTiO_3$ (BNT), $BiKTiO_3$ (BKT), $KNaNbO_3$ (KNN); these, despite the presence of alkali metals which leads to some

drawbacks (*i.e.*, narrow sintering temperature range, high corrosivity, high volatility), are the most studied because of their superior piezoelectric properties.

In particular, the discovery of an extraordinarily large strain generated by the field-induced phase transition in Bismuth-Sodium-Titanate based solid solutions draw the attention of researchers to this material system, which seems to be a valid alternative to PZT for actuator applications. BNT was first reported by G.A. Smolenskii and A.I. Agranovskaya in 1960 [97], however, to date, its complex perovskite-based crystal structure is still under debate [98]. By combining electron, X-ray and neutron diffractions with dielectric, ferroelectric and piezoelectric measurements, the coexistence of a rhombohedral and a monoclinic phase, the latter associated to local structural and strain heterogeneities, has been supposed at room temperature. In addition, the similar charge and size of the cations imply long-range ordering is unlikely.

As concerns higher temperatures, it is generally believed that BNT exhibits at least two different phase transitions during cooling: from cubic to tetragonal at about 520°C and from tetragonal to rhombohedral at about 250°C. However, BNT has a peculiar ferroelectric behaviour which does not seem to completely reflect its structural changes. In fact the high leakage currents prevent the measure of loss peak around 500°C, and the permittivity shows just a broad maximum at 320°C (paraelectric-antiferroelectric transition) and a small hump at 200°C (antiferroelectric-ferroelectric transition).

To induce the formation of a morphotropic phase boundary (MPB) and thus enhance the electric and piezoelectric properties of BNT, different solid solutions with other ferroelectric materials including $BiFeO_2$, $CaTiO_3$, $Bi_{1/2}K_{1/2}TiO_3$, $K_{1/2}Na_{1/2}NbO_3$ and $BaTiO_3$ have been studied.

To the purpose of this work, the solid solution of BNT and BT is of particular interest. The phase diagram of the binary system BNT-BT (often called BNBT) is shown in Figure 2.20 where the existence of a rhombohedral-tetragonal MPB around 6-8 mol% of $BaTiO_3$ is clearly visible.

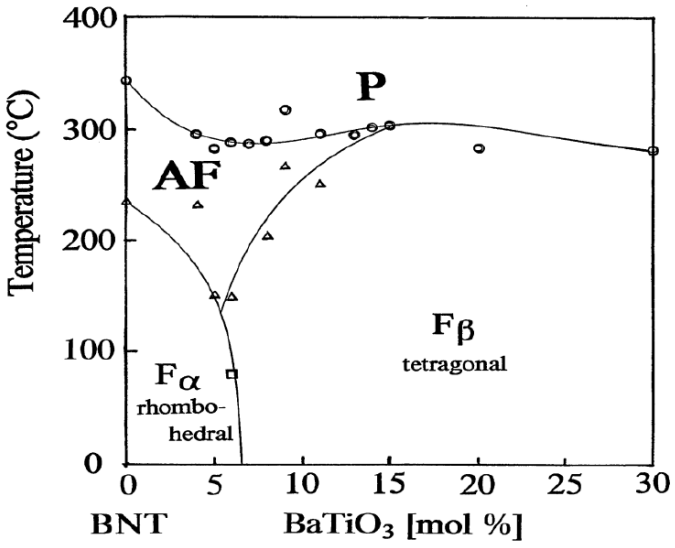

Figure 2.20: Phase diagram of BNT-based solution with BT, for poled ceramics [99].

3 MATERIALS AND METHODS

3.1 Polymer matrices

Poly(vinylidene fluoride) (PVDF) was chosen as the principal polymer matrix. In particular, PVDF pellets of Solef 1008 grade ($\overline{M}_w$ = 244000 g/mol, $\overline{M}_n$ = 114000 g/mol, T_m = 170-175°C**)** purchased from Solvay were employed for the preparation of neat polymer or composites films from melt blending, solvent casting and/or compression molding. Another grade, in the form of powders, purchased from Alfa Aesar (T_m = 155-160°C) was used to obtain films directly from hot-pressing.

Also a PVDF copolymer was investigated in this research: namely, a poly(vinylidene fluoride-*co*-hexafluoropropylene) (PVDF-HFP) ($\overline{M}_w$ = 455000 g/mol, $\overline{M}_n$ = 110000 g/mol,) purchased from Sigma Aldrich, and used neat or for composites preparation.

3.2 Filler particles

For the composites preparation, different ceramic fillers were used.

3.2.1 PZT

Both commercial and synthesized lead zirconate titanate (PZT) powders were used for the preparation of the composites.

The commercial PZT [$Pb_{1.22}(Zr_{0.52}2Ti_{0.48})O_{3.22}$] particles with diameter ranging from 0.5 to 5 μm were purchased by Reade Advanced Materials.

The synthesized particles were prepared by ISTEC-CNR group. PZTN (*i.e.*, PZT doped with Nb) ceramics was synthesized starting from PbO (Sigma-Aldrich, Inc. Darmstadt, Germany), ZrO_2 (SC 101, Mel Chemicals, Flemington, NJ, USA), TiO_2 (P 25, Evonik Degussa, Essen, Germany), Nb_2O_5 (Sigma-Aldrich, Inc. Darmstadt, Germany). A sequence of ball milling for 48 h, calcination at 850°C for 4 h and further ball milling for 96 h in ethanol was followed, leading to a partial conversion into the perovskite phase [100]. Then, suitable thermal treatments were carried out in order to obtain powders fully reacted to the perovskite phase.

In particular, the different types of powders used with the relative specifications are listed below:

- PZT1: particles thermally treated at 930°C for 2 h (average size ≈ 200 nm);
- PZT2: particles thermally treated at 1200°C for 30 min (average size ≈ 700 nm);
- PZT3: particles thermally treated at 1100°C for 30 min (average size ≈ 400 nm);
- PZT4: particles sintered under pressure at 1200°C for 30 min and then crushed (average particles size ≈ 1μm, average sintered aggregate dimension ≈ 5 μm).

3.2.2 Barium titanate

As ceramic inclusions barium titanate, $BaTiO_3$ (BT), particles were used as such or differently coated.

Neat BT nanoparticles were synthesized by the CNR-ICMATE group, using two different procedures: *(i)* one based on a well-consolidated hydrothermal-like synthesis [101] starting from $BaCl_2 \cdot H_2O$ (Aldrich, 99.9%) and $TiCl_4$ (Aldrich, 99.9%) precursors and *(ii)* another exploiting a solid-state reaction [102,103] between TiO_2 (Toho Titanium, Chigasaki, Japan, HT305117, SBET = 2.76 m^2/g, dBET = 511.95 nm) and $BaCO_3$ (Solvay Bario e Derivati, BCL500F, SBET = 3.27 m^2/g, dBET = 423.83 nm).

The hydrothermal-like method was used for the preparation of particles with small and intermediate dimensions (average diameter of ≈ 60 and 120-130 nm, respectively). This synthesis, occurring under continuous agitation in a batch reactor, is realized in two steps: at first, the addition of a concentrated NaOH aqueous solution to another solution containing the precursors induces the hydrolysis leading to a jelly-like suspension of amorphous TiO_2; subsequent heating at 90°C induces the crystallization of $BaTiO_3$ leading to the formation of ceramic particles whose dimensions depend on the concentration of the initial solution containing the metal chlorides.

The solid-state method was instead employed to prepare bigger particles (average diameter of ≈ 750 nm). In this case, TiO_2 and $BaCO_3$ precursors in stoichiometric amounts were first mixed in water by ball milling, adding a solution of an ammonium salt of polyacrylic acid (Acros Chimica, Milano, Italia, MW 2000) as a dispersant. After mixing, the obtained suspension was dried at 80°C in a vented oven and subsequently sieved. A thermal treatment at 1100°C for 4 h led to the formation of monophasic $BaTiO_3$. A grinding in water for 4 h, followed by drying and sieving was finally carried out to improve the particles dispersion.

3.2.3 Core-shell particles

Coating of the BT particles with binary oxides was realized by the CNR-ICMATE group. Except where indicated otherwise, chemicals were purchased from Sigma-Aldrich and used as received.

As concerns titania coated particles, a method previously optimized for other ceramic powders [104–106] was properly modified to coat $BaTiO_3$ and tune the shell thickness.

The method consists in preparing a dispersion of BT particles in an ammonia solution (pH = 9) containing the $TiCl_4$ (0.1 M) and then inducing the hydrolysis of the titanium (IV) peroxo complex by heating at 90°C for 4 h. The obtained titania coated particles ($BaTiO_3@TiO_2$) are named BxTy in the following, where B = $BaTiO_3$, x = diameter of the core (in nm), T = TiO_2 and y = shell thickness (in nm).

As concerns silica coated particles ($BT@SiO_2$) a Strober-like procedure was employed [107]. Before the reaction, the particles were pre-treated in two acid solutions and then in a basic one. In particular, 0.5 g of $BaTiO_3$ were dispersed by ultrasonication in 10 mL of a nitric acid solution 1M

and then washed with distilled water; subsequently, the powders were dispersed by ultrasonication in a citric acid solution 0.01 M and again washed with distilled water.

Afterward, 200 µL of an NH_3 solution was added to a particles dispersion in distilled water. The obtained solution was poured in a mixture of H_2O/EtOH/NH_3 (75/23.5/1.5 Vol%) and reacted with a proper amount of tetraethyl orthosilicate (TEOS) solution (0.1 M in EtOH), added by dripping with a Hamilton pump (rate 1 mL/10 min). Since 1 mL of solution would theoretically lead to a shell growing of about 0.8 nm, by increasing the reaction time, it is possible to increase the final shell thickness.

The obtained silica coated particles are named BxSiy in the following, were B = $BaTiO_3$, x = diameter of the core (in nm), Si = SiO_2 and y = shell thickness (in nm).

In both cases, the obtained coated particles were separated by double centrifugation of the suspension, then freeze-dried and sieved in order to recover the corresponding powders for the subsequent characterization and composites preparation.

3.2.4 BNBT

The bismuth sodium barium titanate 0.94[($Bi_{0.5}Na_{0.5}$)TiO_3]-0.06$BaTiO_3$ (BNBT in the following) particles used in this work were synthetized by CNR-ISTEC group through solid state route. In particular, two different types of particles were employed: calcined powders, indicated as smaller particles (BNBTs) and sintered and crushed powders, indicated as coarser particles (BNBTc).

To prepare the smaller particles (average size ≈ 100-120 nm), stoichiometric amounts of $BaCO_3$ (99.0%, Merck), TiO_2 (99.9%, Degussa), Na_2CO_3 (99.5%, Merck), Bi_2O_3 (99.9%, Aldrich) were ball milled in ethanol for 48 h. The dried precursors mixture was then sieved at 250 µm and calcined at 800°C for 1 h. The calcined powder was finally ball milled in ethanol for 120 h, dried and sieved at 250 µm.

The coarser particles (average size ≈ 2-3 µm) were obtained with a further treatment on the previous powders, by uniaxially pressing them at 300 kg/cm^2, sintering the resulting pellets at 1150°C for 30 min and crushing them into powder. The last was sieved at 40 µm and finally annealed at 700°C.

3.3 Particles functionalization

Different strategies of particles functionalization were tested and the most promising one was that properly adapted from a procedure used for the modification of silica [108]. This consists in preparing by ultrasonication a dispersion of particles and silane in CH_2Cl_2 using a minimum volume but sufficient to allow silane absorption on the particle surface (*i.e.* 5 mL for 0.5 g of powder); after the evaporation of CH_2Cl_2, the silane condensation is induced by a thermal treatment carried out at 110°C for 1 h. Then, the particles are rinsed with acetone to eliminate the unreacted silane and finally dried.

3.4 Composites preparation

In the literature, only a few examples of dielectric (nano)composites produced through technologies involving the PVDF melting are reported [39,48,109,110]. More frequently, the fillers are added to the fluorinated polymer matrix previously dissolved in large amounts of solvent (dimethylacetamide -DMA- or dimethylformamide -DMF-) and a thin film of nanocomposite is then obtained by solvent casting or spin coating [36,111–115]. Technologies that involve the use of solvents are preferred because they usually lead to a finer dispersion of the filler within the polymer matrix and, at a laboratory scale, appear appropriate when the amounts of available materials (*i.e.*, the polymer matrix and/or the inorganic filler) are limited. However, in a general approach to environmental sustainability, technologies which do not foresee the use of solvents and can be easily scaled-up (for instance melt blending or extrusion) are instead desirable. In this thesis work, the composites preparation was carried out by using three technologies: solvent casting, melt blending and hot pressing. In the first two cases, the obtained composites materials were subsequently compression moulded by using a semi-automatic press P200E (Collin GmbH) in order to prepare the final films suitable for the succesive characterization. Two principal methods of compression moulding were employed: *(i)* a single-step moulding (SS in the following), according to which the final film is directly obtained by moulding the composite material (obtained by solvent casting or melt blending) at a temperature higher than the melting temperature of the polymer matrix; *(ii)* a double-step moulding (DS in the following) which consists in preparing a thicker plate under the SS conditions and then re-pressing it at high pressure and a temperature lower than the melting temperature of the procedures used is reported in Figure 3.1.

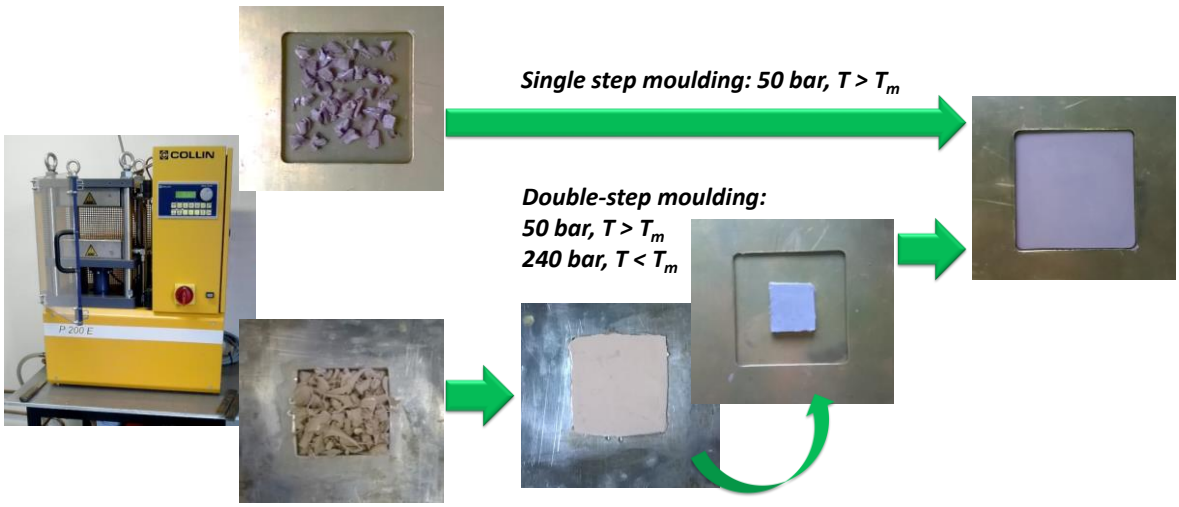

Figure 3.1: Scheme of the two principal procedures used for the compression moulding.

The compression moulding was also employed to directly prepare films of neat polymer. The specific moulding conditions used in the different cases are detailed in the *Results and Discussion* section.

3.4.1 Composites from solvent casting

The solvent casting procedure was optimized in order to obtain a good particle dispersion. Different tests were carried out by varying: the solvent used to dissolve PVDF, concentration of the PVDF solution, procedure used to add the ceramic particles to the polymer solution, method to disperse particles and drying conditions (time, temperature, pressure) of the resultant solvent-cast composite films. The procedure leading to the most suitable morphology was selected and then used for the preparation of all the composites from solvent casting described in this work.

This procedure consists in preparing a powder dispersion in dimethylacetamide (DMA) by ball milling with YSZ media overnight. The dispersion was then added to a solution of PVDF in DMA (20% wt/vol) and the resultant mixture was stirred at 90°C until most of the solvent was evaporated. Finally, it was poured on a glass substrate, dried on a vacuum oven and then on a vented oven (complete DMA removal was verified by infrared spectroscopy). A scheme of the procedure used is reported in Figure 3.2.

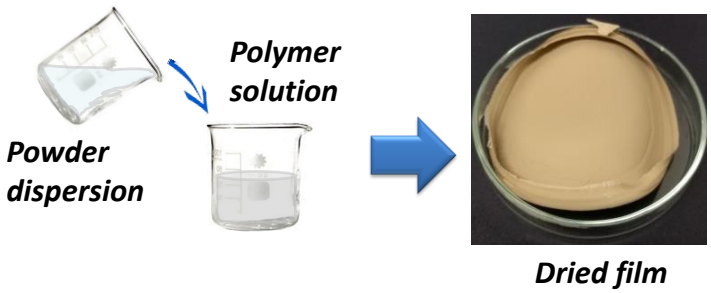

Figure 3.2: Scheme of the solvent casting procedure employed for the preparation of the composites.

3.4.2 Composites from melt blending

The composites from melt blending were prepared by adding to the pre-melted polymer pellet the proper amount of ceramic particles and mixing them with an internal batch mixer W50 EHT Plasti Corder (Brabender).

The melt blending conditions were properly adjusted on PVDF/$BaTiO_3$ composites containing commercial particles, the most suitable ones being identified as 200°C, 60 rpm, 30 min. These conditions were employed for all the composites prepared in this work.

3.4.3 Composites from hot-pressing

For the preparation of composites from hot-pressing, proper amounts of PVDF powder and ceramic particles were dispersed in about 5 mL of isopropanol through 15 min of sonication. The resultant dispersion was then dried in a venting oven at 60°C and finally hot-pressed between two sheets of Kapton. During the hot-pressing the mixture of powders was heated from room temperature to 160°C without applying any pressure; then heated to 190°C under 5 MPa of pressure maintaining the final temperature for 10 min; finally, the sample was naturally cooled by releasing the pressure when the temperature reached 160°C. A scheme of the procedure used is reported in Figure 3.3.

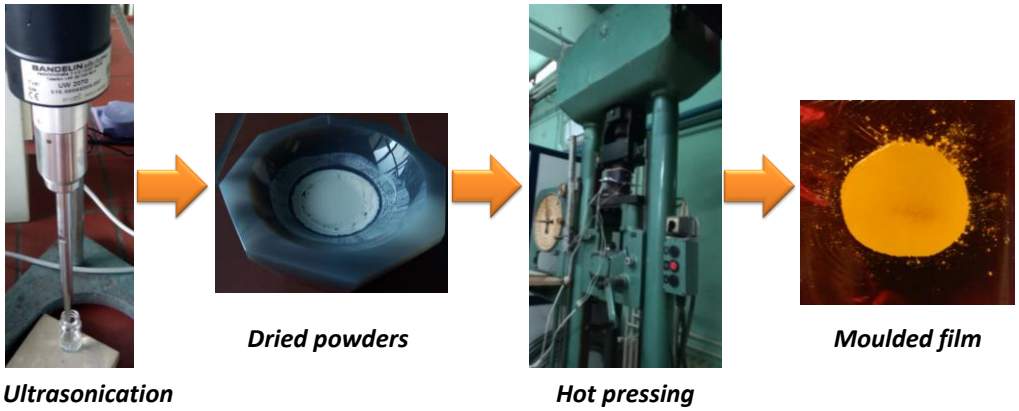

Figure 3.3: Scheme of the procedure used to prepare composites from hot-pressing.

3.5 Materials Characterization

The prepared composites materials, as well as the ceramic particles and the polymer matrices used as components, were thoroughly characterized by means of several techniques.

Fourier transformed infrared (FTIR) spectroscopy was employed to investigate the polymorphism of the PVDF matrix. The neat polymer matrices and composites were characterized by using a PerkinElmer Spectrum Two™ FTIR spectrometer, operating in the attenuated total reflectance (ATR) mode. At least six measurements for each sample were carried out by recording the spectra in the 4000-400 cm^{-1} wavenumber range. The relative fraction of the electroactive phase(s) (F_{EA}) was determined on normalized spectra by applying Equation 3.1, as suggested by X. Cai *et al.* and other authors [116]:

$$F_{EA} = \frac{I_{EA}}{\left(\frac{K_{840^*}}{K_{763}}\right) \cdot I_{763} + I_{EA}} \tag{3.1}$$

where I_{EA} is the absorbance of the band at about 840 cm^{-1} that can be assigned to β and/or γ phase, I_{763} is the absorbance of a characteristic band of the α phase, and K_{840^*} and K_{763} are the absorption

coefficients whose values, at the respective wavenumbers, are 7.7 x 10^4 and 6.1 x 10^4 cm^2/mol. The F_{EA} value expresses the amount of electroactive polymorphs with respect to the total crystalline phase(s) present in a given sample; in order to distinguish the contribution of β (F_β) and γ (F_γ) phase, when they are present simultaneously, the peak-to-valley height ratio between the two peaks around 1275 and 1234 cm^{-1} was considered.
As for the composites, the ATR-FTIR spectrum corresponding to neat filler was subtracted from the spectra of the composite material.

Films of composite materials as well as of neat PVDF were subjected to differential scanning calorimetry (DSC) in order to establish the crystallinity degree (X_C). Two or three repeats for each sample (10-15 mg) were performed with a Mettler DSC 821^e instrument, by heating from 0 up to 220°C at a scan rate of 10°C/min in air or under N_2 atmosphere. The value of X_C was calculated as the ratio between ΔH_m and ΔH_0, where ΔH_m is the measured enthalpy value, normalized with respect to the actual content of PVDF in the composite samples, and ΔH_0 is the enthalpy of fusion of a perfect PVDF crystal (ΔH_0 = 104.6 J/g) [117,118]

X-ray diffraction analysis was carried out on the neat PVDF films in order to validate the spectroscopic and calorimetric results. Wide angle X-ray diffraction (WAXD) patterns were obtained at room temperature with a Siemens D-500 diffractometer equipped with a Siemens FK 60-10 2000 W tube (Cu K_α radiation, λ = 0.154 nm), operating at 40 kV and 40 mA, and collecting data from 5 to 35° 2θ at 0.02° 2θ intervals. The degree of crystallinity (X_{cW}) and the amount of β phase ($X_{\beta,A}$ or $X_{\beta,I}$) were estimated, also by this technique using the following Equations:

$$X_{cW} = \frac{A_c}{A_c + A_a} \tag{3.2}$$

$$X_{\beta,A} = \frac{A_\beta}{A_c} \tag{3.3a}$$

$$X_{\beta,I} = \frac{I_\beta}{I_c} \tag{3.3b}$$

where *A* indicates the peak area related to the overall crystalline phases (A_c, in this case α+β as specified in the *Results and Discussion* section), or the amorphous phase (A_a) or the β phase (A_β, in particular, the peak at 20.8° 2θ), respectively; whereas *I* refers to the corresponding peak intensities [34]. All the calculations were made after proper deconvolution of the WAXD patterns.

Thermogravimetric analysis (TGA) measurements, two or three repeats for each sample, were performed with a PerkinElmer TGA7 analyzer. This technique was principally used to characterize the pristine ceramic particles and to estimate the amount of coupling agent grafted onto their

surface as a consequence of the functionalization. After 5 min at 50°C the specimens (10-15 mg) were heated from 50 to 700°C at 20°C/min in N_2 atmosphere and then from 700°C to 850°C at 20°C/min in O_2 atmosphere.

As for the morphological characterization, scanning electron microscopy (SEM) was used to investigate composites microstructure. Basically, a Hitachi TM3000 benchtop SEM microscope, implemented by a probe for energy dispersive X-ray analysis (EDX), was used; while, for higher magnification images, a LEO 1450VP (LEO Electron Microscopy Ltd) SEM microscope was employed. Specimens were cryo-fractured in liquid nitrogen in order to induce a fragile fracture; the obtained transversal surfaces were gold or silver sputtered prior observation.
Morphological analysis of particles and nanoparticles was carried out by SEM observations at high magnification and/or by transmission electron spectroscopy (TEM). For the acquisition of the TEM micrographs, some drops of (nano)particles dispersion in acetone were dropped onto a carbon-coated TEM grid after 5 min ultrasonication and soon after the samples were analyzed by using a Zeiss EM 900 TEM microscope operating at 80 kV.
Besides, a Leica DMR polarized optical microscope (POM) was used to observe polymer orientations possibly present in the moulded polymer films.

The mechanical performance of neat polymer and composites samples was tested with a strain-controlled rotational rheometer MCR301 (Anton Paar), operating in the torsion mode.
The dynamic-mechanical analysis (DMA) is an effective method to study the viscoelastic behaviour typical of the polymeric materials, by measuring the response of a sample subjected to a mechanical stimulus as a function of frequency or temperature.
When a material is subjected to a dynamic load it manifests a phase lag in the deformation. Considering the dynamic force to be oscillating and sinusoidal, the corresponding stress (σ) and strain (γ) can be written as:

$$\gamma = \gamma_0 sen(\omega t) \tag{3.4}$$

$$\sigma = \sigma_0 sen(\omega t + \varphi) \tag{3.5}$$

where γ_0 and σ_0 are the maximum strain and stress, respectively, and φ is the phase lag, whose value is: *(i)* null for an elastic material (*i.e.*, stress and strain are directly proportional); *(ii)* equal to $\pi/2$ for a pure viscous material (*i.e.*, the stress is proportional to the shear rate); *(iii)* between 0 and $\pi/2$ for a viscoelastic material. In this case, the elastic (instantaneous) and viscous (delayed) responses can be distinguished by expressing the Equation 3.5 as:

$$\sigma = \sigma_0 cos\varphi sen(\omega t) + \sigma_0 sen\varphi \cos(\omega t) \tag{3.6}$$

and dividing by the maximum strain:

$$\frac{\sigma(t)}{\gamma_0} = \frac{\sigma_0 cos\varphi sen(\omega t)}{\gamma_0} + \frac{\sigma_0 sen\varphi \cos(\omega t)}{\gamma_0} = G' sen\,(\omega t) + G'' \cos(\omega t) \qquad (3.7)$$

Thus, the storage or elastic (*G'*) and loss or dissipative (*G''*) moduli are obtained, which are related to the stored energy and to the energy lost through dissipation as frictional heat, respectively. The ratio between the dissipative and the elastic component is named loss tangent ($tan\delta_G = G''/G'$).
Amplitude sweep tests were carried out at 1 Hz and 25°C in the strain range 0.001/1% on rectangular specimens (thickness 0.5-0.8 mm, width 10 mm, length 50 mm) to determine the range of linear viscoelasticity (LVE). Temperature sweep tests were then performed on at least two specimens for each film between −100 and 140°C (3°C/min scan rate) by fixing the frequency at 1 Hz and the amplitude deformation at 0.005% (in the LVE range). Elastic and dissipative components of the modulus as well as the loss tangent values were determined.

The obtained films were also thoroughly characterized by the dielectric point of view. The surfaces of the films were prior sputtered with Au, Au/Pd or Ag in order to obtain electrodes with a diameter of 22.6 mm suitable for the subsequent characterization. All the samples were subjected to frequency sweep measurements: real (*ε'*) and imaginary (*ε''*) part of relative permittivity and the related loss tangent (*tanδ*) were measured at room temperature at different frequencies (from 1 Hz to 0.1 or 1 MHz) in parallel-plate capacitor geometry by using a frequency response analyzer (Solartron, SI1260) equipped with a Novocontrol BDC dielectric interface. At least two measurements for each sample were carried out.
For some films the dielectric properties were studied more in depth with measurements acquired as a function of temperature and carried out by using an impedance bridge Agilent E4980A at frequencies of 0.1 kHz - 1.5 MHz in the 25-150°C temperature range. The real (M') and imaginary (M") part of the dielectric modulus were calculated, by following Equations 3.8 and 3.9:

$$M' = \frac{\varepsilon'}{\varepsilon'^2 + \varepsilon"^2} \qquad (3.8)$$

$$M" = \frac{\varepsilon"}{\varepsilon'^2 + \varepsilon"^2} \qquad (3.9)$$

Selected samples were also subjected to ferroelectric characterization, by using a Precision Multiferroic Test System with High Voltage Interface - Radiant Technologies, Inc or a Radiant Precision Multiferroic II Ferroelectric Test System. For some samples, the applied electric voltage was increased until reaching the breakdown. From 5 to 7 measurements for each sample were performed in different place and with different electrodes. The recovered energy densities were estimated by integrating the area between the polarization axis and the obtained curves while the efficiency was calculated dividing the energy recovered during the depolarization by the energy accumulated during the polarization.

The piezoelectric characterization was carried out on some selected samples.

Silver sputtered electrodes were prepared onto the films surface and three disks were punched from each mother sample and subjected to the analysis.

Samples were poled with an HV DC polarizing facility able to output DC voltages up to 50 kV, immersed in an insulating and thermalizing silicone oil bath at 120°C for 40 min under an applied DC fields. A feedback loop employing a contacting mercury thermometer was used to regulate the temperature of a heating plate, thus keeping the oil bath at a constant temperature during the active phase of poling. The electric field was maintained throughout the cooling phase to RT.

Dielectric dispersion curves and piezoresonance analysis were performed on a Hewlett-Packard HP4194A frequency response analyzer, over the 100 Hz-40 MHz frequency range. Dielectric data were calculated from primary AC impedance data measured under sinusoidal AC excitation at 10 mV amplitude, taking into account the geometry of the samples. Piezoresonance analysis was conducted by locating resonance/antiresonance doublets associated with both radial and along thickness vibration modes of samples shaped into thin disks. A Matlab routine was used to convert resonance and anti-resonance frequency values to those of the piezoelectric and mechanical constants of the materials, consistent with the ANSI/IEEE 176-1977 Standard.

The d_{33} piezoelectric coefficient was then independently measured using a Sinocera d_{33}-meter calibrated with a standard sample (d_{33} = 360 pC/N) provided by the manufacturer.

In some cases, the samples were also subjected to text on force impact, by using a hammer with a force around 100N. A Piezoelectric Charge Accelerometer Types 4371, a Charge Amplifier 2635, Bruel and Kjaer and a Two-channels digital storage oscilloscope WAVE ACE 1002, TELEDYNE Lecroy were used for the detection of the output voltage. A scheme of the testing set-up is shown in Figure 3.4 for the sake of clarity.

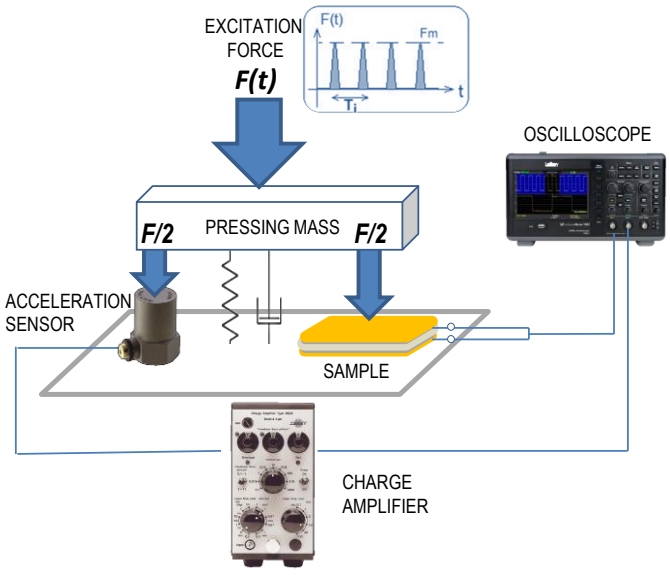

Figure 3.4: Scheme of the testing set-up used to excite the piezoelectric films and collect the signal.

4 RESULTS AND DISCUSSION

4.1 The importance of processing to tune PVDF polymorphism and properties of ensuing composites

Since the properties of PVDF homopolymer and its copolymers depend on their polymorphism, there is an increasing interest in studying new processing methods suitable to induce the crystallization of the electroactive crystalline phases, in particular of the β form, which, being the most highly polar due to its all-trans conformation, is also the most desirable. In literature, different strategies leading to a conformational change of the PVDF chains have been already employed: crystallization from polar solvents at temperatures below 70°C, which, however, leads to porous films characterized by poor mechanical and dielectric properties [119,120]; application of high electric fields, that causes a progressive re-orientation of the moment dipoles, inducing the formation, at first, of δ phase and then of β phase [121,122]; introduction of nucleating agents, such as ceramic nanoparticles, which promote the polar phases due to electrostatic interactions between the filler surface and the polymer chains [123,124]; mechanical deformations, such as stretching [125,126] or rolling [127,128] of α-PVDF films.

The processing method one applies, by changing the polymorphism of PVDF, consequently affects the electric, dielectric and piezoelectric properties of the neat polymer or composite films. However, more in general polymer processing techniques can modify the properties of the final material, also independently from the polymorphism. The processing can indeed affect the overall crystallinity degree of PVDF; as an example, V. Tiwari and G. Srivastava prepared PVDF films from solvent casting and treated them at different annealing and quenching temperature and they found that the different conditions determine not only different relative amounts of crystalline phases but also a different total crystalline content and both these factors in turn influence the dielectric properties [34]. The processing also influences the microstructuration of the polymer, for example in terms of chains orientation and crystallites size. M. Yuan *et al.* investigated the stretching-induced structure development of differently stretched PVDF-HFP films and its correlation with dielectric properties; they found that by stretching, the dipole moment of ferroelectric crystals gradually orients parallel to the electric field and the crystallite size becomes smaller, both these occurrences facilitate ferroelectric switching, resulting in higher dielectric constant [35].

The processing plays an important role also in determining the quality of the ensuing composites for example in terms of filler dispersion or porosity. As an example, K. Silakaew *et al.* tried two different liquid-phase processes for the preparation of PVDF/$BaTiO_3$ composites obtaining different final microstructures and thus different dielectric permittivity not only in terms of attained values but also in terms of trend with frequency [36]. L. Zhang *et al.* prepared PVDF-CTFE/BST composites by using two different configurations in the hot-pressed process, stacking two layers of

as-cast films in different ways; they found a comparatively higher dielectric constant and lower dielectric loss for the sample obtained by joining together the top side of the layers because of the removal of air traps and the achieving of a more compact structure [24].

4.1.1 Double-step moulding: An effective method to induce the formation of β-phase in PVDF

E. Brunengo, G. Luciano, G. Canu, M. Canetti, L. Conzatti, M. Castellano, P. Stagnaro

"Double-step moulding: an effective method to induce the formation of β-phase in PVDF"

Polymer 193 (2020) 122345;
DOI: 10.1016/j.polymer.2020.122345

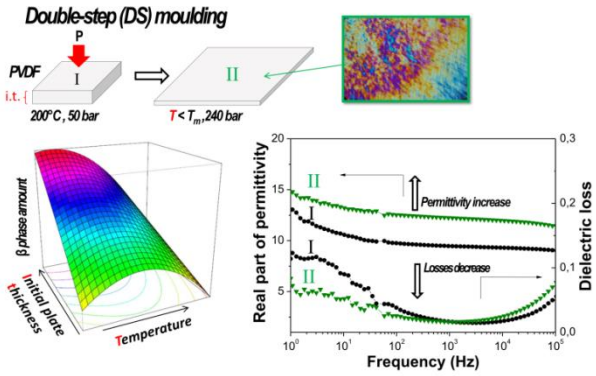

This paragraph is taken from the published work E. Brunengo *et al.* [129], where an alternative and smart approach to tune PVDF polymorphism was proposed, exploiting the compression moulding. Compression moulding is a well-known, simple and easily scalable technique, widely used in polymer processing, that can lead to final materials endowed with different characteristics as a consequence of the processing conditions employed. In such a study, a double-step compression moulding has been used for the first time as an effective method to induce the formation of PVDF β phase, which is the polymorph of the uppermost importance for energy-related applications.

The PVDF pellets were compression moulded by using the two moulding methods described in the *Materials and Method* section (*Paragraph 3.4*). Besides a traditional single-step (SS) moulding a double-step moulding (DS) was used. In particular, in the SS method, the pellets were processed at 200°C and 50 bar for 4 min, while, in the DS method, a thicker plate was first prepared using the SS-conditions and then re-pressed at lower temperature and 240 bar for 4 min. Different DS-conditions were tested, by varying *(i)* the thickness of the initial plate, namely, 1, 2, 3 and 4 mm, and *(ii)* the temperature of the second moulding step, namely, 120, 150 and 170°C.

The obtained films were then characterized by spectroscopic, calorimetric, structural, morphological, dielectric and dynamic-mechanical point of view.

Infrared spectroscopy (IR) is widely used to distinguish the principal PVDF polymorphs, *i.e.*, α, β and γ. Indeed, several peaks can be associated with only one of the crystalline phases. More in detail, characteristic bands of the α polymorph are situated at about 1423, 1383, 1209, 1149, 975, 854, 795, 763, 614, 532, 489, and 410 cm^{-1}; whereas, the peaks around 1275, 473, and 445 cm^{-1} are exclusive for the β phase and, finally, the γ phase is characterized by bands at about 1234, 833,

811, 482, and 431 cm^{-1} [116]. Besides these characteristic peaks, other peaks can originate from the superimposing of signals of two of the three mentioned phases, such as the band around 840 cm^{-1}, which is observable in the presence of β and/or γ crystals.

The ATR-FTIR spectrum of one of the PVDF samples prepared, accompanied by the peaks indication, is shown in Figure 4.1 as an example and a more complete assignment of the bands is reported in Table 4.1

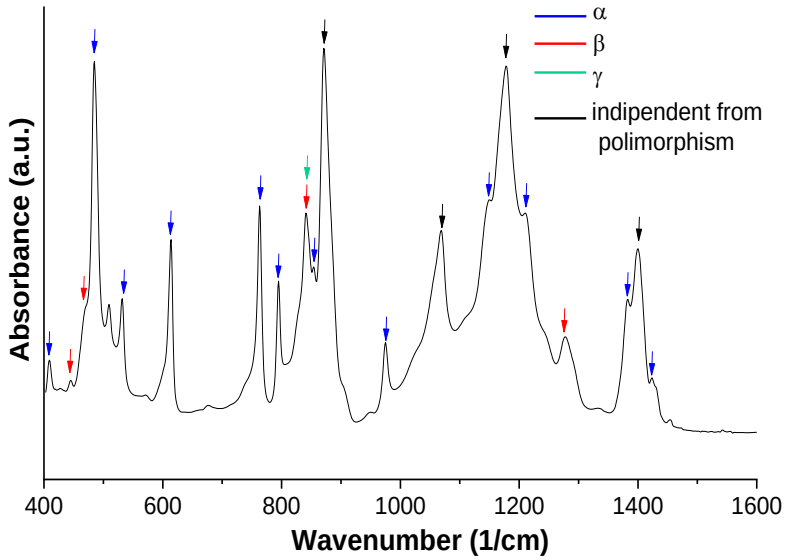

Figure 4.1: ATR-FTIR spectrum of a PVDF film moulded from a starting plate 1 mm thick at 150°C.

Table 4.1: Assignments of the PVDF peaks [130,131].

Wavenumber ± 5 (cm^{-1})	Assignments	Wavenumber ± 5 (cm^{-1})	Assignments
511	δ (CF_2), ω(CF_2)	1167	*vs*(CF_2)
676	Head-to-head and tail-to-tail, ρ(CF_2)	1275	Long trans-sequence of β phase
743	In-plane δ *or* ρ CH_2, CF_2 of β phase	1333	Out-of-plane δ (CH_2)
763	In-plane δ *or* ρ of α phase	1453	In-plane δ (CH_2)
840	ρ(CH_2) and *v*as(CF_2) of β and γ phase	1671	Intermolecular β structure
877	ρ(CH_2)	2980-3020	*vs*(CH_2), *v*as(CH_2)

The infrared spectroscopy is also useful to quantify the amount of these electroactive polymorphs with respect to the total crystalline phase. The fraction of the electroactive phase(s) (F_{EA}) values, calculated for each sample moulded with the DS method, are reported in Table 4.2

The corresponding value for the reference PVDF sample moulded with the SS method is F_{EA} = 29%. The absence of all the characteristics bands of the γ phase (only a faint shoulder at 1243 cm^{-1} is barely visible) and the clear occurrence of the peaks at 445, 470 and 1275 cm^{-1} suggest that, upon double-step moulding, the electroactive phase present in all the films is substantially the β phase.

For the quantitative evaluation only two peaks are considered: the band around 763 cm^{-1} and that around 840 cm^{-1} (see Equation 3.1). However, to the best of our knowledge, no one has so far verified the representativeness of these two peaks, and consequently of the F_{EA} values calculated from them, with respect to the whole infrared spectrum.

To this aim, a PCA (Principal Component Analysis) protocol was applied to all the ATR-FTIR spectra collected on PVDF samples [132].

Table 4.2: Mean F_{EA} values (calculated by Equation 2.1) and crystallinity degrees X_c (calculated by DSC considering ΔH_0 = 104.6 J/g) of PVDF films prepared by the double-step method in different processing conditions.

Sample name	Sample code	Initial film thickness (mm)	Second step moulding T (°C)	F_{EA} (%)	X_c (%)
PVDF1_120	A	1	120	34	56
PVDF1_150	B	1	150	42	57
PVDF1_170	C	1	170	28	59
PVDF2_120	D	2	120	52	55
PVDF2_150	E	2	150	56	57
PVDF2_170	F	2	170	33	59
PVDF3_120	G	3	120	58	55
PVDF3_150	H	3	150	55	54
PVDF3_170	I	3	170	35	57
PVDF4_120	L	4	120	73	56
PVDF4_150	M	4	150	61	54
PVDF4_170	N	4	170	39	62

The principal components analysis is a technique used in the context of multivariate statistics for the simplification of the source data. It allows to individuate new variables, called Principal Components (PCs), which account for the majority of the variability in the set of data under investigation [133]. The loading plot consisting of the wavenumbers of the infrared spectra acquired is reported in Figure 4.2a. The score plot shown in Figure 4.2b represents all the IR measurements carried out on the investigated samples, the obtained points are differently coloured depending on the corresponding F_{EA} value calculated from Equation 3.1. As visible from Figure 4.2, almost all the variance of the system is explained by the first two principal components (PC 1 and PC 2); in particular, the main part of the total variance is described by PC 1. Observing the

loading graphs, one can see two infrared absorbance bands showing a large projection on the PC 1 axis and thus being relevant in describing the variance of the system: namely, the peak around 763 cm^{-1} and that around 840 cm^{-1}. The first one, as expected, is positively correlated with the scores corresponding to samples with lower F_{EA} values (Figure 4.2b), meaning that the intensity of this peak is high for the samples with a low electroactive phase amount. On the other hand, the second one is positively correlated with samples characterized by higher F_{EA} values, meaning that its intensity is high for the samples with a high electroactive phase amount. This result is obviously coherent with the Equation 3.1, but, more than this, indicates that the two bands considered to quantify the relative electroactive phase amount are really important in the description of the whole IR spectrum.

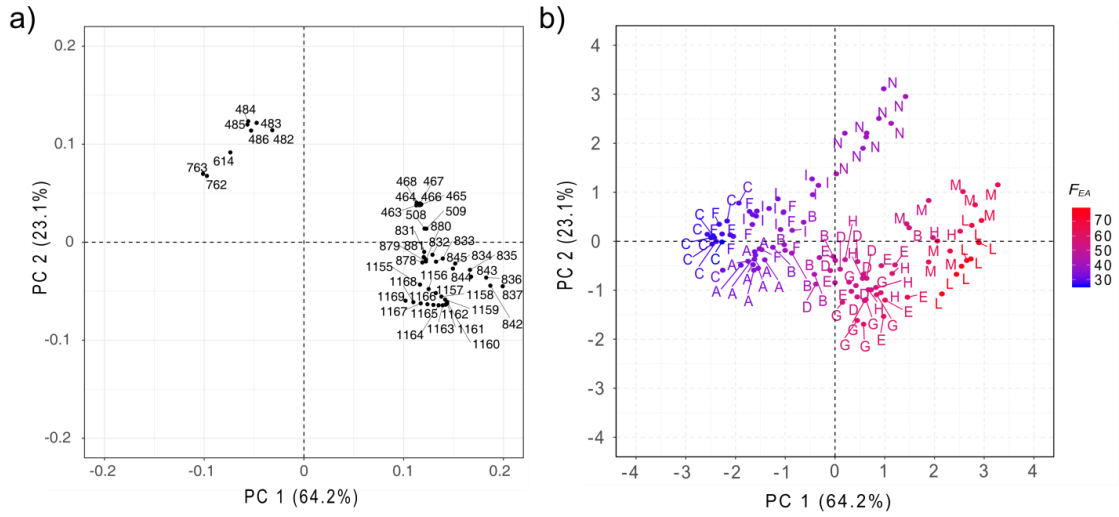

Figure 4.2: a) Loading and b) score plots resulting from PCA performed on ATR-FTIR spectra of PVDF samples. In order to facilitate the reading of the graph, in the loading plot only the first 50 variables having the highest contribution in the loading calculation are reported.

Also the peak around 1167 cm^{-1} seems to have an influence on the variance of the system.

This is an interesting result because this peak, together with the bands in the ranges 876-885, 1067-1075, and 1398-1404 cm^{-1}, is often considered as a peak appearing with similar characteristics in all three PVDF electroactive phases [116,134–136]. On the other hand, by careful inspection of the spectra, it can be noticed that a modification in the range 1160-1180 cm^{-1} occurs, depending on the F_{EA} amount. In particular, as visible in Figure 4.3, where the mean spectra obtained from 8-10 measurements for each sample are reported, the band in the above mentioned range (evidenced by an arrow) tends to broaden and shift to lower wavenumbers with the increasing amount of the electroactive phase, indicating that this band is not completely independent from the PVDF polymorphism.

As inferred by this data elaboration, the processing conditions induce a variation in the PVDF crystalline phases.

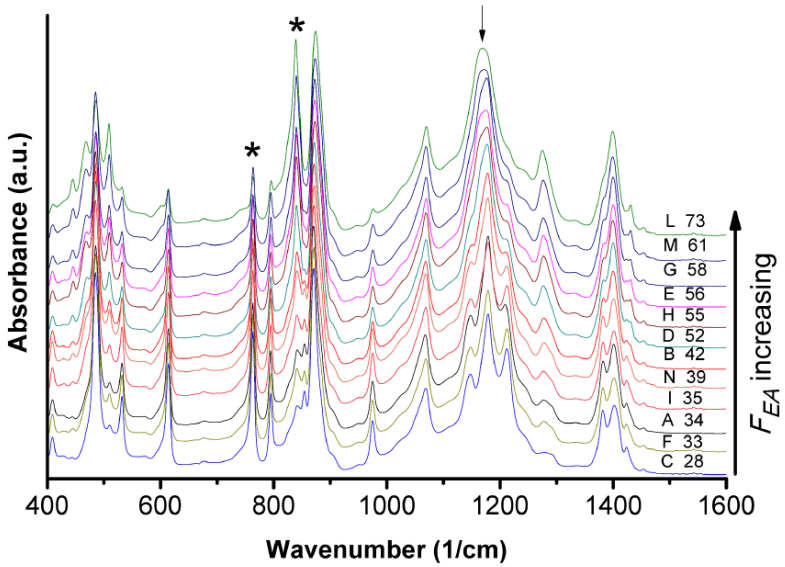

Figure 4.3: IR spectra of the PVDF samples prepared by DS moulding. The letters in the graph code the samples while the numbers indicate the corresponding mean F_{EA} values (see Table 4.2); the asterisks evidence the two peaks considered for the F_{EA} calculation.

In Figure 4.4 the F_{EA} values, already reported in Table 4.2, are represented as a function of the second moulding temperature (Figure 4.4a) or initial plate thickness (Figure 4.4b); for the discussion of F_{EA}* values shown in the inset see below in the text. The electroactive phase amount, at equal initial plate thickness, is low for samples re-pressed at 170°C while is higher when the polymer is moulded at 150°C or 120°C (Figure 4.4a). On the other hand, by considering the samples at equal moulding temperature, the β-phase content tends to increase by increasing the initial plate thickness (Figure 4.4b).

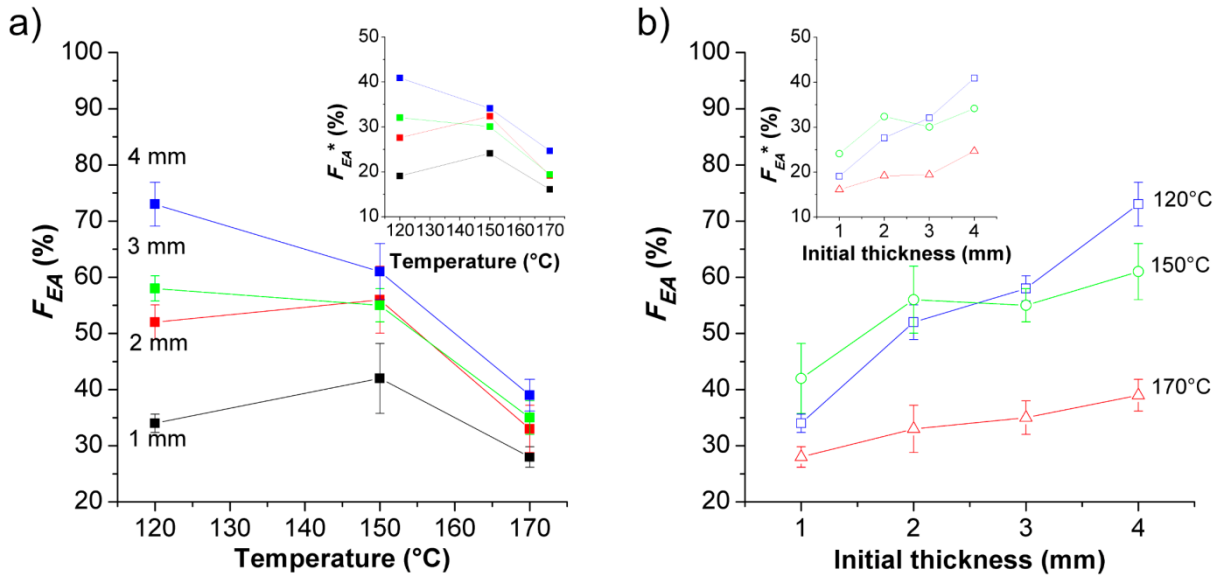

Figure 4.4: F_{EA} and absolute electroactive phase amount (F_{EA}*, in the insets) as a function of: a) temperature of the second step of moulding; b) initial plate thickness.

To better understand the trend of the F_{EA} as a function of the moulding conditions, a multivariate approach was then used. An MLR (Multiple Linear Regression) method [137] was applied to the collected data by considering the initial plate thickness (t_i) and the moulding temperature (T) as the predictors (x), and the electroactive phase amount as the response (Y). Having two input variables, the empirical model assumed in terms of coded factors can be expressed as:

$$Y = b_0 + b_1 x_1 + b_2 x_2 + b_{11} x_1^2 + b_{22} x_2^2 + b_{12} x_1 x_2 \quad (4.1)$$

where x_1 and x_2 correspond to T and t_i, respectively.

It is known that the MLR method allows computing the regression coefficients of the response models in order to minimize the sum of squared residuals [138]. The value of the coefficients and the corresponding standard deviations calculated in the present case are reported in Table 4.3.

Table 4.3: Coefficients calculated by the MLR model. Only the significant ones are reported.

Coefficient	b_0	b_1	b_2	b_{11}	b_{12}
Value	54.60	-11.87	6.11	-7.50	-3.60
St. Dev.	2.03	1.42	0.98	1.46	0.94

The model describes this system with an explained variance of about 93%.

The response surface obtained, shown in Figure 4.5, indicates that, for high initial plate thickness, the F_{EA} increases by decreasing the processing temperature, while, for low t_i, the amount of electroactive phase induced by the moulding reaches the maximum value for intermediate temperatures. This non-monotonous trend can be explained by considering the process of formation of the β phase.

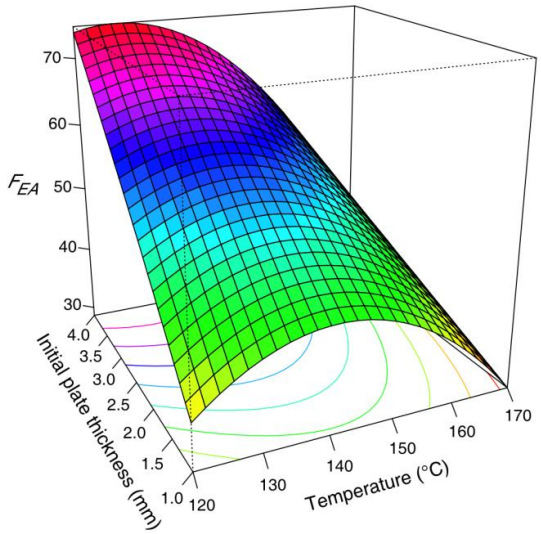

Figure 4.5: Response surface and obtained from the MLR.

It is known that a proper mechanical stress can promote the phase transformation of PVDF and its copolymers. Won June Kim *et al.* [122], by using first-principles simulation methods, modelled different possible transition routes from α to β phase. They theoretically demonstrate the need of the simultaneous application of a mechanical drawing (parallel to the *c-axis* direction) and a compression (along *a-axis* direction) to induce the formation of β phase and enhance PVDF ferroelectric properties.

In practice, to mechanically obtain the most polar PVDF phase two main methods are widely used: namely, stretching or rolling of preformed polymer films. In both cases, the stresses generated within the material bulk as a consequence of longitudinal extension or transversal compression, respectively, cause an alignment of the polymer chains that, in turn, leads to the conversion into β phase. In the present case, an analogous phenomenon occurs with the DS moulding: the promotion of the β phase formation is reasonably due to the internal shear stresses occurring in the material during the second step of moulding, in a similar way to what observed in literature when a PVDF film is subjected to a rolling process.

Several studies were carried out in order to understand how the processing conditions influence the electroactive phase amount obtained in the stretched or rolled PVDF films. Usually, the tested temperatures are set well below the melting temperature of the polymer. Here, because of the limited maximum pressure reached by the semi-automatic press her used (*i.e,*. 240 bar) a partial polymer melting was necessary to outcome the compression of the film. Taking this into account, the trend of the F_{EA} obtained can be explained, by considering two conflicting factors. In the second step of moulding, the film reduces its thickness and increases laterally its surface; the higher the initial thickness and the temperature, the more marked the resultant deformation (see *Appendix A* for more details). However, the higher the temperature, the higher the amount of molten polymer, but, during this process, only the non-molten portion of PVDF undergoes the phase transition. Thus, if the initial plate is thick enough to allow a consistent squeezing of the polymer, the amount of the electroactive phase obtained is mainly determined by the quantity of PVDF that remains solid, which increases by decreasing the processing temperature. On the contrary, if the starting plate is too thin, lower viscosity of the system is necessary to induce a sufficient deformation of the material; that is the reason for the presence in the response surface of a maximum at intermediate temperatures for low t_i values.

F_{EA} value expresses the relative amount of electroactive phase(s), *i.e.,* the content of electroactive polymorph(s) with respect to the total crystalline phase present in a given PVDF sample, without taking into account the remaining amorphous part. Thus, because the different re-pressing conditions can affect polymer crystallization, all the prepared films were subjected to DSC analysis; the relative thermograms are shown in Figure 4.6 and the calculated crystallinity degrees (X_c) are reported in Table 4.2. The corresponding X_c value for the film obtained from SS-moulding is 53%.

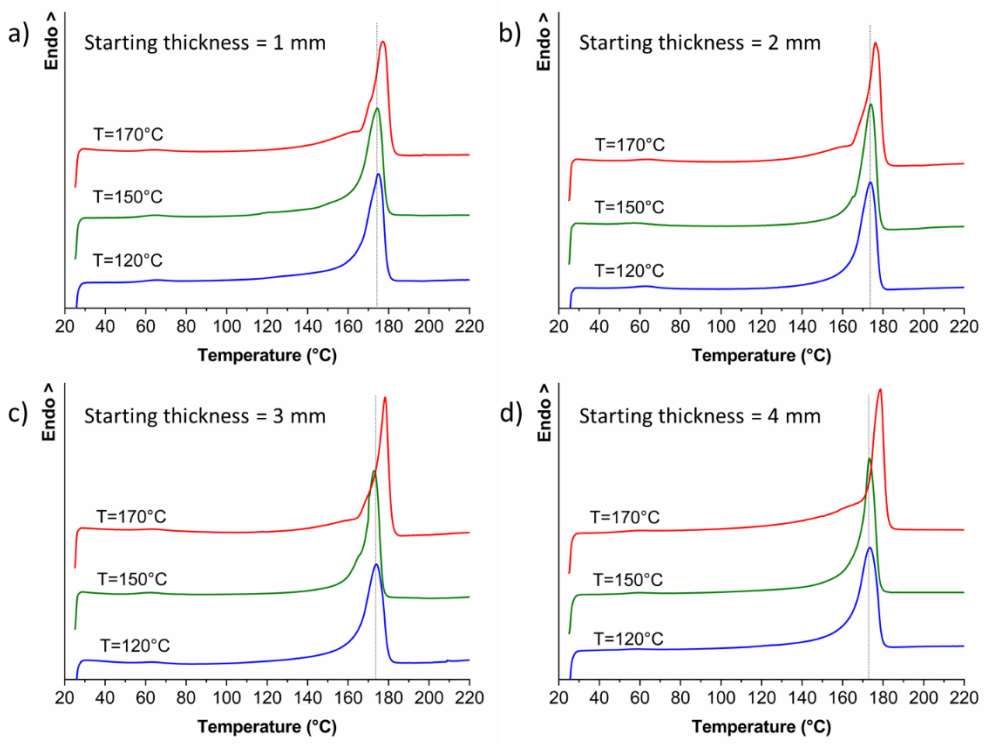

Figure 4.6: DSC heating curves of samples DS-moulded starting from plates: a) 1 mm, b) 2 mm, c) 3 mm, and d) 4 mm thick. The vertical line is placed at 174°C (see the text below).

For sake of completeness, one must say that in literature, discordant values of the fusion enthalpy for a perfect PVDF crystal are reported: many authors, irrespective of the polymorph, α or β, consider a unique value equal to 104.6 J/g [117,139], while few others report different enthalpies for α (93.07 J/g) and β phase (103.4 J/g) [127]. The crystallinity degrees here reported, were calculated by following the first assumption; however, we verified that, also by using the two different values of enthalpies above mentioned, all the following considerations remain still valid (see *Appendix A*). As observable in Table 4.2, no specific trend is individuated as a function of the moulding conditions, except a slight increase of X_c, at equal t_i value, for the films re-pressed at 170°C. These samples are also characterized, as visible in Figure 4.6, by a higher melting point (177°C, red curves) with respect to 174°C measured for both the other DS-moulded films (green and blue curves) as well as for the SS-moulded PVDF (curve here not shown). This suggests that, during the second step of moulding at 170°C, the higher annealing temperature, which increases the chain mobility, combined to the applied shear, contributes to obtain a higher amount of more perfect crystals.

In order to take into account the influence of the crystallinity on the trends described above for F_{EA} (see Figure 4.4 and Figure 4.5), the absolute electroactive phase amount (F_{EA}*) was calculated multiplying the F_{EA} value by the X_c value (Table 4.2). The trends for F_{EA}* are analogous to those observed for F_{EA} (see the insets of Figure 4.4 reporting the results obtained by considering ΔH_0 = 104.6 J/g), this means that the considerations about the relative electroactive phase content can hold also for the absolute electroactive phase amount.

The macroscopic deformation of the polymer can be put in evidence by exploiting the birefringence of the crystalline phase. To this aim, very thin and transparent films of PVDF were prepared in similar conditions with respect to those described above. PVDF films 500 µm thick were re-pressed at 240 bar and 120, 150 or 170°C in order to replicate the DS moulding on a reduced scale. For reference purpose, other two transparent films, one re-pressed at 240 bar and 200°C and one moulded under SS conditions (200°C and 50 bar), were prepared as well. The images obtained by POM are reported in Figure 4.7. An orientation is visible in all the samples prepared through the DS method at a temperature below the melting temperature of PVDF (Figure 4.7a-c). In particular, the deformation increases by increasing the temperature of the second moulding because of the lower viscosity of the system leading to an easier flow of the polymer chains during the compression. Also, the dimensions of the domains tend to increase, as expected, by increasing the temperature.

If the temperature of the second step of moulding is well above the melting temperature of PVDF, the re-pressing at high pressure is ineffective to induce an orientation (Figure 4.7d) and the film appears similar to that obtained through the SS moulding (Figure 4.7e), that is at a temperature above the complete melting of the polymer and at low pressure.

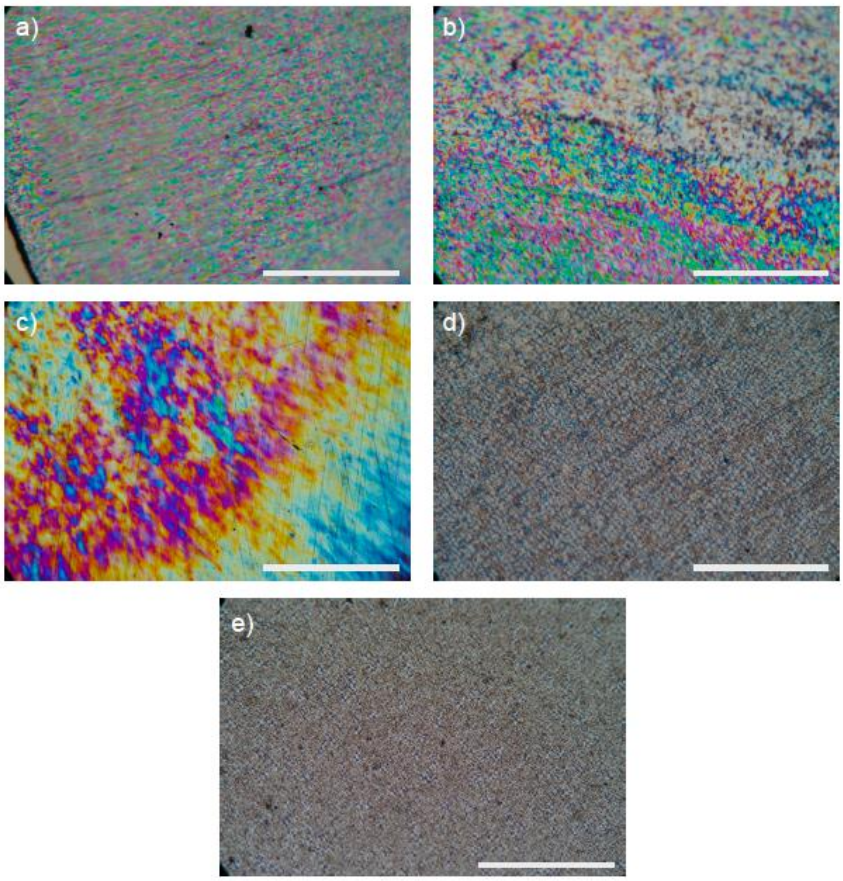

Figure 4.7: Polarized optical micrographs of thin films moulded with the DS method at: a) 120°C; b) 150°C; c) 170°C; d) 200°C; and e) film moulded under SS conditions. The white bar corresponds to 1 mm

Among the series of thicker films, three samples characterized by a significantly different amount of β phase (73, 61 and 39%) were selected for further investigation. Namely, the PVDF films obtained by re-pressing a plate of 4 mm at 120, 150 or 170°C (L, M, and N, respectively in Table 4.2) were subjected first to WAXD analysis, in order to support the results obtained from ATR-FTIR and DSC analyses, and then to dielectric and dynamic-mechanical characterization. For references purpose also a PVDF film prepared by DS moulding at 200°C (named PVDF4_200) and a film prepared by SS moulding (named PVDF_SS) were studied. The amount of electroactive phase of the sample re-pressed at 200°C was 28%, thus exactly comparable to the low amount present in the sample from SS moulding (29%).

The WAXD patterns of the DS-films, reported in Figure 4.8, confirm the infrared spectroscopy results. The reflections relative to the electroactive phase are evident and become more intense by decreasing the temperature of the second step of moulding. This can be appreciated also from a quantitative point of view by considering $X_{\beta,I}$ and $X_{\beta,A}$ values (*i.e.*, the amount of β crystalline phase calculated by considering the intensity or the areas of the peaks, respectively) reported in Table 4.4.

Table 4.4: Crystallinity degree and β phase amount (expressed as %) estimated by WAXD analysis by following Equations 3.2, 3.3a and 3.3b. The corresponding values of F_{EA} and X_c obtained by FTIR and DSC are indicated again for the sake of clarity.

Sample	**FTIR**	**WAXD**			**DSC**
	F_{EA}	$X_{\beta,I}$ (%)	$X_{\beta,A}$ (%)	X_{cW} (%)	X_c
PVDF4_120	73	57	57	43	56
PVDF4_150	61	25	20	45	54
PVDF4_170	39	18	20	54	62

Although the trends are the same, the values of β phase obtained from WAXD are lower than the corresponding ones calculated by IR spectroscopy; this is essentially due to the intrinsic differences between the two techniques: the penetration depth of the X-rays is much higher than that of the penetration depth of the infrared rays and the amount of β phase can be reasonably higher near the sample surface, where the shear stresses are transferred directly from the press plates to the surface of the polymer film, rather than in its core. Indeed, during polymer processing, a gradient of the crystalline structure is frequently observable, especially if samples are quite thick. As an example, M. Favaro *et al.* [140] studied the polymorphism and the molecular orientation in isotactic polypropylene (*i*-PP) subjected to injection moulding and found different characteristics between the skin and the core of the investigated samples.

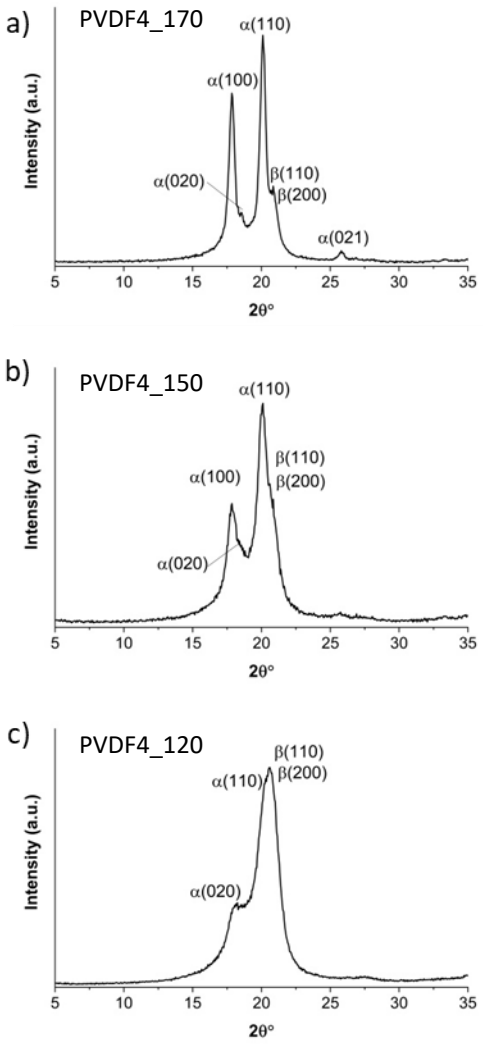

Figure 4.8: WAXD patterns of the PVDF films prepared by the DS moulding at a) 170°C, b) 150°C, and c) 120°C starting from a plate 4 mm thick.

Regarding the α form, for the PVDF films re-pressed at 150 and 170°C the reflection relative to the (100) plane is more intense than that related to the (020) plane, as opposed to what visible for the sample re-pressed at 120°C; this is probably ascribable to the material anisotropy, consequence of the deformation (induced by processing), that is more evident for the samples re-pressed at high temperature, in accordance with the POM images.

It can be also noticed that the crystallinity degree values obtained from WAXD are lower than those calculated from DSC, as already observed in literature [141,142] However, following the results reported in Table 4.2, the X_{cW} value can be considered significantly higher for the film PVDF DS-170 with respect to the other samples, in accordance with what previously observed from calorimetric characterization.

The dielectric permittivity and the loss tangent measured by impedance spectroscopy are shown in Figure 4.9. The reported curves are representative of several replicas for each sample.

If the temperature of the second step of moulding is lower than the melting temperature of PVDF, the dielectric permittivity of the film is high and tends to increase by decreasing the temperature of moulding; this is due to an increase of the PVDF β phase amount. In particular, the permittivity at

10^3 Hz results similar (9.5 and 9.7) for the films prepared through the SS moulding and DS re-pressed at 200°C, respectively, which contains a β phase amount of about 30%. Whereas, as concerns the other PVDF films from the DS method, the permittivity values are 10.9 for the sample re-pressed at 170°C (β-phase about 40%) and increases to 12.2 and 12.5 for those re-pressed at 150°C (β-phase about 60%) and 120°C (β-phase about 70%), respectively.

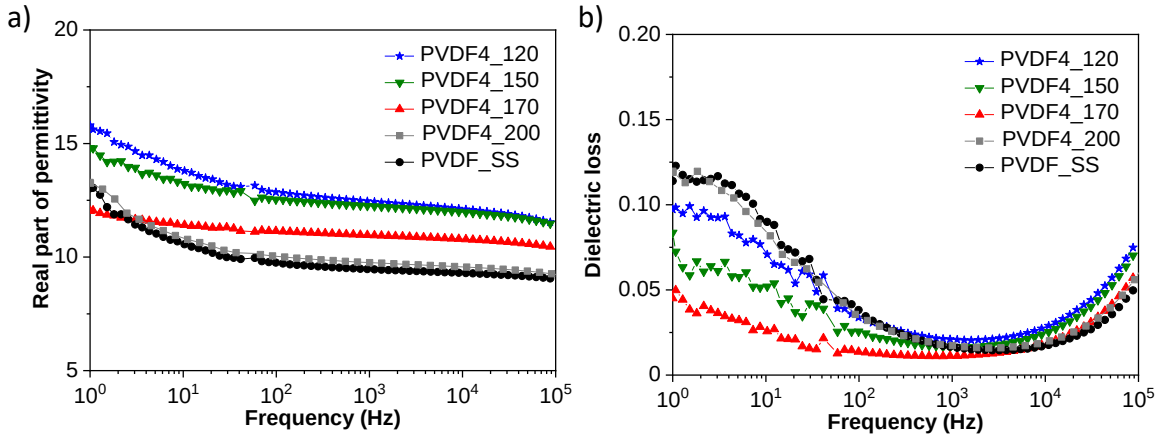

Figure 4.9: a) Dielectric permittivity and b) loss tangent (*tanδ*) of the PVDF films prepared with the DS moulding starting from a plate 4 mm thick and a PVDF film obtained by SS moulding.

The dielectric properties are affected by the polymorphism, but also by the crystallinity degree of the polymer. In particular, it is important not only the amount of β phase present with respect to the other crystalline phases but its quantity with respect to both the total crystalline phase and the amorphous counterpart. Actually, if two PVDF films are characterized by the same F_{EA} but have different crystallinity degrees, the dielectric permittivity will be higher for the more crystalline sample. The absolute elecroactive phase amount F_{EA}*, previously introduced, takes into account both of the above mentioned factors. As shown in Figure 4.10, the increasing trend of the dielectric permittivity observed *versus* the relative electroactive phase amount is valid also for this parameter (inset Figure 4.10).

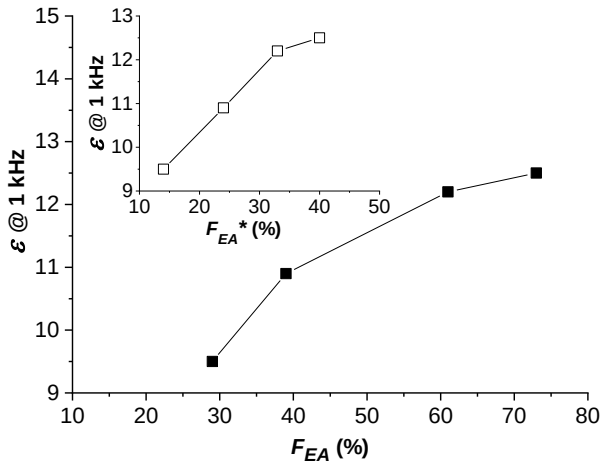

Figure 4.10: Real part of dielectric permittivity at 1 kHz *vs.* relative or absolute (inset) amount of β phase.

Also dielectric losses are affected by the processing conditions. More in detail, the *tanδ* at low frequency is lower for the films prepared by the DS method at 120°C, 150°C and 170°C than for the PVDF samples obtained from DS moulding at 200°C and from SS moulding. Besides, the losses tend to decrease by increasing the temperature of the second step moulding.

This trend is opposite with respect to the behaviour of dielectric permittivity and suggests that not only the polymorphism contributes to the overall dielectric properties of the PVDF. In literature analogous results were obtained for PVDF films subjected to rolling [127,143,144]: the rolled films are characterized by a reduction in dielectric losses at low frequency with respect to the same PVDF films prior rolling (taken as a reference). This is indicated as a consequence of a shift of the relaxation processes to lower frequency values (only visible when measurements are carried out in a wider range of frequencies) and it is ascribed to the reduction of the free volume in the bulk material, induced by the process. Based on these literature results, the experimental evidence here founded can be explained: the higher the re-pressing temperature, the lower the viscosity of the system and the more marked the compacting effect.

The processing conditions clearly influence also the molecular motions of the PVDF as evidenced by the dynamic-mechanical response (Figure 4.11).

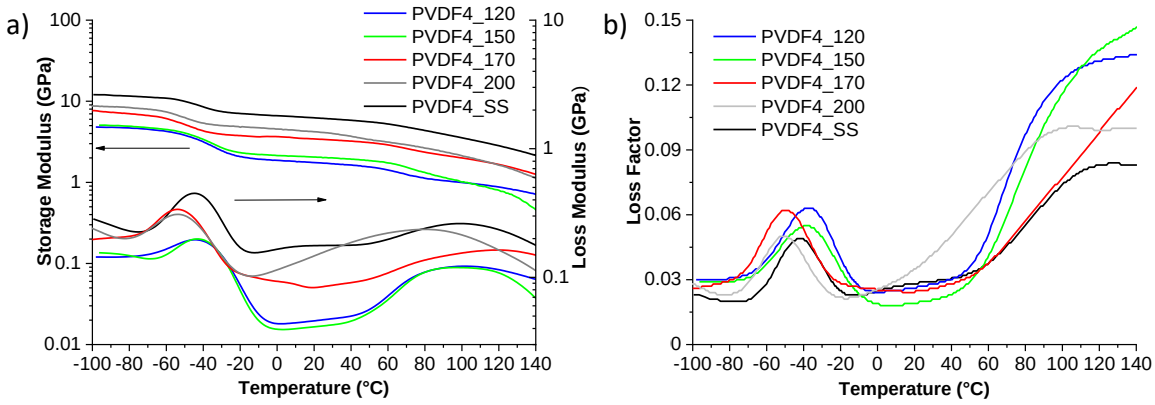

Figure 4.11: Dynamic-mechanical response of the PVDF films moulded under different conditions: a) storage and loss moduli; b) loss factor ($tan\delta_G$).

Indeed, it is known that different processes can have an effect on the architectural organization of polymers, in terms of crystalline, rigid-amorphous and amorphous phases, that in turn can affect the thermal dynamic-mechanical properties of the semi-crystalline polymers.

It is known as well that the mechanical response of polymers can be affected by the crystallinity degree, *i.e.*, higher the X_c higher the elastic modulus. However, in our case, even though the crystallinity degree of the SS-moulded PVDF film is comparable or lower than that of the DS-moulded samples (see Table 4.4), a slight decrease of the storage modulus (*G'*) upon the second step of moulding is visible in Figure 4.11a. The differences in modulus, here observed, are probably due to the quality of the crystals rather than to their quantity. V. Sencadas *et al.* [145] measured a lower elastic modulus (*E'*) for PVDF stretched samples with respect to the un-stretched

one, while D. Samios *et al.* stated a decrease in *E'* when iPP was subjected to plane strain compression at temperatures below the melting temperature [146]. This suggests that the lower shear modulus of the samples from DS moulding is probably due to the introduction of defects in the crystalline phase as a consequence of re-pressing at high pressure, an effect which is more marked if the second moulding temperature is lower. Anyway, the mechanical performance of the films remains sufficiently high for practical applications.

As concerns the mechanical losses, the curve of the PVDF prepared with the SS moulding shows three main relaxations located in the -80 ÷ -10°C, 0 ÷ 50°C and 50 ÷ 140°C temperature ranges. The first, usually labelled as β or α_α relaxation, is due to cooperative segmental motions of the main chains within the amorphous phase and is related to the glass transition ($T_g \approx$ -40°C) of PVDF [145,147,148]. Between the glass transition and the melting temperature, the semi-crystalline polymers generally show, at least, one absorption peak [149]. The peak at lower temperatures might be assigned to the *γ'* relaxation, attributed to the folding movements in the amorphous phase [150]. The broad relaxation process occurring at higher temperatures (labelled as α or α_c relaxation) has given rise to discrepancies in the literature, being ascribed to the rigid-amorphous region [151] or molecular motions within the crystalline fraction [145,148,152]. In general, it must be considered that multiple relaxation processes are inherently broad and tend to be poorly resolved from each other. Moreover, in the mechanical response, the effect of the molecular motions in the crystal, responsible for the α_c process, can be transferred to the closest amorphous fraction [153].

In literature, there are some examples which demonstrate that the intensity and the position of the PVDF transitions are influenced by sample processing [142,151,154] and are affected not only by the fraction of amorphous phase but also by the architecture of the crystalline phase [148]. More in general, in semi-crystalline polymers, the orientation of the crystalline lamellae induced by a given processing procedure can modify the thermal dynamic-mechanical response, especially above the glass transition [145,155]. Different responses have been already observed not only by deforming the specimen in tensile mode but also in bending and torsional modes [155]. By considering the rolling process, which can be assumed similar to the DS moulding method here used, Z. Bartczak *et al.* found that side-constrained rolled HDPE and PP films [156,157] showed a different relaxation behaviour compared to the corresponding not rolled reference samples.

As for the samples here prepared, the shape of the curve changes: the shoulder occurring at intermediate temperatures becomes less evident and the peak that identifies the α_c relaxation appears at different temperatures as a consequence of the different moulding conditions (Figure 4.11b). In particular, for the films re-pressed at 150 and 170°C, it occurs at higher temperatures with respect to the other samples. This shifting is ascribable to the re-processing at a higher temperature that, on one hand, causes an increase of the crystal thickness and, on the other hand, according to the above reported results, leads to a more compact structure, in which the polymer chains have higher difficulties to relax.

The good performances of the DS-moulded films suggest that the proposed method of moulding could also lead to an improvement of the ferroelectric and piezoelectric properties of neat PVDF. However, these kinds of characterization require the preparation of thinner films, which can be obtained by the DS processing starting from PVDF plates of lower thickness, due to the limited maximum pressure reached by the press (see above in the text what said regarding the films prepared for POM observations). In order to obtain suitably thin PVDF films with analogous characteristics analogous, in terms of phases amount and crystallinity degree, to those of the thicker samples here presented, a deeper study of the DS moulding on a reduced scale will be necessary.

4.1.2 The effect of double-step moulding on PVDF-HFP copolymer

The study of the influence of compression moulding on polymorphism of PVDF homopolymer was then extended to another fluorinated matrix, namely poly(vinylidene fluoride-*co*-hexafluoropropylene) (PVDF-HFP), which is a PVDF copolymer consisting of randomly distributed vinylidene fluoride (VDF) and hexafluororepropylene (HFP) units.

For PVDF, as in general for the other polymers, copolymerization is an effective way to control the crystallinity and improve the processability. The incorporation of HFP units reduces the length of the crystallizable VDF homosequences, in turn reducing the melting temperature and crystallinity degree, while enhancing the chain flexibility with respect to the homopolymer. PVDF-HFP copolymer has been widely studied for applications in membranes, separators between the electrodes of batteries and gel electrolytes [158–160] and, more recently, it is arousing interest also in the field of energy storage and conversion [27,161–166]. However, compared to the extensive literature present for the PVDF, only few works about the investigation of PVDF-HFP polymorphism its crystalline transformations are available [167–171].

Taking into account of the obtained results, single-step and double-step moulding procedures were here applied also to PVDF-HFP, by varying the moulding temperatures in relation with the different characteristics of the copolymer. Indeed, its melting temperature, measured by DSC (T_m about 160°C), is lower than the melting temperature of the homopolymer (T_m 175-180°C). The moulding conditions were therefore properly selected as follows: 190°C, 50 bar, 4 min for the SS moulding and 120 or 150°C, 240 bar, 4 min for the second step of the DS moulding.

The obtained films were thoroughly characterized by spectroscopic, calorimetric, morphological, dielectric and dynamic-mechanical point of view.

Gathered results are in accordance with the experimental evidence we previously found for the homopolymer. The α phase is the predominant polymorph (F_{EA} = 29%) in films obtained by the SS moulding. The re-processing at high pressure and below the melting temperature (DS moulding) has two effects on the copolymer: first, it induces a partial orientation of the molecular chains, evidenced at the macroscopic level by POM (See inset Figure 4.12a) and, second, it determines a partial conversion from α phase to β phase, quantified by ATR-FTIR. As detailed in *Paragraph*

4.1.1 the phase transformation is due to the mechanical deformation occurring during the second step of moulding with a mechanism similar to that involved in a rolling process. Also for the copolymer, the lower the temperature of the second step of moulding, the higher the amount of β phase formed (Figure 4.12a), because only the not molten portion of the polymer undergoes the phase transition. From the DSC thermograms, it was estimated for the copolymer that the relative amount of not molten material with respect to the total crystalline phase, is analogous to that already found for the homopolymer, being it equal to about 60% or 95% when the samples are re-pressed at 150 or 120°C, respectively. However, under analogous conditions, F_{EA} values obtained for PVDF-HFP are lower than those reached by PVDF. This is probably due to the fact that, as estimated by DSC, the crystallinity degree present in the sheet obtained from the first step of moulding is lower for the copolymer ($X_c \approx 40\%$) than for the homopolymer ($X_c \approx 50\%$) and thus, at equal moulding temperature, lower shear stresses arise during the re-compression step.

The increase of the electroactive phase amount as well as the polymer orientation induced by the DS moulding, in turn, affect the dielectric properties, leading to an increase in permittivity, which reaches the value of 15.5 at 10^3 Hz for the PVDF-HFP DS 120°C film, and a decrease of dielectric losses (Figure 4.12b). In particular, the *tanδ* at low frequency is lower for the PVDF-HFP sample re-pressed at 150°C than for that re-pressed at 120°C, in accordance with what observed for the homopolymer.

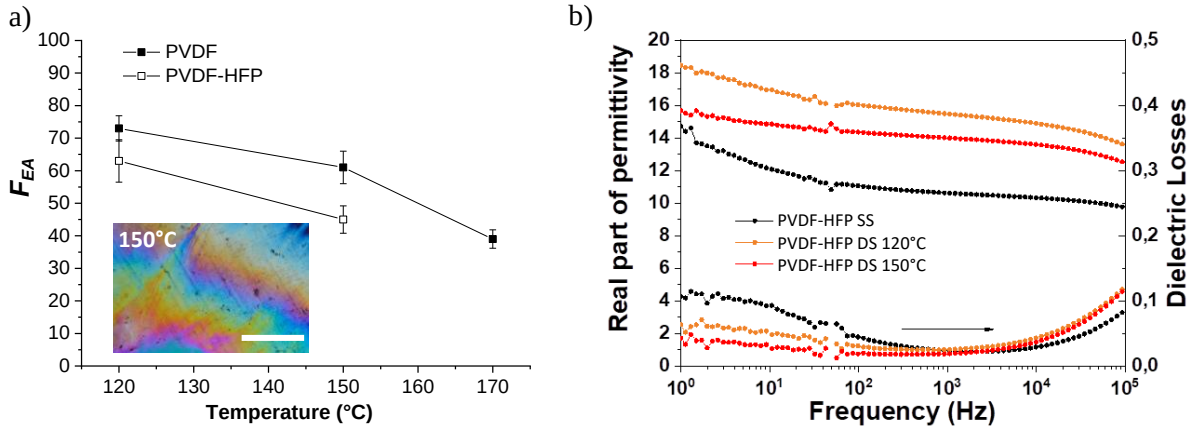

Figure 4.12: a) Electroactive phase amount for PVDF homopolymer and PVDF-HFP copolymer as a function of the temperature of the second step of moulding and POM image of a thin sample re-pressed at 150°C (inset). The white bar corresponds to 500 µm; b) Dielectric properties of the PVDF-HFP films prepared with SS or DS moulding at different temperatures.

The dynamic-mechanical characterization indicates that the shear modulus of the copolymer is lower than that of the homopolymer. For istance, the *G'* value at room temperature is about 2 GPa for the PVDF-HFP SS and about 6 GPa for the PVDF SS. This is due to the lower crystallinity degree exhibited by the copolymer.

As already observed for PVDF, the processing conditions also modify the polymer chains mobility: the DMTA measurements carried out on the copolymer films (Figure 4.13) showed that α_c

relaxation is more evident and shifts to a higher temperature for the samples obtained from DS moulding with respect to the corresponding transition measured for the films prepared by SS moulding.

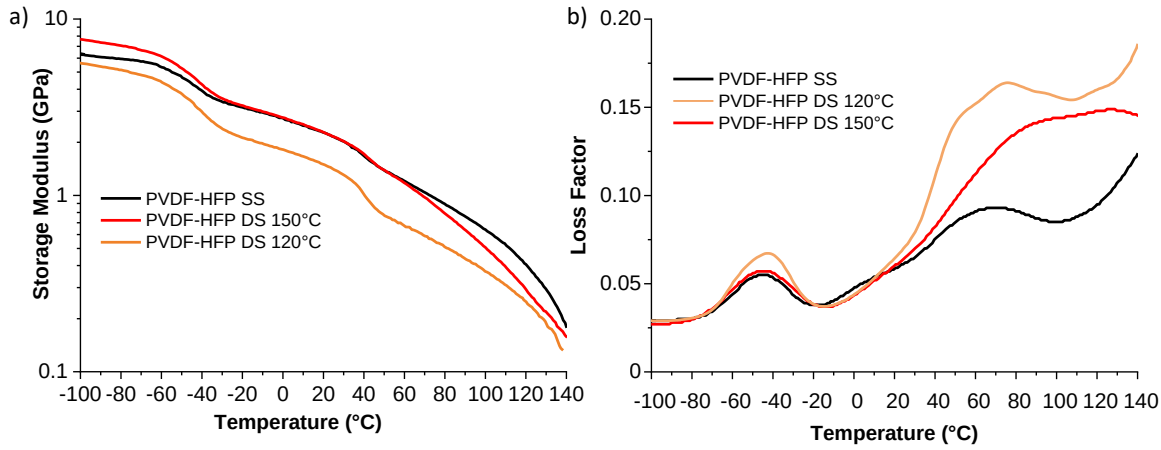

Figure 4.13: Dynamic-mechanical response of the PVDF-HFP films moulded under different conditions: a) storage modulus; b) loss factor ($tan\delta_G$).

In the light of the above experimental evidence, it was considered of interest to study the effect of the DS moulding on different PVDF-based composites, by selecting suitable moulding conditions. From the results obtained for the neat polymer matrices it was found that the temperature of the second step of moulding affects in an opposite way the dielectric permittivity and the loss tangent; in particular, the lower the second-step temperature the higher the permittivity while the higher the temperature the lower the dielectric losses. One can therefore reasonably foresee that the introduction of a ceramic filler in a polymer matrix, by increasing the viscosity of the resulting system, consequently contributes, during the re-processing, to the generation of the shear stresses necessary for the β phase formation, even at relatively high temperatures. In addition, if the temperature of the second moulding step was too low, the limited maximum pressure of the press may not be sufficient to reduce the sheet thickness down to that suitable for the subsequent characterization. Taking into account all these considerations, 170°C and 240 bar were selected as suitable conditions for the second step of moulding in the preparation of the PVDF-based composites. In this case, for the sake of clarity in the sample name attribution, the SS and the DS moulding are indicated as P1 and P2 in the composite films labels.

Taking into account that a too high filler content, leading to an increase in porosity and/or stiffness, tends to decreases the dielectric/piezoelectric performance of the composites (See *Paragraph 2.2* and *2.3*), compositions not higher than 50Vol% filler were chosen. Moreover, different filler concentrations were selected for the different materials studied, depending on the single aspects under examination. In some cases also the amount of ceramic powders available coupled with the time necessary to prepare the composites with a certain methodology had to be taken into account. More than one composition was tested for the composites from melt blending and hot-pressing and for those containing commercial particles while, for samples from solvent casting prepared with

synthesized particles, the filler amount was fixed at 30 Vol%. Nevertheless, the concentrations were always set in order to allow a comparison among all types of composites under investigation.

4.1.3 PVDF-based composites containing PZT particles: How processing affects the final properties

E. Brunengo, M. Castellano, L. Conzatti, G. Canu, V. Buscaglia, P. Stagnaro

"PVDF-based composites containing PZT particles: How processing affects the final properties"

Journal of Applied Polymer Science 137 (2020) 48871;
DOI: 10.1002/APP.48871.

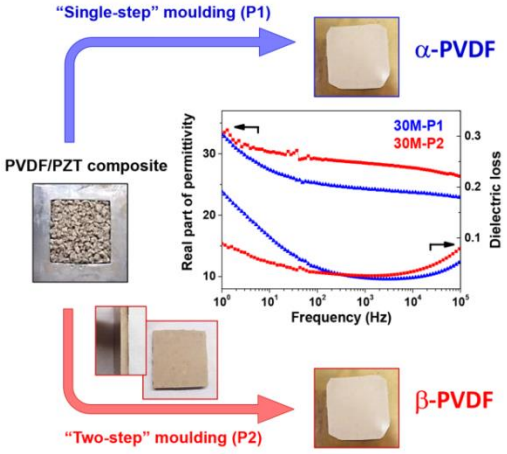

This paragraph is taken from the published work Brunengo *et al.* [154].

PVDF-based composites containing 10, 20 and 30 Vol% of commercial lead zirconate titanate (PZT) particles were prepared by means of two different techniques: solvent casting (S) and melt blending (M) (procedures detailed in *Paragraph 3.4.1 and 3.4.2*). In both cases (S and M composites), the obtained materials were then compression moulded by using two different procedures: a single-step (SS) and a double-step (DS) method. As already described for the neat polymer matrices, in the latter method a second moulding step was applied to induce the formation of the electroactive β polymorph of PVDF through the stresses generated by compression, exploiting an approach similar to that used in the rolling process.

The ensuing samples were respectively named xM-P1, xM-P2, xS-P1 or xS-P2, where x = 10, 20 or 30, depending on PZT Vol%, M or S are referred to the preparation technique, P1 = SS and P2 = DS moulding method.

For reference purpose, analogous films of neat PVDF obtained from melt blending or solvent casting, were moulded following the two methods; these samples are named PVDFM-P1, PVDFM-P2, PVDFS-P1 and PVDFS-P2.

The influence of the preparation technique and moulding method on the fluorinated matrix polymorphism, as well as on the dielectric and dynamic-mechanical properties of the composites were studied.

A careful morphological observation of the prepared PVDF/PZT composites was firstly carried out to evaluate filler distribution/dispersion within the polymer matrix. In Figure 4.14 representative SEM images of the xM-P1 and xS-P1 composites at the three different compositions are reported.

The subsequent moulding method does not affect the morphology which resulted analogous for the P2-samples (see *Appendix B*). As a whole, composites from melt blending show a quite good particles distribution throughout their cross-section, but are characterized by the presence of large agglomerates (Figure 4.14a,c,e), essentially constituted by PZT particles, as revealed by EDX element mapping (Figure 4.15a); on the contrary, in the samples prepared from solvent casting, the ceramic filler is very finely dispersed, as shown in Figure 4.14b,d,f and Figure 4.15b.

Thus, the different preparation technique affects the morphology of these composites. On one hand melt blending, although advantageous for processing large amounts of material because it avoids the use of solvents, does not lead to an optimal dispersion of PZT particles. On the other hand, in the solvent casting method, the pre-dispersion of the ceramic particles in the solvent seems to be a fundamental step to attain a fine and even morphology in the ensuing composites.

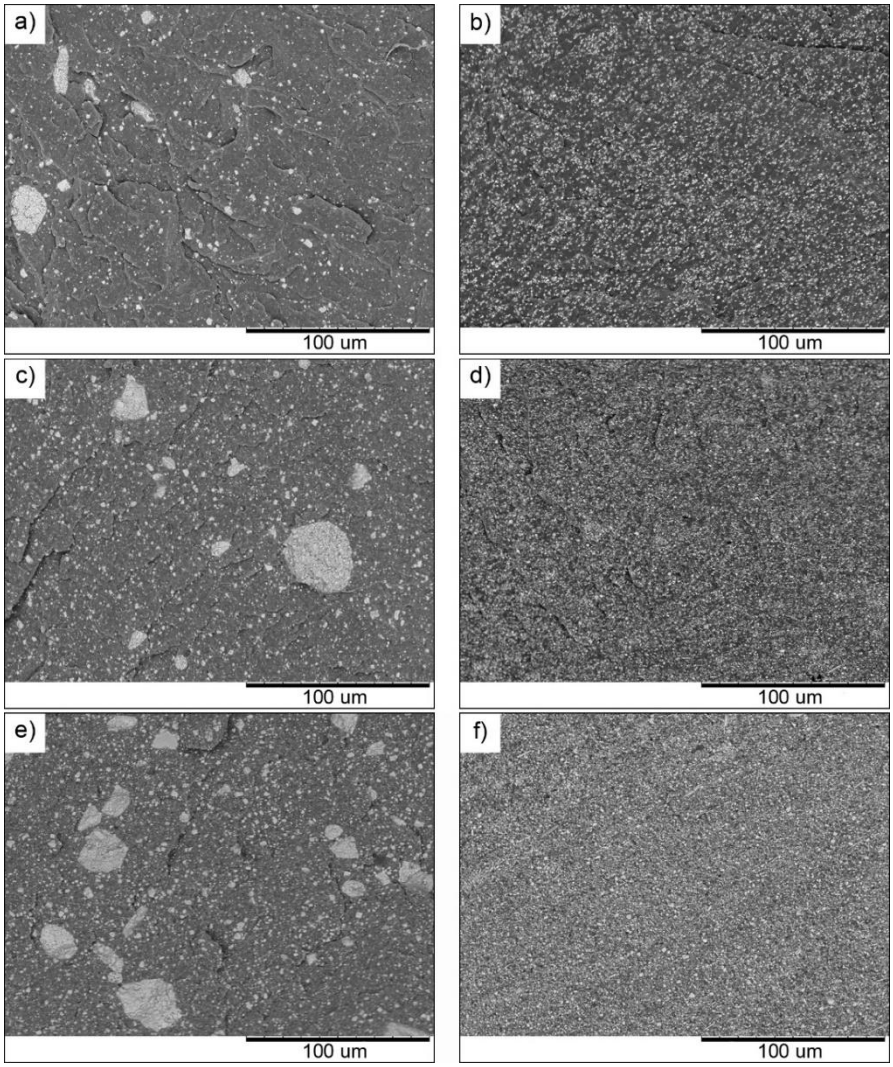

Figure 4.14: SEM micrographs of PVDF/PZT composites: a) 10M-P1; b) 10S-P1; c) 20M-P1; d) 20S-P1; e) 30M-P1 and f) 30S-P1.

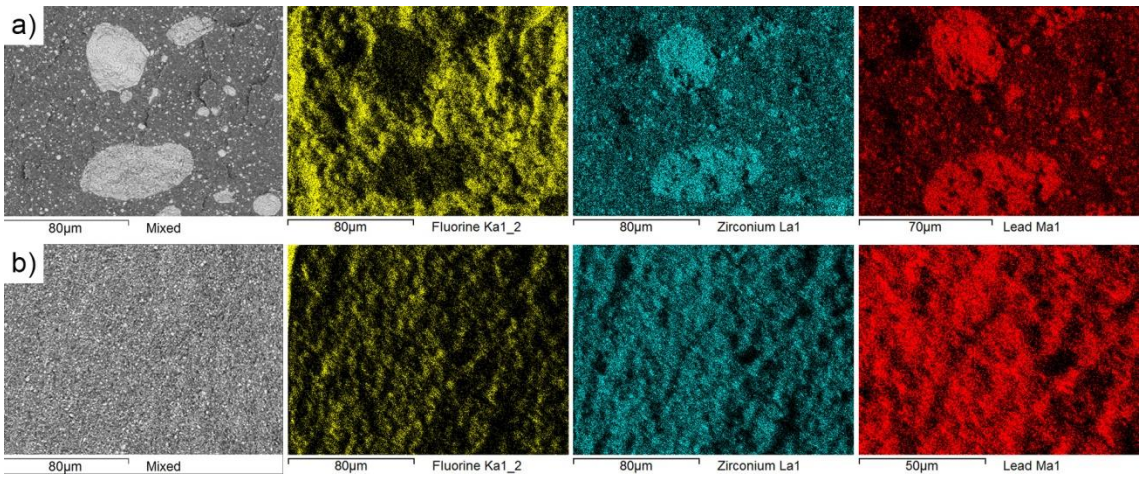

Figure 4.15: EDX element mapping of the 30 Vol% PVDF/PZT composites from: a) melt blending; b) solvent casting. See the *Appendix B* for the corresponding images of the composites containing 20 and 10 Vol% of PZT.

The PVDF/PZT composites were then subjected to ATR-FTIR measurements to study the polymorphism of the polymer matrix.

In Figure 4.16 the infrared spectra of the composites from melt blending and solvent casting are reported (spectra of neat PVDF are reported for comparison).

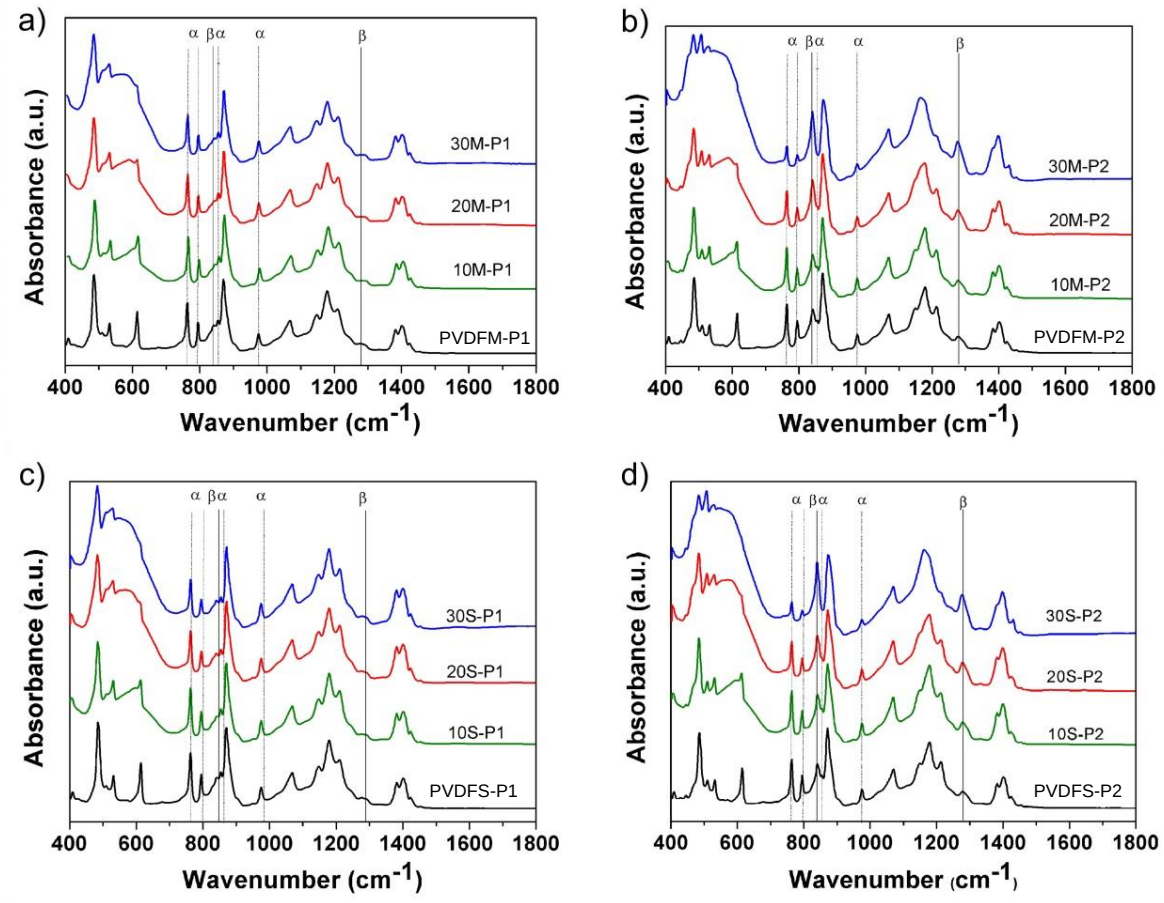

Figure 4.16: ATR-FITR spectra of the PVDF/PZT composites prepared by melt blending and solvent casting: a) XM-P1 and b) XM-P2; c) XS-P1 and d) XS-P2.

In the composites moulded by SS method (P1-samples), PVDF tends to crystallize predominantly as α phase, regardless of the PZT powder content and the preparation technique. On the contrary, in the spectra of the samples obtained from DS moulding (P2-samples) procedure, two peaks are visible at 840 and 1275 cm^{-1}, whose simultaneous presence indicates the formation of the β phase. Moreover, the intensity of these bands tends to increase with the amount of PZT.

The relative fraction of the electroactive phase (F_{EA}) of PVDF, in the present case ascribable only to the β phase, was calculated by using Equation 3.1. The results relative to the composites are reported in Table 4.5.

The β phase amount in the samples prepared by the SS method is about 30%, irrespective of the composition and preparation method (M or S). Its value increases for the composites obtained by DS moulding, reaching about 40% for the samples containing 10 Vol% PZT (10M-P2 and 10S-P2), 50% for the samples containing 20 Vol% PZT (20M-P2 and 20S-P2) and 70% for the composites containing 30 Vol% PZT (30M-P2 and 30S-P2).

Table 4.5: Relative amount of electroactive phase (coincident in this case with β phase) in the PVDF/PZT composites. For the sake of clarity, it is here recalled that the obtained values for the films of neat PVDF are F_{EA} = 29% and F_{EA} = 38% for samples moulded by SS and DS method, respectively.

Samples from melt blending	***F_{EA} (%)***	**Samples from solvent casting**	***F_{EA} (%)***
10M-P1	35	10S-P1	28
20M-P1	32	20S-P1	32
30M-P1	35	30S-P1	33
10M-P2	42	10S-P2	44
20M-P2	53	20S-P2	52
30M-P2	69	30S-P2	71

The F_{EA} value expresses the content of electroactive polymorphs with respect to the total crystalline phase present in the sample. Thus, taking into account that the calculated crystallinity degree is about 50% for the P1-samples and about 60% for the P2-samples, the absolute β phase content can be considered even higher in the composites obtained from the double-step moulding method.

These results are in accordance with what already observed for the neat PVDF. In particular, the hypothesis of a "rolling-like" effect, by which the local shear stresses, induced in the not completely molten polymer matrix, promote the formation of the β phase, is supported by the fact that the electroactive phase amount also increases with the filler content which, in turn, increases the viscosity of the system and the frictions generated during the compression in the mould.

The PVDF/PZT composites were also characterized from the dielectric point of view; the curves of the real part of permittivity (ε) and the dielectric loss ($tan\delta$) as a function of frequency are shown in Figure 4.17.

The dielectric properties of the pristine PVDF are maintained despite the additional processing consisting of melt blending or solvent casting. As for the reference neat polymer samples, the permittivity is comprised between 9 and 12 in the 1-10^5 Hz frequency range and its variation with frequency is well in line with literature data [172]. The introduction of PZT particles induces an increase of dielectric permittivity with respect to the neat PVDF both for composites from melt blending and those from solvent casting. Thus, in spite of the different dispersion of filler particles achieved through the two different techniques (S or M) of preparation, the dielectric properties of two series of samples are dictated by the subsequent moulding to which they are subjected (SS or DS).

In particular, as already observed for the neat PVDF, at equal composition, the dielectric properties of the composites obtained from DS moulding are enhanced: their dielectric permittivity is higher and dielectric losses are lower at low frequency if compared to those obtained for the composites by SS moulding. It is reasonable to think that the changes in dielectric properties are, at least partially, due to the same reasons described above for the neat polymer (see *Paragraph 4.1.1*). A not completely clear relation is identifiable between the electroactive phase amount and the corresponding permittivity values; as an example, the increase in ε with the DS moulding is higher for the 30M than for the 30S samples, although the F_{EA} values between the two series of composites are comparable. This can be partially ascribed to the experimental error in dielectric measurements but also to other factors coming into play during processing. Guan *et al.* [161] found interesting results by processing PVDF-HFP differently: they prepared copolymer films from solvent casting or melt blending and then stretched them. They observed that the stretched films from melt blending, despite having amount of β phase comparable to that present in the stretched films from solvent casting, possess higher permittivity. This was attributed to a different orientation of the crystals (measured with a 2D WAXD) independently from the polymorphism. They assessed that if the polymer crystals in a film are oriented with their *c*-axes perpendicular to the applied electric field, they exhibited large polarizability because the CF_2 dipole moments are randomly distributed in a plane parallel to the electric field. This hypothesis has not been verified in the case of our composites but it can be taken into account at a speculative level.

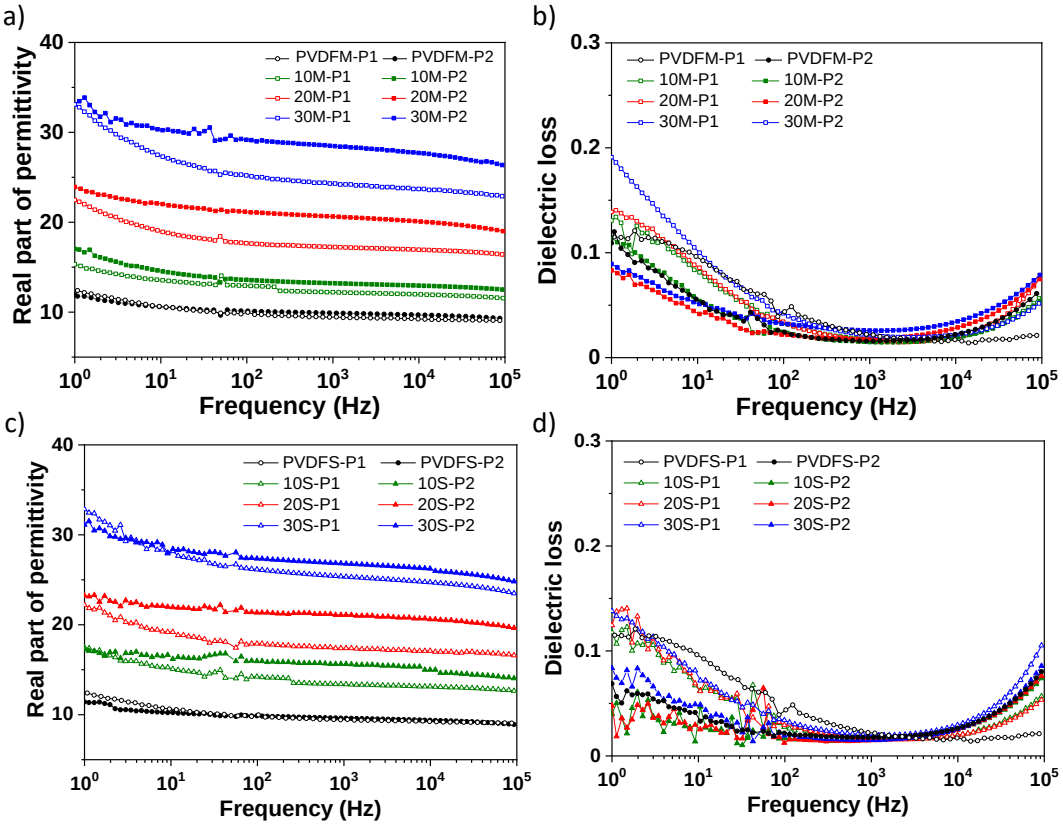

Figure 4.17: Dielectric measurements of the samples: a) real part of permittivity (ε) and b) dielectric loss ($tan\delta$) of composites from melt blending; c) ε and d) $tan\delta$ of composites from solvent casting. Curves of neat PVDF are reported for comparison.

Taking into account that electroactive materials (dielectrics, piezoelectrics, ferroelectrics, multiferroics) are often subjected to mechanical loads (some of them cyclic) in many of their applications, a study of the dynamic-mechanical performance of the prepared composites was also carried out.

Because the additional processing, necessary for the preparation of the composites, can affect the mechanical properties of the polymer matrix, also the reference PVDF films were subjected to DMA measurements. The results obtained for PVDF films from melt blending and solvent casting followed by compression moulding are reported in Figure 4.18. In both cases, the processing necessary to prepare composites leads to a decrease in the mechanical response (Figure 4.18). In particular, *G'* at room temperature is about 1 GPa for the PVDFM-P1, PVDFM-P2, PVDFS-P1 and PVDFS-P2 while results about 6 and 3 GPa for the PVDF directly moulded with the SS or the DS method, respectively. However, the same kind of modifications of the molecular relaxations with the method of moulding are visible from the loss factor.

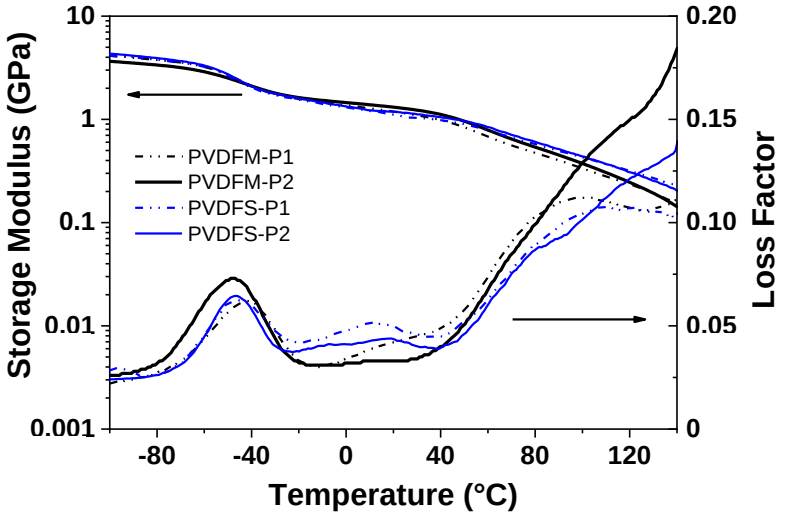

Figure 4.18: Dynamic-mechanical response of the PVDF reference films moulded with the SS and DS methods.

The elastic modulus of the composites results higher with respect to that of the neat PVDF, as expected. However, the increment in *G'* is not monotonic with the composition and is influenced by the composites preparation method, M or S (Figure 4.19).

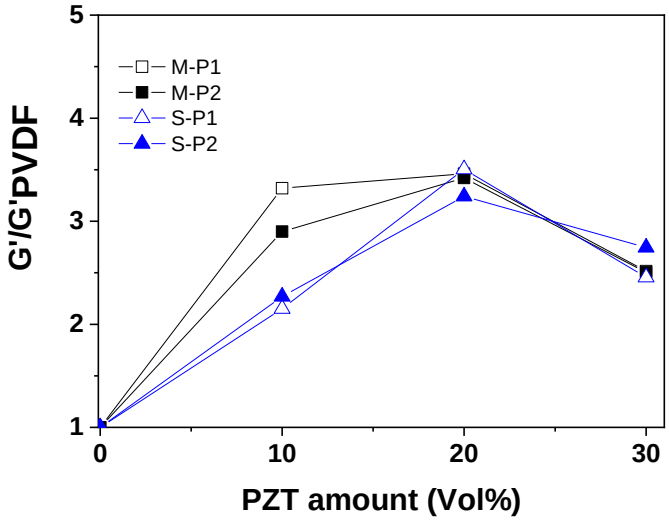

Figure 4.19: Elastic modulus of the samples normalized respect to that of reference PVDF as a function of filler content.

In particular, for the composites from melt blending the elastic modulus triplicates with the introduction of 10 Vol% of filler; while for the composites from solvent casting, an amount of 20 Vol% of PZT is necessary to reach similar values. The observed trend suggests a different position of the percolation threshold between the two series of composites (*i.e.,* M or S). Theoretically, a percolation threshold of about 0.16 (the so-called Sher-Zallen invariant) has been accepted for an homogeneous composite containing fillers of spherical shape and similar size [173]. However, in practice, this is not always observed due to the numerous factors involved that can affect a real system. Indeed, the percolation threshold is strongly dependent on filler geometric parameters such

as particle size, shape and orientation, on a number of characteristics of the polymer matrix such as viscosity, crystallization degree and polarity and mainly on the microstructure of the composite. In this case the different threshold are determined by the different preparation technique and, in turn, by the different dispersion of particles in the polymer matrix.

A change in the percolation threshold depending on the processing strategy was already found by J.G. Meier *et al.* in elastomeric composites containing CNTs [174].

The dynamic-mechanical loss factor curves recorded as a function of temperature for the composites are reported in Figure 4.20.

The introduction of the PZT powder determines a change in the molecular motions of the PVDF matrix. The intensity of the peak relative to the glass transition is lower for the composites with respect to that observed for the neat PVDF and a relaxation process, which is not present in the neat polymer, takes place centred at about -10°C. Such a peak, present in all the composites regardless of the preparation technique and moulding method, is probably associable to a molecular movement induced by the presence of the filler.

The method of moulding also affects the molecular relaxations at high temperature: a peak (XM-P1 samples) or a shoulder (XS-P1 samples), clearly visible for the samples prepared by the SS method at about 100°C and ascribable to the α_c, become less visible for the samples obtained from DS method; the curves of the XM-P2 and XS-P2 samples are steeper at high temperature and reach higher values of loss factor, showing a trend similar to that observed for the neat polymer.

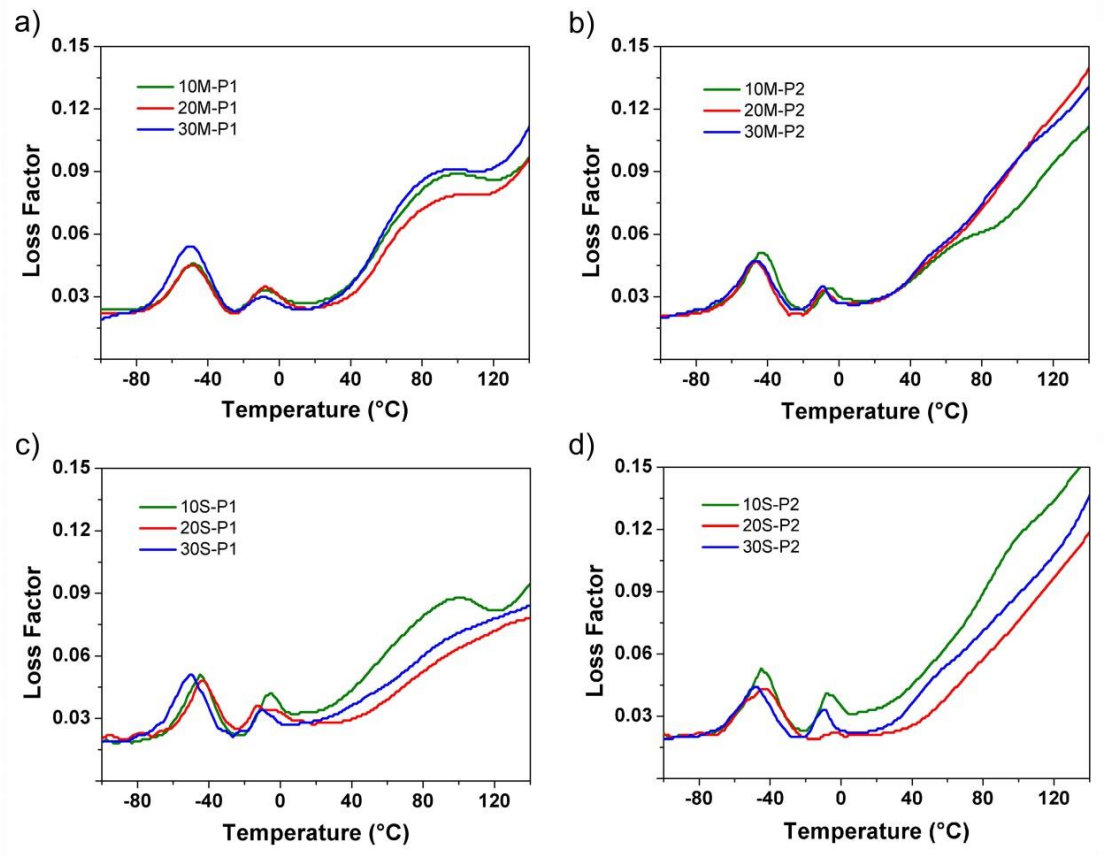

Figure 4.20: $tan\delta_G$ *vs* temperature of samples: a) XM-P1; b) XM-P2; c) XS-P1 and d) XS-P2

Gathered results indicate that the different moulding processes have a much stronger effect on the formation of PVDF crystalline phases, dielectric response and molecular relaxations of the composite materials with respect to the preparation techniques, which rather influence the filler dispersion in the polymer matrix. The double-step moulding was extended to PVDF/PZT composites giving the same consequences evidenced for the neat PVDF. In particular, despite the different (and less homogeneous) morphology, the composites from melt blending possess dielectric characteristics that are similar, or in some cases superior, with respect to those of composites obtained from solvent casting; furthermore, in both the series of samples, the performances are improved by the double-step moulding. This thorough investigation has interesting consequences because it opens the possibility of *(i)* preparing performing polymer-ceramics composites through an easily scalable and solvent-free technique and *(ii)* improving their dielectric properties by simply tuning the moulding conditions.

Taking into account all this, by exploiting the combination of the melt blending technique with the double-step moulding, it was decided to employ another type of filler commonly used in the field of energy storage (*i.e.* $BaTiO_3$) in order to obtain more sustainable dielectric PVDF-based composites at the same time endowed with enhanced ultimate properties.

4.1.4 Improved dielectric properties of PVDF – $BaTiO_3$ composites by solvent-free processing

---

E. Brunengo, M. Castellano, L. Conzatti, I. Schizzi, C. Costa, M.T. Buscaglia, G. Canu, L. Curecheriu, L. Padurariu, L. Mitoseriu, P. Stagnaro, V. Buscaglia

"Improved dielectric properties of PVDF–$BaTiO_3$ composites by solvent-free processing"

Journal of Applied Polymer Science (2021) 138:e50049
DOI: 10.1002/app.50049.

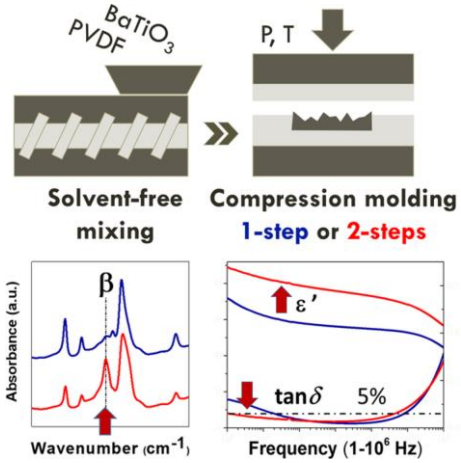

This paragraph is taken from the published work E. Brunengo *et al.* [175].
As already discussed in *Paragraph 3.4* the use of fabrication technologies based on polymer melting is rarely found in the literature related to the preparation of dielectric composites, although

such polymer-melt-based technologies would be preferable for economic and environmental reasons, as they avoid the use of costly if not harmful solvents and enable a facile scale-up in view of industrial production (*e.g.*, extrusion, compression moulding). It is worth remembering that neat polymer films used for industrial manufacturing of film capacitors are fabricated by a solvent-free extrusion and stretching process [176,177].

PVDF-based composites containing either 10 or 30 Vol% of $BaTiO_3$ (BT) nanoparticles (of about 125 nm) were prepared by melt blending followed by compression moulding using both the SS (200°C, 50 bar, 4 min) and the DS (200°C, 50 bar, 4 min and then 170°C, 240 bar, 4 min) method previously described. The resulting composites were labelled as xBM-P1 or xBM-P1, where x is the volume percentage of $BaTiO_3$ inclusions (B in the composite sample label), M indicates the melt blending preparation, P1 and P2 are referred, respectively, to the adopted SS or DS moulding procedure.

A thorough characterization of the prepared PVDF/$BaTiO_3$ composites was carried out, with particular attention to the dielectric response and the study of molecular motions, which was deepened by correlating the results from dynamic-mechanical analysis and dielectric spectroscopy.

SEM micrographs of the DS-moulded composites are shown in Figure 4.21. The images of the cryo-fractures reveal a fine dispersion of BT nanoparticles in the PVDF matrix, with rare aggregates of dimensions lower than 50 μm.

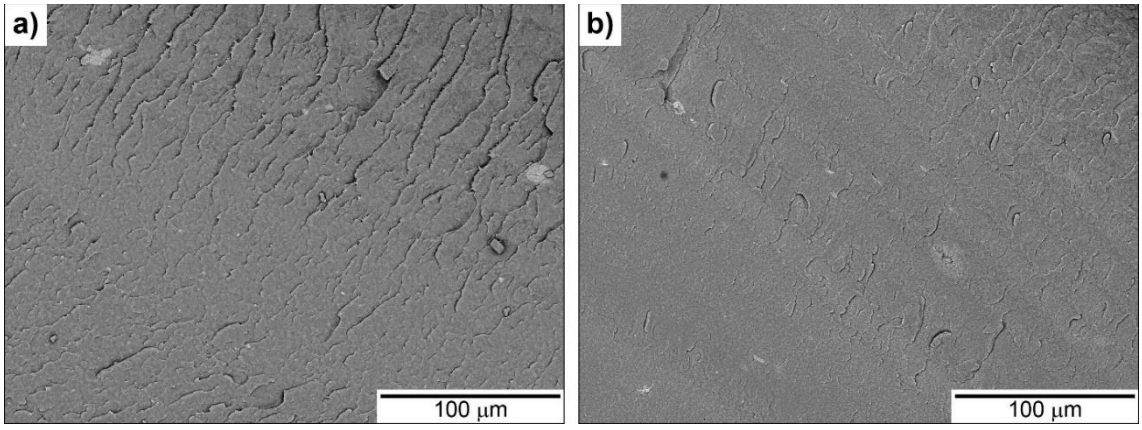

Figure 4.21: SEM micrographs of fragile fractures of the composites with: a) 10 Vol% or b) 30 Vol% BT moulded with the SS method.

Higher magnification SEM images (Figure 4.22a), taken in backscattering mode, confirm that BT nanoparticles are well dispersed and suggest that BT aggregates are loosely packed and permeated by the polymer matrix (Figure 4.22b).

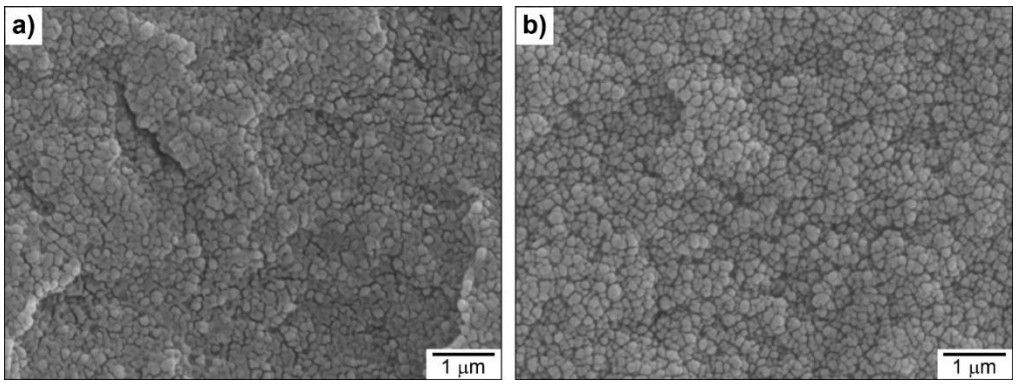

Figure 4.22: SEM backscattering micrographs of fragile fractures of the 30BM-P1 composite taken a) outside an aggregate b) inside an aggregate.

This observation is supported by SEM-EDX analysis: a significant amount of fluorine, characteristic of the PVDF matrix, is found well distributed within the BT aggregates. As an example, in Figure 4.23 the elemental mapping (fluorine, titanium, barium) recorded for 30BM-P1 sample is shown. It is worth noticing that the aggregates also show a very diffuse boundary (Figure 4.23a).

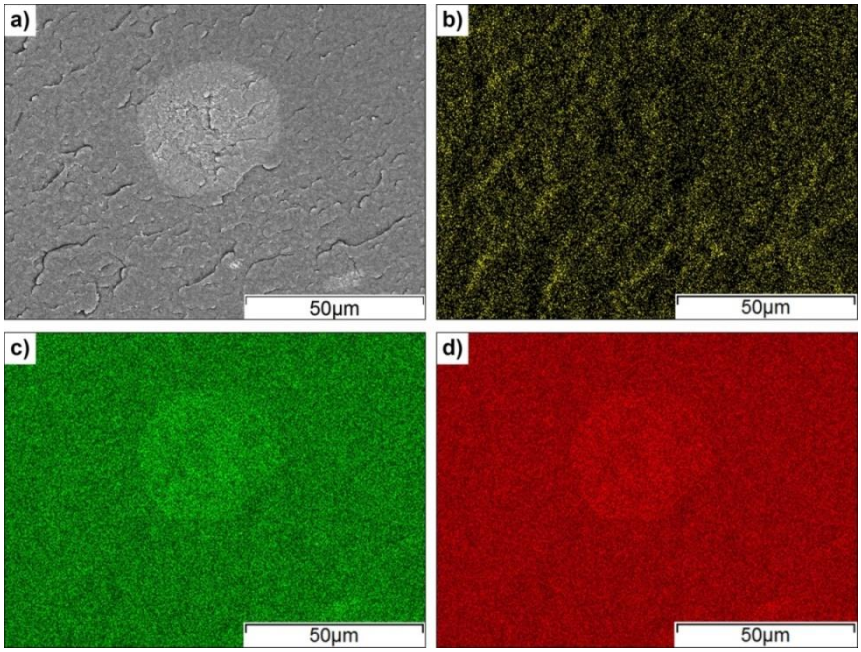

Figure 4.23: SEM-EDX analysis of 30BM-P1 sample. a) Morphology of the sample. Elemental maps of: b) fluorine, c) titanium and d) barium.

ATR-FTIR analysis was then carried out for evaluating the relative fraction of the electroactive phase (F_{EA}) of PVDF. In the composite samples processed through the SS method, only crystallization occurs predominantly in the α form (Figure 4.24a). Irrespective of the composition, the values of F_{EA} are around 30% and, since the degree of crystallinity, measured from DSC, is around 50%, the corresponding F_{EA}* amount is about 15% for all the films obtained by SS moulding (Table 4.6).

The double-step process promotes the formation of the β phase, which is also favoured by the presence of the inorganic particles (see Figure 4.24b and Table 4.6), according to the results obtained for PVDF/PZT composites. In particular, the amount of β phase increases by reaching values of F_{EA} higher than 60% and F_{EA}* higher than 30% for the composite containing 30 Vol% of BT nanoparticles.

Table 4.6: Temperature of the second step moulding (T_2), crystallinity degree (X_C), relative and absolute fraction of electroactive phase(s) (F_{EA} and F_{EA}*) of PVDF/BT composites. The corresponding results of the reference PVDF films from melt blending are reported for sake of clarity.

Sample	T_2 (°C)	X_C (%)	F_{EA} (%)	F_{EA}* (%)
PVDFM-P1	170	53	29	15
PVDFM-P2	170	58	38	22
10BM-P1	170	53	28	15
10BM-P2	170	57	54	31
30BM-P1	170	50	31	16
30BM-P2	170	52	66	34

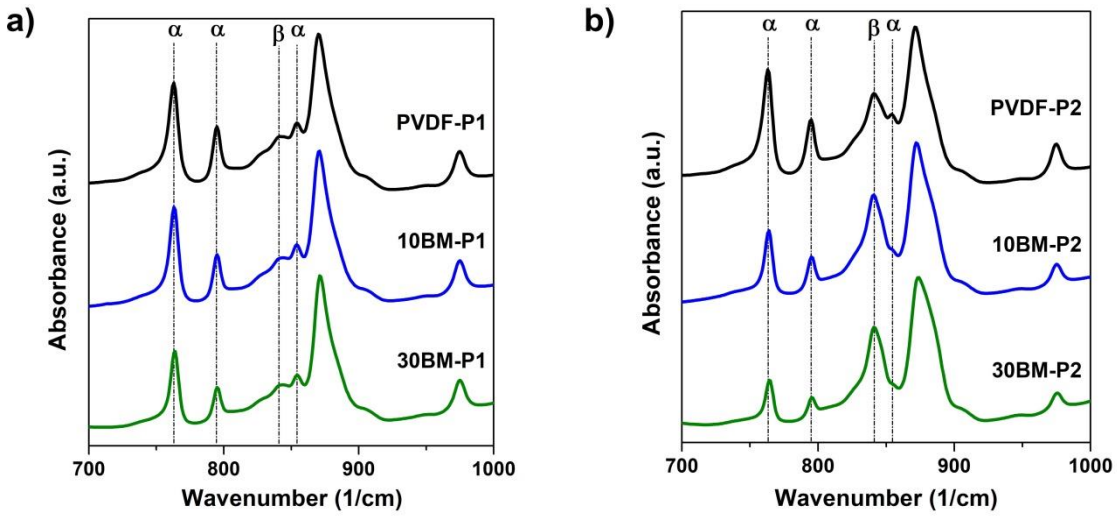

Figure 4.24: ATR-FTIR spectra of PVDF/BT composites compression moulded with: a) single-step moulding; b) double-step moulding. The corresponding spectra of the PVDF are reported for reference purpose.

Low magnification SEM images of samples with 10 and 30 Vol% BT nanoparticles obtained by double-step moulding, *i.e.*, samples 10BM-P2 and 30BM-P2, are shown in Figure 4.25. As found for the corresponding 10BM-P1 and 30BM-P1 samples, a good dispersion of the BT particles is obtained. However, the spherical aggregates, appear in this case elongated, especially for the

30BM-P2 sample. This indicates that the polymer penetrated in the BT powder aggregates (of roughly equiaxial shape) found in the composite films prepared with a single-step moulding makes them deformable and, when the composites are moulded through the double-step process, the aggregates tend to stretch and align because of the internal stresses originated by the high pressure applied to the only partially molten matrix.

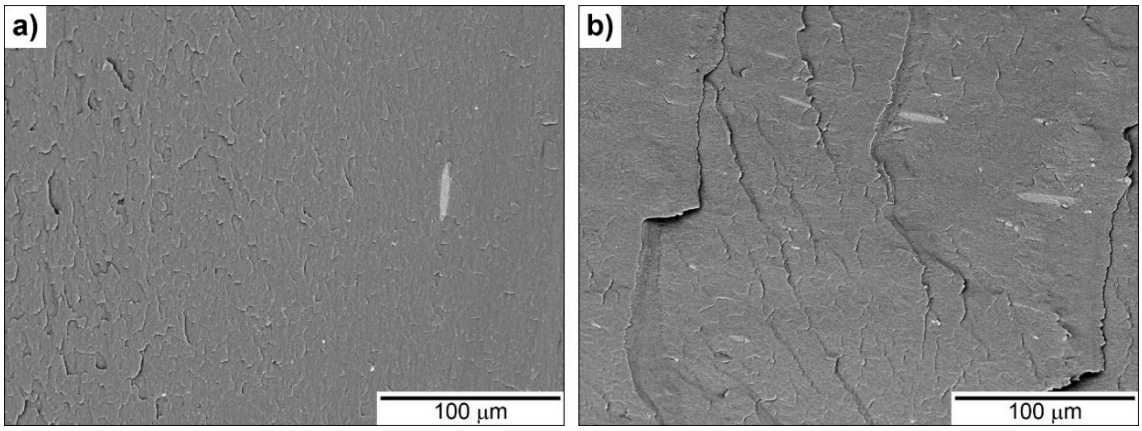

Figure 4.25: SEM micrographs of fragile fractures of the composites with: a) 10 Vol% or b) 30 Vol% BT moulded with the DS method.

A DMA characterization was carried out on these PVDF-based composites to evaluate the effect of *(i)* BT nanoparticles amount and *(ii)* moulding conditions on the PVDF macromolecular mobility. The resulting temperature dependence of the elastic component (*G'*) of the mechanical modulus and the corresponding loss tangent ($tan\delta_G$) are shown in Figure 4.26.

The curves of *G'* reported in Figure 4.26a indicate an increasing reinforcing effect by increasing the amount of BT nanoparticles. For example, the *G'* values at 25°C for PVDFM-P1, 10BM-P1 and 30MP-P1 are about 1140, 1580 and 2700 MPa, respectively; thus, the introduction of 10 or 30 Vol% of ceramic inclusions leads to an increase in the storage modulus of 39 or 137%, respectively, compared to the neat PVDF.

As concerns the samples moulded by SS method, the curves of $tan\delta_G$ obtained for the composites show all the three main relaxations already described for the neat PVDF (Figure 4.26b). The composites show β relaxation peaks lower in intensity than those of the reference polymeric film; in particular, the peak intensity decreases by increasing the amount of BT nanoparticles. As suggested by F.S. Mendes *et al.* [152], this can be ascribed to a low dissipation of mechanical energy due to the presence of ceramic inclusions that hinder the cooperative motions of polymer chains within the amorphous phase. This effect of restriction in mobility can also be observed at higher temperatures: in the samples moulded by SS method, the transitions above T_g are less visible for composites than for the reference polymer. By comparing the curves obtained for samples with the same amount of BT nanoparticles but moulded through the two different processing conditions, in the case of samples moulded by DS method, the broad relaxation around 25°C becomes less evident and the one above 50°C (α_c relaxation) seems to shift towards higher temperatures.

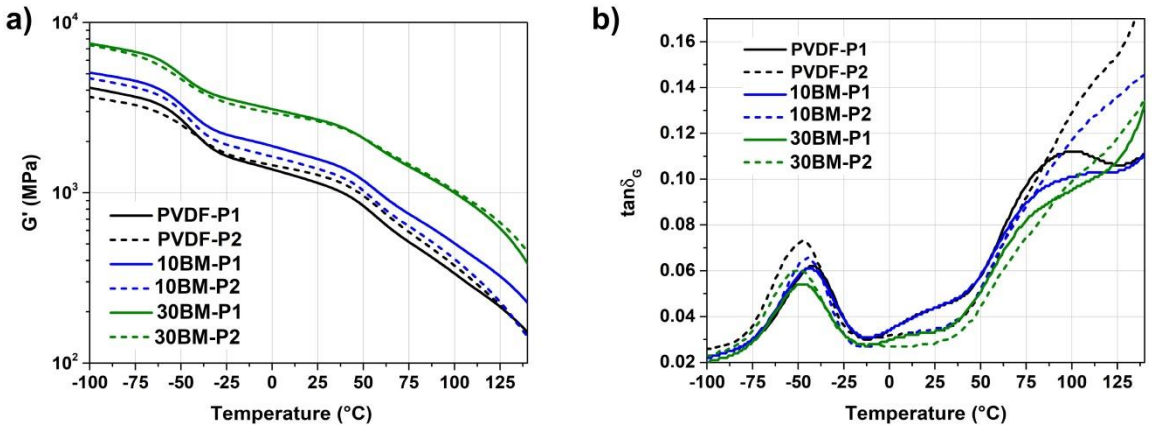

Figure 4.26: Temperature dependence of: a) *G'* and b) $tan\delta_G$ for the PVDF/BT composites moulded with the two methods. The corresponding curves of the PVDF are reported for reference purpose.

The above described dynamic-mechanical features are analogous to those already observed for the neat PVDF films and for the PVDF/PZT composites. In particular, the hypothesis that the effects of the DS moulding method on the molecular relaxation can be attributed to a more oriented and compact polymeric structure obtained upon the re-pressing, is here supported at the macroscopic level by SEM analysis (see Figure 4.25).

The dielectric properties were measured in the 1 Hz - 1 MHz frequency range at room temperature for all the samples.

For all the compositions, the permittivity curves are relatively flat over the explored frequency range, with a slight increase at low frequency, due to extrinsic contributions (Figure 4.27a).

For the samples processed in SS conditions, an increase in permittivity in the presence of the ferroelectric BT particles is observed with respect to the neat PVDF; the values at 1 kHz for PVDFM-P1, 10BM-P1 and 30BM-P1 samples are 9, 13 and 28, respectively, and are comparable to literature values [178,179] found for analogous samples obtained from solution casting. This suggests that good dielectric performances can be obtained with a smart solvent-free and easily scalable technique. It is worth noting that, while the inclusion of 10 Vol% nanoparticles in the polymer matrix results in a moderate increase of ε, the permittivity increases by a factor of three compared to the neat PVDF when the load is 30 Vol%.

The impact of moulding processing on permittivity depends on the volume fraction of BT inclusions. In the case of composites with 10 Vol% BT, the permittivity is only slightly larger for the sample moulded with DS method than for that moulded with the SS method. In contrast, for the composite with 30 Vol% BT inclusions moulded in DS conditions, the value of permittivity increases significantly from 28 to 38 at 1 kHz.

In *Paragraph 4.1.1. and 4.1.2* the increasing of permittivity induced by the DS moulding was ascribed to the increasing of electroactive phase amount in PVDF and PVDF-HFP, respectively. This behaviour has been already observed in the literature for neat PVDF [128,129,172]. By considering that the amount of β phase in 30BM-P2 is higher than in the 10BM-P2 sample, but not

so higher to justify such a difference in the permittivity values, this suggests that, in this case, the increase cannot be ascribed exclusively to the increase of F_{EA}.

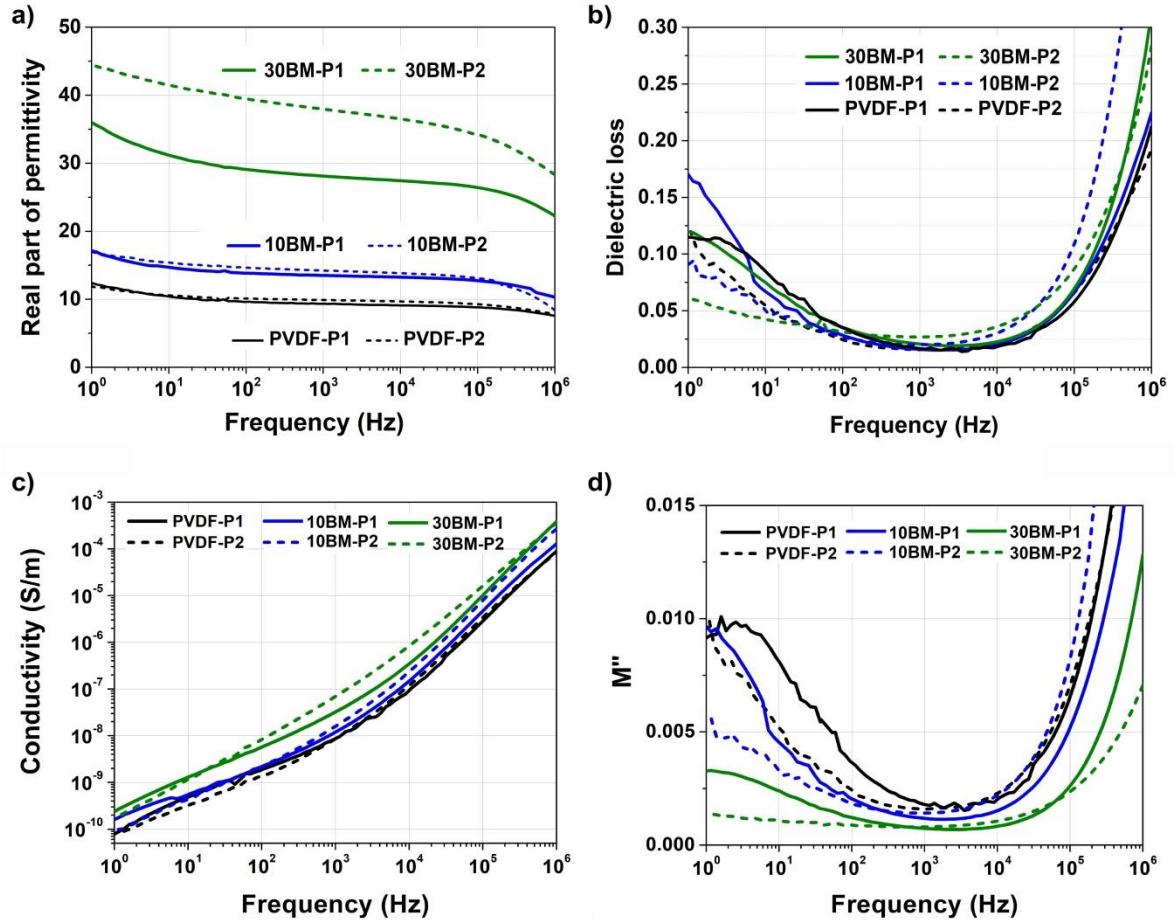

Figure 4.27: a) Real part of permittivity, b) dielectric loss, c) ac-conductivity and d) imaginary part of the dielectric modulus for PVDF and PVDF/BT composites as a function of frequency, at room temperature.

In *Paragraph 4.1.3* the variation in dielectric permittivity of the PVDF/PZT composites was attributed to the polymer matrix polymorphism, but without excluding other influencing factors related to the reciprocal orientation between the polymer crystals and the applied dielectric field.

In the case of PVDF/BT composites a similar phenomenon may occur leading to the remarkable permittivity increase observed for the 30BM-P2 composite. To support this hypothesis, we have nothing else the experimental evidence that the combination of melt blending and suitable conditions for compression moulding leads to composites characterized by an improved quality that results in higher permittivity and lower losses, as discussed in the following.

Dielectric losses (Figure 4.27b) are, in general, larger for the composites compared to neat PVDF films. They show a moderate increase at low frequencies, resulting however relatively low, *i.e.* lower than 17%, in the 1-10^5 Hz frequency range. In all cases, the samples moulded with DS processing benefit of a decrease of dielectric losses at low frequency. The small increase in permittivity associated with an increase of loss tangent at low frequency is usually ascribed to interfacial polarisation [180]; the reduced losses at low frequency (< 100 Hz) measured for P2

composites support the hypothesis that the double-step processing improves the overall quality of the samples. It is worth pointing out the low general values of losses when moulding with the DS process: tanδ is lower than 5% in the frequency range from 10 to $3 \cdot 10^4$ Hz.

Furtherly, it is worth noticing the samples show stable dielectric properties with time after storage in air: indeed, by comparing the permittivity and losses of the samples as prepared and after two months, the permittivity data are very similar and only a slight decrease of *tanδ* at high frequency is observed, indicating limited aging. The two curves for 30BM-P2 are reported in *Appendix C* as an example.

Usually, the presence of filler in the polymer matrix tends to result in a conductivity increase in related PVDF-based composites [181]. However, irrespective of composition, all the present samples processed in both SS and DS conditions show a remarkable low conductivity, not saturated yet to the value characteristic of the dc conductivity plateau, meaning that their dc conductivities would be below 10^{-10} S/m (Figure 4.27c). The increase of losses (Figure 4.27b) as well as of the imaginary part of dielectric modulus (Figure 4.27d) both at ultralow frequencies (below 100 Hz) and above 100 kHz indicates at least two distinct relaxation mechanisms. Since they are present in both neat PVDF samples and composites, they are originated from the polymer chain field-induced movements.

The study of the relaxation mechanisms was deepened by measuring the dielectric properties as a function of temperature and as a function of frequency at different temperatures. The temperature dependence of permittivity at few selected frequencies (Figure 4.28a,c,e) shows a maximum in the range of 90-120°C, which is more intense in the composites with higher amount of filler for all the frequencies and less visible at high frequencies for the composites produced by SS processing. This feature was observed in other PVDF-based composites and considered related to wide angle oscillation of dipoles, followed by their rotation with main chain cooperation appearing in the crystalline phase [182–184].

For the samples 10BM-P1 and mostly for 30BM-P1, another weak and broad maximum around 60°C is noticed (measurement at 1 MHz, Figure 4.28e); the same peak is probably also present for the P2 films at this frequency and shifted at higher temperature (around 80°C), but it is difficult to be distinguished because its broadness, small intensity and its overlapping with the previous described peak. This maximum is a known PVDF relaxation (γ), whose origin has been related to an interfacial polarisation of the amorphous-crystalline boundaries, and to folding movements of the amorphous regions of the polymer matrix [150]. The two maxima in the temperature dependence of permittivity indicate the existence of two dielectric relaxation processes whose characteristic frequency changes with temperature, that might be related to the phenomena observed at low frequency in the dynamic-mechanical experiment, in the same temperature range.

In agreement with DMA results, also with dielectric spectroscopy a shift of the relaxations at higher temperatures was observed for the samples from DS moulding with respect to those from SS moulding. This could be related to a higher level of orientation of the polymeric chains.

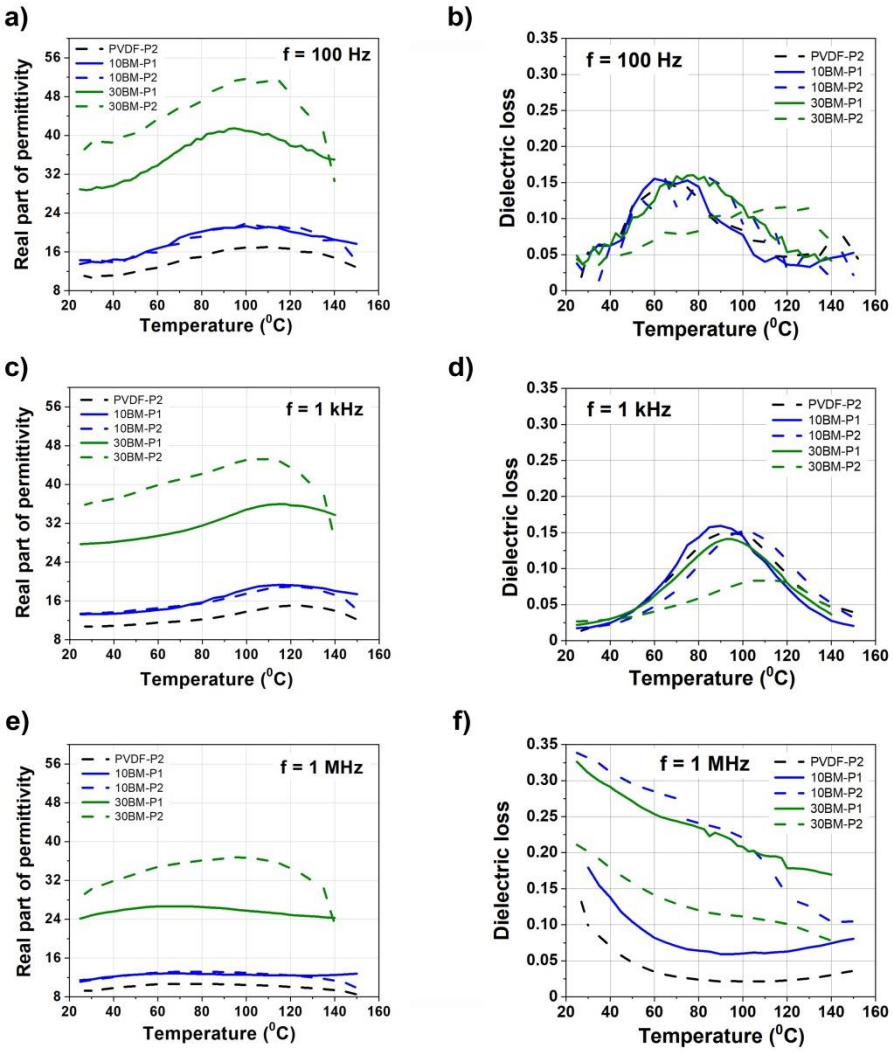

Figure 4.28: Comparative dependence of: a,c,e) the real part of permittivity and; b,d,f) dielectric losses for all the composites on temperature at a few selected frequencies: a,b) 100 Hz; c,d) 1 kHz; e,f) 1 MHz. PVDFM-P2 is reported as a reference sample.

Frequency dependences of the dielectric properties at different temperature are reported in Figure 4.29 for the samples moulded with the DS method.

The role of filler addition on the dielectric relaxations can be observed. For all the temperatures in the investigated frequency range, the filler addition contributes to an increase of permittivity (Figure 4.29a-c), which, however, is also due to extrinsic contributions, as demonstrated by the evolution of the imaginary part of permittivity (Figure 4.29d-f) and dielectric modulus (Figure 4.29g-i).

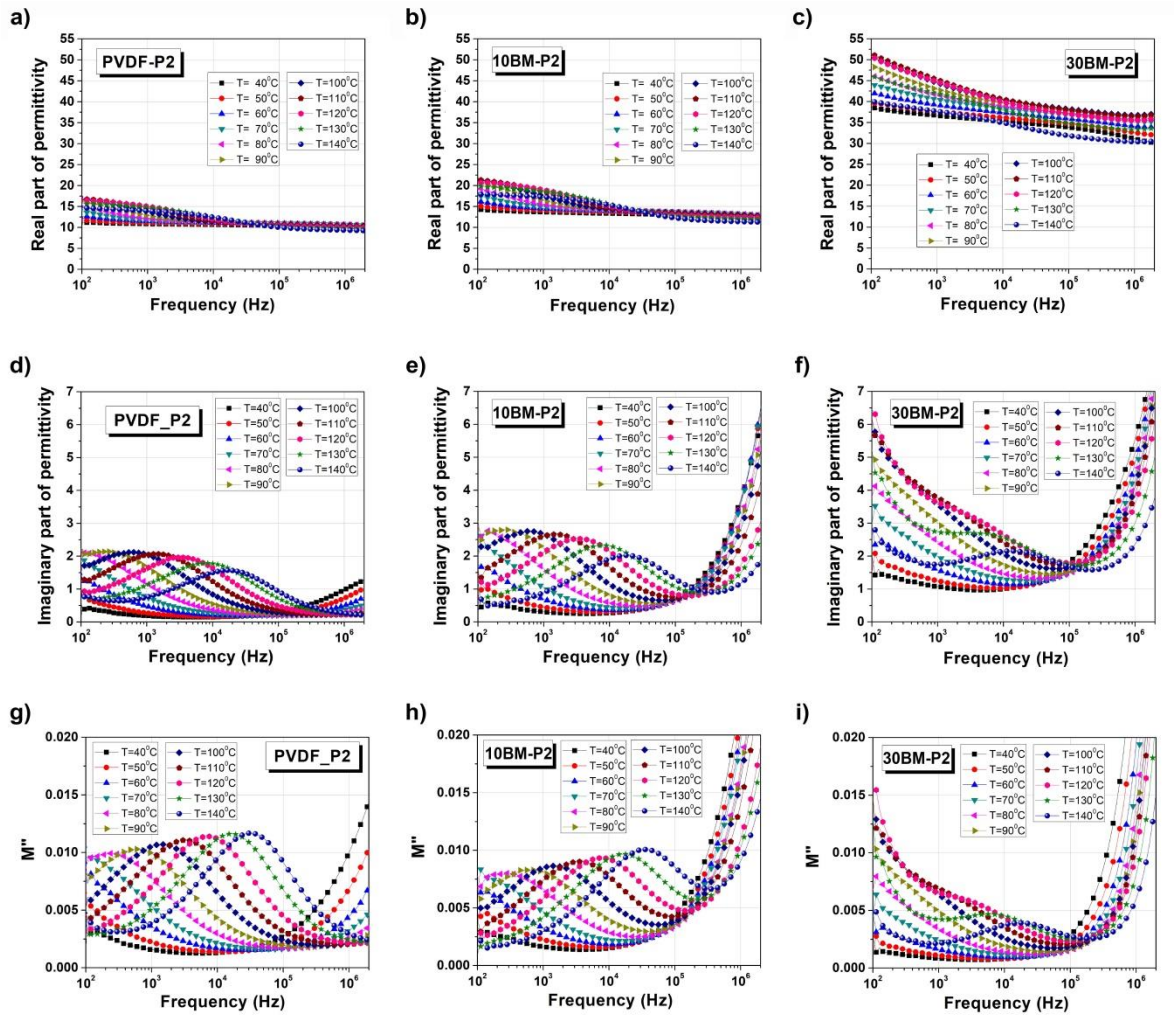

Figure 4.29: Dielectric properties of samples produced by double-step moulding as a function of frequency at selected temperatures: a-c) real part of permittivity, d-f) imaginary part of permittivity, g-i) imaginary part of the dielectric modulus, for neat PVDF and composites with 10 and 30 Vol% of BT particles.

Besides the thermally activated relaxation in the intermediate frequency range 500-10^5 Hz exhibited by all the composites and neat PVDF, a strong increase of the imaginary part of permittivity both at low frequencies (below 500 Hz, Figure 4.29f) and above 10^6 Hz (Figure 4.29e,f) is clearly promoted by the presence of the filler. All the three relaxations are also visible in the spectra of *M"* (Figure 4.29i), which means that they represent thermally activated dielectric relaxation phenomena (not related to conductivity). The high-frequency phenomenon (> 10^6 Hz) was assigned, in the literature, to a dielectric manifestation of the glass transition temperature of PVDF related to the micro-Brownian cooperative segmental motions of the polymer backbone [185]; this phenomenon, which is only slightly observed for the neat PVDF due to the instrumental frequency limit, is shifted towards lower frequencies when increasing the filler load. This can be explained, in agreement with DMA results, by the strong limitation of the chain movement determined by the presence of $BaTiO_3$ nanoparticles. The low-frequency phenomenon is usually assigned to slow interfacial polarisation, or Maxwell–Wagner–Sillars (MWS) mechanism, which is typical of heterogeneous materials, due to local differences in the permittivity and conductivity allowing the trapping of charged ionic or polar species at the interfaces [109]. The semicrystalline PVDF matrix

contains inhomogeneities related to the presence of both amorphous and crystalline regions as well as of α and β chain conformations. The interfacial contribution also increases due to the addition of high permittivity $BaTiO_3$ nanoparticles, as observed by the strong increase of the low-frequency imaginary part of permittivity in 30MB-P2 sample, that overlaps to the middle frequency relaxation maxima (Figure 4.29f).

The intermediate frequency range relaxation occurring in the 10^2-10^5 Hz frequency range, characterized by thermally activated maxima of the imaginary parts of both permittivity and dielectric modulus (Figure 4.29d-i), was observed in neat PVDF and PVDF-based composites [109,186] and seems to be reduced for the high filler content (Figure 4.29f,i). This dispersion is also accompanied by an inflexion of the real part of permittivity and is considered related to an intrinsic dipolar relaxation of PVDF matrix [109,186,187]. The activation energy computed from Arrhenius plots gives values of ~1.10 eV for all the composites, slightly higher than 0.96 eV, which was determined for the neat PVDF. Such values are similar to the ones reported by Chanmal [109], that were assigned to a MWS faster process.

It must be considered that there is no full agreement with respect to the assignment of dielectric relaxations mechanisms in such complex, from the electrical point of view, PVDF-based composites. However, changes in the molecular relaxations of the PVDF matrix with the double-step moulding process and the introduction of the ceramic filler were evidenced both from DMA and dielectric measurements and good accordance were found, despite the different techniques used, and consequently, the different ways to induce the molecular movements.

4.2 Influence of particles coating and dimension on the dielectric properties of the composites

The second part of this work deals with the study of the influence of ceramic particle coating and dimension on the dielectric properties of the composites.

As in other types of composites, also for dielectric composites, amount, dimension, morphology of particles or nanoparticles, as well as polymer/filler interface, are very important factors in determining dielectric properties (as well as other ultimate properties) of the resulting composites.

Many theoretical approaches have been developed to predict the effective dielectric constant of polymer composite systems, that depends on the intrinsic permittivity of the filler and the polymer matrix but can also be affected to extrinsic factors such as the interactions between the components [6,188]. Besides simple models which consider the constituents of composites and nanocomposites as two different phases or treat the filler particles as inclusions in a continuous phase of polymeric matrix [189], there are many theoretical works which take into account the role of the particle/polymer interface in determining the performance of such dielectric materials [190].

Obviously, the role of interfaces depends on their extension: they are more important if the filler dimensions are in the nanometric than in the micrometric scale.

The dielectric properties of interfaces differ from the dielectric properties of either the filler or the polymer matrix and are determined by both the morphology and the charge/polarization distributions around the interface. In fact, as a consequence of the difference in Fermi levels or chemical potential between filler and matrix, part of the whole particle surface gets charged resulting in the formation of an electrical double layer in the polymer matrix, consisting of a layer of counterions (*i.e.,* Stern layer) and an external diffuse layer of negative and positive charges.

When the composite material is subjected to an external electric field, the polarization processes occurring in the filler and in the matrix enhances the electrical fields in the double layers, leading to increased polarization, conduction processes around the interfaces and possible formation of weak points which can cause the breakdown. This implies the need to take measures to modulate the interfaces and thus limits the dielectric losses and contrast reduction of the breakdown strength.

Surface modification of micro- or nanofillers is an effective approach to form robust interfaces and/or to control the charge and dipole distribution around them.

Among envisaged chemical methods, the treatment with coupling agents is the most popular and easiest to be applied. The minimization of particle-particle interactions and the enhancement of particle-polymer interactions, *(i)* improve the filler dispersion, *(ii)* enhance the mechanical performance and *(iii)* can suppress the dielectric loss at the interfaces [191]. Another useful approach is the formation of a "diffuse interface" which provides a more homogeneous distribution of the electric field in the nanocomposite material, mitigating the electric field enhancement at the interfaces: a gradient in ε can be obtained by coating nanoparticles with a polymer [192,193] or another inorganic material [194–197] characterized by a dielectric constant lower than that of the filler itself but higher than that of the matrix. The obtainment of a core-shell structure is also fundamental in the case of conductive nanoparticles (*e.g.,* Ag) because it prevents their direct connection near to the percolation threshold [173,198,199].

Another factor playing an important role in determining the dielectric behaviour of composites and nanocomposites is the size of inorganic particles/nanoparticles used. In particular, in the case of $BaTiO_3$, it is well known that the dielectric properties of the bulk ceramics depend strongly on the size of the crystallites which in turn influences the domain configuration and phase transitions [91,92,94]. $BaTiO_3$ ceramics usually shows a permittivity maximum at a grain size of about 1 μm; such a trend has been interpreted as the superposition of two contrasting contributions: the dilution effect of the grain boundaries, which is predominant for small grain size (<1 μm), and the domain size and mobility, which is the more determining factor for coarse grains (>1 μm) [94,200,201].

Despite the grain size effect in $BaTiO_3$ ceramics is now clear, the effect of particle size on dielectric properties of $BaTiO_3$/polymer composites is poorly understood because they can be

influenced not only by the intrinsic characteristics of the filler but also by its surface and interface with the polymer matrix.

The dimension of BT particles determine the crystalline phase: when the diameter is too small, $BaTiO_3$ tends to crystallize in its cubic form while a transformation into the tetragonal and ferroelectric phase occurs at room temperature for higher particle dimensions. A rather wide range of critical size values has been reported for isolated equiaxed particles: some authors individuate this critical dimension as 10-20 nm, other as 30 nm, other as 44 nm [30,201,202]. T. Hoshina measured the dielectric permittivity of different BT particles slurries and found a maximum for particles around 140 nm size. The author explained this behaviour by supposing the existence of three regions in the particle structure: an inner tetragonal core, a surface cubic layer and an intermediate "gradient lattice strain layer" (GLSL) characterized by high permittivity [203]. In general, the critical size for ferroelectricity is strictly dependent on the synthesis method, which in turn affects the concentration of defects (impurities, lattice defects, nanopores, etc.), as well as on the technique used to analyze the particles [201].

Besides the properties of the particles, also the presence of the polymer matrix has to be considered: indeed, composites containing small cubic nanoparticles often present dielectric permittivity higher than that of composites containing bigger and partially tetragonal particles. This is due to the Maxwell-Wagner polarization [30,204–206] which occurs at low frequency, where extrinsic interfacial phenomena tend to be predominant. In this regard, B.-H. Fan *et al.* prepared by solvent casting PVDF/BT composites containing 50 Vol% of ceramic filler with different dimension and found, after a treatment of cooling to -40°C and subsequent heating to room temperature, a decreasing of permittivity at low frequency, especially in the composite containing the smaller particles (diameter in the range 30-50 nm); they ascribe this evidence to the destruction of interfacial charge accumulation due to the thermal motions induced during the heating run [30]. However, the same authors, by preparing analogous composites but using a thermoset polyimide as polymer matrix, showed that the contribution of the interfacial polarization to the final permittivity also depends on the organic phase nature [207].

In addition, other factors, related to the size of the particles, but independent from their intrinsic or extrinsic properties, can contribute to the dielectric properties of the composite material; as an example, B. Zhou *et al.* found that, by mixing batch of BT particles with different dimensions the dielectric permittivity of the ensuing composite is higher than that of the composites filled with each single batch, because in the former case a denser microstructure and a better film quality is obtained [208].

Moving from the considerations above reported, this part of the research consists of:

- the preparation and characterization of composites containing $BaTiO_3$ particles coated with shells of SiO_2 or TiO_2 of different thickness in order to study the influence of the

surface coating on the final properties of the composites. Experimental evidence was also compared with the theoretical results obtained from finite element modelling (FEM).

- the preparation and characterization of composites containing bare $BaTiO_3$ particles or core-shell particles of different diameter in order to investigate the influence of particles dimensions on the dielectric response of the obtained materials.
- the preparation and characterization of composites containing $BaTiO_3$ particles functionalized with dodecyl triethoxysilane (DDTES) and 1H,1H,2H,2H-perfluorodecyl triethoxysilane (PFDTES) in order to study how these coupling agents affect the dielectric properties of the resultant composites.

Due to the limited amount of available powders, these composites (all containing 30 Vol% of filler) were obtained by solvent casting (the procedure used is detailed in *Paragraph 3.4.1*).

Furthermore, *(i)* taking into account the positive effect induced by the double-step moulding, in particular by the re-pressing stape, and *(ii)* considering that with the solvent casting technique a film of composite material is directly obtained (as opposed to what happens for the melt blending technique which requires a subsequent moulding to prepare films suitable for the successive characterization), it was decided to test another method of moulding. Specifically, the conditions of the "second step of moulding" in this case were applied directly to the films from solvent casting, which, after drying, were moulded as 170°C, 240 bar, 4 min. In fact, ATR-FTIR analysis of the composites before the moulding revealed that the PVDF matrix tends to crystallize as γ phase upon solvent casting, regardless of the type of filler introduced. Since the dipole moment of γ phase is lower than that of β phase but higher than that of α phase, a method of moulding more direct (*i.e.* just one step of moulding) and that induces the formation of β phase limiting the formation of α phase was considered of potential interest.

This procedure was previously tested with a composite containing 30 Vol% of pristine BT in order to verify its effectiveness before extending the method to other composites. In Figure 4.30 the effect of the different processes on the polymorphism of the PVDF matrix is summarized.

Spectroscopic measurements revealed that the composite directly obtained by moulding at 170°C and 240 bar the film prepared from solvent casting is characterized by the presence of both β and γ ferroelectric phases, probably because this method, avoiding the complete polymer melting, allows the partial conversion of γ phase into β phase, while preventing the increase of the α phase amount.

This film (30BS-P3 in the following) was characterized in order to compare its properties with those of other PVDF/30 Vol% BT films processed with SS or DS moulding (named 30BS-P1 and 30BS-P2, respectively).

Electroactive phase(s) amount and crystallinity degree of the samples are reported in Table 4.7. In this case, because of the contemporary presence of two electroactive phases (*i.e.*, β and γ), the two contributions were distinguished by considering the peak-to-valley height ratio between the two peaks centred around 1275 and 1234 cm^{-1} (see *Paragraph 3.5*). As clearly visible, the 30BS-P3

sample is characterized by a very large overall amount of electroactive phase (about 90%), although it contains a lower β phase quantity with respect to the 30BS-P2 sample.

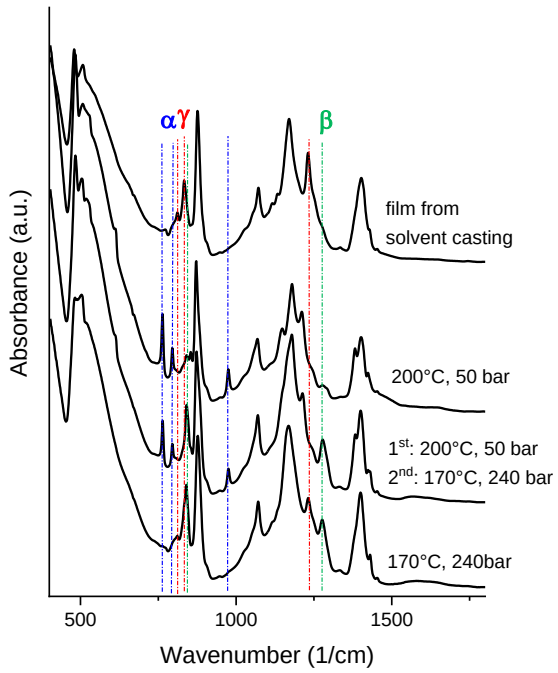

Figure 4.30: ATR-FTIR spectra of PVDF/30 Vol% BT films prepared under different conditions.

Table 4.7: List and characteristics of the PVDF composite samples containing 30 Vol% of BT particles prepared from solvent casting.

Sample	F_{EA} (%)	F_{β} (%)	F_{γ} (%)	X_C (%)
30BS-P1	29	29	-	56
30BS-P2	57	57	-	50
30BS-P3	91	45	46	52

Dielectric spectroscopy measurements revealed, as expected, that 30BS-P2 and 30BS-P3 are characterized by a higher permittivity with respect to 30BS-P1 (Figure 4.31a). However, the double-step moulding is still preferable because it allows to obtain composites with lower losses with respect to those derived by the other methods (Figure 4.31b). This occurs probably because: *(i)* the shear stresses generated inside the material are higher for the DS moulding (the starting sheet is thicker than the film obtained from solvent casting) and *(ii)* the complete polymer melting reached during the first step of moulding may be important to completely eliminate the pores present in the film before the compression treatment and thus consolidate the ensuing composite materials. These observations are in accordance with the hypothesis that the double-step moulding improves the quality of the films, beyond the polymorphism of the matrix.

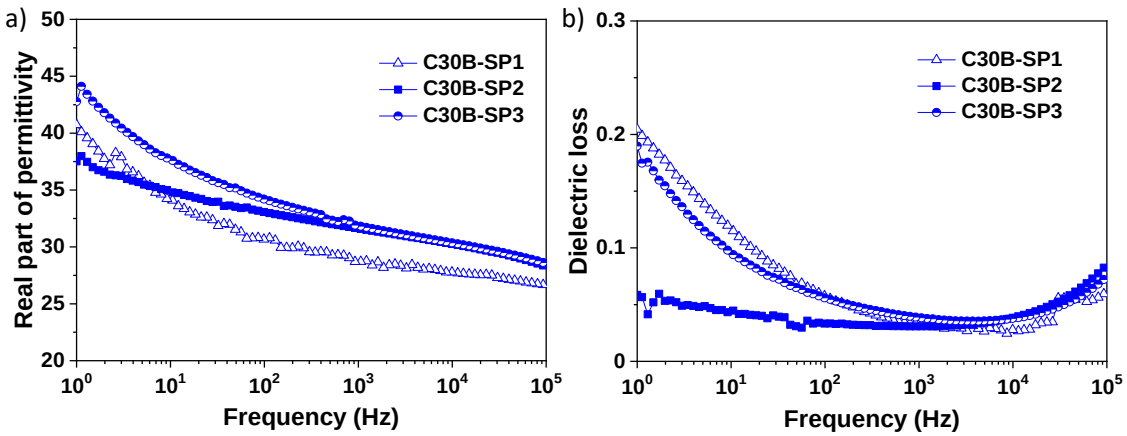

Figure 4.31: a) Real part of permittivity and b) dielectric loss of PVDF/BT composites from solvent casting as a function of the frequency.

Taking into account these results the double-step method was chosen for processing all the composites described in this paragraph.

A list of the prepared composites all containing 30 Vol% of $BaTiO_3$ particles with different dimensions/functionalization/coating is reported in Table 4.8. As they contain the same amount of filler and are moulded under the same conditions, the letters in the sample labels usually referred to these parameters in the previous paragraphs are here omitted.

Table 4.8: List of the samples containing BT particles as such or differently surface modified.

Composite name	Particles name	BT particles diameter (nm)	Coupled silane	Inorganic coating	Coating thickness (nm)
S-B60	BT60	60	-	-	-
S-B125	BT125	125	-	-	-
S-B750	BT750	750	-	-	-
S-B125T6	BT125-Ti6	125	-	TiO_2	6
S-B125T13	BT125-Ti13	125	-	TiO_2	13
S-B125T22	BT125-Ti22	125	-	TiO_2	22
S-B60T6	BT60-Ti6	60	-	TiO_2	6
S-B750T75	BT750-T75	750	-	TiO_2	75
S-B125Si6	BT125-Si6	125	-	SiO_2	6
S-B125Si15	BT125-Si15	125	-	SiO_2	15
S-BPFDTES	BT-PFDTES	125	PFDTES	-	-
S-BDDTES	BT-DDTES	125	DDTES	-	-

The composites prepared, as well as the particles used, were thoroughly characterized.

4.2.1 Influence of particles coating

The pristine and coated BT particles, before being embedded in the PVDF matrix, were characterized by spectroscopic and morphological point of view.

The presence of a shell of silica or titania was confirmed by ATR-FTIR spectroscopy. The infrared spectra of the particles BT125-Ti22 and BT125-Si15, compared with that of the uncoated BT (BT125), are reported in Figure 4.32 as an example.

The IR spectrum of BT powders presents four principal bands: at 490 cm^{-1} due to the Ti-O vibration; around 1420 cm^{-1} ascribed to the stretching of the $–CO_3^{2-}$ groups [209] derived from $BaCO_3$ remaining as synthesis residue; at 3500 and 1630 cm^{-1} attributed to the –OH groups vibration.

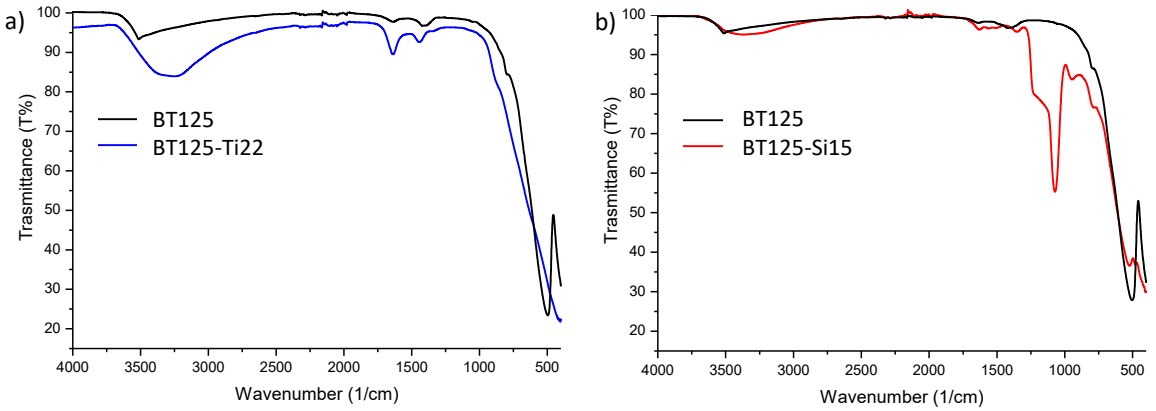

Figure 4.32: ATR-FTIR spectra of: a) BT125-Ti22 and b) BT125-Si15. The spectrum of BT125 is reported for reference purpose.

Compared to the pristine powder, the coated particles are characterized by new bands due to the presence of the shell. In particular, the spectra of particles coated with TiO_2 exhibit two bands, one around 480 cm^{-1} and one around 1440 cm^{-1}; both of them are ascribable to the stretching vibration of the titania Ti-O bond [194,210]. The bands at about 3300 e 1630 cm^{-1} are more intense for the BT125-Ti22 than for the BT125, indicating that the titania shell is more hygroscopic than the bare $BaTiO_3$ surface. This is in accordance with TGA measurements, where the TiO_2 coated particles show a more evident weight decrease with respect to the uncoated ones.

As concerns the silica coated particles, the IR analysis shows the presence of one broad and intense band around 1100 cm^{-1} and one peak at about 950 cm^{-1}, corresponding to the vibration of the Si-O-Si bond and to the stretching of Ti-O-Si [211–213].

The presence of a shell onto the particles surface is also confirmed by the morphological analysis (Figure 4.33). TEM micrographs show that the morphologies of titania and silica coating are

clearly different. In the case of BT@SiO_2 particles, the silica forms a continuous and regular coating, clearly evident in the BT125-Si15 sample, consisting of a homogeneous shell that surrounds the BT core. In this cases the shell thickness was evaluated with Image-Pro Plus software, by taking at least 80 measurements for each sample; the obtained values were 5.5 ± 0.8 nm and 15 ± 1.5 nm for BT125-Si6 and BT125-Si15, respectively. On the contrary, the titania coating appears less uniform, as if it consisted of a set of TiO_2 particles attached to each other (a kind of pearl necklace) rather than of a continuous shell; this irregular morphology prevented an accurate thickness determination. In this case the thickness values reported in Table 4.8 are theoretical shell thickness. It was verified that there are not appreciable loss during the hydrolysis of the titanium(IV) peroxo complex; in addition, the limited losses occurring during the coating reaction, which can reduce the actual shell thickness, are in some way compensate by the fact that the obtained shell consists principally of amorphous titania, whose density is lower than the crystalline one, leading to a higher shell thickness. Taking into account these two contrasting factors, the theoretical shell thickness was estimated by considering a complete formation of TiO_2 onto the BT particles surface.

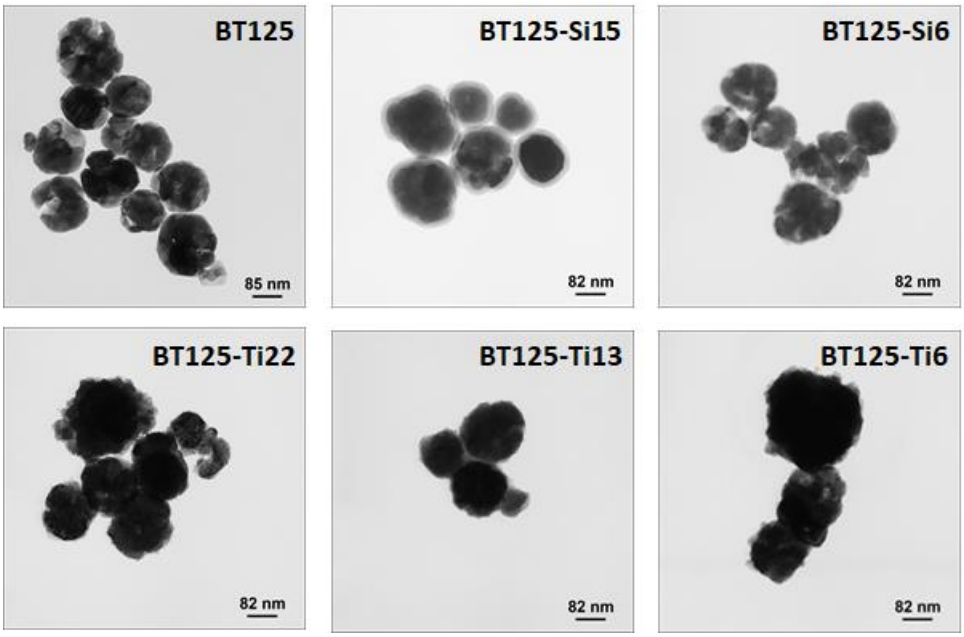

Figure 4.33: TEM micrographs of BT125 particles pristine and coated with shells of TiO_2 or SiO_2.

After the particles characterization, the morphology, the polymorphism of the PVDF matrix, the crystallinity degree and the dielectric properties of the prepared composites were investigated.
Morphological SEM analysis of composites indicated that all samples, either containing pristine or surface-coated BT particles, are characterized by a good filler distribution/dispersion, regardless of the type of coating (TiO_2 or SiO_2). The low and high magnification micrographs of the composites containing pristine BT, BT coated with a TiO_2 shell 13 nm thick and BT coated with a SiO_2 shell

15 nm thick are reported in Figure 4.34 as an example; for the images of the other samples see *Appendix D.*

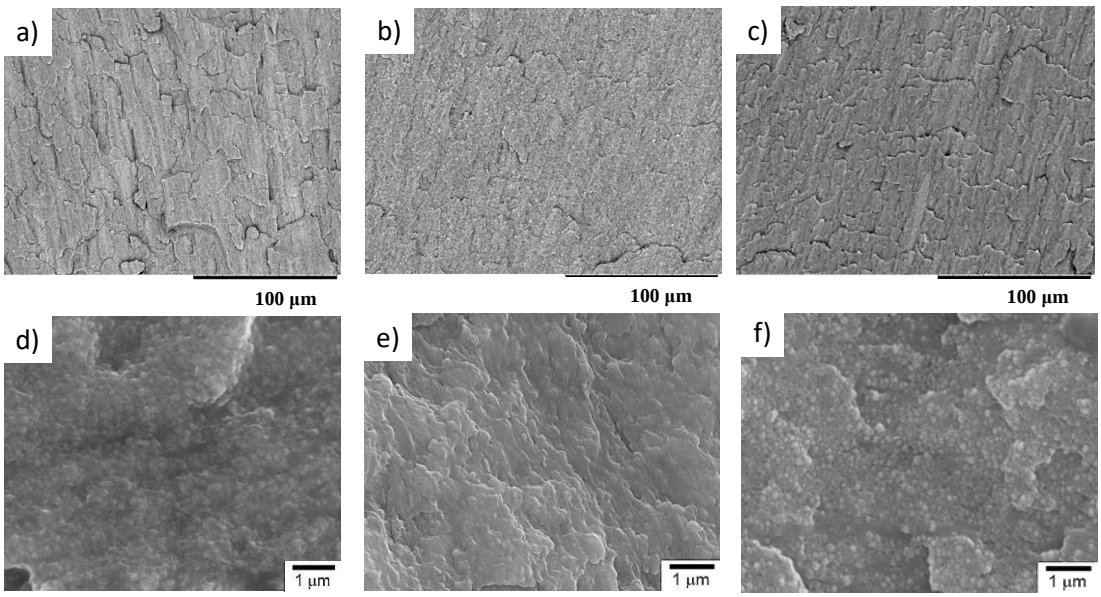

Figure 4.34: SEM micrographs at low and high magnification of: a,d) S-B125; b,e) S-B125T13; c,f) S-B125Si15.

In Table 4.9 the results relative to the calorimetric and spectroscopic characterization are reported. The degree of crystallinity of the PVDF matrix is comparable for all the samples except for those containing BT-Si particles, that are more crystalline than the others; thus, for comparison purpose, the relative electroactive phase fraction (F_{EA}) was recalculated by normalizing the value (F_{EA}*) with respect to the crystallinity degree.

Table 4.9: Crystallinity degree (X_c), relative (F_{EA}) and normalized (F_{EA}*) electroactive phase amount of the composites containing pristine and coated particles with different shell thickness.

Sample	X_c (%)	F_{EA} (%)	F_{EA}* (%)
S-B125	50	57	28
S-B125T6	51	60	31
S-B125T13	49	64	31
S-B125T22	49	68	33
S-B125Si6	61	53	32
S-B125Si15	59	48	28

As concerns the samples containing the coated particles, their electroactive phase amount is, in the overall, to some extent higher than that present in composites containing naked BT particles. In particular, for composites with titania coated particles, the β phase content slightly increases by increasing the shell thickness (see F_{EA} e F_{EA}* of S-B125T6, S-B125T13 and S-B125T22). The

silica coating improves the degree of crystallinity of the polymer matrix; thus, despite the F_{EA} values of the composites containing BT-Si particles are lower than the value obtained for S-B125, the absolute amount of β phase is comparable.

As concerns the dielectric properties, the influence of the shell type and thickness on the dielectric permittivity of the ensuing composites is clearly visible in Figure 4.35**.**

The dielectric losses are not significantly affected by the coating, but, when coated particles are used, the dielectric permittivity of the ensuing composites results lower, especially if the shell consists of silica. In addition, the permittivity decreases by increasing the shell thickness. This evidence is due to the dielectric permittivity of the oxides surrounding the particles, which is much lower ($\varepsilon \approx 4$ for SiO_2 and $\varepsilon \approx 100$ for TiO_2) than that of the $BaTiO_3$ ($\varepsilon \approx 1000$), and is consistent with the trends obtained by the Finite Element Modelling (FEM), presented in the following.

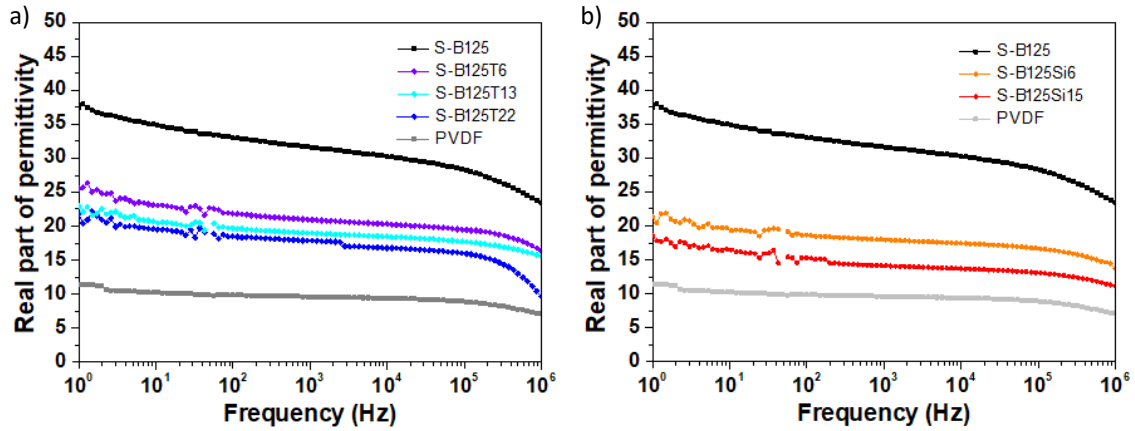

Figure 4.35: Dielectric permittivity of the composites containing: a) BT@TiO_2 and b) BT@SiO_2 particles with different shell thickness. The permittivity of S-B125 and of PVDF are reported as a reference.

In literature, some works about the theoretical prediction and experimental validation of the dielectric behaviour of polymer-based composites are present [4]. Yet, with the exception of few simple cases, the traditional equations (*i.e.*, Maxwell-Garnett, Bruggeman, Lichtenker, etc.) used to calculate the permittivity of a dielectric material consisting of different components, do not lead to reliable results if applied to real and more complicated systems.

The finite element modelling (FEM) analysis can be a good tool to calculate the distribution of the electric field, and thus the effective permittivity, taking into account the intrinsic contributions and neglecting the extrinsic ones, which are instead considered in other theories [190]. In general, FEM calculations have a twofold purpose: *(i)* to determine *a priori* the properties of some simple model-microstructures in order to guide the experimental activity in its first steps and *(ii)* to compare the properties experimentally measured with the calculated ones, reproducing in the best way the real microstructure of the investigated material. A brief explanation of the principles of this modelling is reported in *Appendix E.*

In a PVDF/$BaTiO_3$ composite the dielectric constant of the inorganic filler is much higher than that of the polymer ($\varepsilon \approx 10$), so the electric field tends to be more intense in the matrix, which

dominates the effective permittivity. The introduction onto filler surface of an inorganic shell with a different (here lower) ε modifies the field inside the resulting composite material and, consequently, the dielectric response. As visible in Figure 4.36, according to the finite element modelling the field distribution in the composite containing particles coated with titania is not so different from that of the composite containing the uncoated particles. In contrast, in the composite containing silica coated particles, the field is higher within the shell layer than in both the polymer matrix and in the BT core.

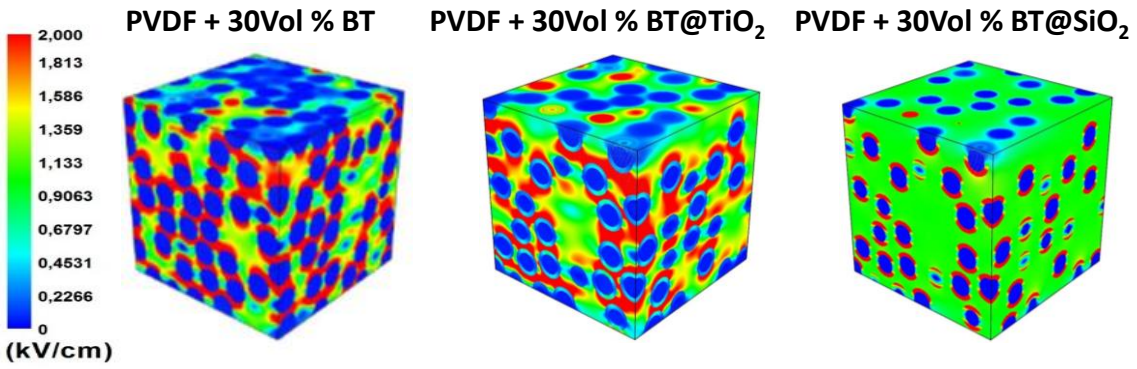

Figure 4.36: Electric field distribution in composites containing 30 Vol% of uncoated or coated particles according to the FEM.

The permittivity of PVDF-based composites containing 30Vol% of BT particles as such or coated with titania/silica were calculated by considering different values of shell thickness, 5, 10, 15 and 20 nm, that is close to those of the synthesized particles used for the samples preparation.

The modification of the electric field distribution induced by the shell leads to the following consequences: *(i)* the effective permittivity of the composites containing titania coated particles is only slightly lower than that of the composite containing uncoated BT particles (theoretical value 26), while when the shell consists of silica the values decrease markedly; *(ii)* the permittivity of composites, at equal type of coating, is affected by the shell thickness of the introduced particles, being the change more pronounced for silica than for titania shell.

The FEM predicted values are compared with the experimental ones in Figure 4.37.

As concerns the composites containing silica coated particles, the measured values are in accordance with those calculated by the theoretical model. The difference between the theoretical and the experimental values is more marked for BT@TiO_2 particles and this might be due to the fact that FEM analysis assumes for the TiO_2 shell a permittivity of 100; this value is valid for the rutile crystalline polymorph of TiO_2 but, in this case, it is an overestimated value because the shell mainly consists in amorphous titania, which reasonably possesses a lower dielectric constant.

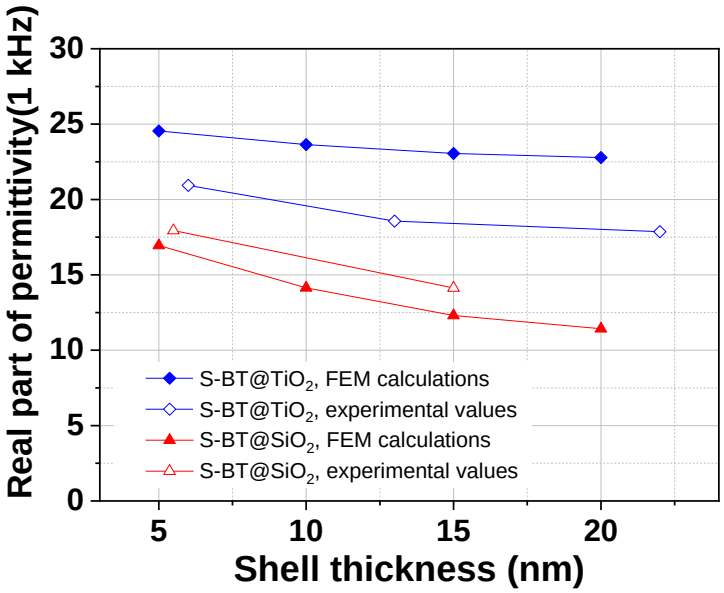

Figure 4.37: Permittivity of the composites (value at 1 kHz) as a function of shell thickness: the values predicted by the FEM are compared to those obtained from dielectric measurements.

The dielectric response was also measured as a function of the applied electric field and the corresponding tunability (n) was calculated as:

$$n = \frac{\varepsilon(0)}{\varepsilon(E)} \tag{4.1}$$

where $\varepsilon(0)$ is the dielectric permittivity when the external electric field is null, while $\varepsilon(E)$ is the dielectric permittivity measured applying an external electric field different from zero.

Figure 4.38 shows that the permittivity decreases when the module of the electric field increases but the change is limited, as confirmed by the tunability values, which slightly differ from 1 even at relatively high electric fields. Moreover, the presence of the shell affects the dielectric response as a function of the applied electric field; the tunability reaches lower values for the composite containing coated particles, especially BT@SiO_2 particles. This characteristic is a not negligible requirement in the field of dielectrics in capacitors, where the dielectric permittivity has to be as constant as possible by changing the applied electric field.

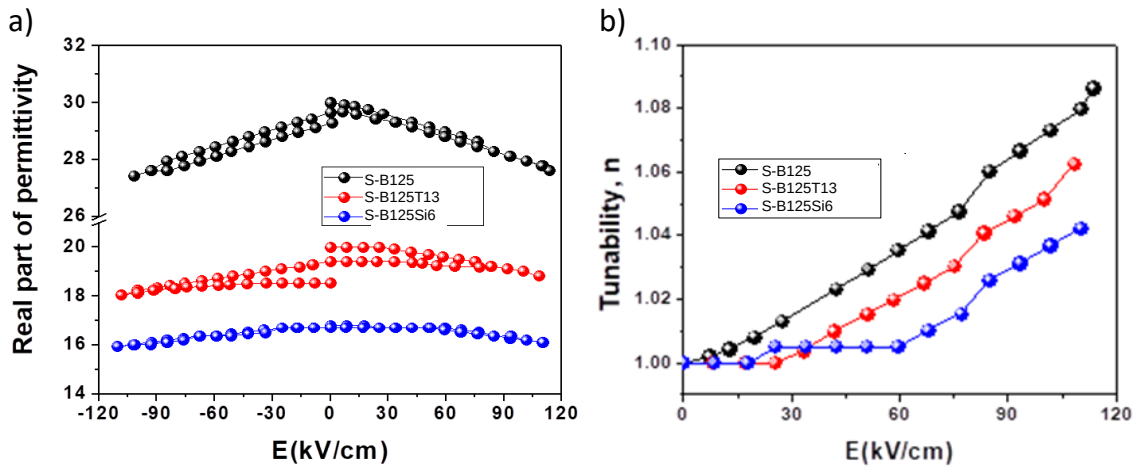

Figure 4.38: a) dielectric permittivity as a function of applied electric field and b) tunability of the composites containing pristine BT and BT coated with silica or titania.

Beside all the previous properties, also the electric field distribution within the material bulk and, consequently, the breakdown field is affected by particles modification. In general, it was found that selecting a material with a moderate dielectric constant to create a buffer layer between BT and PVDF can accomplish a stepwise change in the dielectric constant of the material, reducing the non-uniformity of the electric field in the bulk and increasing the breakdown field [214].

In order to further investigate this aspect, the dielectric characterization of the composites was completed with P-E loops measurements, by repeating the cycles at increasing applied field, until the electric breakdown of the sample. To this purpose, all the composite materials under investigation were re-prepared on a reduced scale in order to obtain thinner films, more suitable for the high-field measurements. Since the electrical breakdown is a statistical process, which depends on the nature of the materials but is strictly affects by extrinsic factors, such as local defects or impurities, the measurements were repeated from 5 to 7 times for each sample.

The maximum electric field (E_{max}) the films can stand before the breakdown occurring, the energy density recovered and the efficiency are reported in Figure 4.39; the permittivity of the samples at 1kHz is there reported as well for sake of clarity.

The BT coating with silica, when thick enough (*i.e.*, 15 nm) leads to a significant increment in the maximum electric field with respect to that measured for the composites containing pristine BT.

However, because the presence of SiO_2 shell leads also to a decrease of the dielectric permittivity, the energy density of the composite with BT@SiO_2 particles results lower with respect to that of the sample containing pristine BT particles.

The composites containing titania-coated particles have a comparable (S-B125T6) or higher (S-B125T13 and S-B125T22) resistance to electric field with respect to the corresponding composites with naked BT particles, but, having lower permittivity, their energy storage capability is overall lower. However, if the thickness of the TiO_2 shell is small enough, the coating of the particles increase the efficiency of the dielectric composite, meaning that it leads to a less lossy ferroelectric loop.

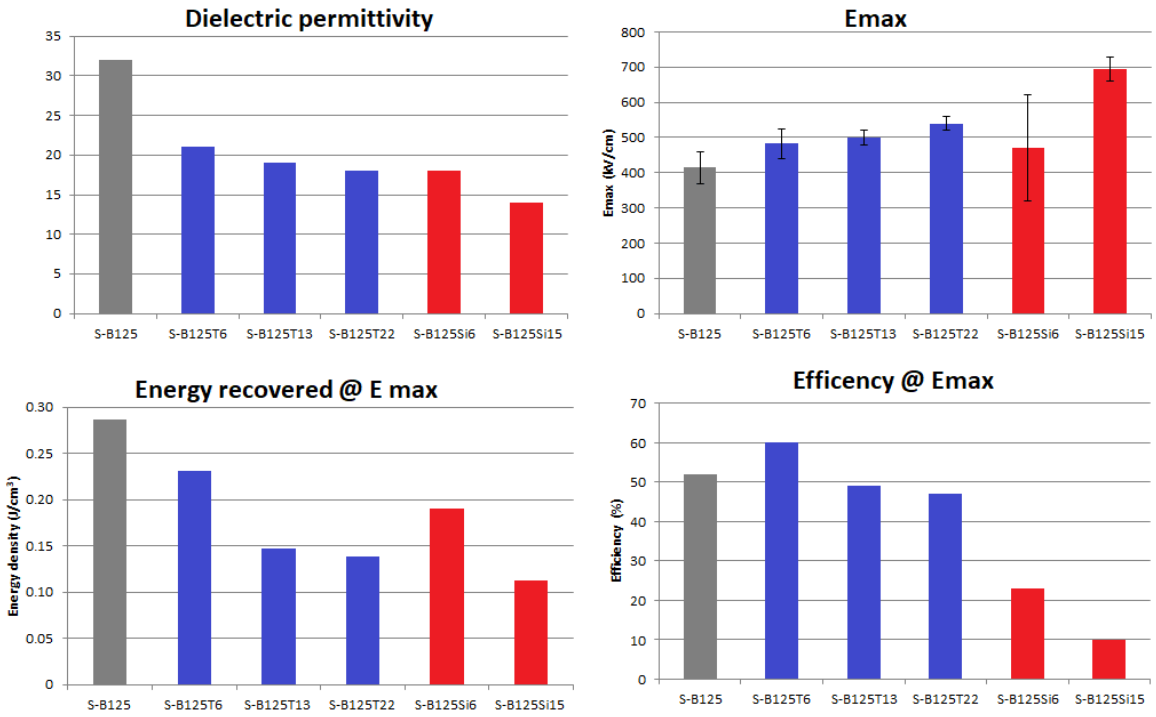

Figure 4.39: Values of: permittivity at 1kHz; maximum electric field; energy density recovered; and efficiency of composites containing BT with different coating.

The ultimate effect of an inorganic shell on the dielectric properties of a dielectric composites is the results of contrasting factors which are difficult to be predicted.

Z. Zhang *et al.* prepared PVDF-based composites containing BT particles coated with silica of different shell thickness (2, 4 and 6 nm) and they found, according to the results here presented, a decrease in permittivity and an increase in dielectric breakdown with the increasing of the shell thickness. They ascribed the decrease in permittivity to the gradually increase of the relative distance between the BT cores due to the presence of SiO_2 shell and the increase in breakdown strength to the good insulation property of the silica, which acts as a passive interlayer preventing charge carrier conduction. They observed that the final energy density released depends on a compromise between the increase in dielectric breakdown and decrease in the maximum polarization, leading to a slight increase in the final performance for the composite containing particles with intermediate shell thickness.

P. Hu *et al.*, prepared PVDF-based composites containing BT particles coated with crystalline titania having different shell thickness (1-3, 3-5 and 5-10 nm). They found that these composites are characterized by permittivity and breakdown strength higher than those of the reference composite with uncoated BT but, also in this case, the trend of this parameters with the shell thickness is non-monotonous. Indeed, the introduction of the buffer layer on particles induces a two-charged interface which tends to expand with the shell thickness, reducing the charge density; this leads to: *(i)* a weakening of the interfacial polarization and thus of the dielectric constant and *(ii)* a homogenization of space charge, which improves the breakdown strength.

As concerns our composites, the relatively high thickness of the coatings is functional to increase, even considerably, the dielectric breakdown, but the intrinsic contributions (*i.e.*, the permittivity of titania and silica) prevail over the extrinsic ones (*i.e.*, interfacial polarization) in determining the dielectric permittivity.

4.2.2 Influence of particles dimensions

Size and scaling effects in ferroelectric materials have attracted great interest over the last 25 years. The current understanding of these effect in perovskite compounds, with particular attention devoted to $BaTiO_3$, has been recently summarized by V. Buscaglia and C. A. Randall [201]. The authors in their Review clearly put in evidence the complexity of the various phenomena which determine the dielectric and ferroelectric properties of the particles and bulk ceramics.

As already discussed in *Paragraph 4.2*, the issue of the size effect comes into play also when perovskite particles are embedded in a polymer matrix; yet, the influence of the filler dimensions in determining the ultimate properties of the composite is not so clear. The problem is that, by varying the particles diameter, other factors result inevitably changed: the intrinsic properties of the particles, in terms of crystalline phase, domains configuration, defects or surface characteristics, but also the extrinsic properties of the ensuing composite, in terms of interface quality, porosity, or filler distribution. In light of this, one must consider all these aspects for the interpretation of the results.

Here, the influence of the particles size on the dielectric properties of the PVDF-based composites was studied by employing BT and BT@TiO_2 particles of different dimensions. The coating thickness was chosen to maintain the same volume ratio between the shell and the entire particle (V_{shell}/V_{tot} = 0.42). The images of the smallest and the biggest uncoated and coated particles are shown in Figure 4.40.

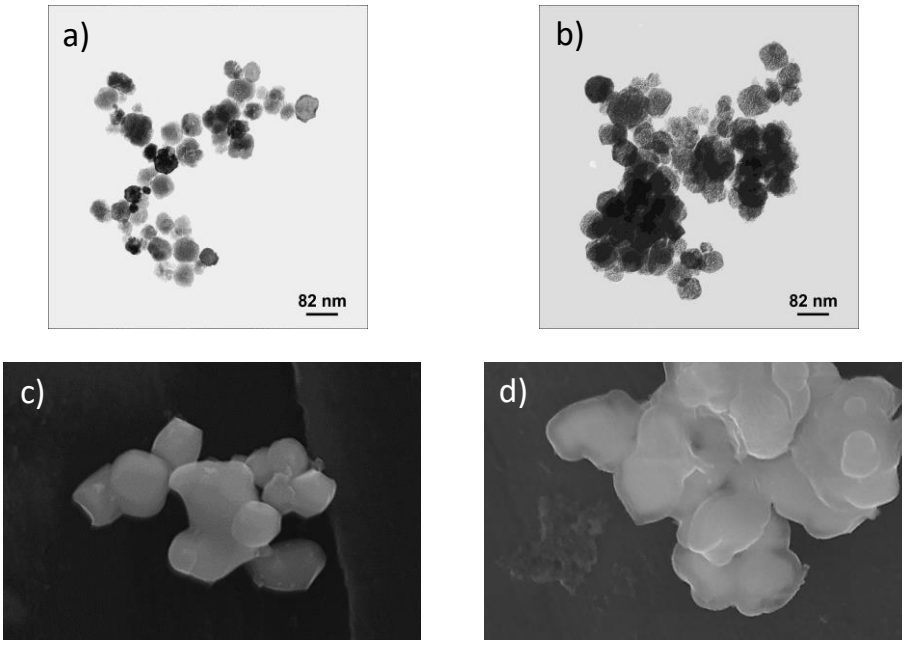

Figure 4.40: TEM images of: a) BT60 and b) BT60-Ti6; SEM images of: a) BT750 and d) BT750-Ti75.

Also for these composites, a good particles dispersion resulted from the morphological analysis (Figure 4.41).

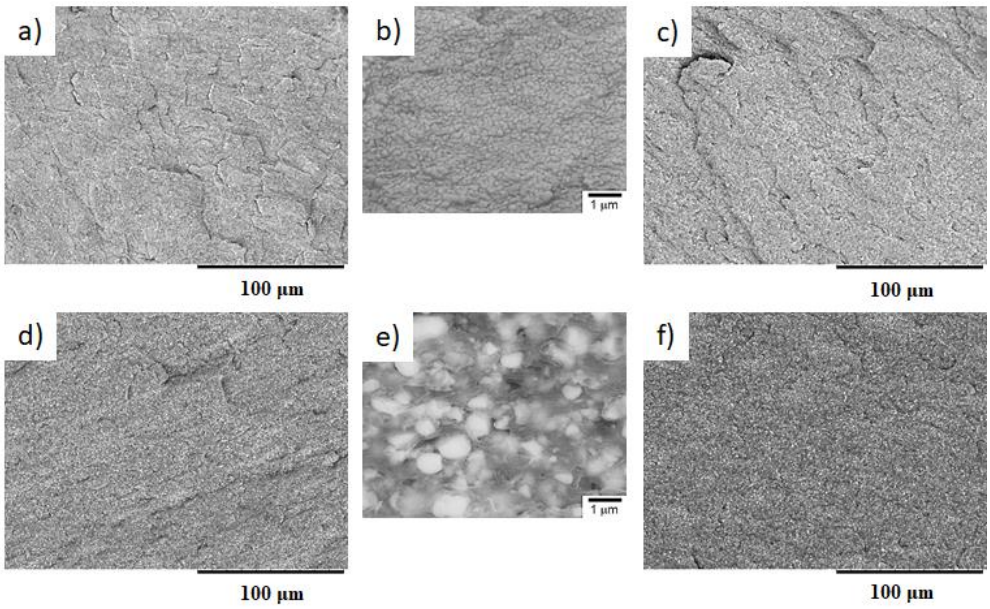

Figure 4.41: SEM micrographs of: a,b) S-B60; c) S-B60Ti6; d,e) S-B750; f) S-B750T75.

The crystallinity degree and electroactive phase amount were estimated as well (Table 4.10); the values for the samples containing particles with intermediate dimensions (*i.e.*, 125 nm) are reported again for comparison purpose. The normalized electroactive phase amount is slightly higher for the composites containing core-shell particles with respect to that of the composites containing pristine BT.

Table 4.10: Crystallinity degree (X_c), relative (F_{EA}) and normalized (F_{EA}*) electroactive phase amount of the composites containing pristine and coated $BaTiO_3$ particles with different diameter.

Sample	X_c (%)	F_{EA} (%)	F_{EA}* (%)
S-B60	49	56	27
S-B125	50	57	29
S-B750	60	47	28
S-B60T6	48	62	30
S-B125T13	49	64	31
S-B750T75	57	57	33

From the dielectric characterization it was revealed that also the particles dimensions affect the dielectric properties of the composites Figure 4.42. However, a different behaviour is visible depending on the particles type used. For the composites containing BT@TiO_2 particles with different dimensions, the dielectric permittivity increases with the filler diameter (60, 125 and 750 nm). On the contrary, the ε value of the samples containing uncoated BT particles is higher for particles with intermediate dimensions and results lower for both the S-B60 and S-B750 samples.

In literature, a different trend has been observed: Y. P. Mao *et al.* studied the size effect on PVDF/60 Vol% BT composites and found a maximum in permittivity for the sample containing particles of 100-150 nm size [205]. They ascribed this trend to an unusual compression along the *c-axis* of the tetragonal structure for the particles with these dimensions, visible from an inverse (002)/(200) peak intensities. On the other hand, according to H.-I. Hsiang *et al*., the permittivity of PVDF/40 Vol% BT composites increases with particles dimensions until 600 nm of diameter and above this value shows an oscillating trend [204]. They claimed that the dielectric constant increased with $BaTiO_3$ particle size, because of the contribution of the ferroelectric domains and then decreased due to the coalescence occurring at calcination temperatures above 1200°C, that leads to disappearance of grain boundaries, consequent elimination of constrained forces from neighbouring crystallites and in turn decreased domain density.

These contrasting results make clear the difficulty in understanding the particles size effect in the composites.

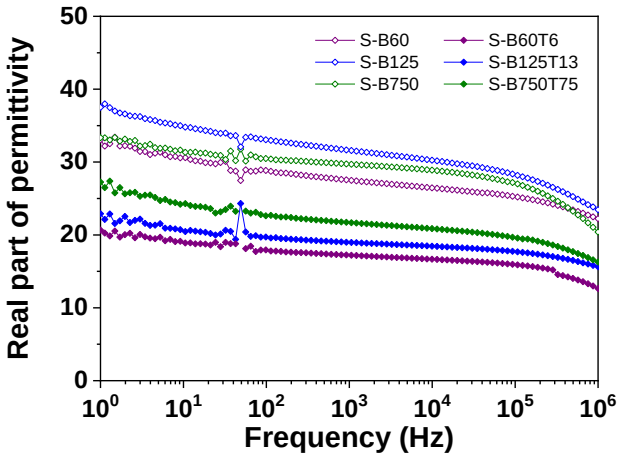

Figure 4.42: Dielectric permittivity of the composites containing BT and BT@TiO_2 particles with different diameter.

An important contribution to the ultimate properties of the composites is given by the intrinsic properties of the filler. Unfortunately, contrary to what happens for bulk ceramics or thin films, the permittivity of ceramic particles is very difficult to determine because it is obtained indirectly from measurements carried out on powder compacts or slurries by applying theoretical models based on mixing rules; this leads to a high margin of error in dielectric constant estimation due to the non-ideality of the system (*e.g.*, for particles agglomeration) [215]. This is the reason why, in literature, the crystalline features of the particles are often considered to explain the difference in dielectric response of the composites on the basis of the expected properties of the filler. The structural characterization of the intermediate and smaller particles (*i.e.*, diameter 60 and 125 nm) here used revealed that they are characterized by a pseudocubic phase, thus they are probably polar but with a mean *c/a* axes ratio close to 1. The structure of the larger particles (*i.e.*, diameter 750 nm) was not investigated. However, it is known that $BaTiO_3$ particles with the size increasing tend to a tetragonal structure. V. Buscaglia and C. A. Randall [201] showed that for BT particles of dimensions higher than 500 nm, the c/a ratio is close to the bulk ceramics value, 1.011, independently from the synthetic method adopted.

This suggests that a higher permittivity is expected by increasing the particles diameter.

However, it is known that also the extrinsic contributions can take part in the dielectric properties.

Anyhow a not negligible factor is that a different method of synthesis was here used for the particles preparation. This is because, in general, it is difficult to prepare spherical particles with different dimensions in a so large range of size, by using the same method of synthesis. In particular, in this case, the BT particles with a mean diameter of 60 and 125 nm were synthesized by a hydrothermal-like method, while those of about 750 nm were obtained through solid-state reactions. The different preparation methods can determine a different particles surface, as confirmed by IR spectra (Figure 4.43a) and this, in turn, could affect the interactions with the polymer matrix, with a consequent impact on the dielectric properties of the ensuing composites. In particular, by observing the SEM micrographs with more attention, the BT750 particles seem to be less adhered to the polymer matrix than the BT750T75 and this can decrease the overall quality of

the composite, and in turn, of the permittivity. This hypothesis can explain the different behaviour observed for the composites containing these two particle types: the presence of the titania shell probably deletes the surface differences (as visible from the ATR-FTIR spectra of the particles, shown in Figure 4.43b) leading to the expected trend.

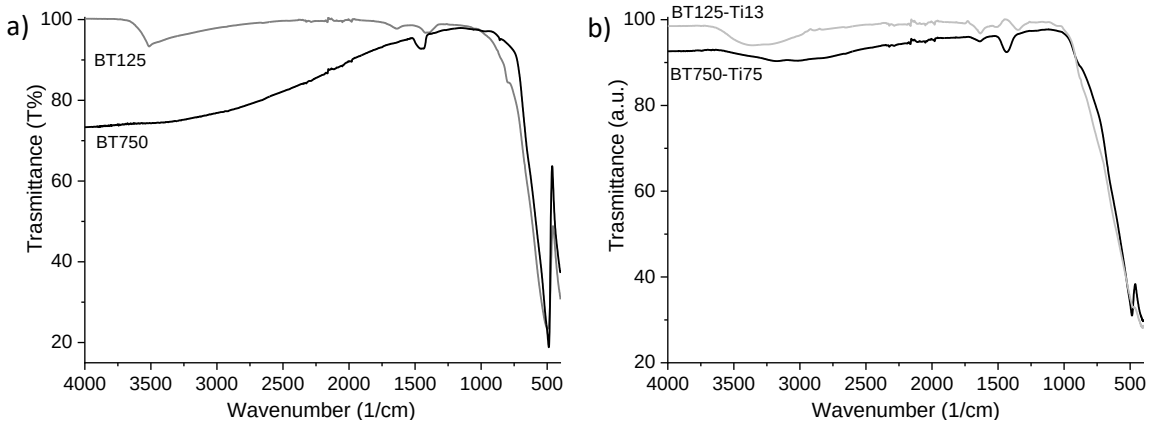

Figure 4.43: ATR-FTIR spectra of: a) BT125 and BT750; b) BT125-T13 and BT750-Ti75.

The particles size can affect the electric field distribution inside a composite material.

In general, it was found that the local electric field concentration generated from the composites containing coarser particulate fillers is higher than that of the composites filled with smaller particles and this can facilitate the breakdown [216].

The maximum electric field and the parameters related to the energy storage capability were measured also for these samples; the relative results are reported in Figure 4.44.

The measured trend seems to be opposite to what reported in literature: the mean maximum electric field increases by increasing the particles size both for the composites containing pristine BT and for those with coated particles. However, taking into account the values dispersion, the response can be considered similar for all the samples.

The composite with neat BT particles having intermediate size (125 nm) is characterized by higher energy storage density with respect to the other films.

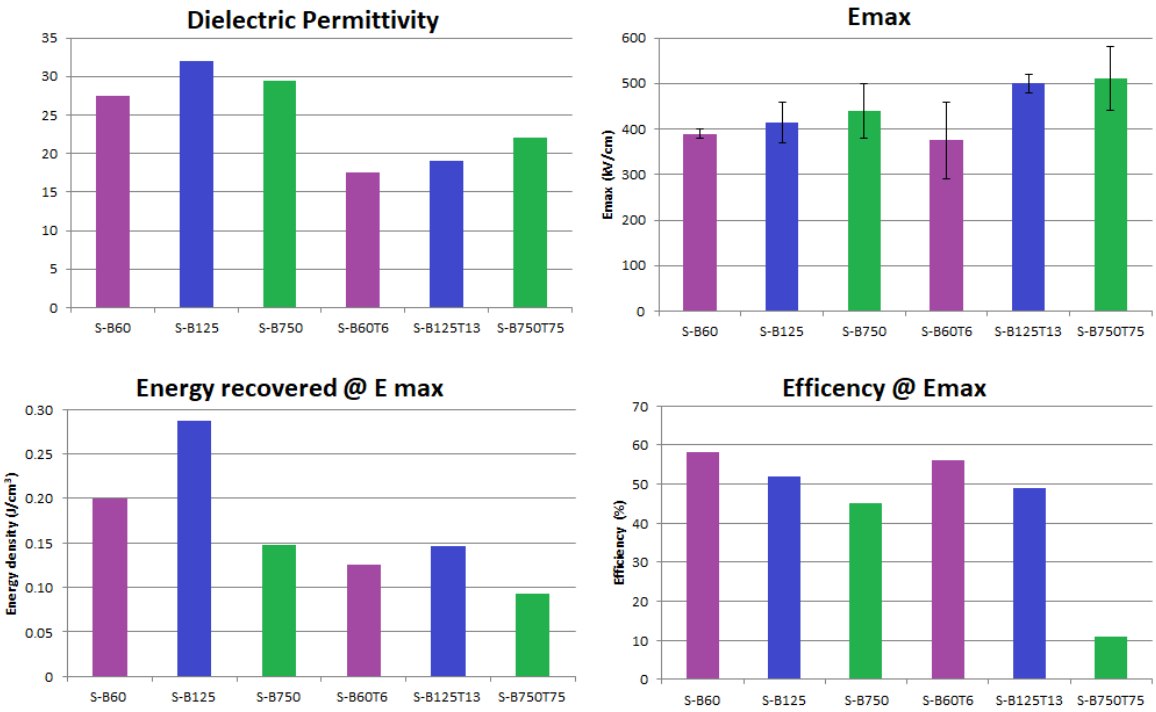

Figure 4.44: Values of: maximum electric field, energy storage density , and efficiency of composites containing BT and BT@TiO_2 with different dimensions. The permittivity values at 1 kHz are reported for sake of clarity.

4.2.3 Influence of particles functionalization

The surface modification of particles with suitable organic molecules can be important to enhance their interaction with the polymer matrix thus possibly improving phase adhesion and filler dispersion, while reducing dielectric losses. In literature, beside phosphonic acids, also organosilanes, are widely used as coupling agents for dielectric nanocomposites [217,218]; in particular (3-aminopropyl)triethoxysilane (APTES) is largely employed because, thanks to the polarity of its aminic group, it provides good compatibility with fluorinated polymer matrices.

Therefore, the optimization of the functionalization procedure was here carried out on a small amount of particles (*i.e.*, 0.5 g) using APTES as the coupling agent. At first, the BT powder (125 nm) was treated with hydrogen peroxide [219] in order to increase the amount of –OH groups onto the particles surface, that can then react with the silane coupling agent during the subsequent functionalization. However, TGA measurements indicated that this pre-treatment does not affect significantly the degree of grafted silane and so can be avoided. Then, two procedures were tested: in the first one, properly modified from the literature [220], the reaction between the silane and the –OH groups originally present on nanoparticles surface was started in the presence of a silane solvent and completed after the solvent medium removal; whereas, in the second one, the condensation of the silane, previously adsorbed, by using a minimum amount of a volatile solvent, on the nanoparticles surface, was carried out by thermal treatment directly on BT powders (this procedure is detailed in *Paragraph 3.3*). The overall results indicated that the second procedure is

more advantageous because allows obtaining a large amount of grafted silane by using a very limited quantity of solvent and, for this reason is also more suitable for a scale-up.

ATR-FTIR analysis carried out on BT particles modified with 20 wt% APTES (with respect to BT), by using the second procedure, is shown in Figure 4.45 as an example. The spectrum clearly revealed the appearance of bands characteristic of the organo-silane moiety: 3400-3100 cm^{-1} ($–NH_2$ stretching); 2926 cm^{-1} ($–CH_2$- symmetric stretching); 2860 cm^{-1} ($–CH_2$- antisymmetric stretching); 1570 cm^{-1} ($–NH_2$ bending); 1190 cm^{-1} (Si-O-$BaTiO_3$ vibration); 1120 and 1030 cm^{-1} (polysiloxane C-Si-O and Si-O). The grafted silane, being present in large amount, is also clearly visible by TEM.

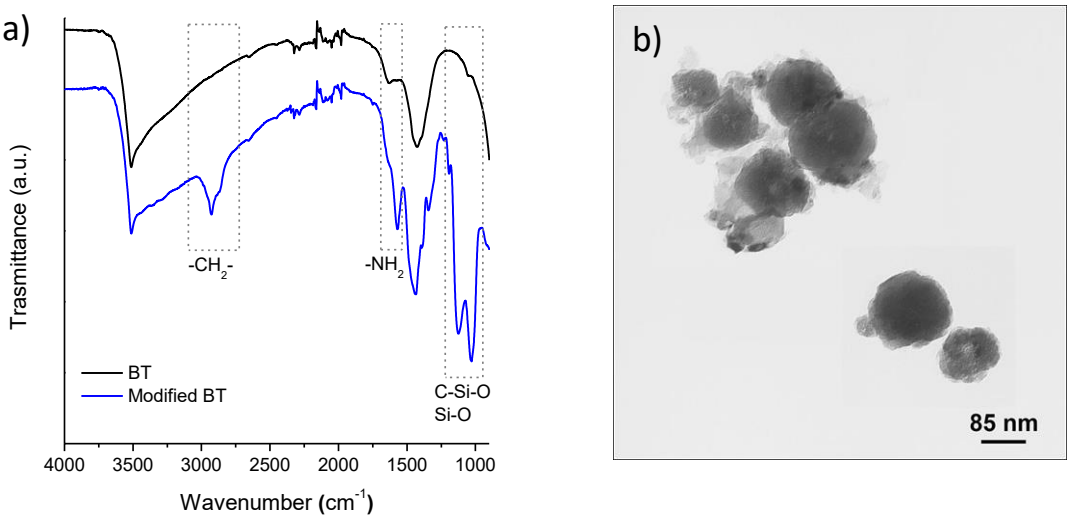

Figure 4.45: a) ATR-FTIR spectra of neat and functionalized BT powders; b) TEM micrograph of modified powders.

The functionalization was then extended to BT@TiO_2 powders in order to verify the procedure efficacy on core-shell particles.

In literature, other organic molecules are employed to enhance the compatibility between inorganic fillers and fluorinated polymer matrices; among these, coupling agents bearing an alkylic chain or fluorinated groups are used [221–223]. Thus, the coated particles were surface modified by using different types of silane: beside APTES, also dodecyl triethoxysilane (DDTES) and 1H,1H,2H,2H-perfluorodecyl triethoxysilane (PFDTES) were tried. The former of the last two molecules, being characterized by a relatively long alkyl chain, could promote the compatibilization through entanglements with the polymer matrix chains while the latter, due to the presence of C-F dipoles, could interact with the PVDF matrix of similar nature.

The chemical formulas of the three silanes employed are shown in Figure 4.46.

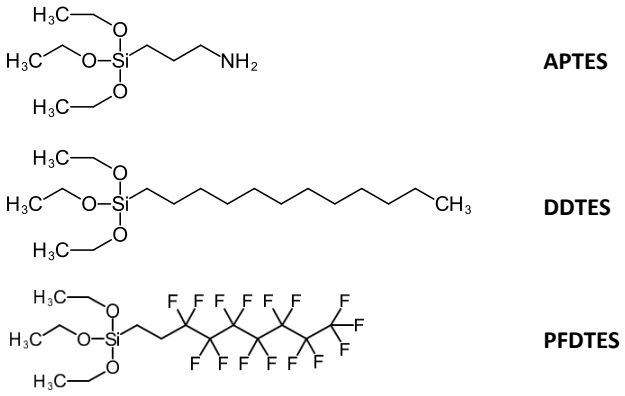

Figure 4.46: Organosilanes used for the BT particles functionalization.

Since the molecular weights of the three silanes are different from each other (M_{ATPES} = 221,37 g/mol; M_{DDTES} = 332,59 g/mol; M_{PFDTES} = 610,38 g/mol), the amount of coupling agent to be used was calculated on equal moles.

In Table 4.11 the list of modified powders and the relative amount of silane used for the functionalization are reported (the number in the sample name indicate an increasing amount of silane in the feed). Also for the core-shell particles, ATR-FTIR analysis confirms that the functionalization was successfully carried out. In Figure 4.47a the spectra relative to the BT@TiO_2 particles modified with an increasing amount of PFDTES are reported as an example; the characteristic bands of the fluorinated silane are clearly visible and their intensity increases by increasing the amount of silane used in the feed.

Table 4.11: List of BT-TO modified with different silanes.

Sample	Fed silane (wt%)	Sample	Fed silane (wt%)	Sample	Fed silane (wt%)
BT-TO 1APTES	5	BT-TO 1DDTES	7.5	BT-TO 1PFDTES	13.8
BT-TO 2APTES	10	BT-TO 2DDTES	15	BT-TO 2PFDTES	27.6
BT-TO 3APTES	15	BT-TO 3DDTES	22.5	BT-TO 3PFDTES	41.4
BT-TO 4APTES	20	BT-TO 4DDTES	30	BT-TO 4PFDTES	55

TGA analysis allowed to roughly estimate the amount of coupling agent present onto the particles surface (Figure 4.47b). Before measurements all the samples were dried overnight at 120°C to

remove the excess water; however, the physi-adsorbed water is not completely eliminated by such a treatment, as suggested by the weight loss that occurs between 50°C and 150°C, visible in the thermogram derivative (DTG) curve (Figure 4.47c).

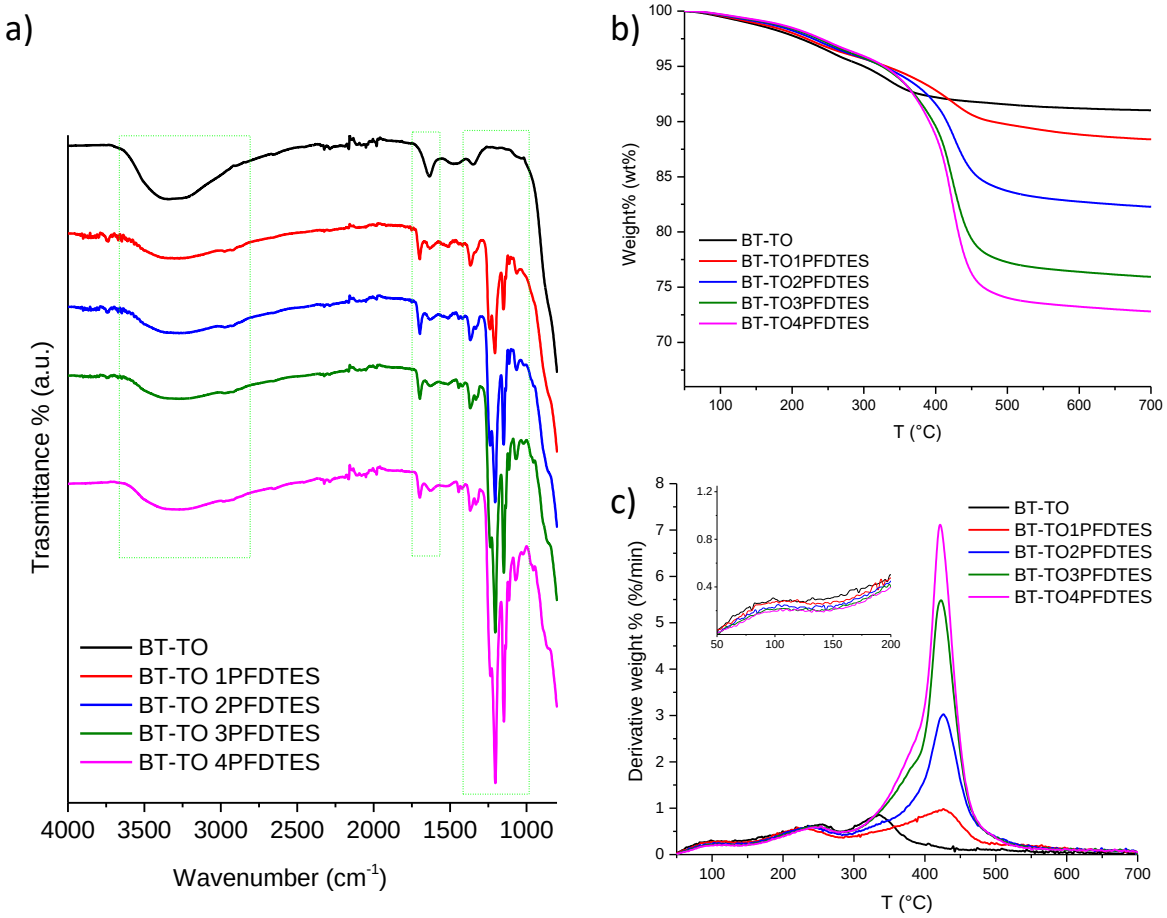

Figure 4.47: a) ATR-FITR spectra, b) TGA thermogram and c) DTG curve of neat BT@TiO_2 and BT@TiO_2 modified with increasing amount of PFDTES. For the results relative to the modification with the other coupling agents see *Appedix F*.

The water adsorbed is around 1 wt% but, being this value not the same for the neat and modified particles, it can lead to an error in the quantification of grafting. The amount of grafted silane was estimated by subtracting to the weight loss of functionalized particles between 150 and 700°C that of pure powders in the same range of temperature. The curves of grafted silane *vs.* silane used in the feed are shown in Figure 4.48.

The different types of silane, more correctly, should be compared to each other by converting these results in terms of moles. Unfortunately, the evaluation of the moles of grafted silane is not so simple because the molecular mass of the grafted silane changes depending on the number of ethoxy groups that react with the –OH groups present on particles surface, releasing ethanol. A more correct grafting degree of the silanes onto the particles requires a combination of the TGA results whit those obtained by Elemental Analysis [224,225], which, however, is beyond the scope of this work.

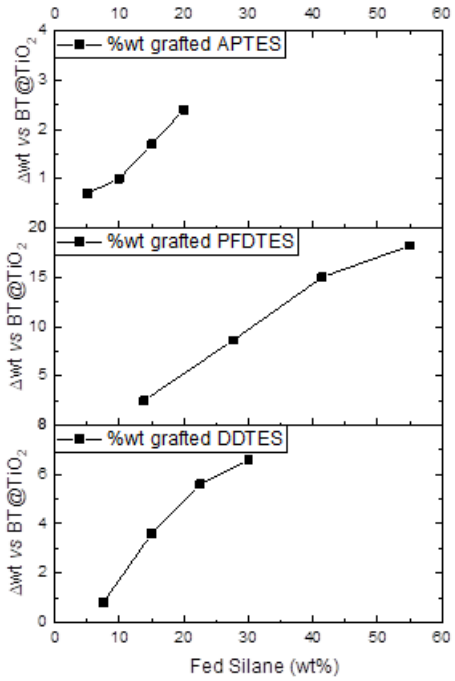

Figure 4.48: Grafted silane *vs.* silane in the feed of the BT-TO powders modified with APTES, DDTES or PFDTES.

For our purpose, the above reported values give an indication of the amount of grafted silane that can be obtained with this method of functionalization. This has been useful for the subsequent step, that consisted of the scale-up of the functionalization method in order to modify an amount of particles high enough to prepare composites.

On the basis of previous results and of the works present in literature [217,220], the minimum amount of organosilane was chosen and the procedure of functionalization was scaled-up to modify an amount of powder sufficient for the subsequent composites preparation.

In particular, BT125 powders were functionalized with DDTES or PFDTES with the purpose of studying the effect of these coupling agents, not yet used in literature, on the dielectric properties of the ensuing composites.

The effective presence of silane on the particles surface was verified by FTIR-ATR analysis (Figure 4.49).

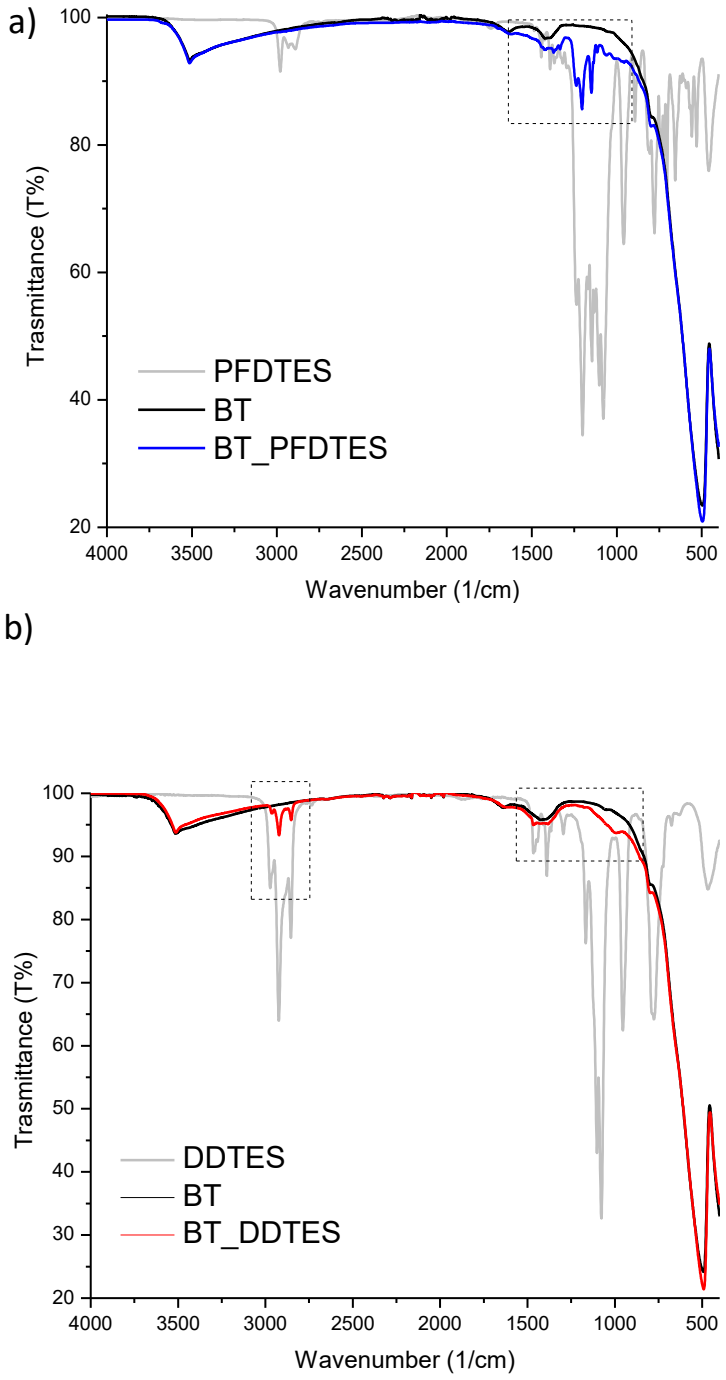

Wavenumber (cm^{-1})	Assignements
2980	νas (CH_3)
2932	νas (CH_2)
289	νs (CH_2)
1485	δ (CH_2)
1444	δas (CH_3)
1392	δ (CH_3)
1237	ν(CF_3)
1168	ρ (-CH_3)
1146	νs(CF_2)
1103	νas (Si-O-C)
1079	νs (Si-O)
959	νs (Si-O-C_2H_5)

Wavenumber (cm^{-1})	Asignements
2972	νas (CH_3)
2923	νas (CH_2)
285	νs (CH_2)
1465	δ (CH_3), δ (CH_2)
1389	δ (CH_3)
1295	ω (CH_2)
1166	ρ (-CH_3)
1102	νas (Si-O-C)
1077	νs (Si-O)
954	νs (Si-O-C_2H_5)
780	ρ $(CH_2)_n$

Figure 4.49: ATR-FTIR spectra of the BT particles functionalize with a) PFDTES and b) DDTES and for the composites preparation. The relative peaks attributions are reported on the right (ν, stretching; δ, bending; ω, wagging; ρ, rocking).

The amount of coupling agent anchored, estimated with TGA measurements, was about 20% of the corresponding quantity used in the feed (Table 4.12).

Table 4.12: Estimated amount of silane anchored on BT surface.

Sample	Silane in the feed (wt%)	Weight variation @ 700°C (wt%)
$BaTiO_3$+PFDTES	13.8	3.0
$BaTiO_3$+DDTES	7.5	1.4

The so modified particles were used to prepare composites that were then characterized.
SEM analysis revealed that the presence of the coupling agent does not improve further the filler dispersion, which was already very fine in the composite containing unmodified BT (Figure 4.50).

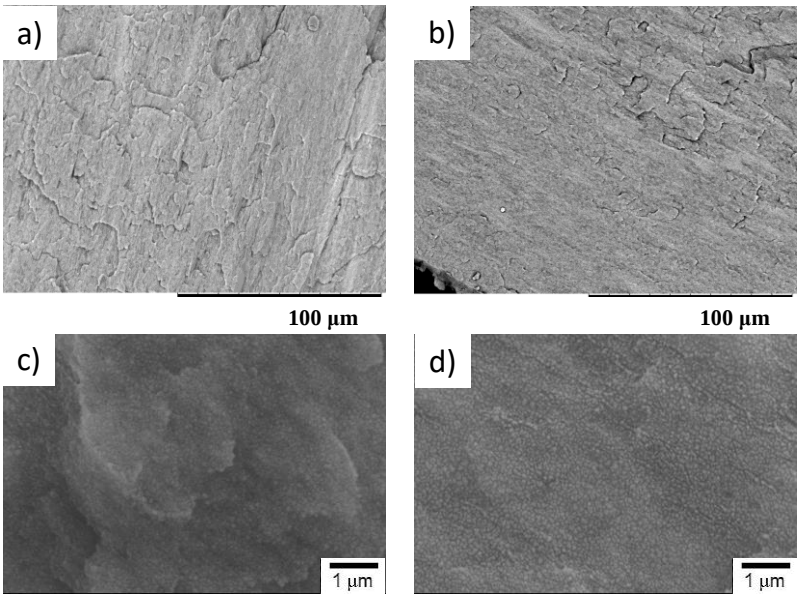

Figure 4.50: SEM images of the composites: a,c) S-BPFDTES; b,d) S-BDDTES.

Instead, the presence of the coupling agent strongly affects the electroactive phase amount obtained in the PVDF matrix: in the composite containing unmodified particles the calculated F_{EA} was 57%, in the S-BPFDTES and S-BDDTES samples it was 30 and 37%, respectively. This suggests that, in both cases, the presence of the silane coupling agent, despite not worsening the particles dispersion, contrary to what envisaged, probably leads to a weaker particles/matrix interaction which decreases the frictions generated during the second step of moulding, partially hampering the formation of β phase.
The dynamic-mechanical measurements are in accordance with this hypothesis (Figure 4.51).

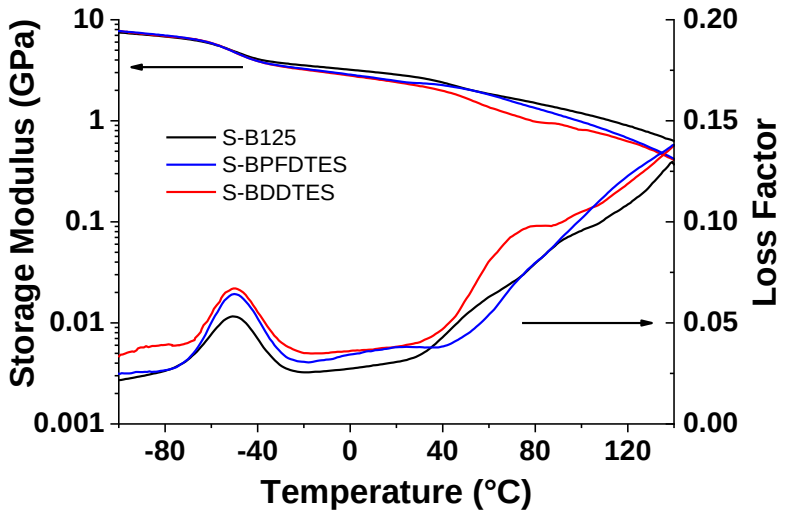

Figure 4.51: Dynamic-mechanical response of the composites from solvent casting containing neat or functionalized BT.

The particles functionalization does not improve the mechanical response of the composites: *G'* is slightly lower for the composites containing functionalized particles with respect to that observed for the corresponding composite containing neat BT, confirming that the effect of compatibilization is not obtained with these silanes.

The dielectric losses remain unchanged but, unfortunately, the permittivity decreases (see Figure 4.52)

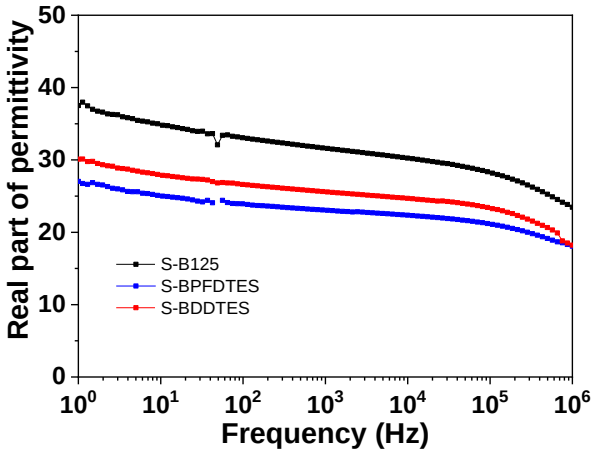

Figure 4.52: Dielectric permittivity of the composites containing functionalized BT particles. The curve of the composite containing pristine BT is reported for reference purpose.

This is ascribable both to the lower amount of β phase induced in PVDF and the very low intrinsic permittivity of the organosilanes, that, in the absence of a marked compatibilizing effect, lead to a deterioration rather than to an improvement of the dielectric properties of the resultant composite materials. Analogous evidence was observed by Delle Vacche *et. al* [220], preparing composites PVDF–TrFE/$BaTiO_3$ with particles as such or modified with APTES; they observed that the introduction of silane enhanced the dielectric properties for the composites from solvent casting,

improving the affinity with the polymer matrix and reducing the porosity of the system, but had a negative effect for the compression moulded composites, where, as in the present case, no differences were found in the morphology with respect to the samples containing unmodified particles.

The influence of the particles functionalization on the final dielectric properties was also studied by R. Li *et al.* [46] who found a contrasting effect of a silane (KH-570) and a titanate (NDZ-101) coupling agent on the permittivity and loss tangent of PVDF/PZT composites, also depending on the concentration of the introduced molecules.

In general, the effect a coupling agent introduced in a composites material can produce is not so obvious and predictable, especially on the electrical point of view. In literature, the improvement of the performance of a dielectric composite as a consequence of the introduction of a coupling agent, is often due not to an increase of the dielectric permittivity, but to an enhancement of the electric breakdown, which leads to higher energy storage capability. This aspect was investigated on our composites and the experimental evidences (Figure 4.53) show that the presence of PFDTES and DDTES clearly increases the maximum electric field and thus the corresponding composites, despite having a lower permittivity, are able to recover the same energy density recovered by the film containing pristine BT.

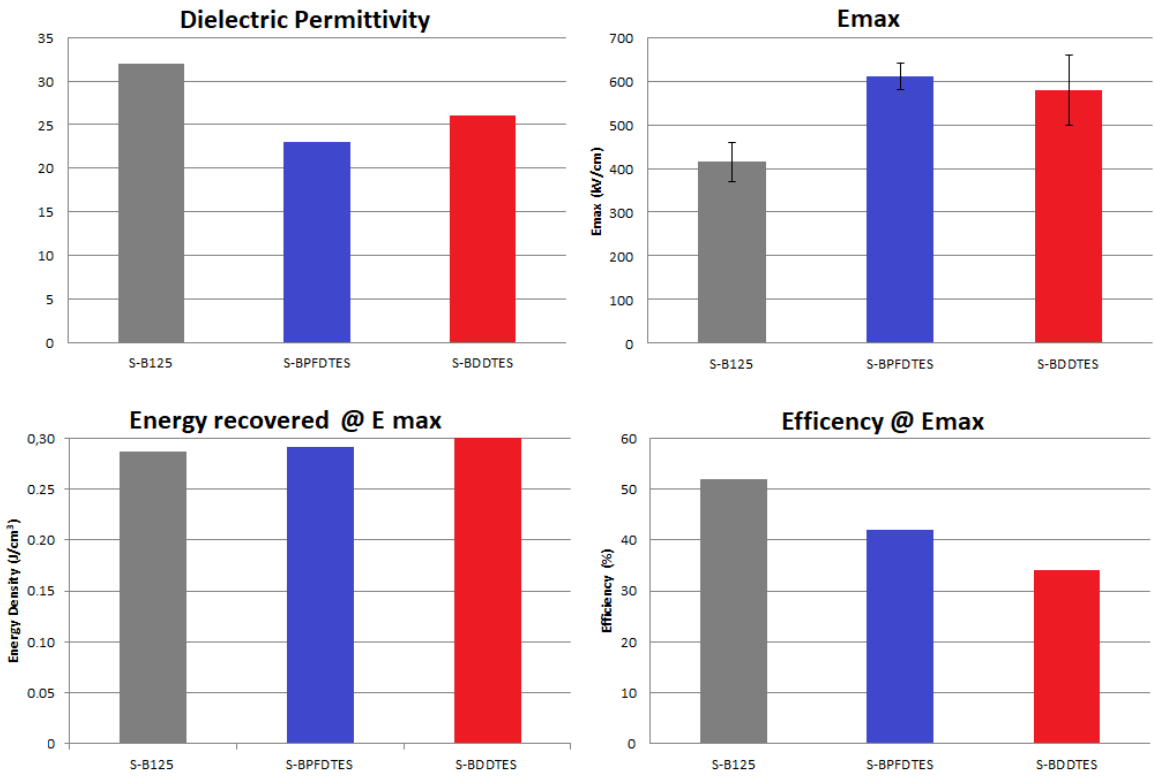

Figure 4.53: Values of: maximum electric field, energy storage density, and efficiency of composites containing pristine and functionalized BT. The permittivity values at 1 kHz are reported for sake of clarity.

4.3 Piezoelectric composites

As reported in the *Introduction*, this part of the work was carried out in the framework of a Serbian-Italian Bilateral Project (Project code: RS19MO01), whose main scope is to prepare and characterize flexible lead-free piezoelectric films for energy harvesting applications.
Piezoelectric generators exhibit a great potential for powering up low-power portable devices and self-powered electronic systems by extraction of mechanical energy. The advantage of piezoelectric mechanism over other conversion mechanisms lies in its high energy density and scalability across a wide range of dimensions. A recent challenge in electronics is also the exploitation of flexible electronics with the ability to bend into diverse shapes, that expands the applications of modern electronic devices in different areas, allowing their implementation in clothing, shoes and other accessories, as an example [226,227]. Thus far, piezoelectric generators commercially available were mostly lead-based materials, which are dangerous during their manufacturing, use and pose environmental issues for their disposal. Recent global restrictions are demanding the removal of lead from all consumer items, this has stimulated urgent solicitation for lead-free substitutes that can have piezoelectric properties comparable to the ones obtained from the lead-containing materials. Polymer-based composites containing piezoelectric lead-free fillers are growing in interest as suitable candidates.

This part of the research work regarding the piezoelectric properties of PVDF-based composites started with a preliminary study carried out by employing as piezo-active filler the classical lead zirconate titanate (PZT), widely used in this field, and then continued with the use of a more recent and suitable lead-free ceramics, namely bismuth sodium barium titanate (BNBT).

4.3.1 PVDF/PZT composites

At first, for the preliminary study on PVDF/PZT piezoelectrics, composites containing 50 Vol% PZT particles were prepared by solvent casting.
The high amount of active phase was chosen to verify the possibility of measuring a piezoelectric response whit the available instrumentation.
In particular, the films were obtained by using the two different methods of moulding (*i.e.*, single-step and double-step moulding) described in *Paragraph 3.4* and ceramic powders deriving from different thermal treatments were employed. The ensuing samples were indicated as PZTy-P1 or PZTy-P2, where y = 1, 2, 3 according to the thermal treatment the particles were subjected to (1 = 930°C for 2 h; 2 = 1200°C for 30 min; 3 = 1100°C for 30 min, see *Paragraph 3.2.1* for more details about the synthesis method) while P1 and P2 is related to SS and DS moulding, respectively, as in the labels of the previously discussed composites.

Some representative SEM micrographs are reported in Figure 4.54a-c. Despite the high filler percentage, also in this case, the preparation procedure guarantees a very good particle dispersion; in addition, the increasing dimensions of the particles with the temperature of treatment can be appreciated.

As already observed for the previously investigated composites, the double-step moulding (P2-samples) leads to a higher β phase amount (Figure 4.54d) and improved dielectric performance with respect to the single-step moulding (P1-samples). However, in this case, the differences in dielectric permittivity values between the samples moulded with the two methods, is less marked (Figure 4.54e) than what observed for the composites previously presented in *Paragraph 4.1.3*, probably due to the higher PZT content, which predominates in the dielectric response.

The piezoelectric coefficient d_{33} of the films prepared through the double-step moulding is lower than that of the corresponding samples obtained by the single-step moulding (Figure 4.54f).

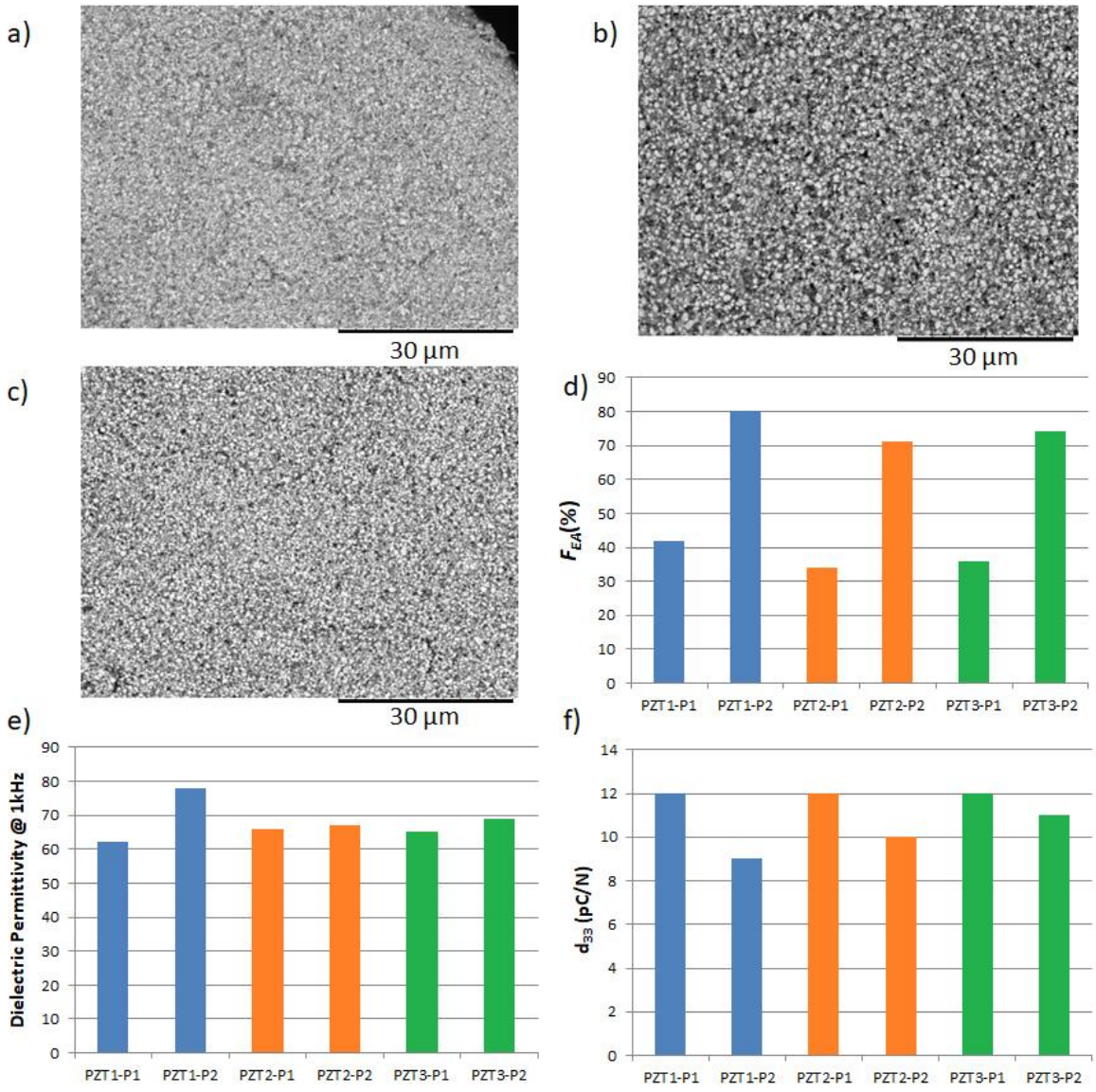

Figure 4.54: SEM micrograph of: a) PZT1-P1, b) PZT2-P2 and c) PZT3-P1 composites. d) Electroactive phase amount, e) dielectric permittivity and f) piezoelectric coefficient of the composites containing 50 Vol% of PZT.

This is reasonably due to the fact that the transversal piezoelectric coefficients of PVDF and its copolymers are positive, but the longitudinal one (that is d_{33}) is negative; indeed, if when an electric field is applied in the direction of polarization most ferroelectric materials expand, these fluorinated polymers tend to contract [228]. Thus, as concerns the piezoelectric response measured in the longitudinal direction, the contribution of the polymer matrix subtracts from the contribution of the ceramic filler (which possess a positive d_{33}); moreover because the higher the electroactive phase amount, the higher (*i.e.*, more negative) the piezoelectric coefficient of PVDF, the composites derived from the double-step moulding are characterized by lower d_{33} values.

Although the obtained piezoelectric coefficients are not so high, they are nevertheless comparable with data found in literature for analogous PVDF/PZT composites [48,229].

The experimental evidences suggest that, at equal moulding method used, the particles treatment does not remarkably affect the final properties of the composites.

Since such a high filler amount hampers too much the flexibility of the films, and also taking into account the project purpose, the work was carried on by preparing other samples with a lower PZT content (*i.e.* 30 Vol%). In this case, both as synthetized PZT1 and sintered and crushed PZT4 particles were used while SS method was chosen for the compression moulding.

The mild sintering used for the preparation of PZT4 leads to the formation of aggregates which can be to a large extent destroyed by the prolonged milling with zirconia spheres, required by the solvent casting procedure. For this reason, the milling time was reduced to 2 h. The SEM images of the ensuing composites are shown in Figure 4.55. The differences between the two composites are clearly visible: in 30PZT1-P1 composite particles are finely dispersed into the polymer matrix, while the morphology of sample 30PZT4-P1 is characterized by the presence of well separated particles accompanied by aggregates resulting from the sintering process, homogeneously distributed along the sample cross-section.

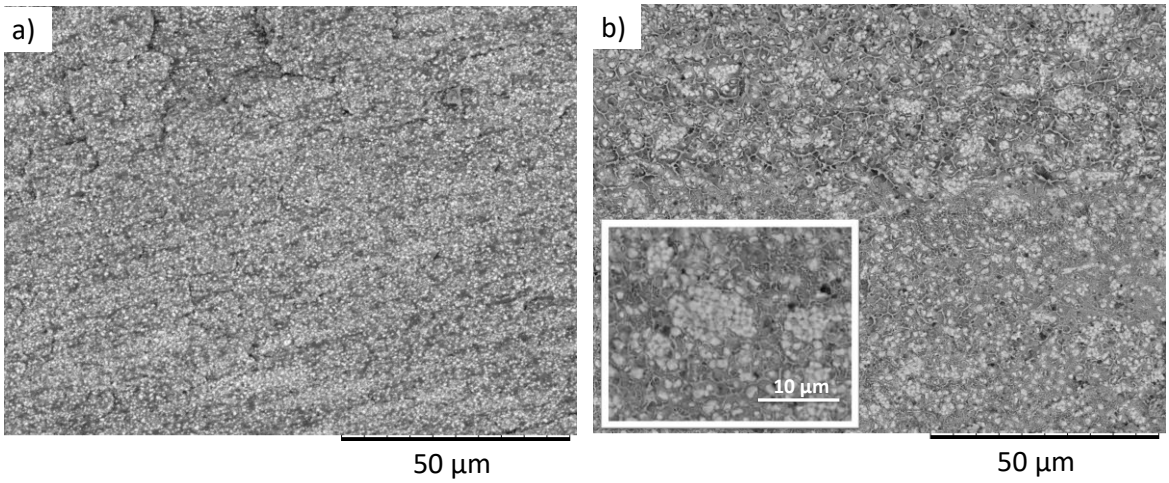

Figure 4.55: SEM micrographs of: a) 30PZT1-P1; b) 30PZT4-P1.

The results deriving from spectroscopic, dielectric and piezoelectric characterization are summarized in Table 4.13.

The composite containing PZT4 is characterized by a piezoelectric coefficient which is more than the double than the d_{33} of the film containing PZT1 particles and this is coherent with what observed in literature concerning the influence of filler dimensions (*see Paragraph 2.3*). More specifically, since in this case the coarser particles mainly consist of agglomerates, also the effect of a different filler dispersion can be important in determining the final piezoelectric properties.

J. E. Q. Quinsaat *et al.* [230], by preparing PDMS/PZT composites at different concentration and with two different filler sizes, found that the samples containing larger and less dispersed particles were more performing. In particular, they ascribe the higher d_{33} values to the higher connectivity between the particles into the agglomerates; the shorter inter-particle distance leads to higher stresses at the contact point between particles, increasing the piezoelectric response of the material.

Table 4.13: Electroactive phase amount, dielectric permittivity and piezoelectric coefficient of the composites containing 30 Vol% PZT.

Sample	F_{EA} **(%)**	ε	d_{33} **(pC/N)**
30PZT1-P1	32	30	2
30PZT4-P1	30	27	4.4

For the composite containing PZT4 particles, the effect of the poling conditions on the dielectric and piezoelectric response was also studied. In particular, the sample was subjected to two different poling processes. A first poling was carried out at 120°C for 40 min under a 6 kV/mm electric field (resulting d_{33} reported in Table 4.13), and a second poling was repeated at 120°C for 40 min but increasing the electric field to 18 kV/mm. In both cases the electric field was maintained during the cooling until the film reached the room temperature.

The sample was subjected to measurements before and after the first and the second poling process: the obtained results are reported in Figure 4.56.

As expected, the resonance and anti-resonance peaks, not present in the unpoled film, appear, at about 39 Hz, in the poled sample, their intensity increasing by increasing the polarization field (Figure 4.56a). As a consequence, also the piezoelectric coefficient increases from 4.4 up to 8 pC/N (Figure 4.56b) because, at fixed temperature and time of poling, the stronger the polarization field, the easier the electric domain begin to align in the piezoelectric material [48].

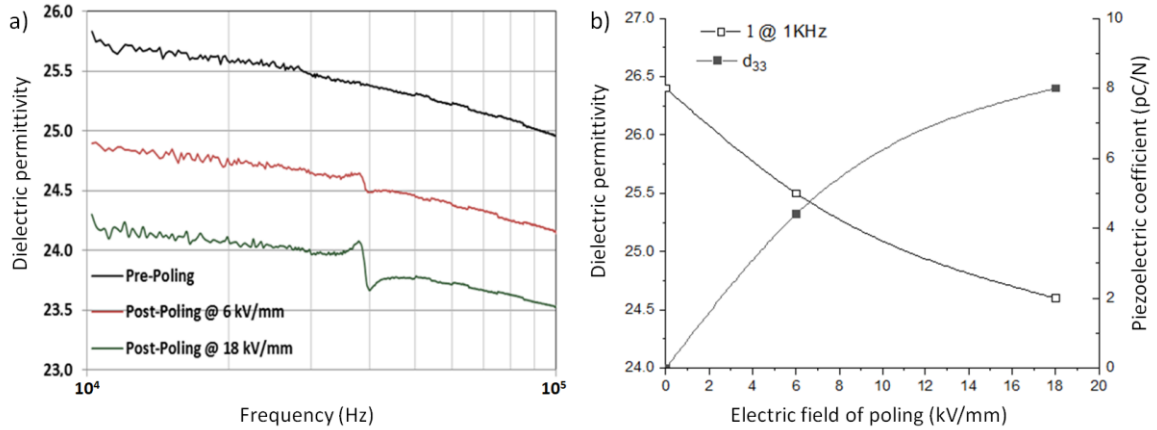

Figure 4.56: a) Resonance and anti-resonance peaks of dielectric permittivity of 30PZT4-P1 composite before and after poling; b) Permittivity at 1 kHz and piezoelectric coefficient of the film as a function of polarization field.

The polarization process has also an effect on the dielectric response: the permittivity of the composite after poling is slightly lower and the dielectric losses (here not shown) slightly higher with respect to the unpoled sample.

As concerns the single components, in literature, an increase of permittivity upon poling has been observed for PVDF; this increment was ascribed to dipole alignment and preferred orientation in the interface regions between crystalline and non-crystalline regions [231]. The behaviour of the ceramic counterpart appears more complex. As an example, J. K. Hong *et al.* [232], studying the properties of PMWN-PZT ceramics, found that the dielectric constant of the poled ceramics is increased in the tetragonal phase and decreased in rhombohedral phase with respect to the unpoled ceramics. They explain this trend by considering that the dielectric constant of piezoelectric ceramics is determined by compromising effects between two contrasting factors: *(i)* the dipole rotation to the poling direction, which is a decreasing factor because, for a single crystal, the permittivity is lower along the dipole axis with respect to perpendicularly to it and *(ii)* the stress induced by electrostriction, which leads to an increase of permittivity.

More in general, the variation of the dielectric permittivity with poling in composites based on PVDF or its copolymers is not clear. Different trends have been measured and explanations are often missing or not properly supported.

For instance, A. Sasmal *et al.* [233] found that the permittivity of PVDF/$Bi_{0.95}Ba_{0.05}Fe_{0.95}Zr_{0.05}O_3$ poled composites is higher than that of the unpoled ones, and the value increases by increasing the field of poling; they ascribe this trend to the improvement in dipolar polarization.

On the contrary, K. L. Ng *et al.* [234] and K.-H. Lam *et al.* [235] found a slight decrease in the dielectric permittivity with the poling process for PVDF-TrFE/PZT and PVDF-TrFE/BNBT composites, respectively. In particular, K.-H. Lam *et al.*, attribute this effect to the reduction of permittivity measured for the single polymeric and ceramic phases as well; indeed poled BNBT ceramics and PVDF-TrFE copolymer showed lower dielectric constant values with respect to the corresponding unpoled materials.

4.3.2 Lead-free composites

After the preparatory study on the PVDF/PZT composites, the work was carried on with the preparation and characterization of the PVDF/BNBT composites.

These composites were prepared by using two different techniques, hot-pressing and solvent casting, and two types of BNBT particles with different dimensions, namely, BNBTs and BNBTc. Such ceramic particles were morphologically characterized by SEM: two representative images are reported in Figure 4.57a,b. As for the previously investigated PVDF/PZT composites (see *Paragraph 4.3.1*), also in this case, the particles with larger dimensions consist actually of smaller (as synthesized) particles which form aggregates as a consequence of a mild treatment of sintering. Thus, as concerns the composites preparation by solvent casting technique, to preserve the filler dimensions, 2 h of ball milling was used; this treatment was verified to be enough to guarantee a good filler distribution within the polymer matrix while maintaining the aggregates dimensions (Figure 4.57c).

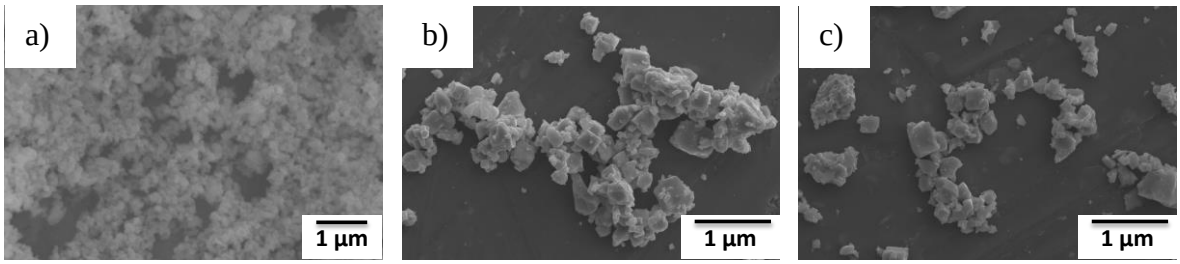

Figure 4.57: Morphological SEM analysis of: a) smaller particles (BNBTs); b) coarser particles (BNBTc); c) coarser particles after 2h milling.

Composites from hot pressing. The PVDF/BNBT composites from hot-pressing were prepared during the stay in Serbia, at the Institute for Multidisciplinary Research (University of Belgrade).

Through the procedure described in *Paragraph 3.4.3*, composite films with different compositions (up to 40 Vol%) were prepared, by using BNBTs as filler. The composites are named xBNBTs-hp, where x is the amount of filler and hp indicates the hot-pressing method. A reference PVDF film (named PVDF-hp) was also prepared for comparison purpose.

The films were, at first, characterized from the spectroscopic and calorimetric point of view.

ATR-FTIR analysis of the samples revealed the co-presence of both β and γ phase of PVDF, with a total electroactive phase amount ranging from 50 to 65%. The neat PVDF sample is characterized by 54% of electroactive phase, of which the main part (50%) consist of γ phase. The results relative to the composites are reported in Table 4.14. The presence of the filler induces the formation of β phase but, contrary to what observed for the composites prepared by melt blending or solvent casting and then moulded with the double-step method, here, the fraction of β phase *F(β)* decreases by increasing the filler amount, being remarkably reduced in the composite with the highest BNBT content. This happens probably because the formation of the all-trans conformation is, in this case,

dominated not by the mechanical frictions generated inside the polymer during the moulding, but by the physico-chemical interaction between the matrix and the filler.

H. S. Mohanty *et al.* [236] ascribed the formation of β phase in PVDF/BNBT composites to the interaction between the partially positive charge of $–CH_2$ dipole of the polymer matrix and the negatively charged filler surface; they found that the amount of β phase increases up to the composition of the percolation threshold and then decreases because the ion-dipole interactions decrease with the filler agglomeration. Based on this explanation, as concerns the composites here prepared by hot-pressing, the trend of *F(β)* suggests that the composition of the samples is above the percolation threshold: in this range an increase in filler amount leads to progressive reduction of the polymer/particles contact area which promotes the formation of β phase.

Table 4.14: Crystallinity degree and electroactive phase(s) amount of the PVDF/BNBTs composites prepared by hot-pressing.

Sample	X_c (%)	F_{EA} (%)	F_{EA}^* (%)	F(β) (%)	F(γ) (%)
30BNBTs-hp	44	65	29	45	20
35BNBTs-hp	40	50	20	32	18
40BNBTs-hp	42	56	23	7	49

The morphology of the films from hot-pressing (see Figure 4.58 as an example) is characterized by the presence of darker strips consisting almost exclusively of PVDF matrix, as indicated from EDX analysis. Outside these areas, the particles are anyhow finely dispersed.

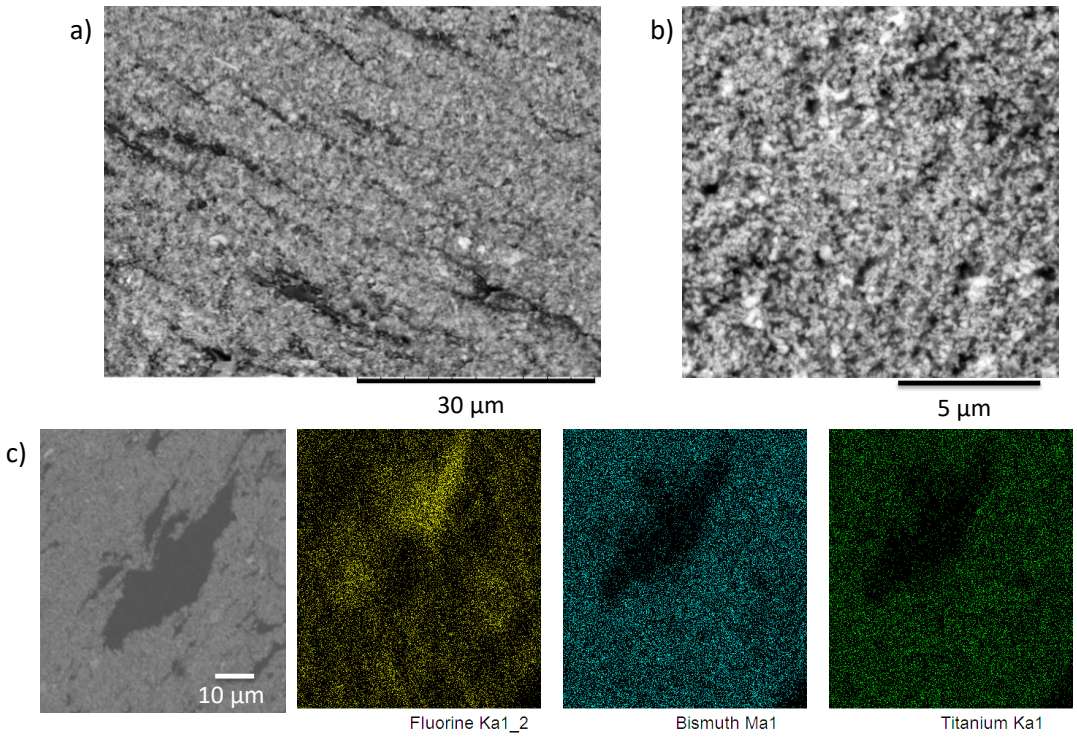

Figure 4.58: a) Low- and b) high-magnification SEM micrographs and c) EDX mapping of 30BNBTs-hp.

P-E hysteresis loops of pure PVDF and its composites measured at room temperature, up to 170 kV/cm electric field and 100 Hz frequency are presented in Figure 4.59a. Ferroelectric measurements revealed, in general, the difficulties of obtaining fully saturated hysteresis loops in inhomogeneous ferroelectric materials; these are due to the formation of charge layers at the ferroactive-polymer phase interfaces, combined with the limitation of the voltage source (4000 V). This behaviour can be seen in literature quite often for PVDF-based composites [25,237,238] and prevent the possibility of comparing the remnant polarization values of the films with high accuracy.

Many parameters can influence the ferroelectric properties such as interface areas, agglomerations, voids in the composites, inhomogeneous distribution of filler in the polymer matrix etc. [25,237,238]. However, there are a couple of more important effects that can influence the ferroelectric properties of these composite materials and have to be considered.

The sintered BNBT ceramics, obtained from the same powders introduced in the composites, possesses good ferroelectric properties with saturated square shaped hysteresis loop (Figure 4.59b); the remnant polarization (P_r) field measured at 50 kV/cm are 38 μC/cm^2, which is in agreement with the data available from literature [51-52].

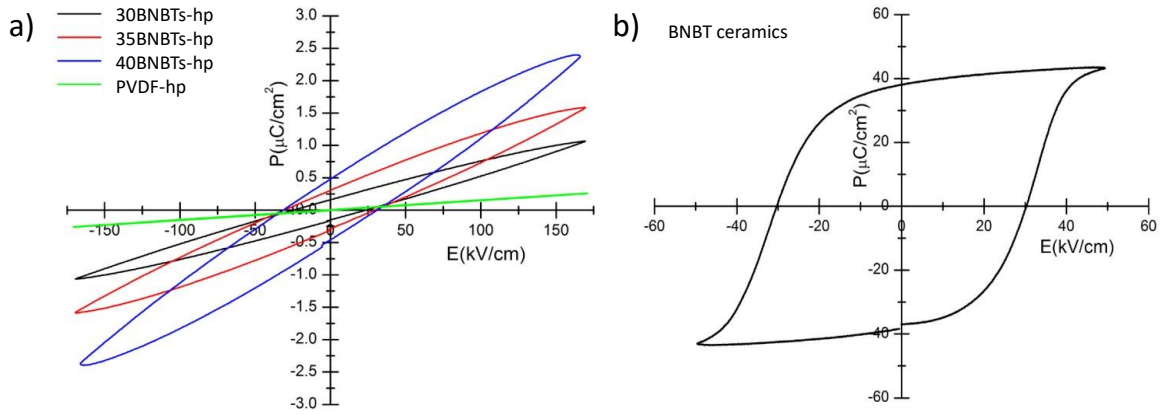

Figure 4.59: Ferroelectric properties of: neat PVDF and of the composites at 170 kV/cm and b) BNBT ceramics at the highest field reached.

Likewise, the literature about ferroelectric properties of pure α, β and γ PVDF films points to the possibility of a profound effect of PVDF phases on the ferroelectric properties of the composites. Neat PVDF β phase shows typical characteristic of normal ferroelectric in the squared shaped loops for its all-trans conformations. α and γ PVDF phases have smaller remnant polarization under the same conditions, and the value for γ-PVDF is slightly higher than that for α-PVDF [33-34]. Thus, in the case here reported, there can be a combined effect of both influence of the filler amount and effect of PVDF crystal phases present in the each film. The 30BNBT-hp has the lowest amount of the filler but also the highest concentration of the ferroelectric β- phase (45%) and it shows a bit lower P_r value in comparison with the 35BNBT-hp sample which has 32 % of β phase but a higher concentration of the filler. The largest loop area which is connected with high losses can be seen

for the 40BNBT-hp sample that possesses the highest amount of filler but the lowest concentration of the ferroelectric β phase (7%).

The overall dielectric characterization showed that the dielectric permittivity increases by increasing the filler amount, reaching (at room temperature and 1 kHz) values around 40 for the composite containing 30 Vol% of filler and around 80 for the composites with 40 Vol% BNBT amounts (Figure 4.60). The losses measured in the same conditions remain below 3%.

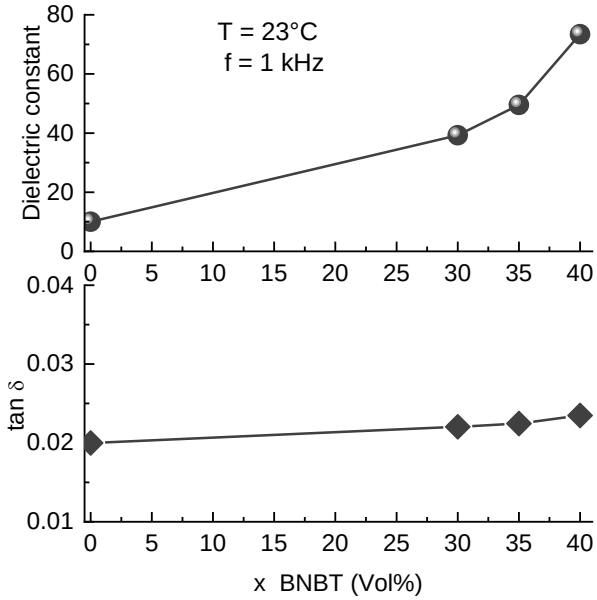

Figure 4.60: Dielectric permittivity (above) and dielectric losses (below) at room temperature and 1 kHz of the composites prepared from hot-pressing and containing BNBTs particles.

The piezoelectric response of these composites was also tested. The flexible films were subjected to poling at 120°C for 40 min at field 5 kV/mm detecting the voltage output generated by them as a consequence of a cyclic force impact of about 100 N.

As visible from Figure 4.61 the output voltage is about 3 for 30BNBTs-hp, about 2 for 35BNBTs-hp, and about 1 for 40BNBTs-hp. This counterintuitive trend seems to follow the amount of β phase, which increases by decreasing the filler content. With a roughly estimation, the total piezoelectric active phase (BNBT + PVDF β phase) results about 62% for 30BNBTs-hp, 56% for 35BNBTs-hp and 44% for 40BNBTs-hp, respectively. However, a viewpoint that cannot be ignored is that, in literature, is often reported that the piezoelectric constants of the ceramic filler and the PVDF matrix have positive and negative values, respectively which may cancel, and not improve, the effect of each other. Thus, such a trend could be explained by assuming that the contribution of the polymer matrix dominates the composites response. Added to this is the relative density of the films which was around 97% for the 30 and 35 Vol% of BNBT and around 92% for the 40 Vol% of BNBT, indicating a higher porosity for the composites with the highest filler amount, that can negatively affect the piezoelectric performances. Nevertheless, another interesting hypothesis is related to the particular microstructure of these films, which are characterized by the presence of strips consisting of neat PVDF embedded in a composite material. P. Hu *et al.* [239]

prepared double-layer (DL) PVDF/BT – PVDF composites and compared their properties with those of traditional single-layer (SL) PVDF/BT composites. The DL composites were characterized by higher output voltage than the corresponding SL composites because the inductive charges accumulated at the additional interlayer interface between BT/PVDF layer and PVDF layer produce more polarization and enhance the total piezoresponse. An analogous phenomenon probably occurs in the present composites from hot-pressing, at the interfaces between the PVDF strips and the rest of the material; this hypothesis is also in accordance with the fact that the extension of the strips decreases by increasing the filler amount.

Anyway, these measurements clearly show the capability of charge generation of these flexible lead-free composites when subjected to a deformation, indicating that they are promising candidates in the field expanding of energy harvesting.

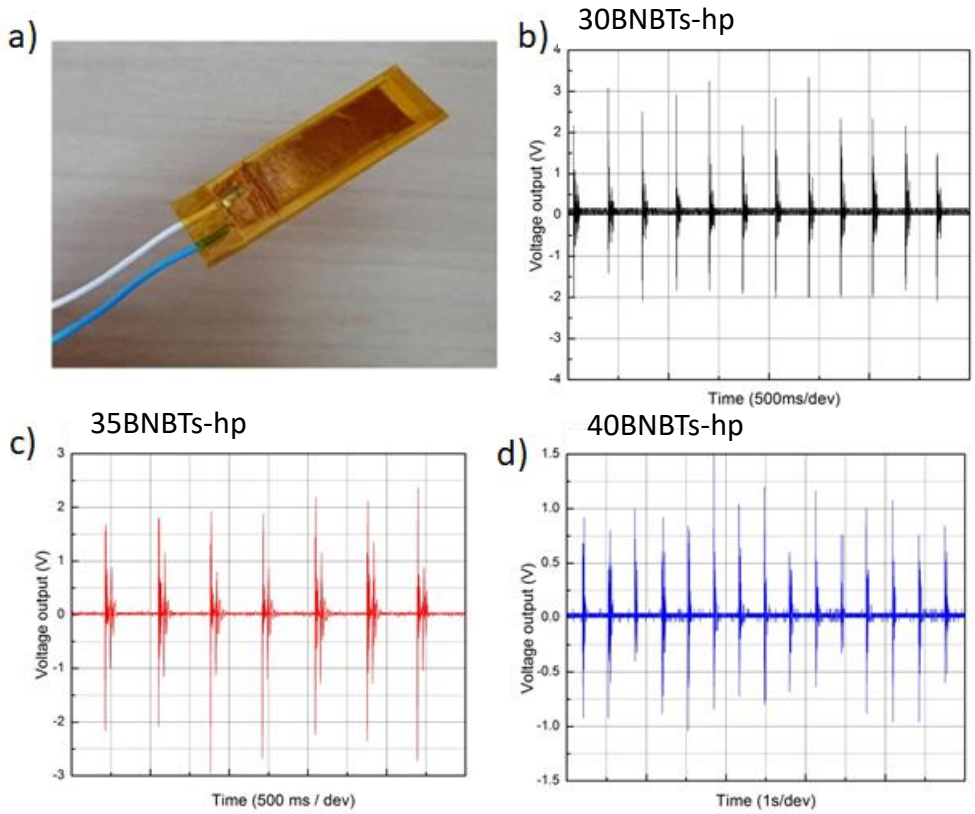

Figure 4.61: a) Image of a PVDF/BNBT composite sputtered with Ag, wired and integrated in the Kapton tape. Voltage output of: b) 30BNBTs-hp; c) 35BNBTs-hp; d) 40BNBTs-hp.

Composites from solvent casting. The composites from solvent casting were prepared by fixing 30 Vol% of BNBT as composition, in order to be able of comparing these samples with the other composites previously prepared. In this case, two different types of matrices (*i.e.*, PVDF and PVDF-HFP) were employed. Taking into account the experimental evidences obtained for the PVDF/PZT composites, the single-step process was chosen as method of moulding.

These samples were named 30BNBTy-P1, where 30 is referred to the composition and y = c or s indicates the coarser or smaller powder batch, respectively; the label is accompanied by “copo” when PVDF-HFP was used as the polymer matrix.

As already observed with the previous films from solvent casting, also in this case the filler resulted finely dispersed within the polymer matrix (Figure 4.62). As concerns the composites containing particles with higher dimensions, there appears to be better filler/matrix adhesion with the copolymer than with PVDF homopolymer.

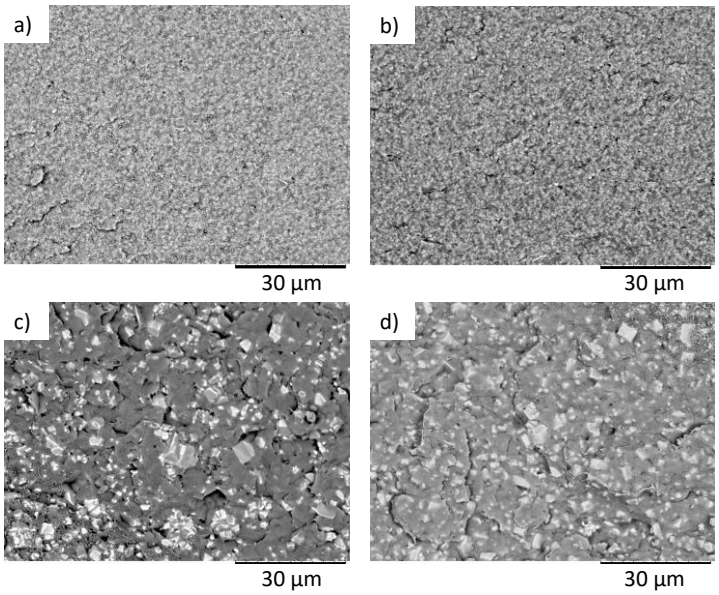

Figure 4.62: SEM micrographs of: a) 30BNBTs-P1; b) 30BNBTs-P1copo; c) 30BNBTc-P1; d) 30BNBTc-P1copo.

The results relative to the spectroscopic (ATR-FTIR) and calorimetric (DSC) characterization of the samples are summarized in Table 4.15.

Coherently with what observed in the previous study comparing the neat polymer matrices, the copolymer crystallinity degree in PVDF-HFP based composites is lower than that observed in the PVDF based counterparts.

In this case, it is interesting to note that the electroactive phase amounts of samples containing the BNBTc particles are comparable to those of the previously reported films moulded with SS method (*i.e.*, around 30%) while F_{EA} values of the composites containing BNBTs particles are higher. This suggests a more pronounced interaction between this type of filler and the polymer matrix, promoting β phase formation also in absence of high pressure.

Table 4.15: Crystallinity degree and electroactive phase amount of PVDF/BNBT composites prepared by solvent casting.

Sample	X_C	F_{EA}	F_{EA}*
30BNBTs-P1	54	41	22
30BNBTc-P1	64	26	17
30BNBTs-P1copo	35	52	18
30BNBTc-P1copo	34	31	10

The composites were then characterized from the dielectric point of view, before and after being subjected to poling procedure at 6 kV/mm. The corresponding values of permittivity are reported in Figure 4.63b.

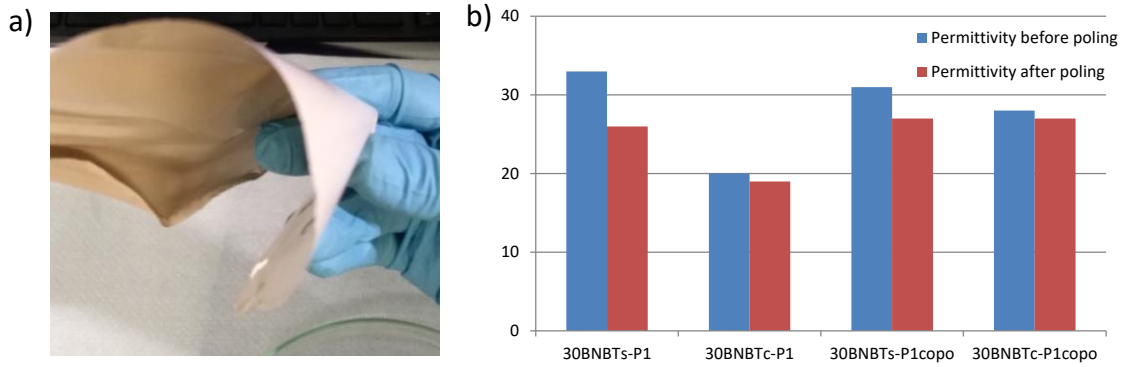

Figure 4.63: a) Picture of one of the flexible lead-free composites from solvent casting; b) dielectric permittivity at 1 kHz of the PVDF/BNBT composites from solvent casting before and after poling.

At equal polymer matrix, the permittivity results higher for the composite containing the smaller BNBTs particles than for those with coarser filler. This result can be ascribed to the different polymorphism of the matrix, which is characterized by higher β phase amount in the samples containing BNBTs. As already observed in *Paragraph 4.3.1*, the permittivity decreases after poling; in particular, its reduction is less marked for the composites containing BNBTc.

After poling, the piezoelectric characterization was carried out. The piezoelectric coefficient was appreciable only for two samples: 30BNBTc-P1 and 30BNBTc-P1copo, being their d_{33} value equal to 3.3 and 6 pC/N, respectively. The response of 30BNBTs-P1 and 30BNBTs-P1 is probably too low to be detected with the Berlincourt method.

The composites were also subjected to impact force test and the results are reported in Figure 4.64.

In line with the measurements of d_{33} values, 30BNBTc-P1 and 30BNBTc-P1copo composites, reaching the value of about 8 V, show a significantly enhanced output voltage with respect to 30BNBTs-P1 and 30BNBTs-P1 (whose maximum output voltage is around 2 V).

The higher piezolectric performance of the samples containing the coarser particles is in accordance with the trend observed for the PVDF/PZT composites and with what reported in literature [229].

By comparing these results with respect to those obtained for the composite series from hot-pressing, at equal filler type (*i.e.*, BNBTs) and composition (*i.e.*, 30 Vol%) the dielectric permittivity and the output voltage are, in this case, slightly lower. This can be due to the different processing procedure, leading to different microstructure: the improved particles distribution which characterized the composites from solvent casting also results in the absence of large discontinuity areas (*i.e.*, PVDF strips) which potentially enhance the interface polarization in the composites from hot-pressing [239]. As already observed in *Paragraph 4.3.1* for the PVDF/PZT samples not

always a flawless homogeneity of the composite necessary leads to an improved dielectric/piezoelectric response.

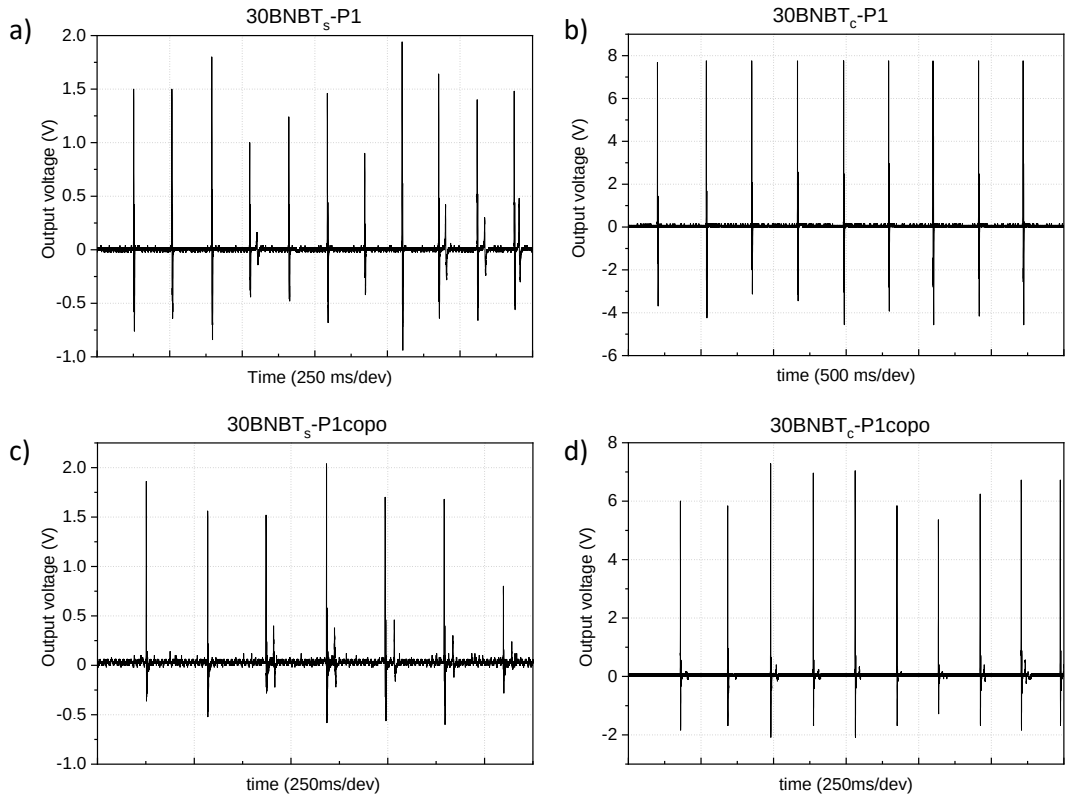

Figure 4.64: Output voltage measurements of the lead-free composites from solvent casting: a) 30BNBTs-P1; b) 30BNBTc-P1; c) 30BNBTs-P1copo; d) 30BNBTc-copoP1.

As far as we know, in literature, only few examples of fluorinated polymer-based composites containing BNBT particles are present [114,236,240,241]. In these papers the authors characterized the composites from the dielectric point of view without analysing their piezoelectric response.

The performance of the PVDF/BNBT and PVDF-HFP/BNBT films here presented are in line with those of many flexible piezoelectric composites made with other lead-free particles. As an example, S. A. Riquelme *et al.* [39,242] prepared PVDF-based composites containing from 35 to 65 wt% of BZT-BCTZ or KNNS-BNKZ particles and obtained d_{33} values ranging from 1 to 11 pC/N; M. Alexandre *et al.*[38] studied the effect of the introduction of $NaNbO_3$ nanoparticles or nanowires into PVDF matrix, measuring piezoelectric coefficients up to 4 pC/N; K. Yu *et al.* [40] prepared PVDF/KNNL-Z composites and found d_{33} around 5 and 12 pC/N for the films containing 40 and 50 wt% of particles, corresponding to 24 and 33Vol%, respectively.

This suggest that the flexible composites here prepared containing only 30 Vol% of BNBT particles have high potential to be used for environmentally safe energy harvesting devices.

5 Conclusions

The presented research activity was carried out in the framework of two CNR research projects: the POLYCOM Project (IDROL 10359) and a Serbian-Italian Bilateral Cooperation Project (Project code: RS19MO01), concerning the preparation, characterization and improvement of polymer-ceramics composites/nanocomposites for energy storage and conversion, respectively.
Specifically, this PhD research work mainly consisted of:

(i) the fabrication of 0-3 connectivity composites by using different starting materials (*i.e.*, inorganic filler and polymer matrix) and different processing techniques;

(ii) the investigation on process-structure-properties correlations.

A preparatory study of the individuated neat polymer matrices, namely poly(vinylidene fluoride) (PVDF) homopolymer and poly(vinylidene fluoride-*co*-hexafluoropropylene) (PVDF-HFP) copolymer, was performed, by focusing on the optimization of compression moulding technique to tune their polymorphism.
In particular, besides a traditional single-step moulding, carried out at temperatures above the melting temperature of the polymer, a double-step moulding was thoroughly studied by testing different processing conditions (*i.e.*, different starting plate thickness and different second step moulding temperature). This was revealed a promising method to induce the most polar electroactive crystalline polymorph, that is β phase. The formation of β phase during this processing is due to the internal shear stresses generated inside the material as a consequence of the transversal compression applied to the not completely molten polymer.

A principal component analysis (PCA) was performed on the infrared spectra of the moulded PVDF samples to validate the equation usually employed for the electroactive phase amount (F_{EA}) determination; it was found that:

(i) the two bands considered for such a calculation (*i.e.*, 763 and 840 cm^{-1}) are actually representative and important in the description of the whole IR spectrum, evidence which, as far as we know, had not yet been proven in literature;

(ii) the band around 1167 cm^{-1}, which is often considered independent from the PVDF polymorphism, tends instead to change by increasing the electroactive phase amount.

A multiple linear regression (MLR) was then applied to better understand how the processing parameters affect the F_{EA} value. A non-monotonous trend was found, which was explained by considering two contrasting factors:

(i) the effectiveness of compression, which increases by increasing the amount of molten polymer, and thus, by increasing the moulding temperature;

(ii) the phase transition of PVDF, which involves only the solid portion of the polymer, whose amount is higher for lower temperatures.

The double-step moulding also affects the dielectric and dynamic-mechanical properties, determining: an increase in permittivity, a reduction of the dielectric losses and a change in terms of molecular relaxations of PVDF chains with respect to the reference film moulded under simple single-step moulding conditions. The same behaviour was observed both for the PVDF homopolymer and its PVDF-HFP copolymer.

An analogous study was then extended to different PVDF-based composites.

Composites containing 10, 20 and 30 Vol% of PZT particles were prepared through solvent casting or melt blending procedures and then were compression moulded by using the two different methods previously mentioned.

The experimental evidences, derived from various characterizations carried out on the resulting composite materials, indicate that the different moulding processes have a strong effect on:

(i) the polymorphism of the polymer matrix, that is electroactive phase(s) amount;

(ii) the macromolecular relaxations;

(iii) dielectric response of the composites, resulting improved by the double-step moulding.

On the other hand, the preparation technique (solvent casting or melt blending) significantly influences the filler dispersion and, consequently, the elastic modulus of the composites, without remarkably impacting on other properties.

This experimental evidence suggests the possibility of preparing polymer/ceramics composites endowed with an overall good performance by a solvent-free and easily scalable technique (*i.e.*, melt blending) and then tune the moulding conditions to obtain suitable dielectric characteristics, very important for the application of such kind of materials.

Taking this into account, the melt blending technique was combined with the double-step moulding in order to obtain more green and performing PVDF/$BaTiO_3$ composites (composition 10 and 30 Vol%). For these composites, a more in-depth investigation of the molecular relaxation was carried out, by correlating the results from dynamic-mechanical analysis to those obtained from dielectric spectroscopy. It is worth noting that the attained PVDF/$BaTiO_3$ samples are characterized by very limited ageing and by dielectric properties comparable or even superior than those of analogous composites from solvent casting present in literature.

The work continued with the study of the influence of particles engineering and size on the final properties of the composites. To this purpose, PVDF-based composites containing 30 Vol% of $BaTiO_3$ particles with different dimensions and/or different surface modification/coating were prepared. Beforehand, particles functionalization was optimized by using a procedure that limits the amount of solvent in order to make it suitable for possible scale-up.

As concerns the engineered core-shell particles, coating of silica or titania were used.

For this study solvent casting was chosen as the preparation technique in light of the limited amount of powders available, while the double-step moulding was selected for the compression moulding. The obtained samples were thoroughly characterized and gathered results indicate that:

(i) the tested coupling agents, namely dodecyl triethoxysilane (DDTES) and 1H,1H,2H,2H-perfluorodecyl triethoxysilane (PFDTES), despite decreasing to a certain extent the dielectric permittivity of the ensuing composites (due to the intrinsic low permittivity of the silane moieties) increase the maximum electric field, thus leading to an energy recovered capability comparable or slightly higher than that of the composite containing pristine BT particles;

(ii) the presence of an inorganic shell around BT particles increases the maximum electric field, even if, as a whole, reduces the energy density values. In addition, the filler coating allows a modulation of the effective permittivity of the composites which, as predicted by FEM calculations, is predominantly due to intrinsic factors (*i.e.*, the permittivity of the components). It is worth noting that the composites containing core-shell particles are characterized by low tunability (*i.e.*, the dielectric response by varying the applied electric field), this parameter plays indeed an important role for application as dielectric capacitors;

(iii) the dielectric response of the composites is affected by the particles dimensions even though the films containing pristine BT and those containing TiO_2-coated particles follow a different trend of dielectric permittivity with filler size; this suggests a not negligible contribution of the interfaces, which varies with the method of particles synthesis. In general, the sample containing barium titanate particles with intermediate size results more performing in terms of energy density recovered.

Finally, the research activity was extended to the piezo-composites.

Also for this part of the thesis work, a preliminary study, performed on “traditional” PVDF/PZT composites, was proven to be useful as it allowed us finding that:

(i) the double-step moulding leads to lower piezoelectric coefficients because improves the amount of PVDF electroactive phase, whose d_{33} is opposite in sign with respect to that of the ceramic filler;

(ii) different thermal treatments of the ceramic particles do not affect the piezoelectric response, while mild sintering and crushing of the powders improve the d_{33}. This probably because the higher connectivity between the particles within the agglomerates, derived from the sintering, leads to higher stresses at the contact point between particles, increasing the piezoelectric response;

(iii) as expected, the poling conditions are important to determine the output performance of the composites; with the increase of the electric field used for poling, the dielectric constant slightly decreases while the piezoelectric coefficient markedly increases.

In line with an environmental sustainability concept, flexible lead-free piezo-active composites containing BNBT particles were lastly prepared by employing different preparation/processing procedures (*i.e.*, solvent casting and hot-pressing), different particles size and different polymer matrix (*i.e.,* PVDF and PVDF-HFP). As far as we know, this is the first time that the piezoelectric properties of composites made of fluorinated polymer matrix and BNBT filler are studied. The characterization of these composites led to these observations:

(i) the different preparation techniques induce a different microstructure of the composites. The films obtained from solvent casting are well homogeneous while those from hot-pressing are characterized by the presence of neat PVDF strips;

(ii) the dielectric permittivity of the composites from hot-pressing increases with the filler amount while the output voltage decreases. This unexpected trend can be explained by considering the polymorphism of the matrix, the density of the composites and their peculiar microstructuration;

(iii) the piezoelectric response of the composites from solvent casting is higher when the coarser BNBT particles (sintered and crushed) are used as the active ceramic filler; the maximum piezoelectric coefficient is 6 pC/N and the maximum output voltage 8 V, the latter being 4 times higher than the corresponding values of the other PVDF/BNBT composites.

(iv) the obtained piezoelectric performances are in line with those of many flexible lead-free composites made with particles different from BNBT, this suggesting the potentiality of these composites in the field of energy harvesting.

As a whole, the PhD research work here presented clearly demonstrates how proper design and engineering of polymer/ceramics composites, based on the combination of fluorinated polymer matrices and perovskitic ceramic fillers, is of uppermost importance to enhance the specific performance and ultimate properties of such kind of composite materials, so important in the increasingly growing field of energy related applications.

Indeed, the preparation technique as well as the subsequent moulding method, by affecting the polymorphism of the polymer matrix and the microstructure of the investigated composites at different level, can be very important in determining their ultimate properties. In particular, I showed that not always a “perfect” particles dispersion necessary leads to the best final performance of the composite and that other structural factors such as the compactness of the films should not be neglected.

At fixed processing conditions, playing on filler size and/or polymer/particles interfaces can be a smart approach to tune the dielectric and piezoelectric performance of the composites.

However, the final effect is not so easy to be predicted because of contrasting factors which play a role in the system. As an example, the particle surface modification leads to an improvement of some parameters, such as an increment in the breakdown field and a reduction of tunability; however, if the low permittivity of the coating (or coupling agent) prevails on the interfacial polarization in determining the dielectric constant, the capability of storing energy of the ensuing composites can be reduced.

As principal achievements, I obtained:

(i) an alternative and smart method to tune the polymorphism of PVDF homopolymer and its copolymers, by exploiting a simple and easily-scalable processing technique;

(ii) solvent-free polymer-based composites with dielectric properties improved by the moulding process;

(iii) a better comprehension about the role of the interfaces, useful to control and steer the final performance of the dielectric composites;

(iv) flexible lead-free polymer-based composites with good piezoelectric response and potential application for safe energy harvesting devices.

6 Bibliography

[1] H.S. Kim, J.-H. Kim, J. Kim, A review of piezoelectric energy harvesting based on vibration, Int. J. Precis. Eng. Manuf. 12 (2011) 1129–1141. https://doi.org/10.1007/s12541-011-0151-3.

[2] Y. Wang, M. Yao, R. Ma, Q. Yuan, D. Yang, B. Cui, C. Ma, M. Liu, D. Hu, Design strategy of barium titanate/polyvinylidene fluoride-based nanocomposite films for high energy storage, J. Mater. Chem. A. 8 (2020) 884–917. https://doi.org/10.1039/C9TA11527G.

[3] Z.-M. Dang, J.-K. Yuan, J.-W. Zha, T. Zhou, S.-T. Li, G.-H. Hu, Fundamentals, processes and applications of high-permittivity polymer–matrix composites, Prog. Mater. Sci. 57 (2012) 660–723. https://doi.org/https://doi.org/10.1016/j.pmatsci.2011.08.001.

[4] Prateek, V.K. Thakur, R.K. Gupta, Recent Progress on Ferroelectric Polymer-Based Nanocomposites for High Energy Density Capacitors: Synthesis, Dielectric Properties, and Future Aspects, Chem. Rev. 116 (2016) 4260–4317. https://doi.org/10.1021/acs.chemrev.5b00495.

[5] Z. Sun, Z. Wang, Y. Tian, G. Wang, W. Wang, M. Yang, X. Wang, F. Zhang, Y. Pu, Progress, Outlook, and Challenges in Lead-Free Energy-Storage Ferroelectrics, Adv. Electron. Mater. 6 (2020) 1900698. https://doi.org/https://doi.org/10.1002/aelm.201900698.

[6] P. Barber, S. Balasubramanian, Y. Anguchamy, S. Gong, A. Wibowo, H. Gao, H.J. Ploehn, H. Loye, Polymer Composite and Nanocomposite Dielectric Materials for Pulse Power Energy Storage, Polym. Compos. Nanocomposite. 2 (2009) 1697–1733. https://doi.org/10.3390/ma2041697.

[7] I. BUNGET, M. POPESCU, Physics of solid dielectrics, 19 (1984) 443.

[8] J. Kuffel, P. Kuffel, High Voltage Engineering Fundamentals, 2nd ed., Elsevier Science, 2000. https://doi.org/doi.org/10.1016/b978-0-7506-3634-6.x5000-x.

[9] J. Artbauer, Electric strength of polymers, J. Phys. D. Appl. Phys. 29 (1996) 446–456. https://doi.org/10.1088/0022-3727/29/2/024.

[10] V.A. Zakrevskii, N.T. Sudar, A. Zaopo, Y.A. Dubitsky, Mechanism of electrical degradation and breakdown of insulating polymers, J. Appl. Phys. 93 (2003) 2135–2139. https://doi.org/10.1063/1.1531820.

[11] L. Roselli, C. Mariotti, P. Mezzanotte, F. Alimenti, G. Orecchini, M. Virili, N.B. Carvalho, Review of the present technologies concurrently contributing to the implementation of the Internet of Things (IoT) paradigm: RFID, Green Electronics, WPT and Energy Harvesting, in: 2015 IEEE Top. Conf. Wirel. Sensors Sens. Networks, 2015: pp. 1–3. https://doi.org/10.1109/WISNET.2015.7127402.

[12] W.R. Cook, H.R. Jaffe, Piezoelectric Ceramics, Academic Press, London, 1971. https://books.google.it/books?id=GJC_MBEM4VMC.

[13] S. Katzir, Who knew piezoelectricity? Rutherford and Langevin on submarine detection and the invention of sonar, Notes Rec. R. Soc. 66 (2012) 141–157. https://doi.org/10.1098/rsnr.2011.0049.

[14] R.S. Dahiya, M. Valle, Robotic Tactile Sensing, Springer Netherlands, Dordrecht, 2013. https://doi.org/10.1007/978-94-007-0579-1_5.

[15] L. Pardo, R. Jiménez, A. Garcia, K. Brebol, G. Leighton, Z. Huang, Impedance measurements for determination of elastic and piezoelectric coefficients of films, Adv. Appl. Ceram. 109 (2010) 156–161. https://doi.org/10.1179/174367509X12502621261497.

[16] Z. Butt, Z. Anjum, A. Sultan, F. Qayyum, H. Muhammad, M. Ali, S. Mehmood, Investigation of Electrical Properties & Mechanical Quality Factor of Piezoelectric Material (PZT-4A), J. Electr. Eng. Technol. 12 (2017) 846–851. https://doi.org/10.5370/JEET.2017.12.2.846.

[17] M. Stewart, M. Cain, Direct Piezoelectric Measurement: The Berlincourt Method, in: M. Cain (Ed.), Characterisation Ferroelectr. Bulk Mater. Thin Film., 2nd ed., Springer Series in Measurement Science and Technology, 2014: pp. 37–64. https://doi.org/10.1007/978-1-4020-9311-1_3.

[18] C.K. Jeong, J. Lee, S. Han, J. Ryu, G.-T. Hwang, D.Y. Park, J.H. Park, S.S. Lee, M. Byun, S.H. Ko, K.J. Lee, A Hyper-Stretchable Elastic-Composite Energy Harvester, Adv. Mater.

27 (2015) 2866–2875. https://doi.org/https://doi.org/10.1002/adma.201500367.
[19] S. Mishra, L. Unnikrishnan, S.K. Nayak, S. Mohanty, Advances in Piezoelectric Polymer Composites for Energy Harvesting Applications: A Systematic Review, Macromol. Mater. Eng. 304 (2019) 1800463. https://doi.org/https://doi.org/10.1002/mame.201800463.
[20] Z.-M. Dang, Y.-H. Lin, C.-W. Nan, Novel Ferroelectric Polymer Composites with High Dielectric Constants, Adv. Mater. 15 (2003) 1625–1629. https://doi.org/https://doi.org/10.1002/adma.200304911.
[21] L. Qi, B.I. Lee, S. Chen, W.D. Samuels, G.J. Exarhos, High-Dielectric-Constant Silver–Epoxy Composites as Embedded Dielectrics, Adv. Mater. 17 (2005) 1777–1781. https://doi.org/https://doi.org/10.1002/adma.200401816.
[22] A.B. da Silva, M. Arjmand, U. Sundararaj, R.E.S. Bretas, Novel composites of copper nanowire/PVDF with superior dielectric properties, Polymer (Guildf). 55 (2014) 226–234. https://doi.org/https://doi.org/10.1016/j.polymer.2013.11.045.
[23] L. Yao, Z. Pan, J. Zhai, G. Zhang, Z. Liu, Y. Liu, High-energy-density with polymer nanocomposites containing of SrTiO3 nanofibers for capacitor application, Compos. Part A Appl. Sci. Manuf. 109 (2018) 48–54. https://doi.org/https://doi.org/10.1016/j.compositesa.2018.02.040.
[24] L. Zhang, P. Wu, Y. Li, Z.-Y. Cheng, J.C. Brewer, Preparation process and dielectric properties of Ba0.5Sr0.5TiO3–P(VDF–CTFE) nanocomposites, Compos. Part B Eng. 56 (2014) 284–289. https://doi.org/https://doi.org/10.1016/j.compositesb.2013.08.029.
[25] W. Nian, Z. Wang, T. Wang, Y. Xiao, H. Chen, Significantly enhanced breakdown strength and energy density in sandwich-structured NBT/PVDF composites with strong interface barrier effect, Ceram. Int. 44 (2018) S50–S53. https://doi.org/https://doi.org/10.1016/j.ceramint.2018.08.260.
[26] Y. Zhang, X. Liu, J. Yu, M. Fan, X. Ji, B. Sun, P. Hu, Optimizing the dielectric energy storage performance in P(VDF-HFP) nanocomposite by modulating the diameter of PZT nanofibers prepared via electrospinning, Compos. Sci. Technol. 184 (2019) 107838. https://doi.org/https://doi.org/10.1016/j.compscitech.2019.107838.
[27] S. Moharana, M.K. Mishra, M. Chopkar, R.N. Mahaling, Enhanced dielectric properties of surface hydroxylated bismuth ferrite–Poly (vinylidene fluoride-co-hexafluoropropylene) composites for energy storage devices, J. Sci. Adv. Mater. Devices. 1 (2016) 461–467. https://doi.org/https://doi.org/10.1016/j.jsamd.2016.08.008.
[28] R.E. Newnham, D.P. Skinner, L.E. Cross, Connectivity and piezoelectric-pyroelectric composites, Mater. Res. Bull. 13 (1978) 525–536. https://doi.org/https://doi.org/10.1016/0025-5408(78)90161-7.
[29] P. Kim, N.M. Doss, J.P. Tillotson, P.J. Hotchkiss, M.-J. Pan, S.R. Marder, J. Li, J.P. Calame, J.W. Perry, High Energy Density Nanocomposites Based on Surface-Modified BaTiO3 and a Ferroelectric Polymer, ACS Nano. 3 (2009) 2581–2592. https://doi.org/10.1021/nn9006412.
[30] B.-H. Fan, J.-W. Zha, D. Wang, J. Zhao, Z.-M. Dang, Size-dependent low-frequency dielectric properties in the BaTiO3/poly(vinylidene fluoride) nanocomposite films, Appl. Phys. Lett. 100 (2012) 12903. https://doi.org/10.1063/1.3673555.
[31] Z.-H. Shen, J.-J. Wang, Y. Lin, C.-W. Nan, L.-Q. Chen, Y. Shen, High-Throughput Phase-Field Design of High-Energy-Density Polymer Nanocomposites, Adv. Mater. 30 (2018) 1704380. https://doi.org/https://doi.org/10.1002/adma.201704380.
[32] Y. Niu, H. Wang, Dielectric Nanomaterials for Power Energy Storage: Surface Modification and Characterization, ACS Appl. Nano Mater. 2 (2019) 627–642. https://doi.org/10.1021/acsanm.8b01846.
[33] P. Martins, A.C. Lopes, S. Lanceros-Mendez, Electroactive phases of poly(vinylidene fluoride): Determination, processing and applications, Prog. Polym. Sci. 39 (2014) 683–706. https://doi.org/https://doi.org/10.1016/j.progpolymsci.2013.07.006.
[34] V. Tiwari, G. Srivastava, Effect of thermal processing conditions on the structure and dielectric properties of PVDF films, J. Polym. Res. 21 (2014) 587. https://doi.org/10.1007/s10965-014-0587-0.
[35] M. Yuan, B. Li, S. Zhang, R. Rajagopalan, M.T. Lanagan, High-Field Dielectric Properties of Oriented Poly(vinylidene fluoride-co-hexafluoropropylene): Structure–Dielectric Property Relationship and Implications for Energy Storage Applications, ACS Appl. Polym.

Mater. 2 (2020) 1356–1368. https://doi.org/10.1021/acsapm.9b01224.
[36] K. Silakaew, W. Saijingwong, K. Meeporn, S. Maensiri, P. Thongbai, Effects of processing methods on dielectric properties of BaTiO3/poly(vinylidene fluoride) nanocomposites, Microelectron. Eng. 146 (2015) 1–5. https://doi.org/10.1016/j.mee.2015.01.029.
[37] A. Jain, K.J. Prashanth, A.K. Sharma, A. Jain, P.N. Rashmi, Dielectric and Piezoelectric Properties of PVDF / PZT Composites : A Review, Polym. Eng. Sci. 55 (2015) 1589–1616. https://doi.org/10.1002/pen.
[38] M. Alexandre, C. Bessaguet, C. David, E. Dantras, C. Lacabanne, Piezoelectric properties of polymer/lead-free ceramic composites, Phase Transitions. 89 (2016) 708–716. https://doi.org/10.1080/01411594.2016.1206898.
[39] S.A. Riquelme, K. Ramam, A. Jaramillo, Ceramics fillers enhancing effects on the dielectric properties of poly(vinylidene fluoride) matrix composites prepared by the torque rheometer method, Results Phys. 15 (2019) 102800. https://doi.org/10.1016/j.rinp.2019.102800.
[40] K. Yu, S. Hu, W. Yu, J. Tan, Piezoelectric and Dielectric Properties of ((K 0.475 Na 0.495 Li 0.03)NbO 3 -0.003ZrO 2)/PVDF Composites, J. Electron. Mater. 48 (2019) 2329–2337. https://doi.org/10.1007/s11664-019-06978-1.
[41] A. Kumar, A. Kumar, K. Prasad, Power generation characteristics of 0.50(Ba0.7Ca0.3)TiO3–0.50Ba(Zr0.2Ti0.8)O3/PVDF nanocomposites under impact loading, J. Mater. Sci. Mater. Electron. 31 (2020) 12708–12714. https://doi.org/10.1007/s10854-020-03822-9.
[42] G. Malucelli, A. Fioravanti, L. Francioso, C. De Pascali, M.A. Signore, M.C. Carotta, A. Bonanno, D. Duraccio, Preparation and characterization of UV-cured composite films containing ZnO nanostructures: Effect of filler geometric features on piezoelectric response, Prog. Org. Coatings. 109 (2017) 45–54. https://doi.org/https://doi.org/10.1016/j.porgcoat.2017.04.020.
[43] G. Rujijanagul, S. Boonyakul, T. Tunkasiri, Effect of the particle size of PZT on the microstructure and the piezoelectric properties of 0-3 PZT/polymer composites, J. Mater. Sci. Lett. 20 (2001) 1943–1945. https://doi.org/10.1023/A:1013182602054.
[44] T. Greeshma, R. Balaji, J. S, PVDF Phase Formation and Its Influence on Electrical and Structural Properties of PZT-PVDF Composites, Ferroelectr. Lett. Sect. 40 (2013) 1–3. https://doi.org/10.1080/07315171.2013.814460.
[45] C. Min, P. Nie, D. Shen, K. Zhao, X. Chen, Preparation and electrical properties of PLZT/PVDF Nanocomposites, J. Polym. Mater. 31 (2014) 199–209.
[46] R. Li, L. Zhang, Z. Shi, J. Pei, Effects of Coupling Agents on the Structure and Electrical Properties of PZT-Poly (Vinylidene Fluoride) Composites, Appl. Sci. 6 (2016) 282. https://doi.org/10.3390/app6100282.
[47] S.J. Priya, H.-C. Song, Y. Zhou, R. Varghese, A. Chopra, S.-G. Kim, I. Kanno, L. wu, D. Ha, J. Ryu, R. Polcawich, A Review on Piezoelectric Energy Harvesting: Materials, Methods, and Circuits, Energy Harvest. Syst. 4 (2017). https://doi.org/10.1515/ehs-2016-0028.
[48] J. Pei, Z. Zhao, X. Li, H. Liu, R. Li, Effect of preparation techniques on structural and electrical properties of PZT/PVDF composites, Mater. Express. 7 (2017) 180–188. https://doi.org/10.1166/mex.2017.1369.
[49] K. Arlt, M. Wegener, Piezoelectric PZT/PVDF-copolymer 0-3 Composites: Aspects on Film Preparation and Electrical Poling, Dielectr. Electr. Insul. IEEE Trans. 17 (2010) 1178–1184. https://doi.org/10.1109/TDEI.2010.5539688.
[50] Z. Dang, Y. Shen, L. Fan, N. Cai, C. Nan, S. Zhao, Dielectric properties of carbon fiber filled low-density polyethylene, J. Appl. Phys. 93 (2003) 5543–5545. https://doi.org/10.1063/1.1562740.
[51] G. Subodh, N. Deepu, P. Mohanan, M.T. Sebastian, Dielectric Response of High Permittivity Polymer Ceramic Composite with Low Loss Tangent, Appl. Phys. Lett. 95 (2009) 62903. https://doi.org/10.1063/1.3200244.
[52] X. Zhu, J. Yang, D. Dastan, H. Garmestani, R. Fan, Z. Shi, Fabrication of core-shell structured Ni@BaTiO3 scaffolds for polymer composites with ultrahigh dielectric constant and low loss, Compos. Part A Appl. Sci. Manuf. 125 (2019) 105521. https://doi.org/https://doi.org/10.1016/j.compositesa.2019.105521.
[53] E.A. Stefanescu, X. Tan, Z. Lin, N. Bowler, M.R. Kessler, Multifunctional fiberglass-

reinforced PMMA-BaTiO3 structural/dielectric composites, Polymer (Guildf). 52 (2011) 2016–2024. https://doi.org/https://doi.org/10.1016/j.polymer.2011.02.050.
[54] M.S. Tamboli, P.K. Palei, S.S. Patil, M. V Kulkarni, N.N. Maldar, B.B. Kale, Polymethyl methacrylate (PMMA)–bismuth ferrite (BFO) nanocomposite: low loss and high dielectric constant materials with perceptible magnetic properties, Dalt. Trans. 43 (2014) 13232–13241. https://doi.org/10.1039/C4DT00947A.
[55] S.-H. Xie, B.-K. Zhu, X.-Z. Wei, Z.-K. Xu, Y.-Y. Xu, Polyimide/BaTiO3 composites with controllable dielectric properties, Compos. Part A Appl. Sci. Manuf. 36 (2005) 1152–1157. https://doi.org/https://doi.org/10.1016/j.compositesa.2004.12.010.
[56] L. Liu, F. Lv, Y. Zhang, P. Li, W. Tong, L. Ding, G. Zhang, Enhanced dielectric performance of polyimide composites with modified sandwich-like SiO2@GO hybrids, Compos. Part A Appl. Sci. Manuf. 99 (2017) 41–47. https://doi.org/https://doi.org/10.1016/j.compositesa.2017.03.029.
[57] Z. Dang, Y.-Q. Lin, H.-P. Xu, C.-Y. Shi, S. Li, J. Bai, Fabrication and Dielectric Characterization of Advanced BaTiO3/Polyimide Nanocomposite Films with High Thermal Stability, Adv. Funct. Mater. 18 (2008) 1509–1517. https://doi.org/10.1002/adfm.200701077.
[58] M.J. Kishor Kumar, J.T. Kalathi, PMMA-LZO Composite Dielectric Film with an Improved Energy Storage Density, J. Electron. Mater. 48 (2019) 7654–7661. https://doi.org/10.1007/s11664-019-07580-1.
[59] B.-H. Fan, Y. Liu, D. He, J. Bai, Achieving polydimethylsiloxane/carbon nanotube (PDMS/CNT) composites with extremely low dielectric loss and adjustable dielectric constant by sandwich structure, Appl. Phys. Lett. 112 (2018) 52902. https://doi.org/10.1063/1.5016543.
[60] I. Rytöluoto, A. Gitsas, S. Pasanen, K. Lahti, Effect of film structure and morphology on the dielectric breakdown characteristics of cast and biaxially oriented polypropylene films, Eur. Polym. J. 95 (2017) 606–624. https://doi.org/https://doi.org/10.1016/j.eurpolymj.2017.08.051.
[61] Q. Chen, Y. Shen, S. Zhang, Q.M. Zhang, Polymer-Based Dielectrics with High Energy Storage Density, Annu. Rev. Mater. Res. 45 (2015) 433–458. https://doi.org/10.1146/annurev-matsci-070214-021017.
[62] D. Bayraktar, F. Clemens, S. Diethelm, T. Graule, J. Van herle, P. Holtappels, Production and properties of substituted LaFeO3-perovskite tubular membranes for partial oxidation of methane to syngas, J. Eur. Ceram. Soc. 27 (2007) 2455–2461. https://doi.org/https://doi.org/10.1016/j.jeurceramsoc.2006.10.004.
[63] D. Naegele, D.Y. Yoon, Orientation of crystalline dipoles in poly(vinylidene fluoride) films under electric field, Appl. Phys. Lett. 33 (1978) 132–134. https://doi.org/10.1063/1.90281.
[64] R.G. Kepler, R.A. Anderson, Ferroelectricity in polyvinylidene fluoride, J. Appl. Phys. 49 (1978) 1232–1235. https://doi.org/10.1063/1.325011.
[65] L. Ruan, X. Yao, Y. Chang, L. Zhou, G. Qin, X. Zhang, Properties and Applications of the β Phase Poly(vinylidene fluoride), Polymers (Basel). 10 (2018) 228. https://doi.org/10.3390/polym10030228.
[66] C. Bowen, C. Wan, Multiscale-structuring of polyvinylidene fluoride for energy harvesting: the impact of molecular-, micro- and macro-structure, J. Mater. Chem. A. 5 (2017) 3091–3128. https://doi.org/10.1039/C6TA09590A.
[67] Y. Chen, L. Zhang, Y. Zhang, H. Gao, H. Yan, Large-area perovskite solar cells – a review of recent progress and issues, RSC Adv. 8 (2018) 10489–10508. https://doi.org/10.1039/C8RA00384J.
[68] A. Bhalla, R. Guo, R. Roy, The Perovskite Structure – A Review of Its Role in Ceramic Science and Technology, Mater. Res. Innov. 4 (2000) 3–26. https://doi.org/10.1007/s100190000062.
[69] M. Wegmann, R. Brönnimann, F. Clemens, T. Graule, Barium titanate-based PTCR thermistor fibers: Processing and properties, Sensors Actuators A-Physical - Sens. ACTUATOR A-PHYS. 135 (2007) 394–404. https://doi.org/10.1016/j.sna.2006.08.008.
[70] X. Zhu, J. Zhu, S. Zhou, Z. Liu, N. Ming, S.-G. (David) Lu, H. Chan, C.-L. Choy, Recent progress of (Ba,Sr)TiO 3 thin films for tunable microwave devices, J. Electron. Mater. - J ELECTRON MATER. 32 (2003) 1125–1134. https://doi.org/10.1007/s11664-003-0098-y.

[71] T. Ren, L.-T. Zhang, X.-N. Wang, C.-G. Wei, J.-S. Liu, L. Lai, Z.-J. Li, High Quality Ferroelectric Capacitor for FeRAM Applications, Integr. Ferroelectr. 46 (2002) 47–53. https://doi.org/10.1080/713718243.
[72] G.M. Krishna, K. Rajanna, Tactile sensor based on piezoelectric resonance, IEEE Sens. J. 4 (2004) 691–697. https://doi.org/10.1109/JSEN.2004.833505.
[73] M. Villegas, A.C. Caballero, T. Jardiel, C. Aragó, J. Maudes, I. Caro, Evaluation of Piezoelectric Properties of Bi4Ti3O12—Based Ceramics at High Temperature, Ferroelectrics. 393 (2009) 44–53. https://doi.org/10.1080/00150190903412838.
[74] B.H. Park, B.S. Kang, S.D. Bu, T.W. Noh, J. Lee, W. Jo, Lanthanum-substituted bismuth titanate for use in non-volatile memories, Nature. 401 (1999) 682–684. https://doi.org/10.1038/44352.
[75] P.K. Panda, B. Sahoo, PZT to Lead Free Piezo Ceramics: A Review, Ferroelectrics. 474 (2015) 128–143. https://doi.org/10.1080/00150193.2015.997146.
[76] W.F. Zhang, Y.B. Huang, M.S. Zhang, Optical properties of ferroelectric (Pb, La)(Zr, Ti)O3 thin films grown by pulsed laser deposition, Appl. Surf. Sci. 158 (2000) 185–189. https://doi.org/https://doi.org/10.1016/S0169-4332(99)00581-4.
[77] A. Paliwal, M. Tomar, V. Gupta, Study of optical properties of Ce and Mn doped BiFeO3 thin films using SPR technique for magnetic field sensing, Vacuum. 158 (2018) 48–51. https://doi.org/https://doi.org/10.1016/j.vacuum.2018.09.018.
[78] O. Bouquin, M. Lejeune, J. Boilot, Multilayer Ceramic Capacitors Based on Pb(Mg1/3Nb2/3)O3, MRS Proc. 72 (2011). https://doi.org/10.1557/PROC-72-73.
[79] C. Fei, Y. Yang, F. Guo, P. Lin, Q. Chen, Q. Zhou, L. Sun, PMN-PT Single Crystal Ultrasonic Transducer With Half-Concave Geometric Design for IVUS Imaging, IEEE Trans. Biomed. Eng. 65 (2018) 2087–2092. https://doi.org/10.1109/TBME.2017.2784437.
[80] C.B. Eom, R.B. Van Dover, J.M. Phillips, D.J. Werder, J.H. Marshall, C.H. Chen, R.J. Cava, R.M. Fleming, D.K. Fork, Fabrication and properties of epitaxial ferroelectric heterostructures with (SrRuO3) isotropic metallic oxide electrodes, Appl. Phys. Lett. 63 (1993) 2570–2572. https://doi.org/10.1063/1.110436.
[81] Y. Xu, U. Memmert, U. Hartmann, Magnetic field sensors from polycrystalline manganites, Sensors Actuators A Phys. 91 (2001) 26–29. https://doi.org/https://doi.org/10.1016/S0924-4247(01)00493-9.
[82] C.-Y. Liu, T.-Y. Tseng, Study of SrTiO3 gate dielectrics, MRS Proc. 966 (2011). https://doi.org/10.1557/PROC-0966-T12-04.
[83] A. Pinheiro, E. Firmiano, A. Rabelo, C. Dalmaschio, E. Leite, Revisiting SrTiO3 as a photoanode for water splitting: Development of thin films with enhanced charge separation under standard solar irradiation, RSC Adv. 4 (2014) 2029. https://doi.org/10.1039/c3ra45066j.
[84] T. Ishihara, J. Tabuchi, S. Ishikawa, J. Yan, M. Enoki, H. Matsumoto, Recent Progress in LaGaO3 Based Solid Electrolyte for Intermediate Temperature SOFCs, Solid State Ionics. 177 (2006) 1949–1953. https://doi.org/10.1016/j.ssi.2006.01.044.
[85] J. Lyagaeva, N. Danilov, G. Vdovin, J. Bu, D. Medvedev, A. Demin, P. Tsiakaras, A new Dy-doped BaCeO3–BaZrO3 proton-conducting material as a promising electrolyte for reversible solid oxide fuel cells, J. Mater. Chem. A. 4 (2016) 15390–15399. https://doi.org/10.1039/C6TA06414K.
[86] S.P. Jiang, Development of lanthanum strontium cobalt ferrite perovskite electrodes of solid oxide fuel cells – A review, Int. J. Hydrogen Energy. 44 (2019) 7448–7493. https://doi.org/https://doi.org/10.1016/j.ijhydene.2019.01.212.
[87] L. Nalbandian, A. Evdou, V. Zaspalis, La1−xSrxMO3 (M = Mn, Fe) perovskites as materials for thermochemical hydrogen production in conventional and membrane reactors, Int. J. Hydrogen Energy. 34 (2009) 7162–7172. https://doi.org/10.1016/j.ijhydene.2009.06.076.
[88] F. Xu, T. Zhang, G. Li, Y. Zhao, Synergetic Effect of Chloride Doping and CH3NH3PbCl3 on CH3NH3PbI3-xClx Perovskite Based Solar Cells, ChemSusChem. 10 (2017). https://doi.org/10.1002/cssc.201700487.
[89] J. Even, D. Sapori, L. Pedesseau, A. Rolland, M. Kepenekian, R. Robles, S. Wang, Y. Huang, A. Beck, O. Durand, C. Katan, Theoretical insights into multibandgap hybrid perovskites for photovoltaic applications, 2015. https://doi.org/10.1117/12.2191953.

[90] Y. Zhang, W. Jie, P. Chen, W. Liu, J. Hao, Ferroelectric and Piezoelectric Effects on the Optical Process in Advanced Materials and Devices, Adv. Mater. 30 (2018) 1707007. https://doi.org/https://doi.org/10.1002/adma.201707007.
[91] P. Zheng, J.L. Zhang, Y.Q. Tan, C.L. Wang, Grain-size effects on dielectric and piezoelectric properties of poled BaTiO3 ceramics, Acta Mater. 60 (2012) 5022–5030. https://doi.org/https://doi.org/10.1016/j.actamat.2012.06.015.
[92] A. V Polotai, A. V Ragulya, C.A. Randall, Preparation and Size Effect in Pure Nanocrystalline Barium Titanate Ceramics, Ferroelectrics. 288 (2003) 93–102. https://doi.org/10.1080/00150190390211972.
[93] R. Waser, Electroceramics. Materials, properties, applications. By A Moulson and J. M. Herbert, Chapman & Hall, London 1990, 464 pp., hardcover, E 49, ISBN 0-412-29490-7, in: Adv. Mater., John Wiley & Sons, Ltd, 1992: pp. 698–699. https://doi.org/https://doi.org/10.1002/adma.19920041031.
[94] T. Hoshina, K. Takizawa, J. Li, T. Kasama, H. Kakemoto, T. Tsurumi, Domain Size Effect on Dielectric Properties of Barium Titanate Ceramics, Jpn. J. Appl. Phys. 47 (2008) 7607–7611. https://doi.org/10.1143/jjap.47.7607.
[95] S. Pramanik, B. Pingguan-Murphy, A. A., Developments of Immobilized Surface Modified Piezoelectric Crystal Biosensors for Advanced Applications, Mater. Des. 40 (2012) 304–313.
[96] N. Horchidan, C.E. Ciomaga, R.C. Frunza, C. Capiani, C. Galassi, L. Mitoseriu, A comparative study of hard/soft PZT-based ceramic composites, Ceram. Int. 42 (2016) 9125–9132. https://doi.org/https://doi.org/10.1016/j.ceramint.2016.02.179.
[97] G.A. Smolenskii, A.I. Agranovskaya, Dielectric Polarization of a Number of Complex Compounds, Sov. Phys. Solid State. 1 (1960) 1429–1437.
[98] K. Reichmann, A. Feteira, M. Li, Bismuth Sodium Titanate Based Materials for Piezoelectric Actuators, Materials (Basel). 8 (2015) 8467–8495. https://doi.org/10.3390/ma8125469.
[99] T. Takenaka, K. Maruyama, K. Sakata, (Bi1/2Na1/2)TiO3-BaTiO3System for Lead-Free Piezoelectric Ceramics, Jpn. J. Appl. Phys. 30 (1991) 2236–2239. https://doi.org/10.1143/jjap.30.2236.
[100] P. Galizia, C. Baldisserri, E. Mercadelli, C. Capiani, C. Galassi, M. Algueró, A Glance at Processing-Microstructure-Property Relationships for Magnetoelectric Particulate PZT-CFO Composites, Materials (Basel). 13 (2020) 2592. https://doi.org/10.3390/ma13112592.
[101] A. Testino, M.T. Buscaglia, V. Buscaglia, M. Viviani, C. Bottino, P. Nanni, Kinetics and Mechanism of Aqueous Chemical Synthesis of BaTiO3 Particles, Chem. Mater. 16 (2004) 1536–1543. https://doi.org/10.1021/cm031130k.
[102] M. Buscaglia, M. Bassoli, V. Buscaglia, R. Alessio, Solid-State Synthesis of Ultrafine BaTiO3 Powders from Nanocrystalline BaCO3 and TiO2, J. Am. Ceram. Soc. 88 (2005) 2374–2379. https://doi.org/10.1111/j.1551-2916.2005.00451.x.
[103] M.T. Buscaglia, M. Bassoli, V. Buscaglia, R. Vormberg, Solid-State Synthesis of Nanocrystalline BaTiO3: Reaction Kinetics and Powder Properties, J. Am. Ceram. Soc. 91 (2008) 2862–2869. https://doi.org/https://doi.org/10.1111/j.1551-2916.2008.02576.x.
[104] M.T. Buscaglia, V. Buscaglia, R. Alessio, Coating of BaCO3 Crystals with TiO2: Versatile Approach to the Synthesis of BaTiO3 Tetragonal Nanoparticles, Chem. Mater. 19 (2007) 711–718. https://doi.org/10.1021/cm061823b.
[105] M.T. Buscaglia, V. Buscaglia, L. Curecheriu, P. Postolache, L. Mitoseriu, A.C. Ianculescu, B.S. Vasile, Z. Zhe, P. Nanni, Fe2O3@BaTiO3 Core−Shell Particles as Reactive Precursors for the Preparation of Multifunctional Composites Containing Different Magnetic Phases, Chem. Mater. 22 (2010) 4740–4748. https://doi.org/10.1021/cm1011982.
[106] M.T. Buscaglia, M. Sennour, V. Buscaglia, C. Bottino, V. Kalyani, P. Nanni, Formation of Bi4Ti3O12 One-Dimensional Structures by Solid-State Reactive Diffusion. From Core−Shell Templates to Nanorods and Nanotubes, Cryst. Growth Des. 11 (2011) 1394–1401. https://doi.org/10.1021/cg101697r.
[107] S. Mornet, C. Elissalde, V. Hornebecq, O. Bidault, E. Duguet, A. Brisson, M. Maglione, Controlled Growth of Silica Shell on Ba0.6Sr0.4TiO3 Nanoparticles Used As Precursors of Ferroelectric Composites, Chem. Mater. 17 (2005) 4530–4536. https://doi.org/10.1021/cm050884r.

[108] M. Castellano, L. Conzatti, G. Costa, L. Falqui, A. Turturro, B. Valenti, F. Negroni, Surface modification of silica: 1. Thermodynamic aspects and effect on elastomer reinforcement, Polymer (Guildf). 46 (2005) 695–703. https://doi.org/http://dx.doi.org/10.1016/j.polymer.2004.11.010.
[109] C. V. Chanmal, Dielectric relaxations in PVDF/BaTiO3 nanocomposites, Express Polym. Lett. - EXPRESS POLYM LETT. 2 (2008) 294–301. https://doi.org/10.3144/expresspolymlett.2008.35.
[110] M. Arjmand, U. Sundararaj, Impact of BaTiO3 as insulative ferroelectric barrier on the broadband dielectric properties of MWCNT/PVDF nanocomposites, Polym. Compos. 37 (2016) 299–304. https://doi.org/10.1002/pc.23181.
[111] A. Jain, S.J. Kumar, M.R. Kumar, A.S. Ganesh, S. Srikanth, PVDF-PZT Composite Films for Transducer Applications, Mech. Adv. Mater. Struct. 21 (2014) 181–186. https://doi.org/10.1080/15376494.2013.834094.
[112] A.K. Zak, W.C. Gan, W.H.A. Majid, M. Darroudi, T.S. Velayutham, Experimental and theoretical dielectric studies of PVDF / PZT nanocomposite thin films, Ceram. Int. 37 (2011) 1653–1660. https://doi.org/10.1016/j.ceramint.2011.01.037.
[113] S. Gupta, R. Bhunia, B. Fatma, D. Maurya, D. Singh, P. Prajapati, R. Gupta, S. Priya, R. Gupta, A. Garg, Multifunctional and Flexible Polymeric Nanocomposite Films with Improved Ferroelectric and Piezoelectric Properties for Energy Generation Devices, 2 (2019) 6364–6374. https://doi.org/10.1021/acsaem.9b01000.
[114] S. Hajra, S. Sahoo, R.N.P. Choudhary, Fabrication and electrical characterization of (Bi0.49Na0.49Ba0.02)TiO3-PVDF thin film composites, J. Polym. Res. 26 (2018) 1–11.
[115] R. Su, Z. Luo, D. Zhang, Y. Liu, Z. Wang, J. Li, J. Bian, Y. Li, X. Hu, J. Gao, Y. Yang, High Energy Density Performance of Polymer Nanocomposites Induced by Designed Formation of BaTiO3@sheet-likeTiO2 Hybrid Nanofillers, J. Phys. Chem. C. 120 (2016) 11769–11776. https://doi.org/10.1021/acs.jpcc.6b01853.
[116] X. Cai, T. Lei, D. Sun, L. Lin, A critical analysis of the α, β and γ phases in poly(vinylidene fluoride) using FTIR, RSC Adv. 7 (2017) 15382–15389. https://doi.org/10.1039/C7RA01267E.
[117] K. Nakagawa, Y. Ishida, Annealing effects in poly(vinylidene fluoride) as revealed by specific volume measurements, differential scanning calorimetry, and electron microscopy, J. Polym. Sci. Polym. Phys. Ed. 11 (1973) 2153–2171. https://doi.org/10.1002/pol.1973.180111107.
[118] F.A. Sánchez, M. Redondo, J. González-Benito, Influence of BaTiO3 submicrometric particles on the structure, morphology, and crystallization behavior of poly(vinylidene fluoride), J. Appl. Polym. Sci. 132 (2015). https://doi.org/https://doi.org/10.1002/app.41497.
[119] R. Gregorio Jr., M. Cestari, Effect of crystallization temperature on the crystalline phase content and morphology of poly(vinylidene fluoride), J. Polym. Sci. Part B Polym. Phys. 32 (1994) 859–870. https://doi.org/10.1002/polb.1994.090320509.
[120] V. Sencadas, R. Jr, S. Lanceros-Méndez, Processing and characterization of a novel nonporous poly(vinilidene fluoride) films in the β phase, J. Non. Cryst. Solids. 352 (2006) 2226–2229. https://doi.org/10.1016/j.jnoncrysol.2006.02.052.
[121] G.T. Davis, J.E. McKinney, M.G. Broadhurst, S.C. Roth, Electric-field-induced phase changes in poly(vinylidene fluoride), J. Appl. Phys. 49 (1978) 4998–5002. https://doi.org/10.1063/1.324446.
[122] W. Kim, M. Han, Y.-H. Shin, H. Kim, First-Principles Study of the α-β Phase Transition of Ferroelectric Poly(vinylidene difluoride): Observation of Multiple Transition Pathways, J. Phys. Chem. B. 120 (2016) 3240–3249. https://doi.org/10.1021/acs.jpcb.6b00881.
[123] P. Martins, C.M. Costa, S. Lanceros-Mendez, Nucleation of electroactive β-phase poly(vinilidene fluoride) with CoFe2O4 and NiFe2O4 nanofillers: a new method for the preparation of multiferroic nanocomposites, Appl. Phys. A. 103 (2011) 233–237. https://doi.org/10.1007/s00339-010-6003-7.
[124] M.S. Sebastian, A. Larrea, R. Gonçalves, T. Alejo, J.L. Vilas, V. Sebastian, P. Martins, S. Lanceros-Mendez, Understanding nucleation of the electroactive β-phase of poly(vinylidene fluoride) by nanostructures, RSC Adv. 6 (2016) 113007–113015. https://doi.org/10.1039/C6RA24356H.
[125] B. Mohammadi, A.A. Yousefi, S.M. Bellah, Effect of tensile strain rate and elongation on

crystalline structure and piezoelectric properties of PVDF thin films, Polym. Test. 26 (2007) 42–50. https://doi.org/https://doi.org/10.1016/j.polymertesting.2006.08.003.
[126] H.-J. Ye, L. Yang, W.-Z. Shao, S.-B. Sun, L. Zhen, Effect of electroactive phase transformation on electron structure and dielectric properties of uniaxial stretching poly(vinylidene fluoride) films, RSC Adv. 3 (2013) 23730–23736. https://doi.org/10.1039/C3RA43966F.
[127] M. Sharma, G. Madras, S. Bose, Process induced electroactive β-polymorph in PVDF: effect on dielectric and ferroelectric properties, Phys. Chem. Chem. Phys. 16 (2014) 14792–14799. https://doi.org/10.1039/C4CP01004C.
[128] L. Yang, J. Qiu, K. Zhu, H. Ji, Q. Zhao, M. Shen, S. Zeng, Effect of rolling temperature on the microstructure and electric properties of β-polyvinylidene fluoride films, J. Mater. Sci. Mater. Electron. 29 (2018) 15957–15965. https://doi.org/10.1007/s10854-018-9681-0.
[129] E. Brunengo, G. Luciano, G. Canu, M. Canetti, L. Conzatti, M. Castellano, P. Stagnaro, Double-step moulding: An effective method to induce the formation of β-phase in PVDF, Polymer (Guildf). 193 (2020). https://doi.org/10.1016/j.polymer.2020.122345.
[130] M.S. Gaur, A.P. Indolia, A.A. Rogachev, A. V Rahachou, Influence of SiO2 nanoparticles on morphological, thermal, and dielectric properties of PVDF, J. Therm. Anal. Calorim. 122 (2015) 1403–1416. https://doi.org/10.1007/s10973-015-4872-x.
[131] S. Mohamadi, Preparation and Characterization of PVDF/PMMA/Graphene Polymer Blend Nanocomposites by Using ATR-FTIR Technique, in: 2012. https://doi.org/10.5772/36497.
[132] F. Husson, J. Josse, S. Lê, FactoMineR: An R Package for Multivariate Analysis, J. Stat. Softw. 25 (2008). https://doi.org/10.18637/jss.v025.i01.
[133] H. Hotelling, Analysis of a complex of statistical variables into principal components., J. Educ. Psychol. 24 (1933) 417–441. https://doi.org/10.1037/h0071325.
[134] D.M. Dhevi, A.A. Prabu, K.J. Kim, FTIR studies on polymorphic control of PVDF ultrathin films by heat-controlled spin coater, J. Mater. Sci. 51 (2016) 3619–3627. https://doi.org/10.1007/s10853-015-9685-6.
[135] S. Satapathy, S. Pawar, P.K. Gupta, K.B.R. Varma, Effect of annealing on phase transition in poly(vinylidene fluoride) films prepared using polar solvent, Bull. Mater. Sci. 34 (2011) 727. https://doi.org/10.1007/s12034-011-0187-0.
[136] M.M. Abolhasani, F. Zarejousheghani, Z. Cheng, M. Naebe, A Facile Method to Enhance Ferroelectric Properties in PVDF Nanocomposites, RSC Adv. 5 (2015). https://doi.org/10.1039/C4RA12221F.
[137] R. Lenth, Response-Surface Methods in R, Using rsm, J. Stat. Softw. 32 (2010). https://doi.org/10.18637/jss.v032.i07.
[138] J.D. Jobson, Multiple Linear Regression, in: J.D. Jobson (Ed.), Appl. Multivar. Data Anal., Springer New York, New York, NY, 1991: pp. 219–398. https://doi.org/10.1007/978-1-4612-0955-3_4.
[139] F. A. Sánchez, M. Redondo, J. Gonzalez-Benito, Influence of BaTiO3 Submicrometric Particles on the Structure, Morphology, and Crystallization Behavior of Poly(vinylidene fluoride), J. Appl. Polym. Sci. 132 (2015). https://doi.org/10.1002/app.41497.
[140] M. Favaro, M. Branciforti, R. Bretas, A X-ray study of β-phase and molecular orientation in nucleated and non-nucleated injection molded polypropylene resins, Mater. Res. J. Mater. - MATER RES-IBERO-AM J MATER. 12 (2009). https://doi.org/10.1590/S1516-14392009000400014.
[141] M. Zhang, A.-Q. Zhang, B.-K. Zhu, C.-H. Du, Y.-Y. Xu, Polymorphism in porous poly(vinylidene fluoride) membranes formed via immersion precipitation process, J. Memb. Sci. 319 (2008) 169–175. https://doi.org/https://doi.org/10.1016/j.memsci.2008.03.029.
[142] P. Atorngitjawat, Effects of processing conditions and crystallization on dynamic relaxations in semicrystalline poly(vinylidene fluoride) films, Macromol. Res. 25 (2017) 391–399. https://doi.org/10.1007/s13233-017-5060-6.
[143] L. Yang, J. Qiu, K. Zhu, H. Ji, Q. Zhao, M. Shen, S. Zeng, Effect of rolling temperature on the microstructure and electric properties of β-polyvinylidene fluoride films, J. Mater. Sci. Mater. Electron. 29 (2018) 15957–15965. https://doi.org/10.1007/s10854-018-9681-0.
[144] A. Peterlin, J. (Holbrook) Elwell, Dielectric constant of rolled polyvinylidene fluoride, J. Mater. Sci. 2 (1967) 1–6. https://doi.org/10.1007/BF00550045.
[145] V. Sencadas, S. Lanceros-Méndez, R. i Serra, A. Andrio Balado, J.L. Gómez Ribelles,

Relaxation dynamics of poly(vinylidene fluoride) studied by dynamical mechanical measurements and dielectric spectroscopy, Eur. Phys. J. E. 35 (2012) 41. https://doi.org/10.1140/epje/i2012-12041-x.
[146] D. Samios, S. Tokumoto, E. Denardin, Investigation of the large plastic deformation of iPP induced by plane strain compression: Stress–strain behavior and thermo-mechanical properties, Int. J. Plast. 22 (2006) 1924–1942. https://doi.org/10.1016/j.ijplas.2006.02.009.
[147] K. Osińska, D. Czekaj, Thermal behavior of BST/PVDF ceramic--polymer composites, J. Therm. Anal. Calorim. 113 (2013) 69–76. https://doi.org/10.1007/s10973-013-3026-2.
[148] J.F. Mano, V. Sencadas, A.M. Costa, S. Lanceros-Méndez, Dynamic mechanical analysis and creep behaviour of β-PVDF films, Mater. Sci. Eng. A. 370 (2004) 336–340. https://doi.org/https://doi.org/10.1016/j.msea.2002.12.002.
[149] J. Rault, The αc Transition in Semicrystalline Polymers: A New Look at Crystallization Deformation and Aging Process, J. Macromol. Sci. Part C. 37 (1997) 335–387. https://doi.org/10.1080/15321799708018369.
[150] A. Linares, J.L. Acosta, Tensile and dynamic mechanical behaviour of polymer blends based on PVDF, Eur. Polym. J. 33 (1997) 467–473. https://doi.org/https://doi.org/10.1016/S0014-3057(96)00182-6.
[151] N. Alves, C.X. Cardoso, A. Job, J.A. Giacometti, Effects of thermal treatment on phase transitions and on the mechanical relaxation in poly(vinylidene fluoride), in: 2002: pp. 263–266. https://doi.org/10.1109/ISE.2002.1042993.
[152] S. Firmino Mendes, C.M. Costa, V. Sencadas, J. Serrado Nunes, P. Costa, R. Gregorio, S. Lanceros-Méndez, Effect of the ceramic grain size and concentration on the dynamical mechanical and dielectric behavior of poly(vinilidene fluoride)/Pb(Zr0.53Ti0.47)O3 composites, Appl. Phys. A. 96 (2009) 899–908. https://doi.org/10.1007/s00339-009-5141-2.
[153] R.H. Boyd, Relaxation processes in crystalline polymers: experimental behaviour — a review, Polymer (Guildf). 26 (1985) 323–347. https://doi.org/https://doi.org/10.1016/0032-3861(85)90192-2.
[154] E. Brunengo, M. Castellano, L. Conzatti, G. Canu, V. Buscaglia, P. Stagnaro, PVDF-based composites containing PZT particles: How processing affects the final properties, J. Appl. Polym. Sci. 137 (2020) 48871. https://doi.org/10.1002/app.48871.
[155] Z. Xia, H.-J. Sue, A.J. Hsieh, J.W.-L. Huang, Dynamic mechanical behavior of oriented semicrystalline polyethylene terephthalate, J. Polym. Sci. Part B Polym. Phys. 39 (2001) 1394–1403. https://doi.org/10.1002/polb.1111.
[156] Z. Bartczak, J. Morawiec, A. Galeski, Deformation of high-density polyethylene produced by rolling with side constraints. II. Mechanical properties of oriented bars, J. Appl. Polym. Sci. 86 (2002) 1405–1412. https://doi.org/10.1002/app.11286.
[157] Z. Bartczak, J. Morawiec, A. Galeski, Structure and properties of isotactic polypropylene oriented by rolling with side constraints, J. Appl. Polym. Sci. 86 (2002) 1413–1425. https://doi.org/10.1002/app.11293.
[158] A.L. Ahmad, U.R. Farooqui, N.A. Hamid, Effect of graphene oxide (GO) on Poly(vinylidene fluoride-hexafluoropropylene) (PVDF- HFP) polymer electrolyte membrane, Polymer (Guildf). 142 (2018) 330–336. https://doi.org/https://doi.org/10.1016/j.polymer.2018.03.052.
[159] J. Barbosa, J. Dias, S. Lanceros-Méndez, C. Costa, Recent Advances in Poly(vinylidene fluoride) and Its Copolymers for Lithium-Ion Battery Separators, Membranes (Basel). 8 (2018) 45. https://doi.org/10.3390/membranes8030045.
[160] T. Liu, Z. Chang, Y. Yin, K. Chen, Y. Zhang, X. Zhang, The PVDF-HFP gel polymer electrolyte for Li-O2 battery, Solid State Ionics. 318 (2018) 88–94. https://doi.org/https://doi.org/10.1016/j.ssi.2017.08.001.
[161] F. Guan, J. Pan, J. Wang, Q. Wang, L. Zhu, Crystal Orientation Effect on Electric Energy Storage in Poly(vinylidene fluoride-co-hexafluoropropylene) Copolymers, Macromolecules. 43 (2010) 384–392. https://doi.org/10.1021/ma901921h.
[162] B. Neese, Y. Wang, B. Chu, K. Ren, S. Liu, Q.M. Zhang, C. Huang, J. West, Piezoelectric responses in poly(vinylidene fluoride/hexafluoropropylene) copolymers, Appl. Phys. Lett. 90 (2007) 242917. https://doi.org/10.1063/1.2748076.
[163] H. Parangusan, D. Ponnamma, M.A.A. Al-Maadeed, Stretchable Electrospun PVDF-HFP/Co-ZnO Nanofibers as Piezoelectric Nanogenerators, Sci. Rep. 8 (2018) 754.

https://doi.org/10.1038/s41598-017-19082-3.
[164] D. Ponnamma, A. Erturk, H. Parangusan, K. Deshmukh, M.B. Ahamed, M. Al Ali Al-Maadeed, Stretchable quaternary phasic PVDF-HFP nanocomposite films containing graphene-titania-SrTiO3 for mechanical energy harvesting, Emergent Mater. 1 (2018) 55–65. https://doi.org/10.1007/s42247-018-0007-z.
[165] M. Wegener, W. Künstler, K. Richter, R. Gerhard-Multhaupt, Ferroelectric polarization in stretched piezo- and pyroelectric poly(vinylidene fluoride-hexafluoropropylene) copolymer films, J. Appl. Phys. 92 (2002) 7442–7447. https://doi.org/10.1063/1.1524313.
[166] Z. Zhou, M. Mackey, J. Carr, L. Zhu, L. Flandin, E. Baer, Multilayered polycarbonate/poly(vinylidene fluoride-co-hexafluoropropylene) for high energy density capacitors with enhanced lifetime, J. Polym. Sci. Part B Polym. Phys. 50 (2012) 993–1003. https://doi.org/https://doi.org/10.1002/polb.23094.
[167] S. Divya, J. Hemalatha, Study on the enhancement of ferroelectric beta phase in P(VDF-HFP) films under heating and poling conditions, Eur. Polym. J. 88 (2017) 136–147.
[168] C.-H. DU, B.-K. Zhu, Y.-Y. Xu, The effects of quenching on the phase structure of vinylidene fluoride segments in PVDF-HFP copolymer and PVDF-HFP/PMMA blends, J. Mater. Sci. 41 (2006) 417–421. https://doi.org/10.1007/s10853-005-2182-6.
[169] X. He, K. Yao, B.K. Gan, Phase transition and properties of a ferroelectric poly(vinylidene fluoride-hexafluoropropylene) copolymer, J. Appl. Phys. 97 (2005) 84101. https://doi.org/10.1063/1.1862323.
[170] D. Yuan, Z. Li, W. Thitsartarn, X. Fan, J. Sun, H. Li, C. He, β phase PVDF-hfp induced by mesoporous SiO2 nanorods: synthesis and formation mechanism, J. Mater. Chem. C. 3 (2015) 3708–3713. https://doi.org/10.1039/C5TC00005J.
[171] S. Prathipkumar, J. Hemalatha, Enhancement in β phase and dielectric property of P(VDF-HFP)/SrFe12O19 nanofiber composite films, AIP Conf. Proc. 2115 (2019) 30183. https://doi.org/10.1063/1.5113022.
[172] R. Gregorio, E.M. Ueno, Effect of crystalline phase, orientation and temperature on the dielectric properties of poly (vinylidene fluoride) (PVDF), J. Mater. Sci. 34 (1999) 4489–4500. https://doi.org/10.1023/A:1004689205706.
[173] C.-W. Nan, Y. Shen, J. Ma, Physical Properties of Composites Near Percolation, Annu. Rev. Mater. Res. 40 (2010) 131–151. https://doi.org/10.1146/annurev-matsci-070909-104529.
[174] J.G. Meier, C. Crespo, J.L. Pelegay, P. Castell, R. Sainz, W.K. Maser, A.M. Benito, Processing dependency of percolation threshold of MWCNTs in a thermoplastic elastomeric block copolymer, Polymer (Guildf). 52 (2011) 1788–1796. https://doi.org/https://doi.org/10.1016/j.polymer.2011.02.024.
[175] E. Brunengo, L. Conzatti, I. Schizzi, M.T. Buscaglia, G. Canu, L. Curecheriu, C. Costa, M. Castellano, L. Mitoseriu, P. Stagnaro, V. Buscaglia, Improved dielectric properties of poly(vinylidene fluoride)–BaTiO3 composites by solvent-free processing, J. Appl. Polym. Sci. 138 (2021) 50049. https://doi.org/https://doi.org/10.1002/app.50049.
[176] T.R. Jow, F.W. MacDougall, J.B. Ennis, X.H. Yang, M.A. Schneider, C.J. Scozzie, J.D. White, J.R. MacDonald, M.C. Schalnat, R.A. Cooper, S.P.S. Yen, Pulsed power capacitor development and outlook, in: 2015 IEEE Pulsed Power Conf., 2015: pp. 1–7. https://doi.org/10.1109/PPC.2015.7297027.
[177] W.J. Sarjeant, J. Zirnheld, F.W. MacDougall, J.S. Bowers, N. Clark, I.W. Clelland, R.A. Price, M. Hudis, I. Kohlberg, G. McDuff, I. McNab, S.G. Parler, J. Prymak, Chapter 9 - Capacitors—Past, Present, and Future, in: H.S. Nalwa (Ed.), Handb. Low High Dielectr. Constant Mater. Their Appl., Academic Press, Burlington, 1999: pp. 423–491. https://doi.org/https://doi.org/10.1016/B978-012513905-2/50023-6.
[178] M. Bi, Y. Hao, J. Zhang, M. Lei, K. Bi, Particle size effect of BaTiO3 nanofillers on the energy storage performance of polymer nanocomposites, Nanoscale. 9 (2017) 16386–16395. https://doi.org/10.1039/C7NR05212J.
[179] K. Yu, H. Wang, Y. Zhou, Y. Bai, Y. Niu, Enhanced dielectric properties of BaTiO3/poly(vinylidene fluoride) nanocomposites for energy storage applications, J. Appl. Phys. 113 (2013) 34105. https://doi.org/10.1063/1.4776740.
[180] Y. Niu, K. Yu, Y. Bai, H. Wang, Enhanced Dielectric Performance of BaTiO3/PVDF Composites Prepared by Modified Process for Energy Storage Applications, IEEE Trans.

Ultrason. Ferroelectr. Freq. Control. 62 (2015) 108–115. https://doi.org/10.1109/TUFFC.2014.006666.
[181] K. Prasad, A. Prasad, K.P. Chandra, A.R. Kulkarni, Electrical Conduction in 0–3 BaTiO3/PVDF Composites, Integr. Ferroelectr. 117 (2010) 55–67. https://doi.org/10.1080/10584587.2010.489425.
[182] V. Tomer, E. Manias, C. Randall, High Field Properties and Energy Storage in Nanocomposite Dielectrics of Poly(Vinylidene Fluoride)-Hexafluropropylene, J. Appl. Phys. 110 (2011) 44107. https://doi.org/10.1063/1.3609082.
[183] B. Hilczer, J. Kułek, E. Markiewicz, M. Kosec, B. Malič, Dielectric relaxation in ferroelectric PZT–PVDF nanocomposites, J. Non. Cryst. Solids. 305 (2002) 167–173. https://doi.org/https://doi.org/10.1016/S0022-3093(02)01103-1.
[184] J. Kułek, I. Szafraniak, B. Hilczer, M. Połomska, Dielectric and pyroelectric response of PVDF loaded with BaTiO3 obtained by mechanosynthesis, J. Non. Cryst. Solids. 353 (2007) 4448–4452. https://doi.org/https://doi.org/10.1016/j.jnoncrysol.2007.02.077.
[185] A. Bello, E. Laredo, M. Grimau, Distribution of relaxation times from dielectric spectroscopy using Monte Carlo simulated annealing: Application to PVDF, Phys. Rev. B. 60 (1999) 12764–12774. https://doi.org/10.1103/PhysRevB.60.12764.
[186] H. Rekik, Z. Ghallabi, I. Royaud, M. Arous, G. Seytre, G. Boiteux, A. Kallel, Dielectric relaxation behaviour in semi-crystalline polyvinylidene fluoride (PVDF)/TiO2 nanocomposites, Compos. Part B Eng. 45 (2013) 1199–1206. https://doi.org/https://doi.org/10.1016/j.compositesb.2012.08.002.
[187] S. Kumar, S. Supriya, M. Kar, Enhancement of dielectric constant in polymer-ceramic nanocomposite for flexible electronics and energy storage applications, Compos. Sci. Technol. 157 (2018) 48–56. https://doi.org/https://doi.org/10.1016/j.compscitech.2018.01.025.
[188] Z. Pan, L. Yao, J. Zhai, X. Yao, H. Chen, Interfacial Coupling Effect in Organic/Inorganic Nanocomposites with High Energy Density, Adv. Mater. 30 (2018) 1705662. https://doi.org/https://doi.org/10.1002/adma.201705662.
[189] D.-H. Yoon, J. Zhang, B.I. Lee, Dielectric constant and mixing model of BaTiO3 composite thick films, Mater. Res. Bull. 38 (2003) 765–772. https://doi.org/https://doi.org/10.1016/S0025-5408(03)00075-8.
[190] T. Tanaka, M. Kozako, N. Fuse, Y. Ohki, Proposal of a multi-core model for polymer nanocomposite dielectrics, IEEE Trans. Dielectr. Electr. Insul. 12 (2005) 669–681. https://doi.org/10.1109/TDEI.2005.1511092.
[191] M.Z. Rong, M.Q. Zhang, W.H. Ruan, Surface modification of nanoscale fillers for improving properties of polymer nanocomposites: a review, Mater. Sci. Technol. 22 (2006) 787–796. https://doi.org/10.1179/174328406X101247.
[192] K. Yang, X. Huang, Y. Huang, L. Xie, P. Jiang, Fluoro-Polymer@BaTiO3 Hybrid Nanoparticles Prepared via RAFT Polymerization: Toward Ferroelectric Polymer Nanocomposites with High Dielectric Constant and Low Dielectric Loss for Energy Storage Application, Chem. Mater. 25 (2013) 2327–2338. https://doi.org/10.1021/cm4010486.
[193] X. Zhang, S. Zhao, F. Wang, Y. Ma, L. Wang, D. Chen, C. Zhao, W. Yang, Improving dielectric properties of BaTiO3/poly(vinylidene fluoride) composites by employing core-shell structured BaTiO3@Poly(methylmethacrylate) and BaTiO3@Poly(trifluoroethyl methacrylate) nanoparticles, Appl. Surf. Sci. 403 (2017) 71–79. https://doi.org/https://doi.org/10.1016/j.apsusc.2017.01.121.
[194] X. Wang, H. Chen, A new approach to preparation of TiO2@void@SiO2 rattle type core shell structure nanoparticles via titanyl oxalate complex, Colloids Surfaces A Physicochem. Eng. Asp. 485 (2015) 25–33. https://doi.org/https://doi.org/10.1016/j.colsurfa.2015.08.036.
[195] Prateek, R. Bhunia, S. Siddiqui, A. Garg, R.K. Gupta, Significantly Enhanced Energy Density by Tailoring the Interface in Hierarchically Structured TiO2–BaTiO3–TiO2 Nanofillers in PVDF-Based Thin-Film Polymer Nanocomposites, ACS Appl. Mater. Interfaces. 11 (2019) 14329–14339. https://doi.org/10.1021/acsami.9b01359.
[196] Y. Wang, J. Chen, Y. Li, Y. Niu, Q. Wang, H. Wang, Multilayered Hierarchical Polymer Composites for High Energy Density Capacitors, J. Mater. Chem. A. 7 (2019) 2965–2980. https://doi.org/10.1039/C8TA11392K.
[197] V. Buscaglia, M. Buscaglia, Core-Shell Heterostructures: From Particle Synthesis to Bulk

Dielectric, Ferroelectric, and Multiferroic Composite Materials: Key Processing and Characterization Issues, and Nanoscale Effects, in: 2016: pp. 72–99. https://doi.org/10.1002/9781118935743.ch3.
[198] Prateek, D. Singh, N. Singh, A. Garg, R.K. Gupta, Engineered thiol anchored Au-BaTiO3/PVDF polymer nanocomposite as efficient dielectric for electronic applications, Compos. Sci. Technol. 174 (2019) 158–168. https://doi.org/https://doi.org/10.1016/j.compscitech.2019.02.015.
[199] H. Zhu, Z. Liu, F. Wang, K. Yan, Influence of shell thickness on the dielectric properties of composites filled with Ag@SiO2 nanoparticles, RSC Adv. 6 (2016) 64634–64639. https://doi.org/10.1039/C6RA08750G.
[200] G. Arlt, D. Hennings, G. de With, Dielectric properties of fine-grained barium titanate ceramics, J. Appl. Phys. 58 (1985) 1619–1625. https://doi.org/10.1063/1.336051.
[201] V. Buscaglia, C.A. Randall, Size and scaling effects in barium titanate. An overview, J. Eur. Ceram. Soc. 40 (2020) 3744–3758. https://doi.org/https://doi.org/10.1016/j.jeurceramsoc.2020.01.021.
[202] W.L. Zhong, Y.G. Wang, P.L. Zhang, B.D. Qu, Phenomenological study of the size effect on phase transitions in ferroelectric particles, Phys. Rev. B. 50 (1994) 698–703. https://doi.org/10.1103/PhysRevB.50.698.
[203] T. Hoshina, Size effect of barium titanate: Fine particles and ceramics, J. Ceram. Soc. Japan. 121 (2013) 156–161. https://doi.org/10.2109/jcersj2.121.156.
[204] H.-I. Hsiang, K.-Y. Lin, F.-S. Yen, C.-Y. Hwang, Effects of particle size of BaTiO3 powder on the dielectric properties of BaTiO3/polyvinylidene fluoride composites, J. Mater. Sci. 36 (2001) 3809–3815. https://doi.org/10.1023/A:1017946405447.
[205] Y.P. Mao, S.Y. Mao, Z.-G. Ye, Z.X. Xie, L.S. Zheng, Size-dependences of the dielectric and ferroelectric properties of BaTiO3/polyvinylidene fluoride nanocomposites, J. Appl. Phys. 108 (2010) 14102. https://doi.org/10.1063/1.3443582.
[206] S.F. Mendes, C.M. Costa, C. Caparros, V. Sencadas, S. Lanceros-Méndez, Effect of filler size and concentration on the structure and properties of poly(vinylidene fluoride)/BaTiO3 nanocomposites, J. Mater. Sci. 47 (2012) 1378–1388. https://doi.org/10.1007/s10853-011-5916-7.
[207] B.-H. Fan, J.-W. Zha, D.-R. Wang, J. Zhao, Z.-F. Zhang, Z.-M. Dang, Preparation and dielectric behaviors of thermoplastic and thermosetting polymer nanocomposite films containing BaTiO3 nanoparticles with different diameters, Compos. Sci. Technol. 80 (2013) 66–72. https://doi.org/https://doi.org/10.1016/j.compscitech.2013.02.021.
[208] B. Zhou, R. Li, J. Cai, J. Xu, Z. Zhao, J. Pei, Grain size effect on electric properties of novel BaTiO3/PVDF composite piezoelectric ceramics, Mater. Res. Express. 5 (2018). https://doi.org/10.1088/2053-1591/aad8a4.
[209] H.A. Al-Abadleh, H.A. Al-Hosney, V.H. Grassian, Oxide and carbonate surfaces as environmental interfaces: the importance of water in surface composition and surface reactivity, J. Mol. Catal. A Chem. 228 (2005) 47–54. https://doi.org/https://doi.org/10.1016/j.molcata.2004.09.059.
[210] A. León, P. Reuquen, C. Garín, R. Segura, P. Vargas, P. Zapata, P. Orihuela, FTIR and Raman Characterization of TiO2 Nanoparticles Coated with Polyethylene Glycol as Carrier for 2-Methoxyestradiol, Appl. Sci. 7 (2017) 49. https://doi.org/10.3390/app7010049.
[211] A.M. El-Toni, S. Yin, T. Sato, Dense silica coating of titania nanoparticles by seeded polymerization technique, Colloids Surfaces A Physicochem. Eng. Asp. 274 (2006) 229–233. https://doi.org/https://doi.org/10.1016/j.colsurfa.2005.10.012.
[212] A.M. El-Toni, S. Yin, T. Sato, Control of silica shell thickness and microporosity of titania–silica core–shell type nanoparticles to depress the photocatalytic activity of titania, J. Colloid Interface Sci. 300 (2006) 123–130. https://doi.org/https://doi.org/10.1016/j.jcis.2006.03.073.
[213] C. Chen, W.Z. Xu, P.A. Charpentier, SiO2 encapsulated TiO2 nanotubes and nanofibers for self-cleaning polyurethane coatings, J. Photochem. Photobiol. A Chem. 348 (2017) 226–237. https://doi.org/https://doi.org/10.1016/j.jphotochem.2017.08.014.
[214] K. Bi, M. Bi, Y. Hao, W. Luo, Z. Cai, X. Wang, Y. Huang, Ultrafine core-shell BaTiO3@SiO2 structures for nanocomposite capacitors with high energy density, Nano Energy. 51 (2018) 513–523. https://doi.org/https://doi.org/10.1016/j.nanoen.2018.07.006.

[215] V. Petrovsky, A. Manohar, F. Dogan, Dielectric constant of particles determined by impedance spectroscopy, J. Appl. Phys. 100 (2006) 14102. https://doi.org/10.1063/1.2206411.
[216] Y. Hao, X. Wang, K. Bi, J. Zhang, Y. Huang, L. Wu, P. Zhao, K. Xu, M. Lei, L. Li, Significantly enhanced energy storage performance promoted by ultimate sized ferroelectric BaTiO3 fillers in nanocomposite films, Nano Energy. 31 (2017) 49–56. https://doi.org/https://doi.org/10.1016/j.nanoen.2016.11.008.
[217] Y. Fan, G. Wang, X. Huang, J. Bu, X. Sun, P. Jiang, Molecular structures of (3-aminopropyl)trialkoxysilane on hydroxylated barium titanate nanoparticle surfaces induced by different solvents and their effect on electrical properties of barium titanate based polymer nanocomposites, Appl. Surf. Sci. 364 (2016) 798–807. https://doi.org/https://doi.org/10.1016/j.apsusc.2015.12.228.
[218] Z.-M. Dang, H.-Y. Wang, H.-P. Xu, Influence of silane coupling agent on morphology and dielectric property in BaTiO3/polyvinylidene fluoride composites, Appl. Phys. Lett. 89 (2006) 112902. https://doi.org/10.1063/1.2338529.
[219] A. Choudhury, Preparation, characterization and dielectric properties of polyetherimide nanocomposites containing surface-functionalized BaTiO3 nanoparticles, Polym. Int. 61 (2012) 696–702. https://doi.org/https://doi.org/10.1002/pi.4181.
[220] S. Dalle Vacche, F. Oliveira, Y. Leterrier, V. Michaud, D. Damjanovic, J.-A.E. Månson, Effect of silane coupling agent on the morphology, structure, and properties of poly(vinylidene fluoride–trifluoroethylene)/BaTiO3 composites, J. Mater. Sci. 49 (2014) 4552–4564. https://doi.org/10.1007/s10853-014-8155-x.
[221] C. Ehrhardt, C. Fettkenhauer, J. Glenneberg, W. Münchgesang, C. Pientschke, T. Großmann, M. Zenkner, G. Wagner, H.S. Leipner, A. Buchsteiner, M. Diestelhorst, S. Lemm, H. Beige, S.G. Ebbinghaus, BaTiO3–P(VDF-HFP) nanocomposite dielectrics—Influence of surface modification and dispersion additives, Mater. Sci. Eng. B. 178 (2013) 881–888. https://doi.org/https://doi.org/10.1016/j.mseb.2013.04.013.
[222] X. Zhang, Y. Ma, C. Zhao, W. Yang, High dielectric constant and low dielectric loss hybrid nanocomposites fabricated with ferroelectric polymer matrix and BaTiO3 nanofibers modified with perfluoroalkylsilane, Appl. Surf. Sci. 305 (2014) 531–538. https://doi.org/https://doi.org/10.1016/j.apsusc.2014.03.131.
[223] H.-J. Ye, W.-Z. Shao, L. Zhen, Tetradecylphosphonic acid modified BaTiO3 nanoparticles and its nanocomposite, Colloids Surfaces A Physicochem. Eng. Asp. 427 (2013) 19–25. https://doi.org/https://doi.org/10.1016/j.colsurfa.2013.02.068.
[224] M. Castellano, A. Turturro, E. Marsano, L. Conzatti, S. Vicini, Hydrophobation of silica surface by silylation with new organo-silanes bearing a polybutadiene oligomer tail, Polym. Compos. 35 (2014) 1603–1613. https://doi.org/https://doi.org/10.1002/pc.22813.
[225] M. Castellano, A. Turturro, E. Finocchio, G. Busca, L. Conzatti, R. Legami, S. Vicini, Innovative Mesoporous Nanosilicas: SBR Nanocomposite for Low Environmental Impact Tread Tyre, J. Nanosci. Nanotechnol. 18 (2018) 1503–1515. https://doi.org/10.1166/jnn.2018.15249.
[226] F.R. Fan, W. Tang, Z.L. Wang, Flexible Nanogenerators for Energy Harvesting and Self-Powered Electronics, Adv. Mater. 28 (2016) 4283–4305. https://doi.org/https://doi.org/10.1002/adma.201504299.
[227] L. Mateu, T. Dräger, I. Mayordomo, M. Pollak, Chapter 4.1 - Energy Harvesting at the Human Body, in: E. Sazonov, M.R.B.T.-W.S. Neuman (Eds.), Academic Press, Oxford, 2014: pp. 235–298. https://doi.org/https://doi.org/10.1016/B978-0-12-418662-0.00004-0.
[228] I. Katsouras, K. Asadi, M. Li, T.B. van Driel, K.S. Kjær, D. Zhao, T. Lenz, Y. Gu, P.W.M. Blom, D. Damjanovic, M.M. Nielsen, D.M. de Leeuw, The negative piezoelectric effect of the ferroelectric polymer poly(vinylidene fluoride), Nat. Mater. 15 (2016) 78–84. https://doi.org/10.1038/nmat4423.
[229] P. Gowdhaman, V. Annamalai, O.P. Thakur, Piezo, ferro and dielectric properties of ceramic-polymer composites of 0-3 connectivity, Ferroelectrics. 493 (2016) 120–129. https://doi.org/10.1080/00150193.2016.1134028.
[230] J.E.Q. Quinsaat, T. de Wild, F.A. Nüesch, D. Damjanovic, R. Krämer, G. Schürch, D. Häfliger, F. Clemens, T. Sebastian, M. Dascalu, D.M. Opris, Stretchable piezoelectric elastic composites for sensors and energy generators, Compos. Part B Eng. 198 (2020)

108211. https://doi.org/https://doi.org/10.1016/j.compositesb.2020.108211.
[231] V. Sencadas, C. Costa, V. Moreira, J. Monteiro, S.K. Mendiratta, J.F. Mano, S. Lanceros-Méndez, Poling of ß-poly(vinylidene fluoride): Dielectric and IR spectroscopy studies, E-Polymers. 5 (2005). https://doi.org/10.1515/epoly.2005.5.1.10.
[232] J.-K. Hong, J.-S. Lee, K.J. Lim, Y.-H. Lee, H.-I. Chae, Poling Effect of Dielectric and Piezoelectric Properties in PMWN-PZT Ceramics, Ferroelectrics. 272 (2002) 261–266. https://doi.org/10.1080/00150190211593.
[233] A. Sasmal, S. Sen, P. Devi, Frequency dependent Energy Storage and Dielectric Performance of Ba-Zr Co-doped BiFeO3 loaded PVDF based Mechanical Energy harvesters: Effect of Corona Poling, Soft Matter. 16 (2020). https://doi.org/10.1039/D0SM01031F.
[234] K. Ng, H. Chan, C. Choy, Piezoelectric and pyroelectric properties of PZT/P(VDF-TrFE) composites with constituent phases poled in parallel or antiparallel directions, Ultrason. Ferroelectr. Freq. Control. IEEE Trans. 47 (2000) 1308–1315. https://doi.org/10.1109/58.883519.
[235] K. Lam, X. Wang, H.L. Chan, Piezoelectric and pyroelectric properties of (Bi0.5Na0.5)0.94Ba0.06TiO3/P(VDF-TrFE) 0–3 composites, Compos. Part A Appl. Sci. Manuf. 36 (2005) 1595–1599. https://doi.org/https://doi.org/10.1016/j.compositesa.2005.03.007.
[236] H.S. Mohanty, Ravikant, A. Kumar, P.K. Kulriya, R. Thomas, D.K. Pradhan, Dielectric/ferroelectric properties of ferroelectric ceramic dispersed poly(vinylidene fluoride) with enhanced β-phase formation, Mater. Chem. Phys. 230 (2019) 221–230. https://doi.org/https://doi.org/10.1016/j.matchemphys.2019.03.055.
[237] J.D. Bobić, G.F. Teixeira, R. Grigalaitis, S. Gyergyek, M.M.V. Petrović, M.A. Zaghete, B.D. Stojanovic, PZT–NZF/CF ferrite flexible thick films: Structural, dielectric, ferroelectric, and magnetic characterization, J. Adv. Ceram. 8 (2019) 545–554. https://doi.org/10.1007/s40145-019-0337-1.
[238] W. Ji, H. Deng, C. Guo, C. Sun, X. Guo, F. Chen, Q. Fu, The effect of filler morphology on the dielectric performance of polyvinylidene fluoride (PVDF) based composites, Compos. Part A Appl. Sci. Manuf. 118 (2019) 336–343. https://doi.org/https://doi.org/10.1016/j.compositesa.2019.01.011.
[239] P. Hu, L. Yan, C. Zhao, Y. Zhang, J. Niu, Double-layer structured PVDF nanocomposite film designed for flexible nanogenerator exhibiting enhanced piezoelectric output and mechanical property, Compos. Sci. Technol. 168 (2018) 327–335. https://doi.org/https://doi.org/10.1016/j.compscitech.2018.10.021.
[240] A. Roy, K. Nath, K. Prasad, A. Prasad, Effective complex permittivity and AC conductivity of (Bi0.5Na0.5)0.94Ba0.06 TiO3-PVDF 0-3 composite, Adv. Mater. Lett. 5 (2014) 100–105. https://doi.org/10.5185/amlett.2013.fdm.77.
[241] H.S. Mohanty, S.K. Sharma, RaviKant, P.K. Kulriya, A. Kumar, R. Thomas, D.K. Pradhan, Enhanced functional properties of soft polymer–ceramic composites by swift heavy ion irradiation, Phys. Chem. Chem. Phys. 21 (2019) 24629–24642. https://doi.org/10.1039/C9CP04206G.
[242] S. Riquelme, K. Ramam, Dielectric and piezoelectric properties of lead free BZT-BCT/PVDF flexible composites for electronic applications, Mater. Res. Express. 6 (2019). https://doi.org/10.1088/2053-1591/ab522c.

APPENDICES

APPENDIX A

During the second step of moulding, the film undergoes contemporary to an *in-plane* (increasing laterally its surface) and *out-of-plane* (reducing its thickness) deformation. To evaluate this change a relative compression ratio ($\varepsilon_{\%}$) was considered (Equation A.1) :

$$\varepsilon_{\%} = \frac{t_i - t_f}{t_i} * 100 \quad \text{(A.1)}$$

where t_i is the initial plate thickness and t_f is the final thickness of the film after the double-step moulding [A1].

The compression ratio depends on both the temperature of moulding and the initial plate thickness as clearly shown in Figure A.1. In particular, at equal moulding temperature, $\varepsilon_{\%}$ increases by increasing the initial plate thickness, while, at equal starting thickness, is higher for higher moulding temperature because the lower viscosity of the polymer allows a more marked deformation. This confirms what reported in *Paragraph 4.1.1* regarding the explanation of the response surface shape.

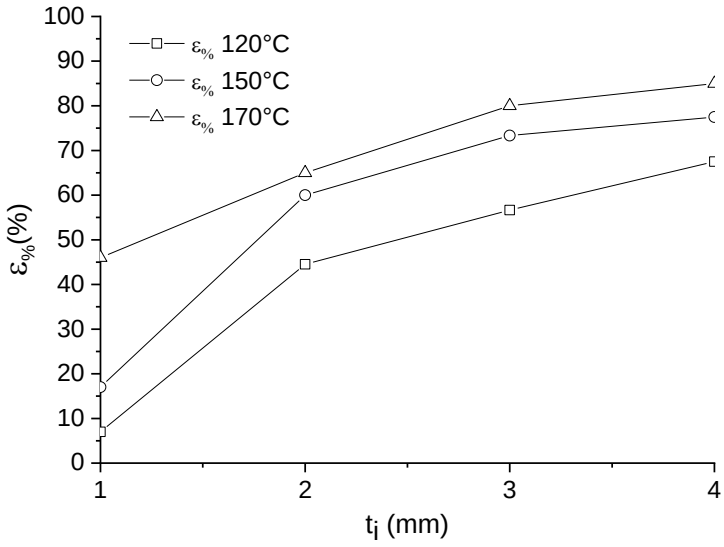

Figure A.1: relative compression ratio as a function of initial plate thickness at different moulding temperature.

Due to the discordant fusion enthalpies values of PVDF present in literature, it was deemed appropriate to calculate the crystallinity degree of the prepared samples by using two different approaches. Table A.1 shows the X_c obtained by considering ΔH_0 = 104.6 J/g independently from the polymorphism (X_c^A) or ΔH_0 = 93.07 J/g and 103.4 J/g for α and β phase, respectively (X_c^B).

Despite the different values obtained, the information derived from the data is the same: the samples re-pressed at 170°C are characterized by an slightly higher crystallinity degree.

Table A.1: PVDF films prepared by the double-step method in different processing conditions and and crystallinity degrees calculated by DSC using different values of fusion enthalpy for PVDF.

Sample name	Sample code	X_c^A (%)	X_c^B (%)
PVDF1_120	A	56	61
PVDF1_150	B	57	62
PVDF1_170	C	59	64
PVDF2_120	D	55	59
PVDF2_150	E	57	60
PVDF2_170	F	59	63
PVDF3_120	G	55	58
PVDF3_150	H	54	57
PVDF3_170	I	57	62
PVDF4_120	L	56	59
PVDF4_150	M	54	57
PVDF4_170	N	62	66

The absolute electroactive phase amount (F_{EA}*) was also calculated in both the cases and the same trend is observable independently from the fusion enthalpy taken as references (Figure A.2)

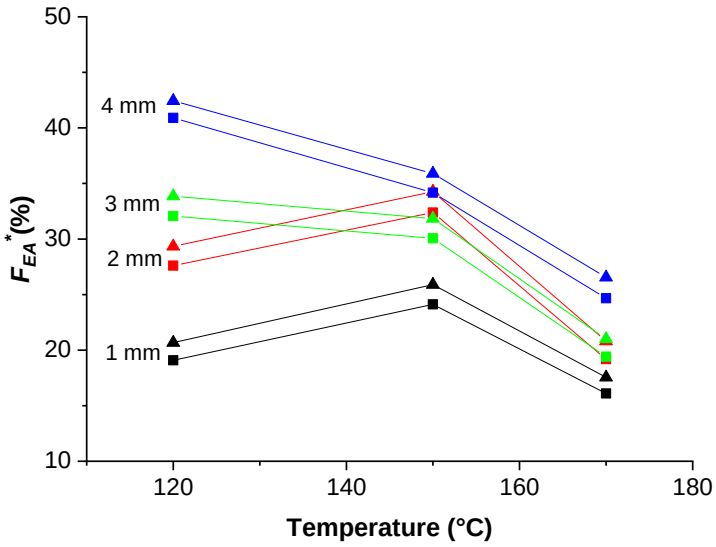

Figure A.2: Absolute electrocative phase amount calculated by considering the crystallinity degree derived from different enthalpies values: X_c^A (square) and X_c^B (triangle).

References

[A.1] S. Satapathy, S. Pawar, P.K. Gupta, K.B.R. Varma, Effect of annealing on phase transition in poly(vinylidene fluoride) films prepared using polar solvent, Bull. Mater. Sci. 34 (2011) 727. https://doi.org/10.1007/s12034-011-0187-0.

APPENDIX B

The filler distribution/dispersion is not affected by the moulding conditions, being determined only by the preparation technique, *i.e.*, melt blending or solvent casting. The morphology of the composites from P2-moulding is here reported for sake of completeness in Figure B.1.

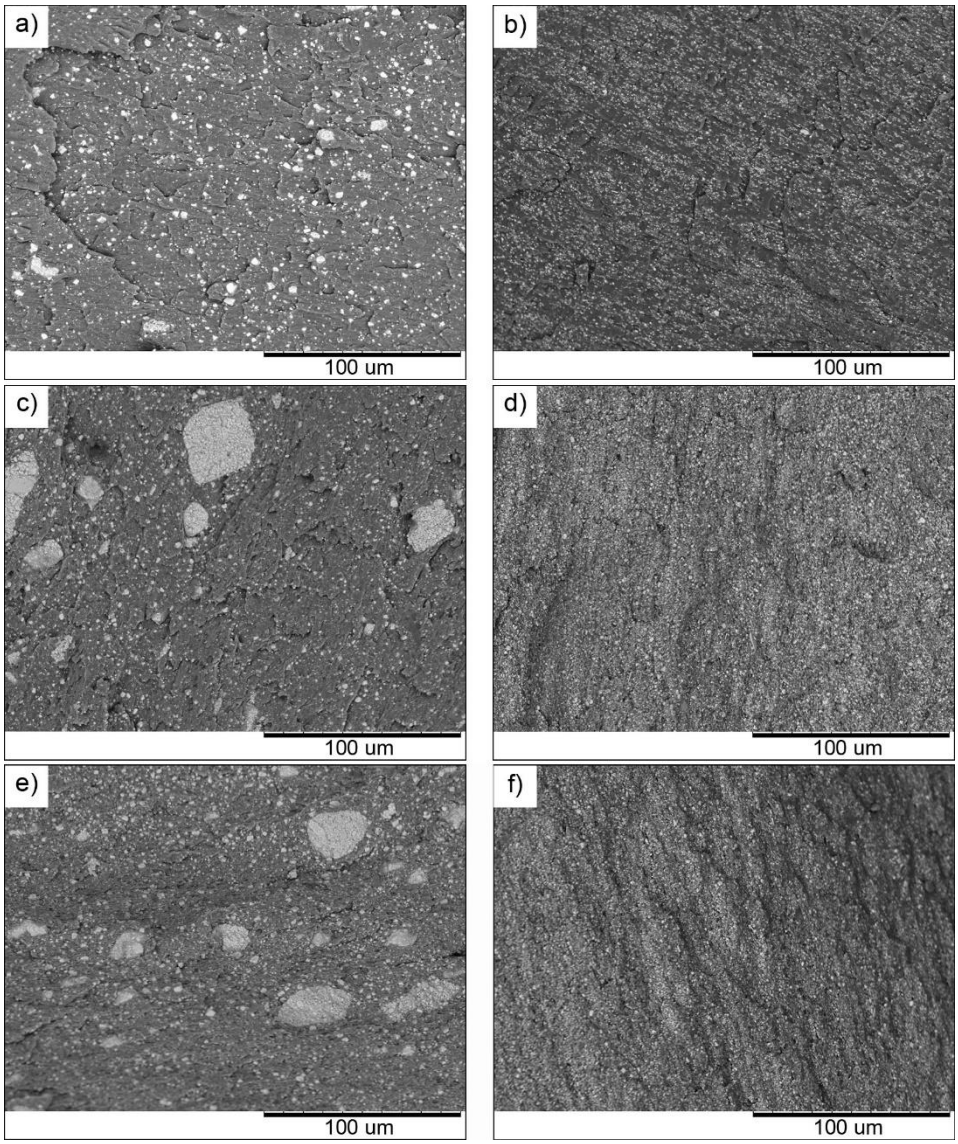

Figure B.1: SEM micrographs of PVDF/PZT composites: a) 10M-P2; b) 10S-P2; c) 20M-P2; d) 20S-P2; e) 30M-P2 and f) 30S-P2

The EDX analysis confirms that, for all the compositions, the agglomerates present in the composites from melt blending are quite dense, consisting predominantly PZT particles. The element mapping of the samples containing 10 and 20 Vol% of particles are reported in Figure B.2 and B.3, respectively.

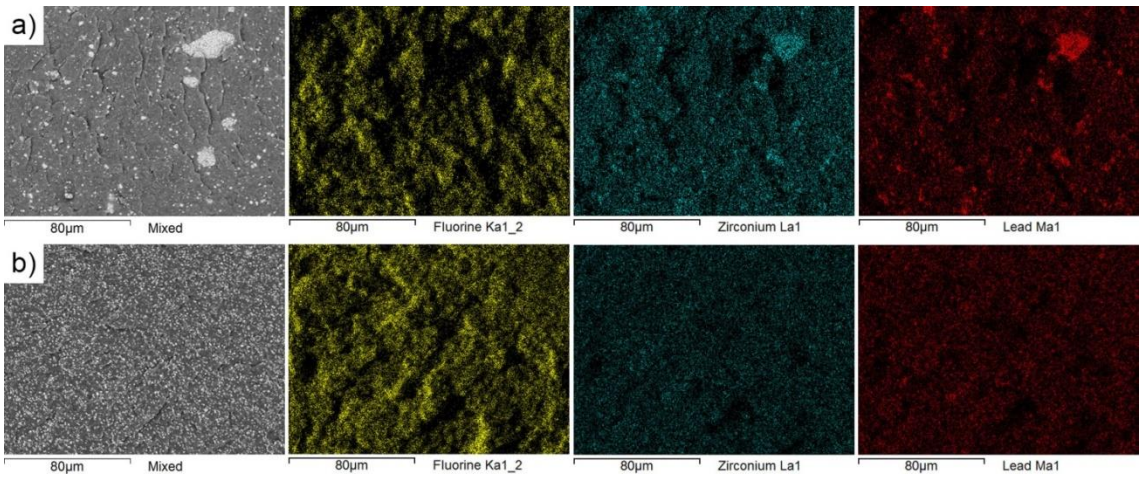

Figure B.2: EDX element mapping of the 10 Vol% PVDF/PZT composite from: a) melt blending; b) solvent casting.

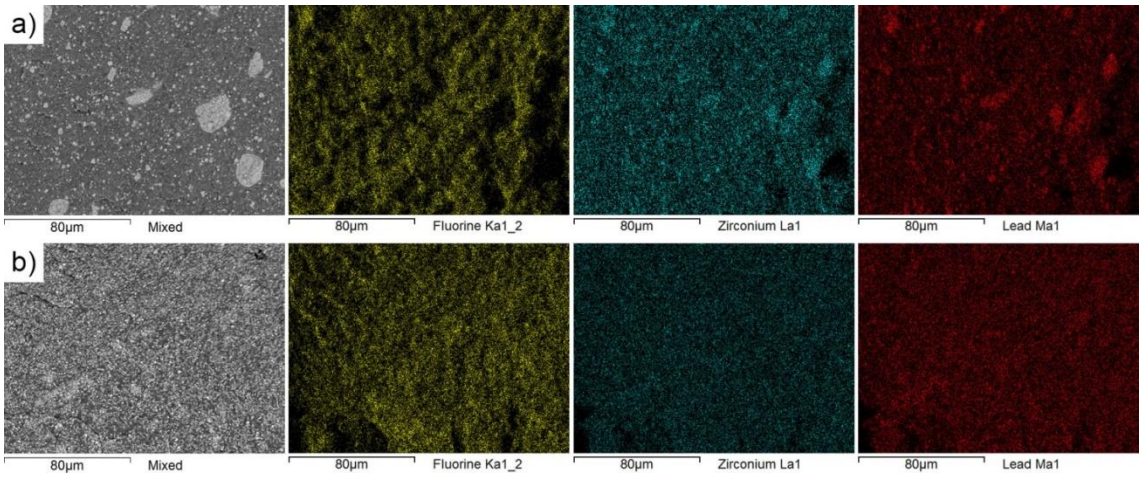

Figure B.3: EDX element mapping of the 20 Vol% PVDF/PZT composite from: a) melt blending; b) solvent casting.

APPENDIX C

The stability over time of some samples was tested by repeating the dielectric measurements 2 months after the preparation.

The stability over time of the 30B-P2 sample is reported in Figure C.1.

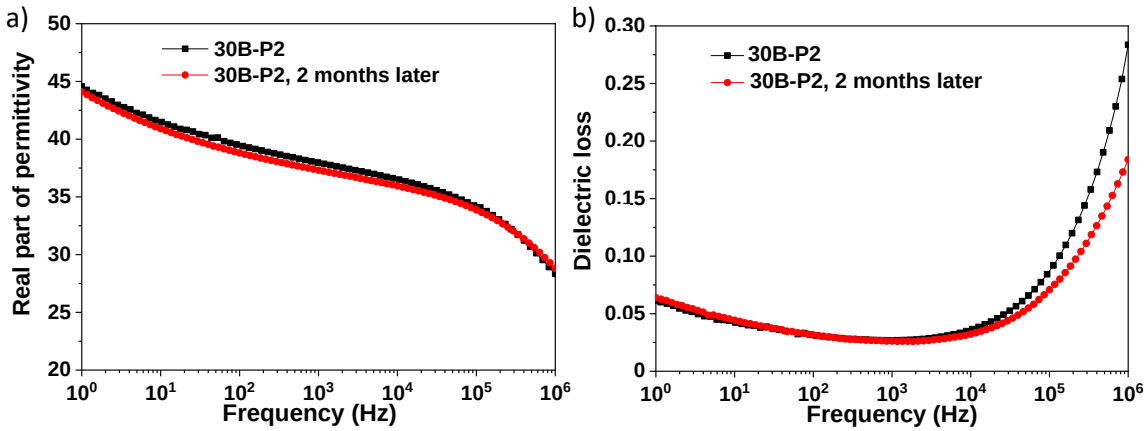

Figure C.1: Stability over time of dielectric properties of C30-P2 sample after two months from preparation: a) real part of permittivity and b) dielectric loss.

The stability over time of the S-B125 sample is reported in Figure C.2.

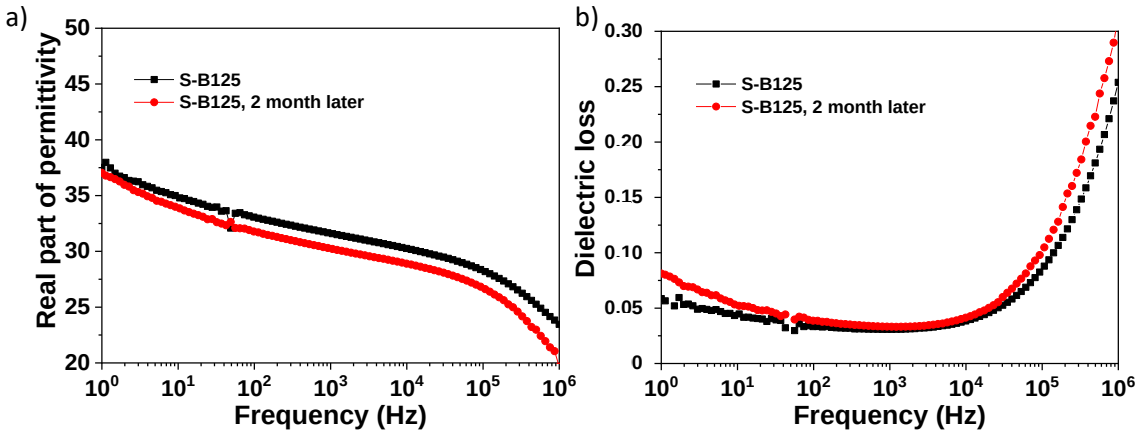

Figure C.2: Stability over time of dielectric properties of S-B125 sample after two months from preparation: a) real part of permittivity and b) dielectric loss.

APPENDIX D

The filler dispersion was not affected by the type of coating (TiO_2 or SiO_2) or the shell thickness; all the sample prepared presented a suitable morphology. The SEM Micrographs of the composites not showed in *Paragraph 4.1.2* are Reported in Figure D.1 for sake of completeness.

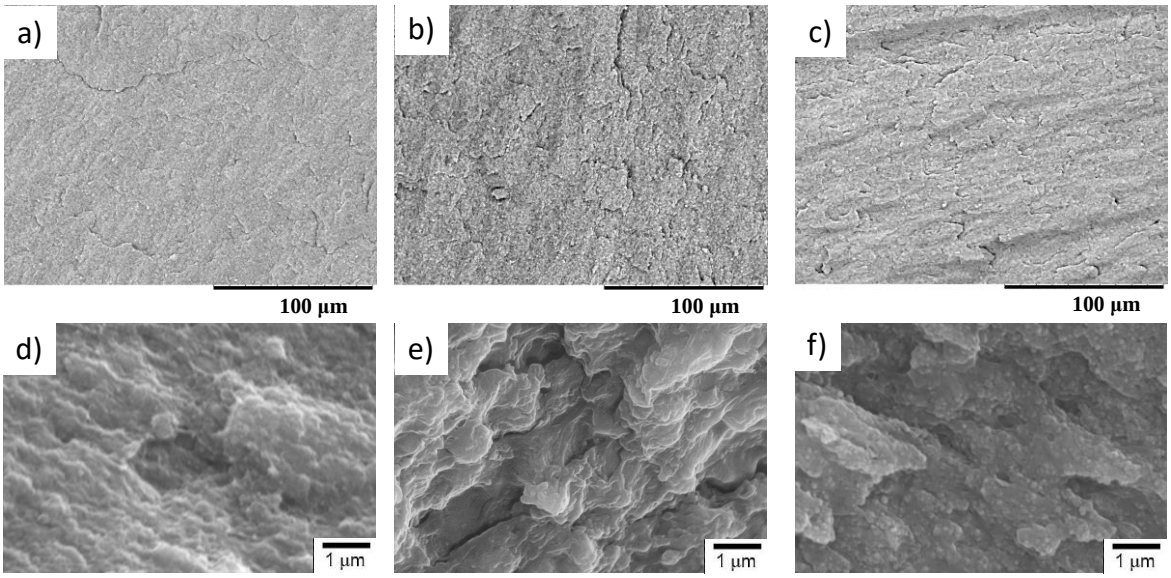

Figure D.1.: SEM micrographs at low and high magnification of: a,d) S-B125T6; b,e) S-B125T22; c,f) S-B125Si6.

APPENDIX E

The finite element method (FEM), which is one of the most widely used method for sort out problems of engineering and mathematical models, is a particular numerical method for solving partial differential equations in two or three space variables. To solve a problem, the FEM subdivides a large system into smaller, simpler parts that are called finite elements, obtained by a particular space discretization consisting in the construction of a mesh of the object. The simple equations that model these finite elements are then assembled into a larger system of equations that models the entire problem.

Here, this method was used to model the dielectric properties of a composite system, that are strongly determined by the local field inhomogeneity due to the co-presence of phases with different permittivity. This aspect is rarely investigate because it requires advanced modeling tool.

The considered system consists of a cube of the dielectric composite with electrodes applied on the top and bottom surfaces, in order to simulate a parallel plate capacitor configuration. The composite is modelled with a 0-3 connectivity, as a dispersion of spherical particles of constant diameters corresponding to the ferroelectric phase in a polymer matrix (see Figure E.1).

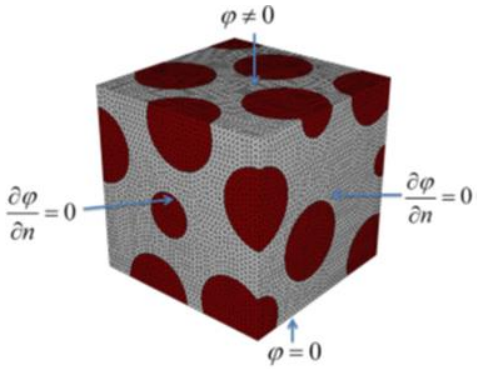

Figure E.1.: Schematic representation of the composite modelled for the permittivity calculation with the FEM [E1].

As a first approximation, the dielectric permittivity of the two phases is considered as field-independent.

Experimentally, only the applied electric field is known. To compute the effective permittivity it must be taken into account that the distribution of the dielectric field within the composite is highly inhomogeneous, because the two components of the material possess very different values of the dielectric constant. For the calculation the system is meshed in a large number of tetrahedral elements and the local electric potential is obtained by solving the Laplace Equation in each element, by using the FEM modelling [E1].

As a result, the distribution of the electric field is obtained and the real part of the effective permittivity (ε_{eff}) is derived from the energy stored by the capacitor, using the additive character of the energy according to Equation E.1:

$$\frac{\varepsilon_{eff}}{2} \cdot \left(\frac{\Delta\varphi}{d}\right)^2 V_t = \sum_{i=1}^{Ne} \frac{\varepsilon_i E_i^2}{2} V_i \qquad \text{(E.1)}$$

where $\Delta\varphi$ is the applied voltage, d is the capacitor thickness, V_t is the capacitor volume ε_i is the real part of permittivity of the i-th element, E_i is the field in the i-th element, V_i is the volume of the i-th element and N is the total number of elements.

References:

[E1] L. Padurariu, L.P. Curecheriu, L. Mitoseriu, Nonlinear dielectric properties of paraelectric-dielectric composites described by a 3D Finite Element Method based on Landau-Devonshire theory, Acta Mater. 103 (2016) 724–734.
https://doi.org/https://doi.org/10.1016/j.actamat.2015.11.008.

APPENDIX F

The results relative to the spectroscopic and calorimetric characterization of the BT@TiO_2 particles functionalized with APTES and DDTES are reported in Figure F.1 and F.2, respectively.

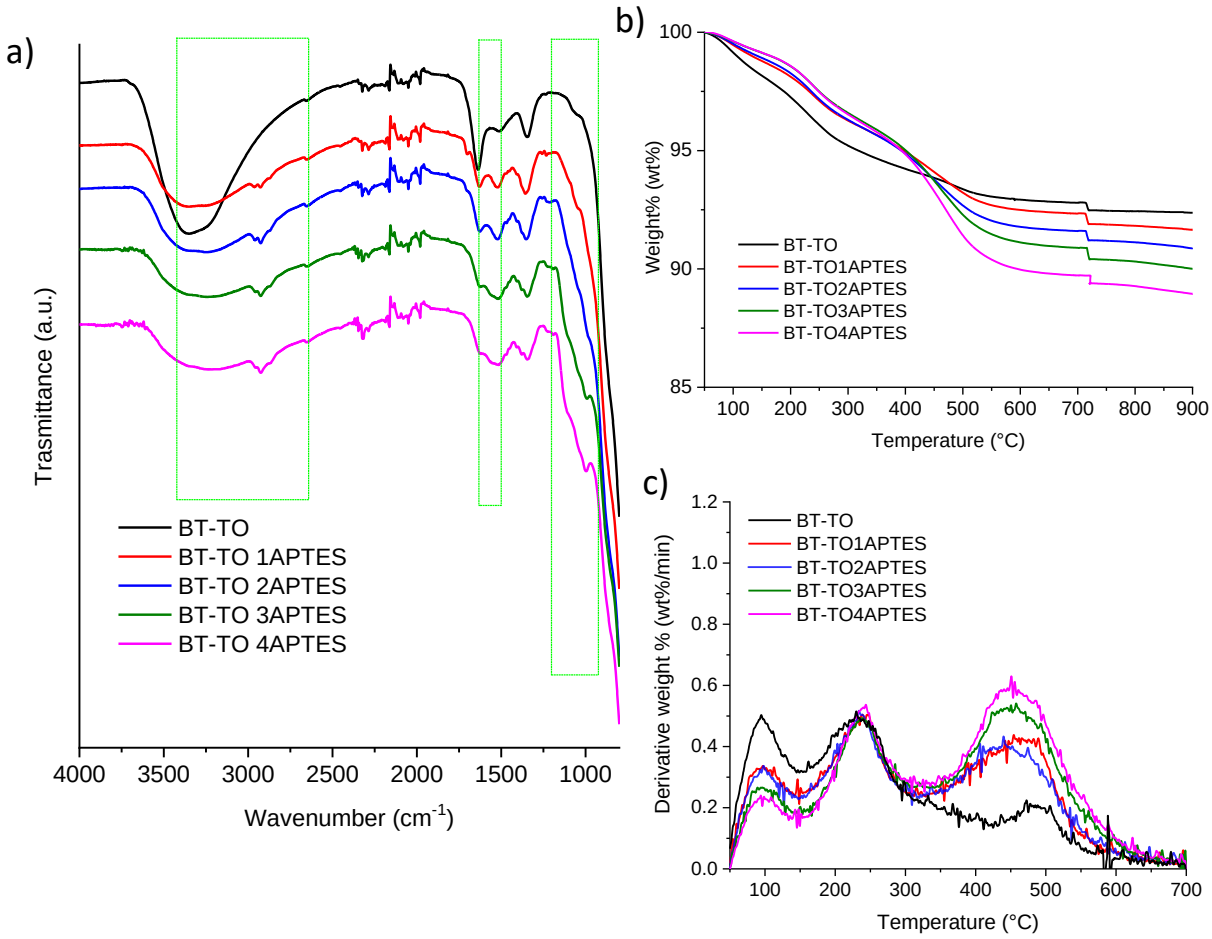

Figure F.1: a) ATR-FITR spectra, b) TGA thermogram and c) DTG curve of neat BT@TiO_2 and BT@TiO_2 modified with increasing amount of APTES.

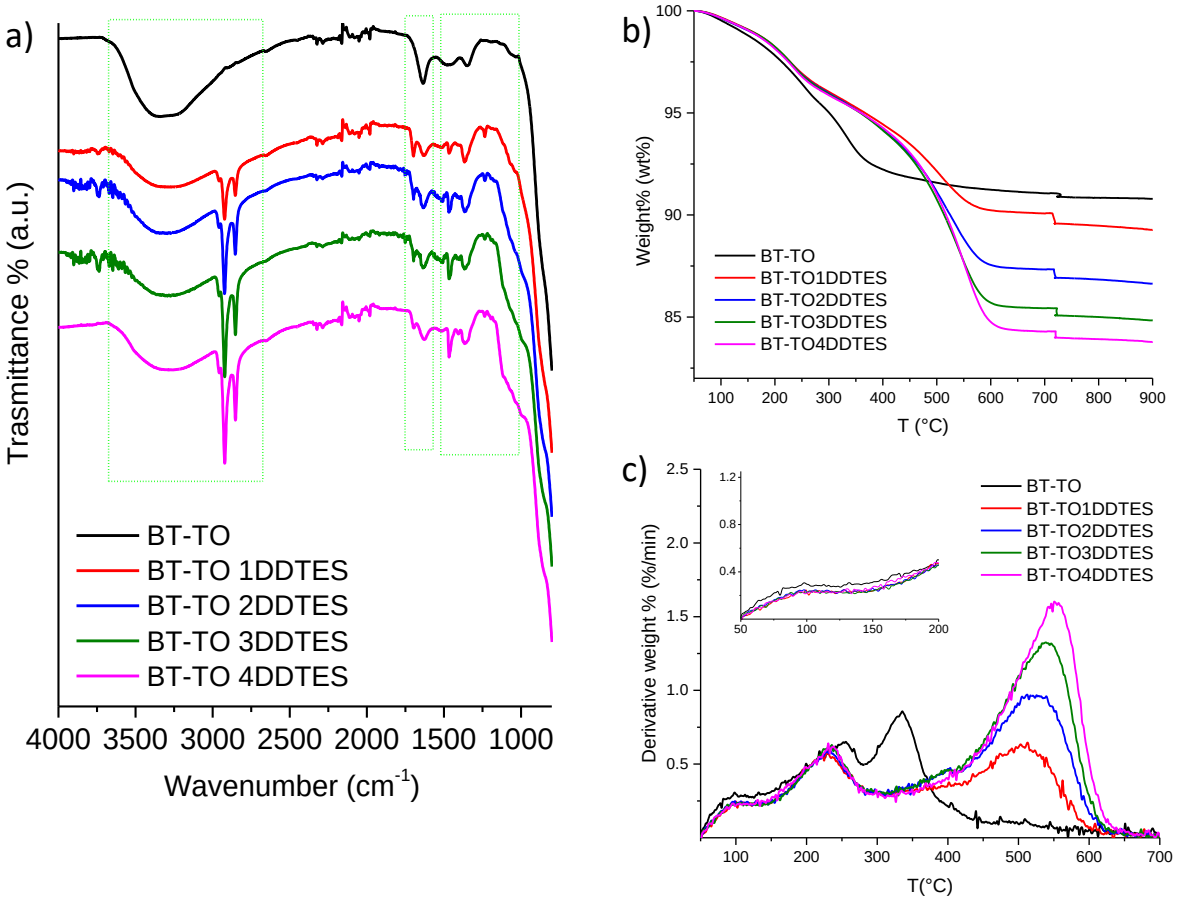

Figure F.2: a) ATR-FITR spectra, b) TGA thermogram and c) DTG curve of neat BT@TiO_2 and BT@TiO_2 modified with increasing amount of DDTES.

7 SCIENTIFIC PRODUCTION

Papers

Related to the thesis:

- E. Brunengo, L. Conzatti, I. Schizzi, C. Costa, M.T. Buscaglia, G. Canu, M. Castellano, V. Buscaglia, and P. Stagnaro, *"PVDF/$BaTiO_3$ composites as dielectric materials: influence of processing on properties",* AIP Conference Proceedings, 1981, 020132 (2018), Code 137840, ISBN: 978-073541697-0, ISSN: 0094-243X; DOI: 10.1063/1.5045994.
- F. Gheorghiu, R. Stanculescu, L. Curecheriu, E. Brunengo, P.Stagnaro, V. Tiron, P. Postolache, M. T. Buscaglia, L. Mitoseriu, *"PVDF-ferrite composites with dual magneto-piezolectric response for flexible electronics applications: synthesis and functional properties"*, Journal of Materials Science 55 (2020) 3926–3939; DOI: 10.1007/s10853-019-04279-w.
- E. Brunengo, M. Castellano, L. Conzatti, G. Canu, V. Buscaglia, P. Stagnaro, *"PVDF-based composites containing PZT particles: How processing affects the final properties",* Journal of Applied Polymer Science 137 (2020) 48871; DOI: 10.1002/APP.48871. Article chosen for the Issue Cover.
- E. Brunengo, G. Luciano, G. Canu, M. Canetti, L. Conzatti, M. Castellano, P. Stagnaro, *"Double-step moulding: an effective method to induce the formation of β-phase in PVDF",* Polymer 193 (2020) 122345; DOI: 10.1016/j.polymer.2020.122345.
- E. Brunengo, L. Conzatti, I. Schizzi, M. T. Buscaglia, G. Canu, L. Curecheriu, C. Costa, M. Castellano, L. Mitoseriu, P. Stagnaro, V. Buscaglia, *"Improved dielectric properties of PVDF–BaTiO3 composites by solvent-free processing"*. Journal of Applied Polymer Science, 2021; 138:e50049; DOI: 10.1002/app.50049

Others:

- L. Conzatti, E. Brunengo, R. Utzeri, M. Castellano, P. Hodge, P. Stagnaro, *"Macrocyclic oligomers as compatibilizing agent for hemp fibres/biodegradable polyester eco-composites",* Polymer 146 (2018) 396-406; DOI: 10.1016/j.polymer.2018.05.053.
- E. Brunengo, L. Conzatti, R. Utzeri, S. Vicini, M. Scatto , E. Verga Falzacappa, M. Castellano, P. Stagnaro, *"Chemical modification of hemp fibres by plasma treatment for eco-composites based on biodegradable polyester",* Journal of Materials Science 54 (2019) 14367–14377; DOI:10.1007/s10853-019-03932-8.
- A. Dodero, E. Brunengo, M. Alloisio, A. Sionkowska, S. Vicini, M. Castellano, *"Chitosan-based electrospun membranes: Effects of solution viscosity, coagulant and crosslinker" ,* Carbohydrate Polymers 235 (2020) 115976; DOI: 10.1016/j.carbpol.2020.115976.
- A. Dodero , E. Brunengo, M. Castellano, S. Vicini , *"Investigation of the mechanical and dynamic-mechanical properties of electrospun polyvinylpyrrolidone membranes: a design of experiment approach",* Polymers 12 (2020), 1524; DOI: 10.3390/polym12071524.

Communications at Conferences

Oral communications:

Personally presented:

- E. Brunengo, L. Conzatti, I. Schizzi, C. Costa, M.T. Buscaglia, G. Canu, M. Castellano, V. Buscaglia, and P. Stagnaro, "*PVDF-$BaTiO_3$ composite dielectrics: influence of processing*

and particles modification on properties", Workshop for young ceramists, CNR Bologna, 26-27 November, 2018. ISBN: 978-88-7586-599-3, p. 119-122.

- E. Brunengo, L. Conzatti, I. Schizzi, C. Costa, M. T. Buscaglia, G. Canu, M. Castellano, L. Curecheriu, L. Padurariu, L. Mitoseriu ,V. Buscaglia, and P.Stagnaro, "*Dielectric PVDF-ceramics nanocomposites: how the coating of the filler affects the final properties*", Eurofillers Polymer Blends 2019, Palermo April 23-26, 2019.
- E. Brunengo, G. Luciano, G. Canu, L. Conzatti, M. Castellano, P. Stagnaro, "A smart approach to modify PVDF polymorphism and properties", Macrogiovani 2020 Digital Edition, 26 June 2020 on Microsoft® Teams.

Co-author:

- V. Buscaglia, E. Brunengo, M. T. Buscaglia, G. Canu, L. Conzatti, C. Costa, L. Curecheriu, L. Mitoseriu, L. Padurariu, I. Schizzi, and P. Stagnaro, «Effective dielectric properties and 3D FEM modelling of field distribution in ferroelectric PVDF composites containing BaTiO3@AO2 (A = Ti, Si) inclusions», International Symposium on Applications of Ferroelectrics (ISAF 2018), Hiroshima (Japan), 27-31 May, 2018.
- L. Conzatti, E. Brunengo, I. Schizzi, C. Costa, M.T. Buscaglia, G. Canu, M. Castellano,V. Buscaglia, P. Stagnaro, «PVDF-based composites with engineered $BaTiO_3$ nanoparticles for energy storage», XXIII Convegno Nazionale AIM, Catania (Italy), 9-12 September, 2018. ISBN: 978-88-7751-449-3, p. 117-118 (oral O4.1)

Poster Communications:

Personally presented:

- E. Brunengo, L. Conzatti, I. Schizzi, C. Costa, M.T. Buscaglia, G. Canu, M. Castellano, V. Buscaglia, and P. Stagnaro, «PVDF/$BaTiO_3$ composites as dielectric materials: influence of processing on properties », 9^{th} Conference on "Times of Polymers (TOP) & Composites", Ischia (Italy), 17-21 June, 2018, p. 95.
- E. Brunengo, L. Conzatti, I. Schizzi, C. Costa, M. T. Buscaglia, G. Canu, M. Castellano, V. Buscaglia, P. Stagnaro, «Influence of processing on PVDF polymorphism in PVDF/BaTiO3 composite dielectrics for energy storage», Fourth Workshop on Polymer Crystallization Genova 2018, Genova (Italy), 3-5 September 2018.
- E. Brunengo, M. Castellano, L. Conzatti, I. Schizzi, C. Costa, M.T. Buscaglia, G. Canu, V. Buscaglia, P. Stagnaro, *"A double-step compression molding to improve the dielectric properties of PVDF and PVDF-based composites"*, Conferenza di Dipartimento 2019 (DSCTM – Dipartimento di Scienze Chimiche e Tecnologie dei Materiali del CNR, Bressanone, 28-30 Ottobre 2019. ISBN:978 88 8080 370 6, p.75

Co-author:

- G. Canu, E. Brunengo, M.T. Buscaglia, L. Conzatti, C. Costa, L. Curecheriu, L. Mitoseriu, L. Padurariu, I. Schizzi, V. Buscaglia, P. Stagnaro, «Engineered ferroelectric PVDF composites containing $BaTiO_3$-based core-shell inclusions: dielectric properties and 3D FEM modelling of field distribution », Electroceramics XVI, Hasselt (Belgium), 9-12 July, 2018.
- I. Schizzi, E. Brunengo, L. Conzatti, C. Costa, M.T. Buscaglia, G. Canu, V. Buscaglia, and P. Stagnaro «Influence of $BaTiO_3$@TiO_2 core-shell inclusions on dielectric properties of PVDF-based composites», XXIII Convegno Nazionale AIM, Catania (Italy), 9-12 September, 2018. ISBN: 978-88-7751-449-3, p. 176-177 (poster P3.6)
- E. Brunengo, G. Canu, M. T. Buscaglia, L. Conzatti, C. Costa, L. Curecheriu, L. Mitoseriu, L. Padurariu, I. Schizzi, V. Buscaglia, P. Stagnaro, «Engineered Ferroelectric PVDF

Composites Containing $BaTiO_3$-based Core-shell Inclusions: Dielectric Properties and 3D FEM Modelling of Field Distribution», CNR-DSCTM Department Conference 2018, Assisi (Italy), 24-26 September, 2018. ISBN: 978 88 8080 339 3, p. 130

- M.T. Buscaglia, G. Canu, E. Brunengo, P. Stagnaro, L. Conzatti, I. Schizzi, C. Costa, L. Curecheriu, L. Padurariu, L. Mitoseriu, V. Buscaglia, "*High-k engineered PVDF-BaTiO3 composites for energy storage*", Conferenza di Istituto 2019 – ICMATE, 21-22 May 2019, Padova (Italia).
- F. Gheorghiu, L. Curecheriu, E. Brunengo, L. Mitoseriu "*The synthesis and characterization of PVDF-based composites for flexible electronics*", 2019 Joint Conference of the IEEE ISAF, EMF, ICE, IWPM and PFM, 14-19 July 2019,Lausanne (Switzerland).
- L. Conzatti, E. Brunengo, R. Utzeri, M. Castellano, M. Scatto, P. Hodge, P. Stagnaro, "Eco-composites based on biodegradable polyester: chemical modification and plasma treatment of hemp fiber reinforcement"Conferenza di Dipartimento 2019 (DSCTM – Dipartimento di Scienze Chimiche e Tecnologie dei Materiali del CNR), Bressanone, 28-30 October 2019. ISBN:978 88 8080 370 6, p. 130.
- M. Vijatovic Petrovic, F. Rusanescu Craciun, F. Cordero, E. Mercadelli, C. Galassi, N. Ilic, J. Bobic, E. Brunengo, P. Stagnaro, "Lead-free piezoelectric flexible films", Electroceramics XVII, Virtual version, 24 - 28 August 2020, p.291 (poster 209).